Investigating the potential of mitochondrial inhibition as an antifungal target in *Cryptococcus neoformans*

Elizabeth Sarah Meta Edrich

2023

A thesis presented for the degree of Doctor of Philosophy in Cell Biology

School of Biosciences

University of Kent

Declaration

No part of this thesis has been submitted in support of an application for any degree or other qualification of the University of Kent or any other University or Institution of learning.

Elizabeth Edrich

December 2023

Acknowledgements

I would firstly like to thank my supervisor, Professor Campbell Gourlay, for his continuous support, encouragement and patience throughout my project, which has enabled me to gain a vast amount of knowledge from him over the years. I would also like to thank the entirety of the Kent Fungal Group (KFG), namely the Gourlay lab, for all the help, advice, company and coffee given during this time, particularly during the COVID-19 pandemic. Without Professor Gourlay and the KFG, this project would not have been possible.

I would also like to thank my collaborators, Professor Robin May (University of Birmingham) and Dr. Tihana Bicanic, (St. George's hospital) for all of their contributions, and the Global Challenges Doctoral Centre (GCDC) for funding my project.

Finally, I would like to thank my family and friends for their unconditional motivation and support throughout the whole duration of this project.

Abbreviations

ABC	ATP Binding Cassette
ADME	Absorption, Distribution, Metabolism, Excretion
ADP	Adenosine Diphosphate
AntA	Antimycin A
Aox	Alternative Oxidase
APS	Ammonium Persulfate
ATP	Adenosine Triphosphate
BBB	Blood Brain Barrier
CFU	Colony Forming Unit
CnMV	*Cryptococcus neoformans* derived Microvesicles
CNS	Central Nervous System
CNV	Copy Number Variation
Cox	Cytochrome *c* Oxidase
DAG	Diacylglycerol
DDR	DNA Damage Response
ECL	Enhanced Chemiluminescence
ERMD	ER-Mitochondrial Division
ERMES	ER-Mitochondria Encounter Structure
ETC	Electron Transport Chain
EV	Extracellular Vesicle
FACS	Fluorescence-Activated Cell Sorter
FCCP	Carbonyl Cyanide-p-trifluoromethoxyphenylhydrazone
FET	Forward Electron Transfer
GAG	Glycosaminoglycan
GXM	Glucuronoxylomannan polysaccharide

GXMGal	Glucuronoxylomannogalactan
H_2DCF-DA	2',7'-Dichlorodihydrofluorescein diacetate
HOG	High Osmolarity Glycerol response
HRR	High Resolution Respirometry
IMM	Inner Mitochondrial Membrane
iNOS	Nitric Oxide Synthase
IPC	Inositol-phosphoryl Ceramide
KCN	Potassium Cyanide
KH_2PO_4	Potassium Dihydrogen Phosphate
L-DOPA	l-3,4-Dihydroxyphenylalanine
MALC	Mono Alkyl Lipid Cation
MAM	Mitochondrial Associated ER Membrane
$MgSO_4$•7H_2O	Magnesium Sulphate Heptahydrate
MIC	Minimum Inhibitory Concentration
MOPS	3-(N-morpholino) propanesulfonic acid
MSR1	Macrophage Scavenger Receptor 1
mV	Millivolts
NAD	Nicotinamide Adenine Dinucleotide
NADH	Nicotinamide Adenine Dinucleotide + Hydrogen
NCR	Nitrogen Catabolite Repression
NIC	Non- Inhibitory Concentration
NO	Nitric Oxide
OMM	Outer Mitochondrial Membrane
pAb	Polyclonal Antibody
PAR	Parallel Respiratory Chain
PBS	Phosphate Buffered Saline

PBS/T	Phosphate Buffered Saline + Tween 20
PCR	Polymerase Chain Reaction
PHO	Phosphate sensing and acquisition
PI	Potassium Iodide
Pi	Inorganic Phosphate
PKA	Protein Kinase A
PKC	Protein Kinase C
PM	Phenotypic MicroArray™
PMF	Proton Motive Force
PMRS	Plasma Membrane Redox System
PPO	Prophenoloxidase
PRR	Pattern Recognition Receptor
PVDF	Polyvinylidene Difluoride
Q_oI	Quinone Outside Inhibitor
RET	Reverse Electron Transfer
redox	Reduction-Oxidation
ROS	Reactive Oxygen Species
rpm	Revolutions Per Minute
SD	Standard Deviation
SDHI	Succinate Dehydrogenase Inhibitor
SDS	Sodium Dodecyl Sulfate
SDS-PAGE	Sodium Dodecyl Sulfate–Polyacrylamide Gel Electrophoresis
SHAM	Salicylhydroxamic Acid
SNP	Sodium Nitroprusside
SOD	Superoxide Dismutase
SPT	Serine Palmitoyltransferase

STAB	Trimethyloctadecylammonium Bromide
TEMED	Tetramethylethylenediamine
TET	Triethyltin Bromide
TF	Transcription Factor
TLR4	Toll Like Receptor 4
TOR	Target of Rapamycin
TPP	Triphenylphosphonium
TPS	Trehalose Phosphate Synthase
WASH	Wiskott-Aldrich syndrome protein and Scar Homolog
WT	Wildtype
YNB	Yeast Nitrogen Base

Abstract

The opportunistic pathogen *Cryptococcus neoformans* is the major causal agent of cryptococcosis and cryptococcal meningitis in HIV patients worldwide, and increasing evidence of antifungal resistance demands that new therapeutic targets are investigated. Here, we review the roles of mitochondria, respiration and metabolism in *C. neoformans* pathogenesis and discuss the role of the Alternative Oxidase enzyme (Aox). Our data suggests that *C. neoformans* was sensitive to mitochondrial disruption and that resistance of this organelle to stress is partly linked to Ypk1, a kinase involved in lipid biosynthesis pathways. We propose that Aox1 plays an important role in the decision to enter quiescence when mitochondria are placed under respiratory stress, potentially as part of a metabolic checkpoint. Investigations into efficacy of the antimicrobial agent sodium nitrite, and the effects of novel, putative fungal-specific inhibitors ALTOX094 and ALTOX102 are discussed. We found that these compounds had potential as dual inhibitors of Aox and cytochrome bc_1, which reduced *C. neoformans* growth and viability. However, these drugs had variable effects on respiration, indicative of different mechanisms of mitochondrial disruption. We suggest that tackling *C. neoformans* infection through mitochondrial inhibition presents a viable future direction for research. Further investigations to extend our findings around the role of mitochondria and metabolism in the control of quiescence may reveal new approaches to tackle the pathogenicity of *C. neoformans*.

Table of Contents

Declaration 2
Acknowledgements 3
Abbreviations 4
Abstract 8
Table of Contents 9
List of Figures 14
List of Tables 17
1. Introduction 18
1.1 Cryptococcosis 18
1.1.1 Clinical presentation and prevalence 18
1.1.2 Cryptococcosis: Host invasion 19
1.1.3 Escape and Dissemination 20
1.2 Pathogenicity and Virulence 22
1.2.1 Cell morphology and the capsule 22
1.2.2 Extracellular vesicles and fungal interactions 24
1.2.3 Signalling adaption to stress within the host 25
1.2.4 Genome plasticity and heteroresistance 27
1.3 Alternative Oxidase – aid or obstacle to combat the rise of fungal pathogens? 29
1.3.1 Abstract 30
1.3.2 Introduction 31
1.3.3 Fungal Respiration 31
1.3.4 The role of mitochondria in fungal pathogenicity 34
1.3.5 Aox function in plant fungal pathogens 37
1.3.6 Aox function in human fungal pathogens 39
1.3.7 Problems and potential for targeting respiration in human fungal pathogens 42
1.3.8 Proposed roles for Aox 44
1.3.9 Conclusion 45
1.4 Existing and new Cryptococcus-targeted antifungals 47
1.4 Project Aims 49
2. Materials and Methods 51
2.1 Strain information 51
2.2 Growth media for C. neoformans strains 52
2.3 Stock preparation of C. neoformans strains 52
2.4 Molecular Biology Techniques 52
2.4.1 Oligonucleotides 52

2.4.2 Genomic DNA Extraction 53
2.4.3 Polymerase Chain Reaction using recombinant Taq DNA Polymerase 53
2.4.4 Agarose Gel Electrophoresis 54
2.4.5 Whole Cell protein extraction 55
2.4.6 Preparation of Polyacrylamide gels 55
2.4.7 SDS-PAGE gel electrophoresis 56
2.4.8 Semi-dry protein transfer 57
2.4.9 Western blot detection using Enhanced Chemiluminescence (ECL) 57
2.4.10 Antibodies used for protein detection 58
2.5 Whole Cell Experimental Procedures 58
2.5.1 Measurement of liquid cryptococcal growth using absorbance 58
2.5.2 Assessment of C. neoformans growth by spotting assays 60
2.5.3 Assessment of C. neoformans viability using colony forming unit (CFU) assays 60
2.5.4 Respirometry Assays 60
2.5.5 BIOLOG screen 62
2.5.6 Flow Cytometry for analysis of cell viability 63
2.5.7 Assessment of melanisation using spotting assays 64
2.6 Pre-clinical testing 65
2.6.1 Use of the Galleria mellonella infection model to assess C. neoformans virulence 65
2.6.2 Haemolysis assay 65
2.7 Recombinant C. albicans Aox assay performed by Dr. Luke Young (University of Sussex) . 66
2.8 Rat liver mitochondrial assay performed by Dr. Luke Young (University of Sussex) 66
2.9 Statistical Analysis 67
3. Mitochondrial function of C. neoformans and its potential as a novel antifungal drug target 68
3.1 Introduction 68
3.2 Results 69
3.2.1 C. neoformans Aox shows low sequence similarity to other human fungal pathogens 69
3.2.2 C. neoformans Aox prediction modelling 72
3.2.3 Confirmation of Aox deletion in C. neoformans 74
3.2.4 C. neoformans Aox does not make a significant contribution to respiration during normal growth 76
3.2.5 Aox is required to provide resistance to Complex III inhibition by Azoxystrobin 78
3.2.6 Azoxystrobin inhibits Δaox1 mutant C. neoformans respiration 80
3.2.7 Azoxystrobin exposure does not reduce C. neoformans viability 82
3.2.8 C. neoformans Aox does not confer resistance to complex IV inhibition 83
3.2.9 Screening a C. neoformans kinase knockout library for KCN sensitivity 85
3.2.10 Ypk1 is required to maintain C. neoformans respiration 89

3.2.11 Loss of Ypk1 does not decrease C. neoformans melanisation under KCN stress 92
3.2.12 Screening for the effect of Azoxystrobin on Δypk1 mutant C. neoformans 95
3.2.13 Δypk1 mutant C. neoformans is sensitive to growth inhibition by Azoxystrobin 96
3.2.14 Δypk1 melanisation is not significantly affected by Azoxystrobin 97
3.3 Discussion 100
3.3.1 C. neoformans Aox shows high sequence homology to oleaginous, non-pathogenic yeasts 100
3.3.2 C. neoformans Aox is required for resistance to Complex III inhibition 100
3.3.3. C. neoformans Aox does not confer resistance to Complex IV inhibition 101
3.3.4 Ypk1 is required for resistance to Complex III and Complex IV inhibition 102
3.3.5 Full kinase activity of Ypk1 is required for melanisation 104
4. Investigating the metabolic requirements of C. neoformans 106
4.1 Introduction 106
4.2 Results 107
4.2.1 BIOLOG metabolite screen for wildtype and Δaox1 C. neoformans 107
4.2.2 Wildtype C. neoformans can utilise a wider range of carbon sources than cells lacking Aox1 109
4.2.3 C. neoformans can utilise peptides as a nitrogen source 113
4.2.4 Phosphorus and sulphur sources significantly increase Δaox1 mutant C. neoformans growth 121
4.2.5 Addition of key biosynthetic pathway substrates does not significantly affect C. neoformans growth 124
4.2.6 Effects of pH on C. neoformans growth 125
4.2.7 C. neoformans is sensitive to osmotic stress 131
4.2.8 Sodium nitrite inhibits the growth of C. neoformans 137
4.2.9 Investigation of sodium nitrite on C. neoformans viability 138
4.2.10 Sodium nitrite affects C. neoformans respiration 139
4.2.11 Sodium nitrite affects the melanisation ability of C. neoformans 141
4.3 Discussion 144
4.3.1 C. neoformans can make use of a variety of nutritional sources to support growth 144
4.3.2 C. neoformans growth is sensitive to pH and osmolarity 146
4.3.3 C. neoformans is sensitive to sodium nitrite 146
4.3.4 Sodium nitrite reduces C. neoformans melanisation 147
5. A search for novel mitochondrial inhibitors reveals a fungal specific role for Decylalkyl in inducing necrosis in C. neoformans 149
5.1 Introduction 150
5.2 Results 151
5.2.1 Inhibitor synthesis and rationale (conducted by Luke Young, University of Sussex) 151

5.2.2 Recombinant Aox and cytochrome bc_1 complex inhibition screening (conducted by Luke Young, University of Sussex) *152*
5.2.3 Identification of novel fungistatic compounds that effect C. neoformans growth *156*
5.2.4 ALTOX094 and ALTOX102 show fungistatic activity even at low concentrations *159*
5.2.5 ALTOX drugs exhibit fungicidal activity *160*
5.2.6 ALTOX094 treatment induces necrosis *161*
5.2.7 ALTOX102 treatment does not induce ROS production *163*
5.2.8 ALTOX treatment affects cellular respiration *166*
5.2.9 Effects of ALTOX drug application on C. neoformans virulence *168*
5.2.10 ALTOX102 induces melanisation in Galleria mellonella larvae *169*
5.2.11 ALTOX drugs do not lead to haemolysis *170*
5.2.12 Determining the active moiety of ALTOX094 and ALTOX102 ..... *172*
5.2.13 Fungistatic action of ALTOX drugs is not reliant on a complete molecule *173*
5.2.14 Fungicidal activity of ALTOX094 reference compounds is based on a mixture of cell death mechanisms *177*
5.2.15 The effects of ALTOX drug components on respiration *183*
5.2.16 Decyl TPP+ inhibits respiration, while Dodecyl TPP+ stimulates respiration *184*
5.2.17 ALTOX102 reference compounds may display a dose-dependent uncoupling activity *186*
5.2.18 MALC compound respiration stimulation is dependent on carbon chain length *190*
5.2.19 ALTOX reference compounds are not haemolytic *192*
5.3 Discussion *194*
5.3.1 ALTOX094 and ALTOX102 reduce C. neoformans growth and viability *194*
5.3.2 ALTOX drugs exhibit fungal specificity *194*
5.3.3 ALTOX drugs affect mitochondrial membranes *196*
6 Final Discussion *198*
6.1 Introduction *198*
6.2 Investigating C. neoformans metabolism *198*
6.2.1 C. neoformans shows optimum growth at low pH *198*
6.2.2 C. neoformans maintenance of membrane integrity *199*
6.3 Assessing C. neoformans use of mitochondria *200*
6.3.1 Mitochondrial function is linked to kinases involved in sphingolipid biosynthesis *200*
6.3.2 The sphingolipid kinase Ypk1 has a role in C. neoformans melanisation *202*
6.3.3 Roles of Aox in C. neoformans *205*
6.4 Antifungal therapeutic strategies *208*
6.4.1 Utilisation of peptides for antifungal targeting *208*
6.4.2 Assessment of C. neoformans mitochondria as a viable antifungal target *209*
6.5 Conclusions and Future Directions *210*
7 Appendix *212*

8 Bibliography *230*

List of Figures

Figure 1.1: Protective and productive roles of the C. neoformans capsule…….. 25

Figure 1.2: Schematic of the Electron Transport Chain (ETC) found in fungal pathogens… 33

Figure 1.3: Key plant fungal pathogens.…… 38

Figure 1.4: Key human fungal pathogens.…….... 41

Figure 3.1: Predicted phylogeny of an Aox monomer from C. neoformans.…….. 71

Figure 3.2: The published crystal structure of TAO.……...…….. 72

Figure 3.3: Predicted model of an Aox monomer from C. neoformans……..…… 74

Figure 3.4: Confirmation of the Aox deletion in the Δaox1 C. neoformans mutant……..… 75

Figure 3.5: Respiratory profiles of C. neoformans strains……...…….. 77

Figure 3.6: Screening the effect of Azoxystrobin on C. neoformans growth……..…….. 80

Figure 3.7: Respiratory profiles of C. neoformans exposed to Azoxystrobin.……..….. 82

Figure 3.8: Viability assay of C. neoformans exposed to Azoxystrobin treatment……..…..… 83

Figure 3.9: Respiratory profiles of C. neoformans strains exposed to KCN.…….. 84

Figure 3.10: Viability assay of C. neoformans exposed to KCN treatment.…… 85

Figure 3.11: Representative example illustrating the determination of KCN sensitive kinase mutants.…….. 86

Figure 3.12: Identification of kinase mutant sensitivity to KCN stress.……... 87

Figure 3.13: Confirmation of Δypk1 mutant sensitivity to KCN stress.……... 88

Figure 3.14: Respiratory profiles of Δypk1 mutant C. neoformans exposed to KCN.…….. 91

Figure 3.15: Melanisation of Δypk1 mutant C. neoformans treated with KCN.…….. 94

Figure 3.16: Identification of Δypk1 mutant sensitivity to Azoxystrobin stress.…….. 95

Figure 3.17: Screening for the effect of Azoxystrobin on Δypk1 mutant C. neoformans.……..... 97

.

Figure 3.18: Melanisation of Δypk1 mutant C. neoformans treated with Azoxystrobin.…….. 99

Figure 4.1: Representative schematic illustrating the determination of AUC values.…… 108

Figure 4.2: C. neoformans carbon source utilisation. 113

Figure 4.3: C. neoformans utilisation of nitrogen sources for growth in PM3. 114

Figure 4.4: C. neoformans utilisation of nitrogen sources for growth in PM6, PM7, and PM8 plates. 120

Figure 4.5: C. neoformans phosphorous and sulphur source utilisation. 123

Figure 4.6: C. neoformans BIOLOG nutrient supplement utilisation. 124

Figure 4.7: C. neoformans pH stress adaption. 130

Figure 4.8: C. neoformans osmotic stress adaption. 136

Figure 4.9: Confirmation of the effect of sodium nitrite on C. neoformans growth. 137

Figure 4.10: Viability assay of C. neoformans exposed to sodium nitrite treatment. 138

Figure 4.11: Respiratory profiles of C. neoformans exposed to sodium nitrite. 140

Figure 4.12: Melanisation of C. neoformans treated with sodium nitrite. 143

Figure 5.1: pIC_{50} values for synthesised compounds against C. albicans. 154

Figure 5.2: Screening of ALTOX compounds and their effect on C. neoformans growth. 158

Figure 5.3: Minimum Inhibitory Concentration (MIC90) values of ALTOX094 and ALTOX102. 160

Figure 5.4: Viability assay of C. neoformans exposed to ALTOX094 and ALTOX102 treatment. 161

Figure 5.5: Flow cytometry assay of C. neoformans exposed to ALTOX094 and ALTOX102 treatment. 162

Figure 5.6: Flow cytometry assay of C. neoformans exposed to ALTOX102 treatment. 165

Figure 5.7: Respiratory profiles of C. neoformans exposed to ALTOX drugs. 167

Figure 5.8: Mortality of Galleria mellonella exposed to ALTOX drugs. 169

Figure 5.9: Melanisation of Galleria mellonella exposed to ALTOX drugs. 170

Figure 5.10: Haemolytic effect of ALTOX drugs. 172

Figure 5.11: Screening of ALTOX reference compounds and their effect on C. neoformans growth. 174

Figure 5.12: Viability assay of C. neoformans exposed to ALTOX reference compounds. 176

Figure 5.13: Flow cytometry assay of C. neoformans exposed to ALTOX reference drugs. 182

Figure 5.14: Respiratory profiles of C. neoformans exposed to ALTOX094 reference compounds. ... 184

Figure 5.15: Respiratory profiles of C. neoformans exposed to ALTOX094 reference compounds. ... 186

Figure 5.16: Respiratory profiles of C. neoformans exposed to ALTOX102 reference compounds. ... 189

Figure 5.17: Respiratory profiles of C. neoformans exposed to MALC compounds. ... 192

Figure 5.18: Haemolytic effect of ALTOX reference drugs. ... 193

Figure 6.1: Proposed roles of Ypk1. ... 204

Figure 6.2: Proposed roles of Aox1 as a quiescence switch. ... 207

Figure 7.1a: Similarity scores of Aspergillus brasiliensis, Histoplasma capsulatum and Aspergillus niger Aox, in comparison to C. neoformans Aox (BLAST) ... 212

Figure 7.1b: Clustal alignment of the Aox sequences of human fungal pathogens whereby yellow residues indicate conservation, red residues indicate iron binding activity and green residues show quinol binding ability, carried out on Clustal 2.1 ... 213

Figure 7.2: Plate maps for the C. neoformans kinase knockout series generated by Kyung-Tae Lee et. al ... 219

Figure 7.3: Kaplan-Meyer survival graph comparing wildtype (H99) and Δaox1 mutant C. neoformans virulence. ... 229

List of Tables

Table 2.1: Strains used for this study 51

Table 2.2: Oligonucleotides used in this study 52

Table 2.3: Recipe for PCR Reaction mix 54

Table 2.4: Taq DNA Polymerase thermocycler settings 54

Table 2.5: Recipe for polyacrylamide gel components 56

Table 2.6: SPECTROstar Nano plate reader settings 59

Table 2.7: Oroboros O2k Oxygraph configuration 61

Table 2.8: Recipe for 48x yeast nutrient supplement (NS) used in BIOLOG plates 62

Table 2.9: Recipe for 12x PM additive solutions used in BIOLOG plates 62

Table 2.10: Recipe for BIOLOG PM plate inoculation 63

Table 2.11: Recipe for melanin agar plate supplementation 64

Table 4.1: Summary of BIOLOG plates 107

Table 5.1: Structures for natural products Colletochlorin B and D, and the analogues synthesised for this study 152

Table 5.2: pIC_{50} value table 154

Table 5.3: IC_{50} value table 154

Table 5.4: Modified Benzofuranone structures used for this study 156

Table 7.1: Summary of additives that increase C. neoformans growth 219

Table 7.2: Summary of additives that inhibit C. neoformans growth 223

Table 7.3 cLogP values 228

1. Introduction

Fungal pathogens are responsible for over one billion human infections and over 1.6 million deaths annually[1-4], as well as a third of all global crop failures[1, 5]. However, despite the threat that fungal strains present to animal species and the threat to food security worldwide, they remain under-researched[3, 6]. *Cryptococcus neoformans,* an opportunistic human fungal pathogen which is the causal agent of cryptococcosis and cryptococcal meningitis in humans[7], is the focus of this study.

1.1 Cryptococcosis

1.1.1 Clinical presentation and prevalence

While *C. neoformans* infections can be fatal, the fungus can be isolated in many regions around the world as a haploid budding yeast, although it has also been documented to grow in a filamentous form through a defined sexual cycle[8]. The fungus itself is relatively abundant and has been found in different soil and tree types, as well as in pigeon faeces[9, 10]. However, invasive cryptococcosis only affects immunocompromised people such as those with HIV or patients treated with immunosuppressant drugs[11]. It is estimated that there are 223,100 cases of AIDS related cryptococcal meningitis per year, attributing 19% of global AIDS related deaths[12], with most cases surfacing in sub-Saharan Africa and countries such as Brazil and Thailand[13].

In immunocompromised patients, pulmonary cryptococcosis presents as a pneumonia-like illness, with coughing, chest pain and fever[14]. Development into cryptococcal meningitis starts with headaches and a high fever, which ultimately leads confusion and behavioural changes[15, 16]. Treatment regimens rely on combination treatment of Amphotericin B and Flucytosine, followed by maintenance with Fluconazole for up to 12 months[17]. However, the varied nature of symptoms presented by patients infected with *C. neoformans* can lead to prolonged misdiagnosis, and inconsistencies in maintenance of the treatment program has led to increases in antifungal resistance[18, 19]. This includes *C. neoformans* heteroresistance to Fluconazole[20] and evidence of resistance providing cross-tolerance to other drug classes through aneuploidy[21]. Anti-fungal

resistance within *C. neoformans* populations has pushed for new alternative anti-fungal targets and better diagnostic tools for earlier detection of cryptococcosis, including antigen screening programmes to initiate earlier lumbar punctures in asymptomatic patients[22].

1.1.2 Cryptococcosis: Host invasion

Invasive cryptococcosis starts with the inhalation of *C. neoformans* basidiospores into the lungs, which form from fruiting bodies and are only 1-2μM in diameter[23-25], allowing for efficient alveolar penetration. Studies suggest that the cell surface of spores facilitates them to survive in harsh environments, including levels of high ultraviolet light (UV) and marked resistance to dry conditions[25], which is attributed to the spore coat. The spore coat has multiple polysaccharide components, displaying high levels of N-acetylglucosamine, glycoproteins and glucuronoxylomannan (GXM)[25]. This, in conjunction with studies showing that genes for the capsule biosynthesis pathway are also activated for sexual development and sporulation[25], may explain the abundance of this polysaccharide in the mature yeast capsule. Once inhaled, the Macrophage Pattern Recognition Receptor (PRR) Dectin1 recognises β-(1,3)-Glucan, and CR3, a leukocyte adhesion receptor, recognises other β-Glucans and mannose present on the spore coat[26]. These spores are readily ingested by alveolar macrophages, and provided they germinate before ingestion, can survive in the acidic environment of the phagolysosome[27]. The phagolysosome derives from a nascent phagosome that serially fuses with endosomes and lysosomes, and development of the mature phagolysosome is mediated by Rho, Rab and Arf GTPases, which has been well reviewed[28]. The mature phagolysosome has characteristics of lysosomes in that it is highly acidic (~pH 4.5) and is rich in hydrolases, including cathepsins, lipases, proteases, and lysozymes[29]. This environment disrupts the regular metabolism of engulfed fungi and consequently prevents the use of microbial metabolites for growth and survival.

Exact mechanisms for *C. neoformans* recognition and phagocytosis by macrophages is still unclear. It is presumed that efficient phagocytosis may be dependent on the M1/M2 polarisation pathway and the use of opsonins and PRR for pathogen-associated molecular pattern (PAMP) recognition[30].

However, recent studies have identified that in the lung environment, non-opsonising uptake is integral for determination of disease progression, which involves Toll-like Receptor 4 (TLR4)/Macrophage Scavenger Receptor 1 (MSR1) crosstalk[31]. Investigations suggest that the use of MSR1, mediated by TLR4, involves multiple signalling pathways for fungal uptake, including SYK, PI3K, p38, and ERK1/2 activation through FcγR receptor activation[31]. Interestingly, both cholesterol and sphingomyelin, key components of lipid rafts, are essential for FcγR receptor activity, namely FcγRIII-mediated phagocytosis of *C. neoformans*[32]. These studies indicate that details of phagocytic interactions between macrophages and *C. neoformans* are multifaceted, but still require further investigation.

1.1.3 Escape and Dissemination

While *C. neoformans* can resist the harsh conditions of the phagolysosome, pathogenic transfer and host evasion are still required for survival and dissemination. There are three known mechanisms of escape from phagocytes that have been reviewed[33]: lytic exocytosis, vomocytosis, and dragotcytosis, although the exact signalling mechanisms behind these processes still requires further research. Lytic exocytosis ruptures the host cell, thought to arise from rapid cryptococcal proliferation[34], and although this process has been observed[35, 36], cryptococcal cell fate after lytic expulsion is not well documented. Vomocytosis, also known as non-lytic expulsion, involves the escape of *C. neoformans* from phagocytes like macrophages and dendritic cells without causing harm to the host cell or incurring damage itself.

Vomocytic mechanisms are thought to be highly regulated in *C. neoformans*[33], including the use of Rab GTPases [37], ERK5 signalling [38], cathepsin [39] and Annexin A2 activity [40]. This involves processes such as actin depolymerisation, phagosome extrusion and antibody agglutination[41, 42]. Once engulfed, if lytic exocytosis through rapid proliferation is not initiated, lateral transfer or ‘dragotcytosis’ can occur, whereby ingested *C. neoformans* may be engulfed by a neighbouring phagocyte shortly after non-lytic expulsion[43].

While the molecular signalling mechanisms behind dragotcytosis are unknown, evidence suggests that there is no observable cross talk between adjacent donor and receiver macrophages involved in the process[33, 43]. It could be postulated that dragotcytosis could simply occur due to close proximity of localised macrophages that actively take up *C. neoformans*, regardless of local vomocytic events. In any case, anti-inflammatory, minimally damaging transfer mechanisms could account for the persistence of the latent infection and the insidious symptoms seen in early-onset patients infected with *C. neoformans*[44].

Transcytosis, the process in which *C. neoformans* transmigrates across the blood-brain-barrier (BBB), relies on both adhesion to the endothelial barrier through glycosaminoglycan (GAG) binding[45] and changes in cryptococcal capsule size and structure[46]. Interestingly, while signalling mechanisms behind BBB migration still require further investigation, studies have shown that *C. neoformans* can induce actin cytoskeleton reorganisation in host endothelial cells, resulting in membrane ruffling and swelling of the mitochondria and ER[33, 47]. This alteration of cytoskeletal morphology in host cells is thought to contribute to cryptococcal migration across the BBB, which is a major step in the advancement of the infection and contributes to late-stage subacute meningitis. It has been proposed that dragotcytosis may enable the localisation of *C. neoformans* to the BBB to initiate transcytosis [43, 48]. Following transcytosis, astrocytes which regulate the BBB and form a secondary component, the glia limitans, provide homeostatic protection against CNS infection from *C. neoformans*[49]. Secondly, reactive astrocytes within the brain are thought to undergo astrogliosis to promote resistance to the infection via complement protein and neurotrophic factor expression. The reviewed interactions between astrocytes and *C. neoformans*[49] suggest that beside homeostatic support, astrocytes could potentially induce cell-mediated immunity through recruitment of phagocytes via MHCII upregulation.

While these dissemination mechanisms require further investigation, both escape from phagocytes and fungal migration require high levels of metabolic flexibility not only for physical transmigration but for adaption in nutrient-limited conditions. This includes the acidic phagolysosome, which

disrupts metabolism and prevents the use of normal metabolic intermediates, and so investigations into *C. neoformans* ability to utilise non-standard metabolites should be explored.

1.2 Pathogenicity and Virulence

1.2.1 Cell morphology and the capsule

A notable virulence enhancing trait of *C. neoformans* is the polysaccharide capsule, a dynamic defence mechanism against environmental pathogens such as amoebae and macrophages in the host[50], which acts as a barrier to phagocytosis[51]. While the *C. neoformans* capsule is integral to survival, exact signalling mechanisms behind capsular growth and plasticity are unclear. However, known roles include inhibiting inflammatory cytokine production, depletion of complement components, and evasion of phagocytosis[52]. Furthermore, the capsule also serves as a ROS scavenger in macrophages and permits resistance to antimicrobial peptides and Amphotericin B[53]. Capsule growth can be induced *in vitro* using low iron, high CO_2 and mammalian serum[54-56]. Capsule sizes vary based on clonal populations and growth conditions, with fluxes of rapid capsular growth reaching up to 2.5μm^3/min, markedly faster than cell body growth (0.3 μm^3/min)[57]. Rapid capsular remodelling is thought to be energetically demanding and therefore dependent on mitochondrial activity, as evidence suggests that capsule enlargement directly correlates with an increase in mitochondrial membrane potential and an increase in ROS production[58] (Fig. 1.1).

The capsule is involved in evading macrophage-based recognition, including impairment of macrophage recognition of cell wall epitopes[59], which is thought to be attributed to adjustment of surface β-glucan levels[60] and high antigenic variation[46]. This variation derives from the structural heterogeneity of GXM, which includes a repeating monosaccharide major triad, like a six-residue repeating unit followed by one or more minor triads, such as β1,2 xylose side chains that can form in multiple combinations and therefore provide differing glucuronic acid positional effects[61, 62]. Approximately 90% of the mature capsule is formed of glucuronoxylomannan (GXM)[63] which contains O-acetylated α-1,3-linked mannose residues with xylosyl and glucuronyl side groups[59].

Another key component in capsular formation is glucuronoxylomannogalactan (GXMGal), an α-1,6-linked galactose polymer with mannose, xylose, and glucuronic acid modifications[64].

Evidence shows that capsule size and signalling is organ-specific. For example, capsular cells extracted from lung tissue are larger than those extracted from cranial samples and include titan cells[46], which may account for delays in immune recognition and prolonged asymptomatic infection[65-67]. Extra-pulmonary cell sizes are heterogenous, with studies citing median diameters of cells extracted from the blood, spleen and brain at 12.7μM, <15μM, and <10 μM, respectively[68]. However, early phase dissemination requires the use of seed-cell morphotypes which are <6 μM in size[69]. Seed cells, as well as titan daughter cells called titanites, are thought to be important in extra-pulmonary dissemination, invasion and proliferation. However, seed cell presence is not preceded by titan cell activation and is interestingly linked to phosphate acquisition, whereby phosphate sourced from either bird guano or tissue damage drives a production of small cell phenotypes[68]. Large capsule sizes, however, have been noted as a key characteristic of titan cells, a phenomenon where *C. neoformans* cells are found between 10μM and 100μM in diameter, with a large cell body, a thick cell wall and highly cross-linked capsule[70-72]. These titan cells are generated during nutrient starvation and hypoxia *in vivo* and are thought to be resistant to multiple stresses including phagocytosis[73]. However, signalling mechanisms behind titan cell formation and roles in pathogenicity are still under-researched due to the difficulties replicating titan cell induction *in vitro*[70].

Capsule production and maintenance is a highly regulated process that places a large metabolic demand on the cell. Adaption of signalling pathways in relation to the host environment, and adaption through early, mid and late-stage infection are required for capsular growth and increased virulence. Several signalling pathways are involved, including at least 35 genes for capsule biosynthesis, such as *CAP10* and *CAP60*, the cAMP and HOG pathways, iron sensing mechanisms and chromatin remodelling[74]. Several transcription factors such as Yap1, Gat201, Ada2, and Bzp4 were involved in capsule production and regulation of capsule-related genes[74]. Interestingly, transcript analysis for energy metabolism was associated with capsule production during infection,

such as downregulation of ATP synthesis in initial infection, increased transcription of HXS1, a high-affinity glucose transporter, and upregulation of ATP synthesis in late-stage infection[69]. This indicates not only that capsule production and development places large energy demands on the cell, but that energy dependent resistance mechanisms for adaption to host induced stress is integral for fungal virulence. Given the known links between capsule size and metabolism, is important that investigations into mitochondrial function in *C. neoformans* and its impact on capsule size and virulence are investigated.

1.2.2 Extracellular vesicles and fungal interactions

Capsular polysaccharides like GXM are abundant on the cell surface and have been found in extracellular vesicles (EVs), along with other virulence enhancing molecules including urease, RNA, antioxidant proteins, laccase, proteases and lipases[75, 76]. EVs are integral in fungal membrane signalling and are also produced by other human fungal pathogens, including *Candida albicans*, *Candida auris*, *Histoplasma capsulatum*, and *Paracoccidioides brasiliensis*[77-79]. While EV signalling is not wholly understood, studies suggest that *C. neoformans* can modulate EV production to enable azole resistance[80] and *C. neoformans* derived microvesicles (CnMV) can enhance cryptococcal transfer across the BBB[81], both of which contribute to pathogenicity. Interestingly, fungal EVs have also been implicated in intraspecies intracellular communication[82]. Given that *C. neoformans* originates from rich polymicrobial environments, evidence suggests that Amoebae such as *Acanthamoeba castellanii* and *Dictyostelium discoideum* form long term environmental interactions with *C. neoformans,* including Wiskott-Aldrich syndrome protein and Scar Homolog (WASH) mediated exocytosis and a vomocytosis-like exocytotic process of *C. neoformans*[83]*.* As these environmental interactions show similarities to interactions with macrophages in the host, adaptive mechanisms developed in these environmental interactions are thought to contribute to the enhanced ability of *C. neoformans* to evade phagocytic killing in the human host and aid in its dissemination[75, 84]. While in-depth discussion surrounding amoeba interactions are outside the scope of this thesis, it is worthwhile to note the importance of capsular adaptability in different niches and

how long-term environmental interactions may pertain to evolutionary adaptions that consequently benefit dissemination and proliferation in the host environment.

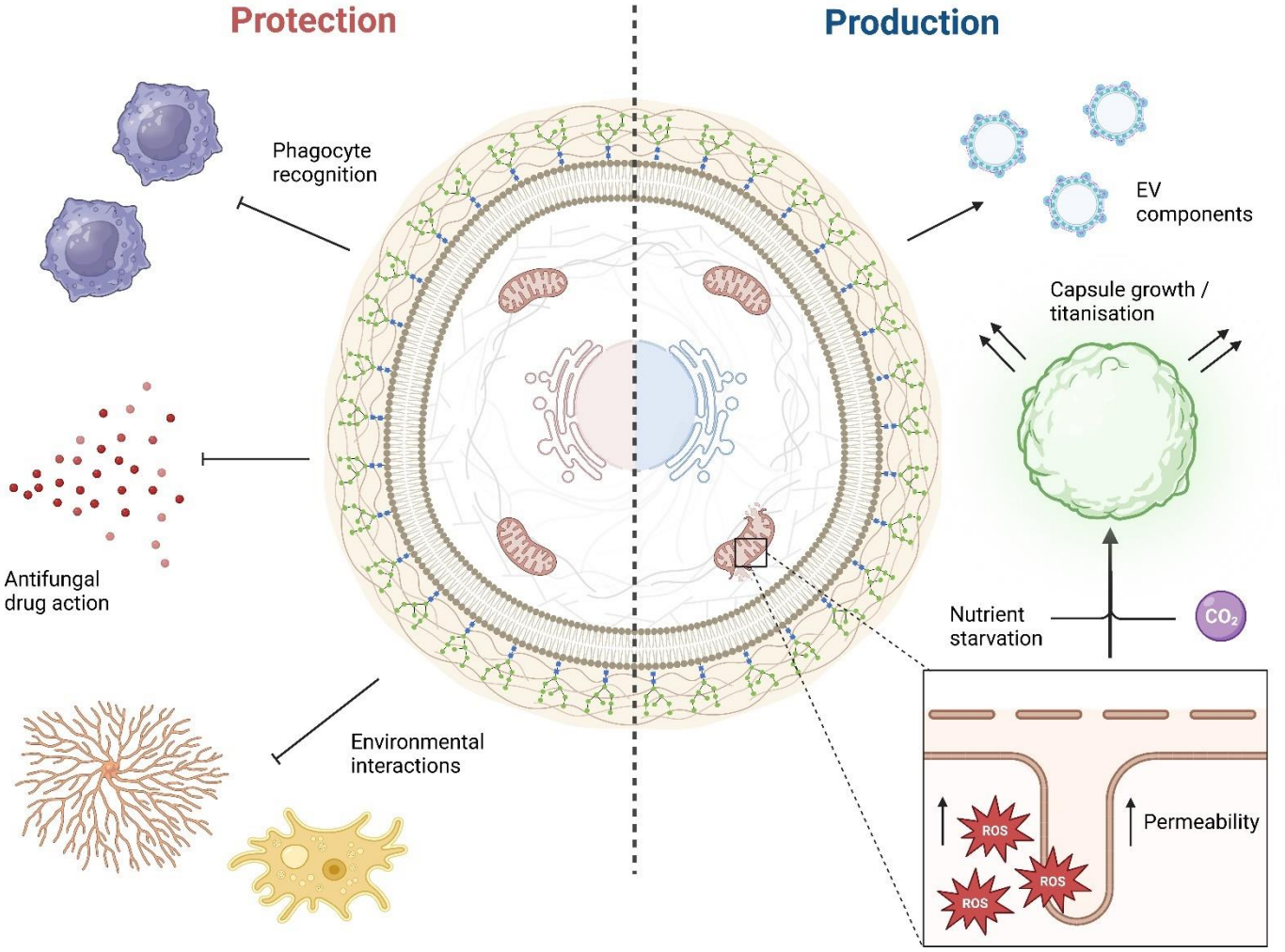

Figure 1.1: Protective and productive roles of the C. neoformans capsule.
Schematic illustrating known capsule production mechanisms and examples of cellular protection against environmental stresses. Production mechanisms include generation of GXM components of EVs for extracellular signalling and rapid capsular growth and titanisation initiated from increases in ROS, CO_2 and nutrient starvation. Protection mechanisms include evasion of phagocyte recognition, antifungal drug resistance, and protection against environmental interactions with *Acanthamoeba castellanii* and *Dictyostelium discoideum.*

1.2.3 Signalling adaption to stress within the host

Although the capsule is a key structure for pathogenicity, *C. neoformans* has a plethora of molecular virulence factors for use against host innate defence systems. Alveolar macrophages in the host rely on multiple signalling mechanisms to counteract *C. neoformans* proliferation, including elevating

free radicals to enhance oxidative and nitrosative stress[85], and elevating copper levels[86]. Excess copper can be negated by *C. neoformans* whereby copper homeostasis machinery such as Cuf1 directs downregulation of copper importers and upregulation of copper-detoxifying metallothioneins such as CMT1 and CMT2[87]. Interestingly, high copper levels in the lungs but a marked decrease in copper levels in the brain initiates a switch between copper detoxification and acquisition [87]. This is indicative that *C. neoformans* signalling allows for rapid adjustment to fluctuating conditions within the host, perhaps through cross-talk between protein regulation pathways.

To tolerate oxidative stress induced by alveolar macrophages, *C. neoformans* undergoes melanisation. Melanisation utilises both the cyclic adenosine monophosphate (cAMP) and high-osmolarity glycerol response (HOG) pathways for induction of laccase enzymes such as Lac1[88, 89], as well as l-3,4-dihydroxyphenylalanine (L-DOPA) as a precursor for melanin production[90]. Complex regulation through kinase cascades synthesise melanin and ensure deposition at the cell wall, where a melanin coat is formed[89]. Melanin production has been shown to enhance resistance to ionising radiation, oxidative stress, acidic conditions, and antimicrobial compounds, making the melanin coat critical for pathogenesis[91]. This may be in part due to the ability of melanin itself to neutralise ROS, and the laccase enzymes responsible for its synthesis can sequester and oxidise iron during infection[92]. In *C. neoformans*, iron acquisition is integral for pathogenicity, melanin production and azole resistance [93]. This involves ferric reductases like Fre4 and iron uptake components such as Cfo1[94] with studies showing that an excess of iron exacerbates the onset of meningoencephalitis in murine models[95].

Murine and rabbit models have not only been used to study drugs that affect disease progression such as corticosteroids like dexamethasone and methylprednisolone [96, 97], but also the effect of mammalian temperature on *C. neoformans* dissemination[98, 99]. Most basidiomycetes are unable to survive temperatures above 35°C, including species like *Cryptococcus podzolicus*, regardless of their capsule and melanin-forming abilities[100]. However, *C. neoformans* is able to grow at the elevated temperatures of the host[99]. The ability to grow at human body temperature has been

attributed to a number of stress response pathways including mitochondrial proteins such as manganese superoxide dismutase (SOD)[101] trehalose biosynthesis[102], HOG signalling, Ras signalling and cell wall integrity pathway[103-105]. Evidence also suggests that gene expression linked to chromatin remodelling is heavily regulated by the histone acetyltransferase Gcn5 during growth at 37°C [106], which allows for host-induced transcriptional responses and increases genomic stability[99, 107].

1.2.4 Genome plasticity and heteroresistance

As has been reported for many fungal pathogens, the adaptation to environmental challenges, such as elevated host temperatures or innate defence mechanisms requires highly functional genomic plasticity[108]. In *C. neoformans*, this is partly attributed to variations in karyotype and chromosome copy number (aneuploidy)[109], an occurrence also observed in *Candida albicans*[110]. Increased or decreased copies of chromosomes can directly affect gene expression and protein synthesis, and while this can be associated with an overall decrease in cell fitness[111] it may allow for adaptability to stress and could facilitate latent survival in the host. *C. neoformans* appears to utilise copy number variation (CNV) as a means to acquire stress tolerance, with aneuploidy being reported to increase rapidly during infection[111]. Evidence suggests that titan cells are genetically unstable and are known to produce highly aneuploid daughter cells[112], which may contribute to a stress tolerant infection via generation of genetically varied progeny.

Aneuploidy has been linked to drug heteroresistance, a phenomenon whereby fungal colonies within a population will show variable growth as an adaptive response to antimicrobial agents. Heteroresistance linked to aneuploidy can therefore lead to a resistant subpopulation of cells that can re-grow or persist during drug re-exposure[113]. This includes *C. neoformans* persister cells, classified as a non-growing, strongly tolerant subpopulation, arising from a heterogenous population[114] of which ergothioneine-mediated persister cells have been documented following Amphotericin B treatment[115]. Increasing incidences of Fluconazole heteroresistant clinical isolates of *C. neoformans* originating from HIV patients in Brazil[116], Thailand[117], Cambodia[118] and Tanzania[20]

have led to trials of combination therapy approaches. Evidence suggests that Fluconazole monotherapy has now been deemed ineffective in the face of emerging resistance[18]. It may be the case that exposure to one drug class, such as an azole like Fluconazole, may provide cross-adaption to other drug classes via aneuploidy. This is supported by the current recommended treatment guidelines for *C. neoformans*, which include a combination of Flucytosine, Amphotericin B, and Fluconazole for efficient containment and treatment of cryptococcosis[17]. Genomic adaption through aneuploidy poses a threat to current antifungal treatment options, which calls for investigations into novel antifungal targets and new collaborations for combination therapies.

In light of increasing cases of heteroresistance, new antifungal targets must be researched. Mitochondria may prove to be a useful target because of links to virulence, and so the following material has been written and submitted as a review article.

1.3 Alternative Oxidase – aid or obstacle to combat the rise of fungal pathogens?

Elizabeth SM Edrich[1], Lucian Duvenage[2] and Campbell W Gourlay[1*]

[1]Kent Fungal Group, School of Biosciences, University of Kent, Kent, CT2 9HY, UK.

[2]CMM AFRICA Medical Mycology Research Unit, Department of Pathology, Faculty of Health Sciences, University of Cape Town, Cape Town, South Africa.

[*]Author for correspondence

DOI: 10.1016/j.bbabio.2024.149031

This review was written by me, with additions from Lucian Duvenage in relation to *Candida albicans* Aox activity. This work was reviewed by me, Lucian Duvenage and Campbell Gourlay prior to submission to the BBA Bioenergetics journal, where it was then published following peer review.

1.3.1 Abstract

Fungal pathogens present a growing threat to both humans and global health security alike. Increasing evidence of antifungal resistance in fungal populations that infect both humans and plant species has increased reliance on combination therapies and shown the need for new antifungal therapeutic targets to be investigated. Here, we review the roles of mitochondria and fungal respiration in pathogenesis and discuss the role of the Alternative Oxidase enzyme (Aox) in both human fungal pathogens and phytopathogens. Increasing evidence exists for Aox within mechanisms that underpin fungal virulence. Aox also plays important roles in adaptability that may prove useful within dual targeted fungal-specific therapeutic approaches. As improved fungal specific mitochondrial and Aox inhibitors are under development we may see this as an emerging target for future approaches to tackling the growing challenge of fungal infection.

1.3.2 Introduction

Given the prevalence of fungal pathogens and their innate ability to overcome antimicrobial challenges presented by the host, there is a growing need to conduct research into new antifungal targets and strategies to prevent fungal infection. As active infection and dissemination is thought to be energetically demanding, mitochondria could prove to be a useful target against plant fungal pathogens[119] and growing evidence, driven by an increase in our understanding of respiratory chain physiology, suggests that inhibitors may also be developed to tackle human infection[120, 121].

1.3.3 Fungal Respiration

As with many eukaryotes, fungal pathogens possess a well conserved classical Electron Transport Chain (ETC) which is used to generate a proton motive force (PMF) that can drive ATP synthesis, which is important for the numerous processes that mitochondrial function supports. Forward electron transfer through the respiratory complexes (FET) provides the thermodynamically favoured reaction that is coupled to oxidative phosphorylation and ATP production. However reverse electron transfer (RET) can occur, whereby electrons flow backwards through Complex I. RET is thought to be induced by reduction of the Ubiquinone pool (UQP) to between 40-60%, requiring a high PMF, a large thermodynamic driving force, and a high ΔpH[122].

Sites for mitochondrial Reactive Oxygen Species (ROS) production, namely superoxide ($O_2^{\bullet-}$) generation, include Complex I and Complex III, particularly sites I_F, I_Q and III_{QO}[122]. Site I_Q is responsible for most of the superoxide production during RET, whereby electrons are forced into Complex I through a high QH_2 / Q ratio and high PMF[122]. Both FET and RET can generate superoxides[122], whereby production and removal depend on substrate availability (like succinate oxidation, which drives RET[123]) QH_2/Q ratio, rate of oxygen consumption, and mitochondrial dysfunction or inhibition[122]. The multifactorial nature of ROS generation and management requires continual homeostasis, as ROS are essential within diverse cellular processes in both host and pathogen[124], but highly inflated ROS levels have been attributed to mitochondrial disease[125].

Induction of ROS production has also been implicated in the mode of action of several antifungals[126, 127] suggesting a role for mitochondria and/or redox homeostasis as a target in current therapeutic approaches. However, understanding the full signalling mechanisms of ROS within fungal pathogenesis represents a growing field of study.

Intuitively the conservation of the classical ETC provides a barrier to its development as an attractive target for human fungal pathogens. However, fungal specific differences that are essential for function have been reported, such as alternative NADH dehydrogenases, which may bypass Complex I activity[128, 129]. One key difference in the respiratory chain of many human fungal pathogens is the presence of a cyanide-insensitive alternative oxidase (Aox), which is not found in mammalian mitochondria. Aox branches from the main respiratory chain at the level of the UQP (Fig. 1.2) and has a catalytic di-iron centre orientated towards the mitochondrial matrix. Interestingly, this membrane-bound oxidase is non-proton motive, and therefore does not have a significant role in ATP production, but rather oxidises ubiquinol and reduces oxygen to water, bypassing the ETC prior to proton translocation by complexes III and IV (Fig. 1.2). However, there is evidence for ATP generation through the Aox/Complex I pathway in *Botrytis cinerea*[128, 130] and inhibition of Aox in *Gaeumannomyces graminis* leads to a decreased rate of ATP synthesis[131], indicating that the extent of Aox involvement in ATP generation may be species specific.

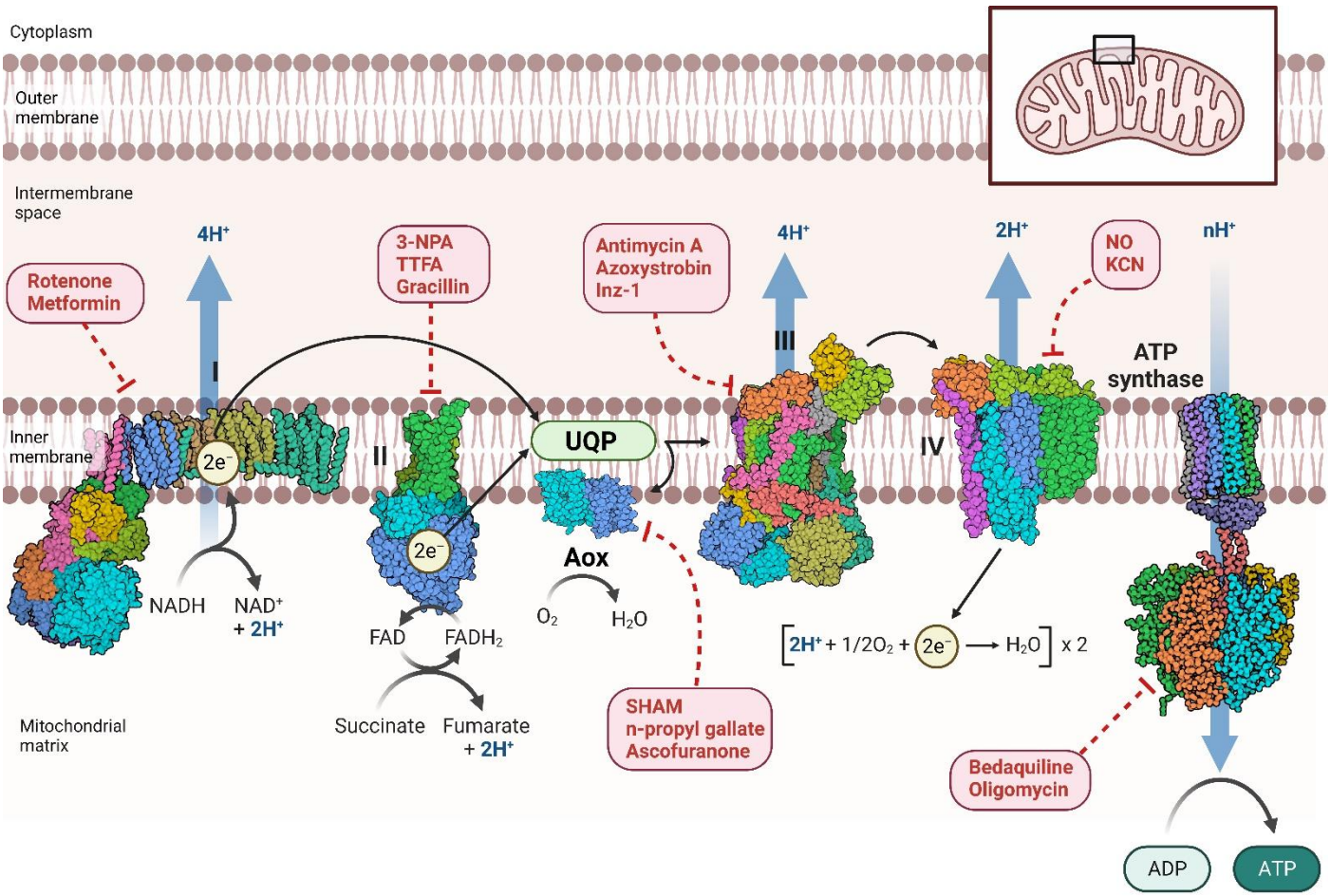

Figure 1.2: Schematic of the Electron Transport Chain (ETC) found in fungal pathogens. Both a classic ETC and an alternative respiratory chain are found in most fungi. Where known, crystal structures of the ETC components are shown [Complex I, Protein Data Bank (PDB) 3M9S[420], Complex II PDB 3VR8 [421], Trypanosomal Aox PDB 3VV9[223], Complex III PDB 1KYO [422], Complex IV PDB 8DH6 (to be published), ATP Synthase PDB 1QO1[423]]. Aox branches from the main respiratory chain at the level of the UQP. This pathway produces little ATP, but instead dissipates energy as heat and bypassing proton transfer through downstream Complexes III and IV. Known inhibitors of each ETC component are listed in red. Created with BioRender.com.

While Aox is not found in mammals, it is highly conserved amongst pathogenic fungi. Some fungal species like *Aspergillus niger*, *Aspergillus flavus* and *Candida albicans* have multiple isoforms[132, 133], there are notable exceptions, for example in *Candida glabrata* and *Pneumocystis jiroveci,* which, like *Saccharomyces cerevisiae*, do not contain a multi-subunit Complex I or Aox. It may be the case that Crabtree positive yeasts, that primarily use aerobic fermentation for increased growth rates

under high glucose availability[134], do not require an Aox for mitochondrial homeostasis, as growth is predominantly supported by fermentation rather than respiration. Crabtree negative yeast, which utilise respiration for energy generation such as *Candida albicans* and *Cryptococcus neoformans,* have retained Aox and maintain metabolic flexibility by utilising both alternative and glucose carbon sources. This flexibility may contribute to host colonisation and virulence in the nutrient-scarce host[134-137] whereby presence of Aox in fungal pathogens may also assist in the maintenance of mitochondrial function upon immune challenge, the regulation of ROS production, and pathogenesis[138-140].

Interestingly, fungi have been shown to utilise multiple respiratory pathways, for example *Aspergillus nidulans* can alternate between both classical and alternative respiratory pathways to generate sterigmatocystin, a precursor to Aflatoxin B_1 [132, 141]. A third 'parallel' respiratory chain (PAR), in *Candida albicans* and *Candida parapsilosis* has been proposed[142, 143] which may contribute up to 10% of total respiration capacity. The ability to utilise alternate routes of respiration suggests that these yeasts may have evolved within an environment that presents regular and significant challenges to electron transport. Alternately, it may be that alternate respiration supports signalling and metabolic changes that are required for adaptability within changing environments. This may include factors produced by competing or co-colonising microbes that damage or inhibit growth[144], such phenazine production by *Pseudomonas aeruginosa*[145], or detoxification of nitric oxide (NO) released by host cells during infection[146, 147]. This could also involve nutritional challenges that limit access to key metabolites, co-factors that support respiration or environmental challenges such as temperature variation or oxygen availability[144, 148].

1.3.4 The role of mitochondria in fungal pathogenicity

An increasing interest in fungal respiration has highlighted several mitochondrial roles which are thought to contribute to human fungal pathogenicity[149], although some of the signalling mechanisms behind this involvement are still unclear. Respiration deficiency leads to diminished virulence in mice

intravenously infected with *Candida albicans*[150], and respiratory inhibition with sodium nitroprusside (SNP), an NO donor, and salicylhydroxamic acid (SHAM), an Aox inhibitor, reduces *Candida albicans* cell viability and increases phagocytic uptake by macrophages[142]. Increased phagocytosis has also been seen after treatment of *Candida albicans* with the Complex III inhibitor Antimycin A, thought to be attributable to β-glucan exposure[151]. However, pre-treatment of the cells with SHAM and SNP prior to murine infection exhibited increased virulence through transcriptional changes and cell wall remodelling, presenting a higher renal fungal burden, and increased immune infiltrate than untreated cells[142]. This data therefore indicates that mitochondrial signalling mechanisms need to be investigated further.

Active infection and dissemination inside the host is presumed to be energetically demanding for pathogenic yeasts, especially for switches to hyphal growth forms for *Candida albicans* via the Ras1/cAMP/PKA signalling pathway[152, 153]. Other instances of increased respiratory demand for ATP in *Candida albicans* include escape from macrophage engulfment through catabolism of amino acids for morphogenesis[154]. This increased ATP demand could be attributed to the action of ATP-driven pumps belonging to the ATP Binding Cassette family (ABC). ABC transporters are profound influx-efflux pumps that rely on ATP hydrolysis to transport a variety of molecules, including sterols, metabolites, and drugs, proving crucial for pathogenic activity of *Magnaporthe grisea*[155, 156] and are thought to contribute to the multi-drug resistant phenotype seen in *Candida auris*[157]*.* As well as heavy reliance on ATP production, Vacuolar ATPases (V-ATPases) generate a pH gradient through ATP hydrolysis which drives secondary transporters to maintain cellular ion homeostasis. This process requires Ergosterol for optimal V-ATPase function and is sensitive to combination treatment with both Fluconazole and Amiodarone in the *Candida albicans* murine candidiasis model[158]. These investigations prove that ATP is crucial for a variety of processes that underpin fungal pathogenesis, although this could be in combination with other mitochondrial signalling pathways.

The maintenance of mitochondrial morphology for stress tolerance and virulence is highlighted in *Cryptococcus neoformans*, whereby fully functioning inherited mitochondria from the *MATa* parent are critical for growth under fluctuating temperature, low oxygen availability and iron regulation[101, 159-162]. Defects occurring in Complex I, II or IV can impair conidiation and sexual development of the yeasts *Neurospora crassa* and *Podospora anserina,* even when alternative NADH dehydrogenases are present, and respiration is maintained by Aox[163-171]. Interestingly, a mutation in the *Cryptococcus neoformans* NADH promoter region increased production of melanin, Glucuronoxylomannan (GXM) release, and ATP, virulence enhancing traits which occurred through serial passage in the *Galleria mellonella* model[172].These studies suggest that while conservation of mitochondrial components and morphology is seen across multiple taxa, mitochondrial plasticity may have a role in enhancing virulence and host evasion.

Mitochondrial morphology is thought to have importance in the ER- mitochondria encounter structure (ERMES), which has been highlighted for cell fitness, immune evasion, and virulence in both *Candida albicans* and *Aspergillus fumigatus* alike[173]. Mitochondrial contact sites with both the ER and peroxisomes have been thought to contribute to lipid homeostasis though shuttling of tricarboxylic-acid (TCA) cycle intermediates like citrate from peroxisomes to the mitochondria, although details of metabolite transfer and regulation of contact sites is still unclear. Interestingly, although direct lipid transit pathways are yet to be elucidated, a recent study by Enkler *et. Al*[174] suggested that Arf1 couples fatty acid β-oxidation to mitochondrial ATP synthesis and can regulate mitochondrial fission and fusion[174]. Adequate regulation of mitochondrial fission and fusion mechanisms is important in *Cryptococcus neoformans*, whereby mitochondrial fusion defects lead to increased ETC inhibitor sensitivity and loss of virulence in a murine model[160]. However, mitochondrial fragmentation in *Aspergillus fumigatus* is seen during human granulocyte killing as a response to oxidative stress[175]. The function of mitochondria in fungal pathogenesis is multi-factorial, with ATP production, organelle signalling and morphology underpinning virulence mechanisms.

However, deeper investigations into virulence signalling pathways involving mitochondria should be explored.

1.3.5 Aox function in plant fungal pathogens

The ETC of plants has been extensively studied[176], and Aox activity has been documented in both plants and phytopathogenic fungi alike. However, evidence shows that the ETC of plants differs to that of other eukaryotes due to the number of subunits found for each mitochondrial complex. For example, the Complex I of plants has nearly 50 different subunits[177], and studies of *Pichia stipitis* and *Neurospora crassa* show that fungal Aox differs from Aox in plants in that it occurs as a monomer and is not induced by α-keto acids such as pyruvate[178]. The disparity between plant and fungal complex subunits, including additional proteins found in plant complexes[179, 180] is thought to assist in antifungal therapies that target phytopathogenic respiration.

In plant fungal pathogens such as *Moniliophthora perniciosa* and *Sclerotina sclerotiorum*, Aox is reported to be more active during the mycelial growth phase, suggesting that the metabolic control provided by alternative respiration is a crucial factor in morphogenesis[181, 182]. Interestingly, the activation of Aox for fungal growth has also been thought to contribute to mycotoxin production by food-colonising fungi, such as Aflatoxins produced by *Aspergillus flavus*[183-185]. It is interesting to note that Aox is activated and upregulated in *Solanum lycopersicum, Arabidopsis thaliana* and *Nicotiana attenuata* in response to bacterial and viral attack, mainly for oxidative and nitrosative stress management[186-190], although the roles of Aox in stress signalling during fungal infection of other plant species requires further research.

For other plant pathogens, such as *Botrytis cinerea, Ustilago maydis* and *Magnaporthe grisea,* Aox is required for active resistance to Quinone Outside Inhibitor (Q_oI) fungicides such as the strobilurins, Azoxystrobin and Pyraclostrobin[191-194]. This class of fungicides inhibit mitochondrial respiration through binding to Cytochrome bc_1, blocking the movement of electrons at the quinone outer binding

site[195], although field resistance is becoming an increasing problem, such as in *Mycosphaerella fijiensis* and *Mycosphaerella musicola* infections of bananas[196] and *Pyrenophora tritici- repentis* infections of Argentinian wheat[197]. Increasing Q_oI resistance has been attributed to the presence of an Aox in *Mycosphaerella graminicola* and *Aspergillus flavus*[132, 198], whereby Aox provides an alternative route for electron transport away from the target site of the Q_oI fungicides to maintain electron flux. In the presence of the strobilurin Azoxystrobin, *Fusarium graminearum* upregulated transcription of Aox and rapidly increased oxygen uptake[199]. To address the emerging antifungal resistance in agricultural practices, research into new succinate dehydrogenase inhibitors (SDHIs), such as Carboxin has begun, whereby fungal respiration is inhibited through blockage of the ubiquinone binding sites of Complex II. SDHIs have been rapidly gaining interest due to their broad, high antifungal activity[200], however phytopathogenic sensitivity to SDHIs is slowly shifting[201] and evidence suggests that SDHI site-specific inhibition may give rise to resistance if not monitored correctly[202]. This may, in part, be due to the presence of fungal Aox at the level of the UQP to provide an alternative respiratory pathway under this inhibition. The potential benefits of Aox inhibitors in the agrochemical industry has been recently reviewed[183].

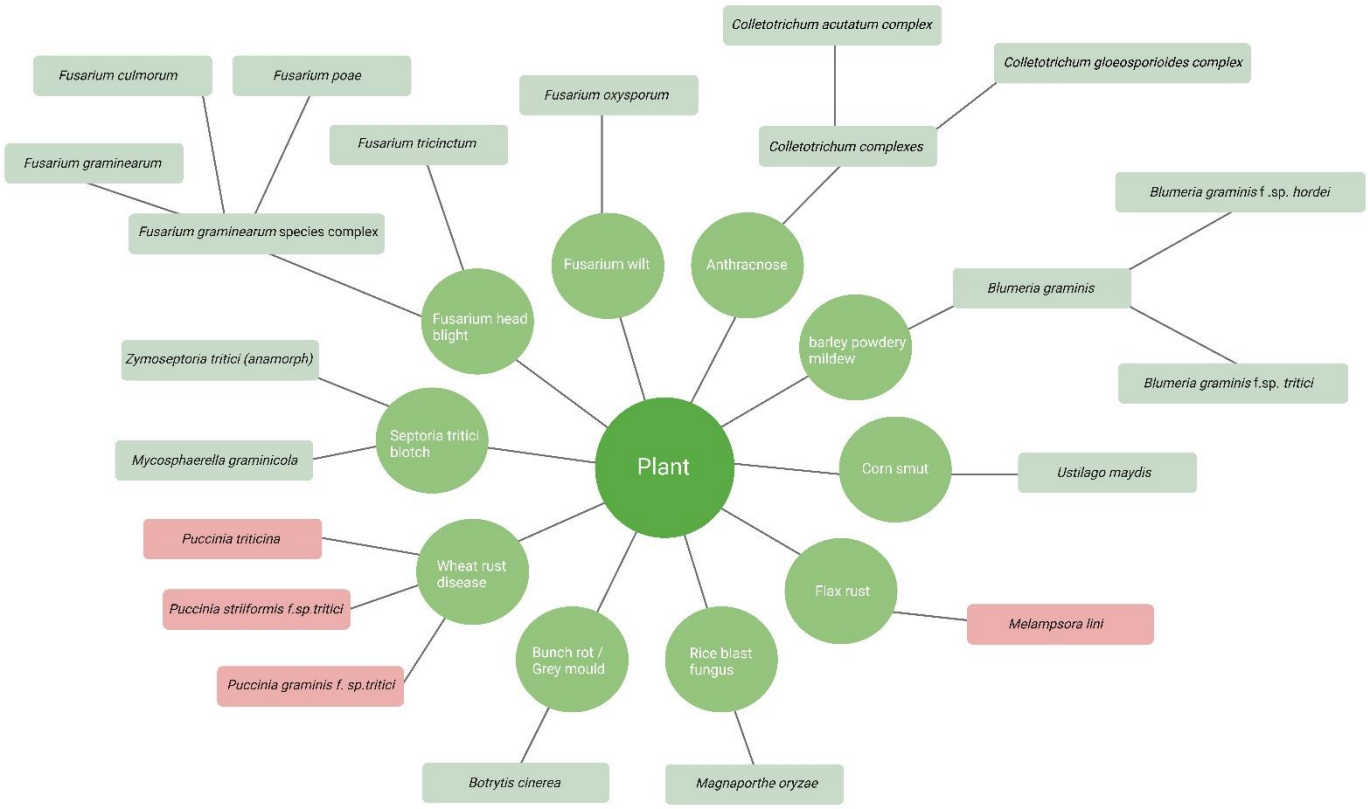

Figure 1.3: Key plant fungal pathogens.
Schematic illustrating key plant fungal pathogens. Pathogenic species without a known or predicted Aox sequence in the UniProt database[286] are highlighted in red. Created with BioRender.com.

Although Aox has proposed functions for virulence in plant fungal pathogens, not all phytopathogens have a predicted sequence, such as the *Puccinia* species responsible for wheat rust disease and *Melampsora lini* which causes flax rust (Fig. 1.3). Interestingly, while resistance mechanisms of wheat and flax towards these pathogens has been documented[203, 204], there are few noted instances of antifungal resistance for these pathogens themselves, which, in conjunction with these other studies, indicates that Aox may have a role in phytopathogenic resistance to antifungal drugs. While much needs to be investigated in plant-pathogen interactions, given that both plants and phytopathogenic fungi can induce Aox independently for multi-factorial stress relief, one cannot rule out the possibility that both fungi and plants may use Aox within the environmental niche of an active phytopathogenic infection. Investigations into the role of Aox on both the host and pathogen sides of an infection could provide an insight into tackling antifungal resistance impacting food security.

1.3.6 Aox function in human fungal pathogens

Most human fungal pathogens possess at least one Aox (Fig. 1.4). The importance of Aox in morphogenesis and resistance to oxidative stress from the human host has been demonstrated in several fungal pathogens. Aox1 from *Cryptococcus neoformans* was shown to be induced at 37 °C and was reported to play a role in virulence in the murine inhalation model[205]. In *Paracoccidioides brasiliensis,* Aox is upregulated in response to oxidative stress and for the mycelial-to-yeast transformation, a crucial step in paracoccidioidomycosis[206, 207]. *Aspergillus flavus* and *Aspergillus fumigatus* have multiple isoforms of Aox, whereby the isoform AoxA was found to attribute resistance to oxidative stress and macrophage killing[132, 208, 209]. Aox is also upregulated in *Candida albicans* and *Candida auris* in response to oxidative stress conditions,[210-212] plays a role in hyphal growth and biofilm formation[213, 214] and deletion of Aox in *Candida albicans* leads to increased Fluconazole

susceptibility[215]. A recent study assessed *Candida albicans* respiratory capacity when exposed to SNP in combination with the known Aox inhibitor SHAM. *Candida albicans* treated with this combination displayed a rapid transition to hyphal growth upon relief from inhibition and *Candida albicans* treated with both SNP and SHAM also displayed a decrease in caspofungin resistance[142]. This indicated that Aox has a significant role in the hyphal switching phenotype in *Candida albicans*, and that transcription of a second alternative oxidase, Aox2, is induced in the presence of ETC inhibitors to buffer respiratory stress and increase alternative respiration capacity[142, 216]. Interestingly, deletion of Aox2 also leads to decreased virulence of *Candida albicans* in the murine model through increased immune recognition[216]. However, some reports suggest that Aox1 is dispensable for virulence in *Candida albicans*[133] and *Aspergillus fumigatus*[208], this may be due to differences between experimental approaches or strain backgrounds and remains a point to be clarified.

Interestingly, both *Candida glabrata* and *Pneumocystis jiroveci* do not have a predicted Aox sequence (Fig. 1.4), however evidence of respiratory inhibition of *Pneumocystis jiroveci* with SHAM has been reported, suggesting an Aox may be present[217, 218]. While incidences of *Candida glabrata* based Candidiasis are increasing, the genetic similarity of *Candida glabrata* to *Saccharomyces cerevisiae* and differences to *Candida albicans* indicate that both species must have evolved different routes to pathogenesis, independently of Aox[219]. Unfortunately, little is known about the metabolic requirements of *Pneumocystis jiroveci* for infection, although it has been postulated that *Pneumocystis* pneumonia is based on reactivation of a latent infection, using the host an as environmental reservoir to facilitate human-human transmission[220, 221], which also appears Aox independent. The importance of Aox in virulence itself appears pathogen specific, as parasitic *Trypanosoma brucei* alternative oxidase (TAO) has proven to be essential for respiration in the bloodstream form of the parasite[222], with intense therapeutic interest providing the only known published crystal structure of Aox[223] and evidence of TAO inhibition with Ascofuranone[224]. However, while interesting links have been made for Aox involvement in parasite infection, this falls out of the scope of this review.

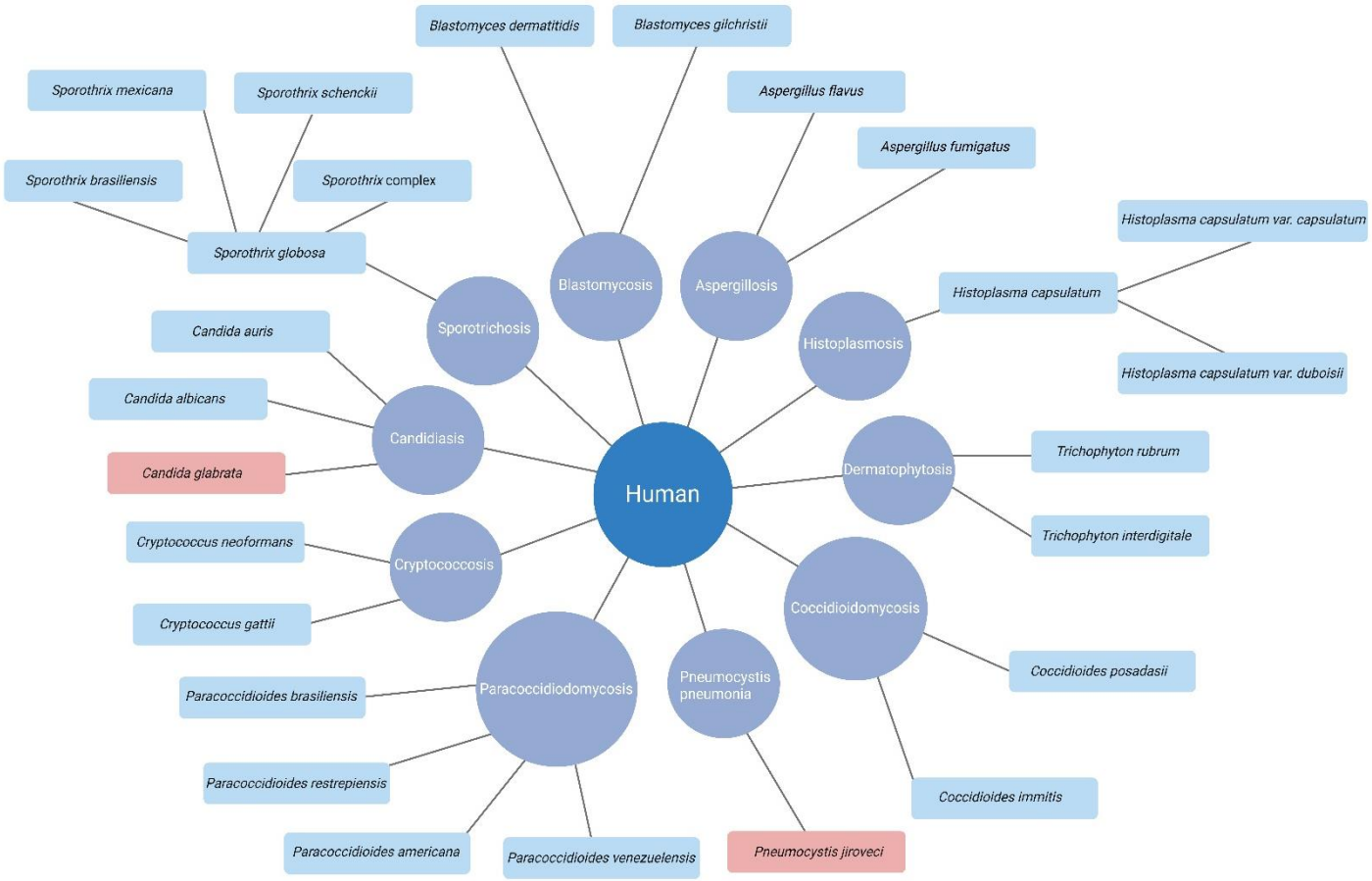

Figure 1.4: Key human fungal pathogens.
Schematic illustrating key human fungal pathogens. Pathogenic species without a known or predicted Aox sequence in the UniProt database[286] are highlighted in red. Created with BioRender.com.

Although human-fungi interactions are widely investigated, direct signalling roles for Aox in fungal pathogenesis and host dissemination are still unclear. Because of its ability to maintain respiration in the presence of classical ETC inhibitors, Aox in human fungal pathogens could be proposed to relieve respiratory stresses induced by the host during infection, such as NO. In humans, NO is produced during host infection by phagocytes via nitric oxide synthase iNOS (or NOS2) as part of the arsenal of oxidants that can inhibit or kill invading pathogens[225]. While no direct links between human NO production and fungal Aox during pathogenesis have been recorded, studies on plant mitochondria show that while NO inhibits cytochrome *c* oxidase, Aox remains uninhibited[226]. The evidence presented suggests that Aox does play a role in fungal pathogenesis, although most likely

as an indirect mediator of oxidative stresses induced by the host and maintenance of fungal morphology in the host environment, rather than a direct virulence component. Perhaps for human fungal pathogens, Aox activity should be seen as a latent, adaptive mechanism which activates under selective pressure for metabolic homeostasis. This would provide a background benefit to fungal pathogens in immune evasion but would be dispensable as an active component of virulence mechanisms required for dissemination in the host. However, further investigations into Aox activation and function within different human fungal pathogens is required to substantiate these postulations.

1.3.7 Problems and potential for targeting respiration in human fungal pathogens

Current antifungal therapies either inhibit biosynthetic machinery for ergosterols (e.g., azoles), nucleic acids (antimetabolites e.g., Flucytosine) or disrupt the cell membrane or wall (e.g., polyenes or echinocandins). While conservation of mitochondrial machinery between both animals and fungi presents a problem for suitable antifungal treatments, current inhibitors of the fungal ETC, highlighted in Fig. 1.2, include both natural and synthetic compounds. Rotenone and Metformin are known inhibitors of Complex I, investigated for their efficacy against cancer and antifungal properties against *Candida albicans* and *Aspergillus niger*[227-231], although Metformin is classically used to treat Type II Diabetes[232]. Complex II is prone to inhibition by 3-nitropropionic acid (3-NPA) or thenoyltrifluoroacetone (TTFA), although new studies have highlighted Gracillin, a natural steroidal saponin as a potential anti-tumour drug[233, 234]. Numerous Complex III inhibitors have been identified, of which Strobilurins such as Azoxystrobin are rapidly gaining interest[185, 235-237]. For example, combination treatment of Complex III and Aox inhibition was found to enhance sensitivity to caspofungin in *C. parapsilosis*[238]. However, while Complex III inhibition is attractive for antifungal activity[120], inhibitors of this kind can often bind to both pathogenic and host complexes alike, so different applications for this inhibitor class are being investigated, such as cancer therapeutics[237, 239-241] While inhibition of yeast ATP synthase is possible using Bedaquiline[242] and Oligomycin[243], the strong conservation between fungal and mammalian isoforms of the mitochondrial ATP synthase

renders this enzyme as an antifungal target obsolete, although it does provide a promising antibiotic target[244].

Prolonged reliance on treatment guidelines has presented increasing numbers of resistance in clinical cases[245-247]. Resistance patterns have begun to emerge in various fungal species, and reliance on combination therapies of azoles, polyenes, echinocandins and anti-metabolites mean that monotherapies are declining in potency against rapidly adapting fungal pathogens. For example, mutations in the ergosterol pathway and sterol biosynthesis of *Candida tropicalis*, *Candida albicans* and *Candida lustiniae* leads to resistance to azoles and Amphotericin B as monotherapies[248-253] and interestingly this mutation in *Candida lustiniae ERG3* is also induced via micafungin monotherapy, which then provides cross resistance to multiple antifungal classes[254]. Treatments are now more aimed towards combination therapy to target invasive fungal infections such as the use of Caspofungin with other antifungal classes to treat Candidiasis[255], and combinations of multiple triazole types such as PC945 and voriconazole for treatment of *Aspergillus fumigatus* based Aspergillosis[256]. The recommended treatment for Cryptococcosis includes a combination of Amphotericin B and Flucytosine, followed by Fluconazole in a maintenance program that can last up to a year[257, 258], although antifungal hetero-resistance and cross-tolerance has been documented[21].

The increasing amount of antifungal resistance and the reliance on combination therapies means focus is shifting towards compounds that can re-sensitise resistant fungal pathogens to current antifungals, rather than identify novel antifungal compounds. Interestingly, a group of Indazole derivates have been identified to convert azoles from fungistatic back to fungicidal for *Candida albicans* infections through inhibition of the cytochrome bc_1 complex[259]. One compound, Inz-5, enhanced the ability of macrophages to contain *Candida albicans*, and Inz-1 showed selection for yeast complex bc_1 over human bc_1, which offsets the current issues other Complex III inhibitors face in host treatment. Other synergisms are beginning to emerge, such as Tetrandrine which increased

the antifungal activity of Fluconazole in the murine Candidiasis model[260] and even a combination of Fluconazole with small molecule ENOblock[261] or SHAM[215] showed synergism against *Candida albicans*. With the indication that research is moving away from monotherapeutic antifungals, inhibition of Aox could be effective in combination therapies with existing antifungal drugs such as Echinocandins and Azoles which are currently circulated for the treatment of *Candidiasis* and *Cryptococcosis,* but not as a monotherapy alone. Another postulation includes the use of known natural stressors for pathogens such as NO, which can be produced by SNP, in combination with Aox inhibitors. While using NO stress in combination with Aox inhibition is an attractive proposal, research into efficacy against fungal pathogens *in vitro* and *in vivo* is required. Research into fungal respiration machinery, especially the role of Aox, and its links to virulence, remain understudied.

In summary, due to the connection of mitochondria to pathogenesis, cell wall regulation and lipid metabolism, fungal-specific respiratory inhibitors may prove to be effective against pathogens either in isolation or in combination with current antifungals. However, the conservation of the respiratory machinery in eukaryotes and the robust and adaptive nature of fungal respiration is a challenge for drug development, so investigation into compounds that can re-sensitise drug resistant fungal pathogens to existing therapies may also provide relief from infection. Characterisation of fungal-specific respiratory chain components are needed, together with a deeper understanding of the roles of those already characterised, such as Aox.

1.3.8 Proposed roles for Aox

Studies so far suggest that Aox does not have a direct role in fungal virulence but does have a role in maintenance of oxidative stress mechanisms, ROS production, and even Complex I driven respiration in *Botrytis cinerea*[262]. It could be postulated that Aox, having close links and established electron transfer from the UQP, and yet no dominant role in ATP synthesis, could act as a switch between FET and RET in response to environmental cues for both ROS production and scavenging. Interestingly, this concept is supported by an investigation in murine mitochondria using xenotopic

expression of Aox from *Ciona intestinalis*[263]. Aox is known to oxidise ubiquinol and reduces oxygen to water, bypassing the ETC prior to proton translocation by complexes III and IV, producing heat as a byproduct. It would make sense, therefore, if Aox acted in FET to stop electron leak through I_Q or III_{QO} by oxidation of quinone which could reduce ROS production in stress conditions induced by host dissemination. More interestingly, as RET induction requires an unfavourable thermodynamic force and high QH_2/Q ratio, one could speculate that Aox could contribute to RET induction itself through generation and release of heat energy as the RET driving force for electron movement into Complex I and maintenance of the reduced quinone state. While induction of RET and induction of ROS production seems counterproductive to fungal pathogens, certain morphological developments induce high ROS, such as capsule development in *Cryptococcus neoformans*[58] and *Aspergillus niger* and *P. penicillium* spore germination[264]. This, in conjunction with studies that show Aox as sensitive to pH changes[265] and other postulations highlighting Aox as important in ROS homeostasis[132, 266, 267] supports the idea that Aox could act a FET/RET switch to provide ROS for energy demanding virulence mechanisms in fungal pathogens or defend against host-generated ROS through induction of FET, independently of ATP production. Experiments investigating ROS production, FET/RET initiation and thermodynamics in relation to Aox activity should be considered.

1.3.9 Conclusion

While fungal pathogens present a growing threat to both human health and food security, research into antifungal therapies are still neglected. Here, we investigated the role of the electron transport chain in fungal virulence and antifungal resistance, including the Aox pathway. Interestingly, while the direct role of Aox in pathogenic virulence remains unclear, studies have showed a potential homeostatic role for metabolism under both biotic and abiotic stresses. This stress tolerance mechanism is thought to contribute to pathogenic survival in the host and contribute to current antifungal resistance through control of ROS and NO accumulation, which is uncoupled from ATP production. To address the issues faced by antifungal resistance, application of an Aox-specific

antifungal may re-sensitise resistant fungal pathogens to drugs such as Fluconazole, although research into combination therapies and Aox-specific inhibitors still needs to be pursued.

1.4 Existing and new *Cryptococcus*-targeted antifungals

Following the studies presented in 1.3.7, *Cryptococcus* specific antifungal therapies are rapidly gaining interest to tackle antifungal resistance. While current treatment plans involve the use of Fluconazole and Amphotericin B, heteroresistance and the induction of persister cells after drug treatment[115] have drawn attention to the slow development of new antifungal classes, and thus research into novel antifungal alternatives is required.

Recently, a promising study followed the clinical development of Olorofim (a dihydroorotate dehydrogenase enzyme inhibitor), Ibrexafungerp (a triterpenoid), Fosmanogepix (a Gwt1 enzyme inhibitor), Opelconazole and Rezafungin (an echinocandin)[268]. Rezafungin inhibits β-1,3-D glucan synthase, and Olorofim inhibits pyrimidine synthesis through dihydroorotate dehydrogenase. Rezafungin and Olorofim showed potency against *Candida*, *Aspergillus* mold and multidrug resistant mold species, respectively, but did not show any efficacy against *C. neoformans* or *G. gattii*[268]*.* Interestingly, Ibrexafungerp, which also inhibits β-1,3-D glucan biosynthesis, but with a different binding site to Rezafungin, is able to inhibit the growth of Candida species, although its potency against *Cryptococcus* species is unknown[268]. Given the unsuccessful use of Echinocandins against *C. neoformans* infection, and the inability of Ibrexafungerp to disseminate to CNS tissues, it would be an unlikely treatment option for those suffering from disseminated cryptococcosis.

Fosmanogepix, which targets GPI-anchored protein maturation through the inhibition of Gwt1, does appear promising against *C. neoformans* and *C. gattii* when combined with Amphotericin B[268]. However, the clearance criteria was based on morphological change and clearance of the blood in ≤ 2 days, rather than loss of growth as with the echinocandin candidates. When considering the low-metabolic dormancy traits of *C. neoformans*, one could suggest that there may be an induction of viable but non-culturable cells (VBNC) or dormancy, rather than cell death. Further investigations to ensure that this drug promotes cell death, rather than induce prolonged latent infection, are required.

Finally, Opelconazole, a nebulised lipophilic triazole that targets lanosterol 14-α demethylase, has also shown potency against *C. neoformans*[268], but questions about suitability for disseminated

infection remain. While these new antifungals are currently circulating in clinical trials, most targets still rely heavily on cell membrane and sterol biosynthesis perturbation, or adaption of current antifungals such as Azoles. Given the resistance patterns emerging against Fluconazole and polyenes and the multi-drug cross tolerance to pyrimidines provided by aneuploidy, new clinical antifungals do little to identify new targets that are not based on previous drug patents. While Opelconazole and Fosmanogepix show efficacy and promise against *C. neoformans* infection in the clinical settling[268], lack of response to Rezafungin and Olorofim suggest that drug repurposing may produce adaptive resistance patterns that will ultimately prolong treatment. Fosmanogepix, however, which has diverted from the currently circulating antifungal classes, does show promise and presents a case for more development in novel antifungal therapies.

Regulation of integrated *C. neoformans* metabolism has been reviewed[269], however emergence of genome-scale metabolic model for *C. neoformans* that emerged in 2023[270] shows promise for identification of new possible drug targets. Within this thesis the use of metabolism, specifically mitochondrial function, is assessed as a novel antifungal target which could circumvent the current resistance strategies. While some studies note concern for conservation between mammalian and eukaryotic respiratory machinery in relation to targeting ability, the identification of novel targets could provide a potent synergism to enable renewed sensitivity against currently circulating antifungals or synergism with other novel therapies such as synthetic small molecule inhibitors. This would allow for any concerns in relation to cross-talk with known resistance mechanisms and dose-dependent off target effects to be addressed and would provide further insight into an otherwise underdeveloped understanding of *C. neoformans* metabolic requirements.

1.4 Project Aims

1. Determine the function of *C. neoformans* Aox and its potential as a novel antifungal drug target

Given the lack of available information we sought to determine how related the Aox of *C. neoformans* is to Aox of other human fungal pathogens at the sequence and predicted structural level. To achieve this, we used the predicted FASTA sequence of *C. neoformans* Aox and compared it to other similar structures using BLAST and aligned the sequence to other enzymes using MEGAX. We then used iTASSER modelling prediction software to generate a predicted structure. Investigations were also carried out to determine whether Aox was actively contributing to respiration and resistance against mitochondrial inhibition through the use of growth and viability analysis, High Resolution Respirometry (HRR), and melanisation assays.

2. Screening to identify regulators of mitochondrial function

We wanted to identify any putative regulators of mitochondrial function through unbiased kinase knockout screens, and assess the impact of kinase loss on growth, respiration, viability and mitochondrial stress signalling. The aim of this screen was to identify regulators of resistance to mitochondrial inhibition, and the impact this had on stress signalling mechanisms in *C. neoformans.*

3. Investigate the metabolic requirements of *C. neoformans* and identification of fungicidal additives

We wished to investigate differences in the metabolic capabilities of wildtype and *Δaox1* mutant cells using a medium throughput screening approach. Using a BIOLOG™ Microarray, we wanted to assess the effect of a broad range of metabolic supplementation and stress challenges on *C. neoformans* growth. The aim of this analysis was to expand our knowledge of the abilities of *C.*

neoformans to utilise metabolites and to identify new roles for Aox in the control of metabolism and stress response.

4. Investigation of a novel antifungal compound against *C. neoformans*

We worked with collaborators at the University of Sussex (Luke Young, Anthony Moore, John Spencer and Andrew McGown) to test new compounds with potential to act as dual inhibitors of both classical and alternate modes of mitochondrial respiration. Compounds with promising *in vitro* activity were tested by assessing effects on growth, respiration, and viability. This was coupled with drug toxicity and virulence assays designed to measure the effects of selected putative inhibitors in *Galleria mellonella* and haemolysis assays. Analysis of drug reference compounds allowed us to identify and propose a mechanism of action for the novel drug compounds.

2. Materials and Methods

2.1 Strain information

Wildtype (H99, Serotype A) and *Δaox1* deletion strains were generously gifted by Elizabeth Ballou (University of Exeter, UK) and were derived from the Madhani laboratory (University of California, San Francisco, California, USA, NIH funding R01AI100272)[271]. *C. neoformans* knockout libraries were provided by the Lee Kyung-Tae lab (Department of Biotechnology, College of Life Science and Biotechnology, Yonsei University, Seoul 03722, Korea)[272]. The parental strain of the mutant (H99P) *Δypk1* mutant, *Δypk1* mutant + YPK1 flag at the locus, and two kinase-dead mutants, *Δypk1* + YPK-K274A and *Δypk1* + YPK-D386A were provided by the Chang lab (Laboratory of Clinical Infectious Diseases, National Institute of Allergy and Infectious Diseases, National Institutes of Health, Bethesda, Maryland, USA)[273]. All genotypes can be found in Table 2.1.

Table 2.1: Strains used for this study

Strain name	Genotype	Source
H99	MAT**a**	Madhani Laboratory[271]
Δaox1	MAT**a** *Δaox1::NAT*	Madhani Laboratory[271]
H99P (*Δypk1* parental)	MAT**a**	Chang Lab[273]
Δypk1 (HL278)	MAT**a** *Δypk1::NEO*	Chang Lab[273]
Δypk1 + YPK1 flag	MAT**a** *Δypk1::NEO, YPK-FLAG-NAT*	Chang Lab[273]
Δypk1 + YPK-K274A	MAT**a** *Δypk1::NEO* + *YPK-K274A-FLAG*	Chang Lab[273]
Δypk1 + YPK-D386A	MAT**a** *Δypk1::NEO* + *YPK-D386A-FLAG*	Chang Lab[273]

2.2 Growth media for *C. neoformans* strains

All media components were mixed in MilliQ de-ionised distilled water (mqH_2O) and heat-sterilised by autoclaving at 121°C for 20 min prior to use, unless stated otherwise. Liquid cultures of wild-type (H99) and *Δaox1* strains were grown in YPD (1% Yeast extract (Difco), 2% Bactopeptone (Difco) and 2% Dextrose (Fisher Scientific)) at 30°C or 37°C for clinical relevance where stated on a rotary shaker at 180 revolutions per minute (rpm) in a sterile falcon tube. Culture plates for solid culture growth contained YPD media with added 20% Oxoid Technical Agar (Agar No. 3) and incubated at 30°C or 37°C where stated.

2.3 Stock preparation of *C. neoformans* strains

5ml of YPD was inoculated with a colony of *C. neoformans* strains and grown overnight at 30°C with shaking at 180 rpm. The following day 750µl of overnight culture was mixed in a cryotube with 40% (w/v) sterile glycerol and frozen at -80°C.

2.4 Molecular Biology Techniques

2.4.1 Oligonucleotides

Table 2.2: Oligonucleotides used in this study

Name	Sequence (5' – 3')	Function
AOX1 Forward Primer	AGAGAAGATTGGTAGCGGCG	Forward primer to check for *aox1* gene deletion
AOX1 Reverse Primer	AAGTGGGGGTGAGTGACCTT	Reverse primer to check for *aox1* gene deletion

2.4.2 Genomic DNA Extraction

5ml of YPD was inoculated with a colony of *C. neoformans* strains and grown overnight at 30°C with shaking at 180 rpm. The next day, 1ml of the cultures were pelleted, washed in sterilised Phosphate Buffered Saline (Oxoid™ tablets, Thermo Scientific, 1 tablet / 100ml mqH_2O) and then resuspended in 500µl Monarch gDNA Cell Lysis buffer (T3012-1). Acid washed beads were added to the suspension, which was then vortexed for 2 min. The lysate was then pipetted into a fresh Eppendorf and 275µl of 7M ammonium acetate (Sigma) was added, and the mixture was incubated at 65°C for 5 min, followed by an incubation on ice for a further 5 min. 500µl of Chloroform (Fischer Scientific) was added to the samples and spun via centrifugation at 13000 rpm for 2 min. Following phase separation, the top phase was removed and precipitated with 1ml of cold isopropanol, and the samples were incubated at 25°C for 5 min. The samples were then spun via centrifugation for a further 5 min at 13000 rpm and the resultant pellet was washed in 70% ethanol. The pellet was finally resuspended in 50µl of mqH_2O. 1µl of the DNA suspension at a concentration between 1-500 ng / µl was used as a template for Polymerase Chain Reaction (PCR) analysis.

To quantify the concentration of DNA samples, the absorbance at 260nm (A260) was measured using a NanoDrop One Microvolume UV-Vis Spectrophotometer (Thermo Scientific). 2µl of DNA samples were pipetted onto the NanoDrop and compared to 2µl of mqH_2O as a control.

2.4.3 Polymerase Chain Reaction using recombinant Taq DNA Polymerase

PCR was carried out for confirmation of the Aox1 gene deletion following a genomic DNA extraction. Mixtures for the PCR reaction (Table 2.3) and thermocycler conditions (Table 2.4) were carried out in accordance with the manufacturer's instructions. Primer annealing temperatures were calculated using an online tool provided by Promega:
(https://www.promega.com/resources/tools/biomath/tm-calculator/).

Table 2.3: Recipe for PCR Reaction mix

Component	Final Concentration	Volume (µl)
10x PCR Buffer, -Mg	1x	5
50mM $MgCl_2$	1.5mM	1.5
10mM dNTP mix	0.2mM	1
10µM Forward Primer	0.5µM	2.5
10µM Reverse Primer	0.5µM	2.5
Template DNA	1-500ng	1
Sterile mqH_2O	Up to desired volume	To 50µl
Taq DNA Polymerase (5U/µl)	1 U/ 50µl	0.2

Table 2.4: Taq DNA Polymerase thermocycler settings

Step	Temperature (°C)	Time	Number of cycles
Initial denaturation	94	3 min	1
Denature	94	45 sec	30
Anneal Cycle	60 (Aox primer dependent)	30 sec	30
Extension Cycle	72	90 sec / kb	30
Final Extension	72	10 min	1
Hold	12	indefinitely	1

2.4.4 Agarose Gel Electrophoresis

For DNA gel electrophoresis following PCR, agarose powder for a 0.8-1% concentration was added to 1x TAE buffer (40mM Tris-base, 20mM Acetic Acid, 1mM EDTA) in a conical flask and heated in the microwave on full power for 1-2 min until the Agarose powder was fully dissolved. The mixture was cooled at 25°C for 5 min, and Ethidium Bromide (Sigma) was added to a final concentration of

0.5µg/ml for DNA visualisation. 25ml of the mixture was poured into a gel cassette and left to set with an inserted comb for 30-45 min. Once set, the gel was submerged in an electrophoresis tank containing 1x TAE. PCR samples were loaded into the gel along with 10x BlueJuice Gel Loading Buffer (Invitrogen, CAT no: 10816015) and a DNA Ladder (1Kb Plus, Invitrogen, CAT no: 11578636). The tank was connected to a Bio-Rad power supply and electrophoresis was carried out at 110V for 25 min. The agarose gel was visualised using the SYNGENE G: BOX gel doc system. Images of the gel were captured using GeneSys software (Version 1.6.5.0) along with a synoptics 6MP camera.

2.4.5 Whole Cell protein extraction

5ml of YPD was inoculated with a colony of *C. neoformans* strains and grown overnight at 30°C with shaking at 180 rpm. The next day, 500µl of the overnight samples were harvested, and pelleted cells were re-suspended in 200µl of lysis buffer (0.1M NaOH, 0.05M EDTA, 2% SDS, 2% β-mercaptoethanol). The samples were then heated for 10 min at 90°C and 5µl of 4M Acetic acid (Fisher Scientific) was added. The samples were then vortexed for 30 sec and a secondary incubation took place at 90°C for 10 min before addition of 50µl of loading buffer (0.25 M Tris-HCl pH 6.8, 50% Glycerol, 0.05% Bromophenol blue). The lysate was cleared through centrifugation and the supernatant was loaded into an SDS PAGE (Sodium Dodecyl Sulfate–Polyacrylamide Gel Electrophoresis) gel.

2.4.6 Preparation of Polyacrylamide gels

All samples were run on a 10% SDS PAGE gel composed of a 5% stacking segment on top of a 12% resolving segment, made in a glass cassette (Bio-Rad, 0.75mm thick). The gel components can be found in Table 2.5. The resolving gel was cast first, with 1ml of isopropanol added on top to ensure resolving gel separation from air. After being left for 1 h to set, the stacking segment was

added up to the top of the cassette and a comb with 12 wells was placed into the top of the cassette. The gel was then left to set for a further hour.

Table 2.5: Recipe for polyacrylamide gel components

Gel	Component	Volume
Stacking	0.5M Tris (pH 6.8) + 0.4% SDS	4ml
	30% Acrylamide Mix (acrylamide/bis-acrylamide 29:1 (3.3% crosslinker) Bio-Rad)	1.34ml
	Tetramethylethylenediamine (TEMED, Sigma)	8µl
	Sterile mqH_20	4.572ml
	10% Ammonium Persulfate (APS, Bio-Rad)	90µl
Resolving	1.5M Tris (pH 8.8) + 0.4% SDS	3.75ml
	30% Acrylamide Mix (acrylamide/bis-acrylamide 29:1 (3.3% crosslinker) Bio-Rad)	6ml
	TEMED (Sigma)	6µl
	Sterile mqH_20	6.156ml
	10% APS (Bio-Rad)	150µl

2.4.7 SDS-PAGE gel electrophoresis

Once set, the gel was submerged in an electrophoresis tank containing 1x SDS running buffer. 10µl of each sample was loaded into the gel along with a PageRuler™ Plus Prestained Protein Ladder

(Thermo Scientific, CAT no: 26619) and additional loading buffer (0.25 M Tris-HCl pH 6.8, 50% Glycerol, 0.05% Bromophenol blue) in any empty wells. The tank was connected to a Bio-Rad power supply and electrophoresis was carried out at 90V for 1 h until the samples had run through the stacking gel, and then run at 110V for a further 2 h.

2.4.8 Semi-dry protein transfer

The resulting separated proteins were transferred onto a Polyvinylidene Difluoride (PVDF) membrane through semidry transfer using a Bio-Rad Trans SD machine. Four pieces of blotting paper of equal size to the resolving layer (4 x 9cm) were wetted in transfer buffer (50ml 10x transfer buffer (29g glycine, 58g Tris-base, 40µl 10% SDS), 100ml methanol (Fischer Scientific), 350ml sterile mqH_2O) and the PVDF membrane (4 x 9cm, Amersham Hybond P) was wetted in methanol to activate it before being soaked in transfer buffer for 15 min. The transfer was layered with two pieces of blotting paper placed first followed by the PVDF membrane, the SDS PAGE gel, and two more pieces of blotting paper, ensuring all air bubbles were rolled out. The transfer was run at 25V for 30 min per gel.

2.4.9 Western blot detection using Enhanced Chemiluminescence (ECL)

After semi-dry transfer, the PVDF membrane was blocked in blocking buffer (5% semi skimmed milk powder, 1x PBS + 0.2% Tween 20 (PBS/T)) for 45 min at room temperature on a rotary shaker. The membrane was then briefly rinsed in PBS-Tween (PBS/T) and then placed in a 50ml Falcon tube with 5ml blocking solution with primary antibody at a dilution recommended by the manufacturer. The list of antibodies used for each gel can be seen in Section 2.4.10. The tube was left to incubate overnight at 4°C on a roller mixer. After overnight incubation, the membrane was removed and briefly washed in PBS/T twice before being washed for 15 min followed by two 5-min washes in PBS/T. The membrane was next placed in a 50ml Falcon tube with 5ml blocking buffer containing a horseradish peroxidase conjugated secondary antibody at a dilution recommended by the

manufacturer. The tube was left to incubate at room temperature for 30 min on a roller mixer. After incubation, the membrane was briefly washed twice in PBS/T twice before being washed for 15 min followed by three 5-min washes in PBS/T and then transferred to PBS. Two Electrochemiluminescence (ECL) solutions were made up as follows: Solution I (1ml of 2.5mM luminol, 440µl of 0.396 mM p-ccumaric acid, 10ml of 1M Tris-HCL pH 8.5, 88.56ml of sterile mqH_2O). Solution II (64µl of 30% hydrogen peroxide, 10ml of 1M Tris-HCL pH 8.5, 89.94ml of sterile mqH_2O). The solutions were mixed at a 1:1 ratio and the membrane was drained of PBS. The mixed solutions were then poured on the membrane and left for exactly one min before the excess was removed and the membrane was transferred to Saran wrap. The membrane in Saran wrap was visualised using the SYNGENE G: BOX gel doc system. Images of the gel were captured using GeneSys software (Version 1.6.5.0) along with a synoptics 6MP camera.

2.4.10 Antibodies used for protein detection

Primary antibody used for Aox1 detection: Rabbit Anti-AOX1 (Biomatik, product ID: AB011129) was generated for use in this study by a custom Polyclonal Antibody (pAb) production service package from Biomatik. We used a *C. neoformans* Aox1 derived peptide sequence as an antigen, cys-DQKRDFNPFALSEASP, that was synthesised by Biomatik and used directly for Western Blotting at a dilution of 1/1000.

Secondary antibody used for Aox1 detection: Anti-Rabbit IgG HRP (Sigma, catalogue number #A0545) and was used at a dilution of 1/5000.

2.5 Whole Cell Experimental Procedures

2.5.1 Measurement of liquid cryptococcal growth using absorbance

5ml of appropriate media (as in 2.2) was inoculated with a colony of *C. neoformans* and grown overnight at 30°C with shaking at 180 rpm. The next morning, either 24 well (1ml), 48 well (500µl)

or 96 well (100µl) Greiner plates were filled with appropriate media and inoculated with the overnight yeast suspensions to an OD_{600} of 0.1 unless specified. Growth was measured as absorbance OD_{600} over 48 h using a SPECTROstar Nano plate reader, with the settings specified in Table 2.6.

Table 2.6: SPECTROstar Nano plate reader settings

Excitation	600nm
Cycle time	360 sec
Shaking frequency	400 rpm
Shaking mode	8-min linear shake and read followed by double orbital shaking
Temperature	37°C
Positioning Delay	0.5 sec

Absorbance readings were collected and analysed by BMG LABTECH MARS data analysis software, which was then imported into Microsoft Excel and further analysed in GraphPad Prism 10 or in R studio using the Growthcurver package where specified. The Growthcurver package fits growth curve data to a logistic equation, to calculate growth rate, area under the curve (AUC), carrying capacity, and initial population size. The parameters were calculated as follows:

Logistic equation:

$$Nt = \frac{k}{1 + \left(\frac{k - N_0}{N_0}\right) e^{-rt}}$$

Where k is the OD_{600} at each measured timepoint, N_0 is the initial OD_{600} of the population, r is the growth rate, assuming there were no limits for population size within the growth environment. This study used the area under the curve (AUC) value to determine growth. Where specified, Minimum

Inhibitory Concentration (MIC) and NIC were calculated where specified using the Gompertz model for growth in GraphPad Prism 10.

2.5.2 Assessment of *C. neoformans* growth by spotting assays

5 ml of YPD was inoculated with a colony of the required *C. neoformans* strain and grown overnight at 30 °C with shaking at 180 rpm. The next day, cells were harvested and diluted to an OD_{600} of 1 and diluted 10-fold over six serial dilutions. Using a replicator, 5 µl drops of cells from all six 10-fold dilutions were stamped onto the agar plate containing the appropriate media. Once the 5 µl drops were dry on the agar, the plates were then incubated at 30 °C or 37°C as indicated for 24-48 h. Plates were then imaged using the SYNGENE G: BOX gel doc system. The GeneSys software (V 1.6.5.0) along with a synoptics 6 MP camera were used to capture images of the agar plates.

2.5.3 Assessment of *C. neoformans* viability using colony forming unit (CFU) assays

5 ml of YPD was inoculated with a colony of the required *C. neoformans* strain and grown overnight at 30 °C with shaking at 180 rpm. The next day, cells were inoculated to an OD_{600} of 0.1 with cells from the overnight in YPD containing inhibitory drugs or solute controls where specified, and the culture was grown at 37°C, 180 rpm shaking for 2 h. After drug exposure, cells were washed three times in Phosphate Buffered Saline (PBS) and diluted to 250 cells per 200µl. 250 cells were then plated onto YPD agar plates and spread using a sterile glass spreader under aseptic conditions. Once dry, plates were then incubated at 37°C for 48 h and viable colonies were counted. Bar charts and statistical tests were carried out in GraphPad Prism 10.

2.5.4 Respirometry Assays

To determine oxygen consumption and capacity of *C. neoformans* strains, respirometry was performed using an O2k Oxygraph (Oroboros) high resolution respirometer, using the settings given

in Table 2.7. 5 ml of YPD was inoculated with a colony of required *C. neoformans* cultures and grown overnight at 30°C with shaking at 180 rpm and 2 ml was added to Oxygraph chambers at a concentration of $1x10^6$ cells / ml after overnight growth. Following a 20-min period of cellular routine respiration to reflect the metabolic activity under cell culture conditions, drugs that inhibited different components of the ETC were investigated. Where indicated, 8µl of 50mM Triethyltin Bromide (TET) was added to each chamber resulting in the leak of respiration caused by compensation for the proton leak after inhibition of ATP synthase. Following the leak 2µl of 12mM Carbonyl Cyanide-p-trifluoromethoxyphenylhydrazone (FCCP) was added to each chamber to uncouple the electron transport chain from the oxidative phosphorylation system through interference of the proton gradient. Finally, 2µl of 20mM Antimycin A (AntA) was added to each chamber for inhibition of complex III. This procedure was repeated for assessment of other respiratory inhibitors where indicated and statistics and respirometry graphs were recorded in Oroboros Datlab Version 4.2.1.62. Bar charts were generated, and statistical testing were carried out in GraphPad Prism 10.

Table 2.7: Oroboros O2k Oxygraph configuration

Control	**Setting (per chamber)**
Protocol	Specific flux per unit sample
Block temperature	37°C
Gain for oxygen sensor	2
Polarisation voltage (millivolts, mV)	800
Stirrer speed (rpm)	750
Data recording interval (s)	2

2.5.5 BIOLOG screen

The BIOLOG screen protocol was carried out as described previously[274]. WT (H99) and *Δaox1* knockout mutant *C. neoformans* were grown overnight in 5ml of YPD at 30°C with shaking at 180 rpm. The next morning, cells were washed three times with sterile mqH_2O and 4.8 OD_{600} units of cells were resuspended in 250µl of 48x yeast nutrient supplement (NS) solution (Table 2.8). 12x Phenotype MicroArray™ (PM) additive solutions were prepared as in Table 2.9 and inoculation mixtures were made according to Table 2.10, whereby each PM plate had individual additives as described. Mixtures were pipetted into the BIOLOG plates using a multichannel pipette and grown as previously stated (2.5.1). AUC values were calculated as described (2.5.1) and heatmaps were made using GraphPad Prism 10.

Table 2.8: Recipe for 48x yeast nutrient supplement (NS) used in BIOLOG plates

Solution	**Concentration (mM)**	**Concentration factor**
L-Histidine HCL monohydrate	0.48	48x
L-Leucine	4.8	48x
L-Methionine	1.2	48x
Uracil	1.44	48x

Table 2.9: Recipe for 12x PM additive solutions used in BIOLOG plates

Solution	**PM1, 2, 5, 9**	**PM3, 6, 7, 8**	**PM4**
D-Glucose	3200mM	3200mM	3200mM
L-Glutamic acid monosodium	60mM	-	60mM
Potassium phosphate monobasic anhydrous (pH 6)	60mM	60mM	-
Sodium Sulphate	24mM	24mM	-

Table 2.10: Recipe for BIOLOG PM plate inoculation

PM stock solution	PM1, 2 (ml)	PM3, 6, 7, 8 (ml)	PM4 (ml)	PM5, 9 (ml)	PM10 (ml)
IFY-0 (1.2x)	10	10	10	10	-
SC media	-	-	-	-	11.75
D-Glucose (32x)	-	0.375	0.375	0.375	-
PM Additive (12x)	1	1	1	1	-
Cells in 48x NS	0.25	0.25	0.25	0.25	0.25
Sterile mqH_2O	0.75	0.375	0.375	0.375	-
Total	12	12	12	12	12

2.5.6 Flow Cytometry for analysis of cell viability

Propidium Iodide (PI) staining was used to assess membrane integrity and 2',7'-Dichlorodihydrofluorescein diacetate (H_2DCF-DA) to detect cellular ROS. H99 and *Δaox1* mutant Colonies of *C. neoformans* strains were grown overnight in 5ml of YPD at 30°C with shaking at 180 rpm. Cells were harvested at indicated time points and resuspended in 300µl of 100µg/ml PI in sterile PBS or H_2DCF-DA at a 0.1µM concentration in PBS and incubated in the dark at 37°C for 10 min. Samples were then washed three times with sterile PBS and analysed by flow cytometry. Fluorescence intensity of cells was analysed using the BD Accuri™ C6 Plus Personal Flow Cytometer (BD Biosciences). Measurement events were gated on the flow cytometer to ensure that singlet yeast cells were being recorded. The flow cytometer was equipped with a Propidium iodide laser (488 nm, 585/40, 670 LP standard filter) and a FITC laser (488 nm, 533/30 standard filter). Approximately 15,000 events were collected per sample and the data was acquired and analysed using the BD Accuri C6 Plus software.

2.5.7 Assessment of melanisation using spotting assays

To assess melanin production, agar plates containing L-DOPA were used as described previously[160]. 5 ml of YPD was inoculated with a colony of the required *C. neoformans* strain and grown overnight at 30 °C with shaking at 180 rpm. The next day, cells from the overnight were inoculated to a concentration of 5 x 10^6 cells / ml in YPD containing inhibitory drugs or solute controls where specified, and the culture was grown at 37°C, 180 rpm shaking for 2 h. After 2 h, cells were washed with PBS and 5µl of cells were pipetted onto Yeast Nitrogen Base (YNB) agar plates containing the supplements found in Table 2.11[160]. Once each 5µl spot was dry, plates were incubated at 30°C and 37°C for 2 or 3 days, respectively. Images were taken and analysed using image J to calculate the mean grey area (light intensity) and values were plotted with statistical testing in GraphPad Prism 10.

Table 2.11: Recipe for melanin agar plate supplementation

Supplement	**Concentration**
D-Glucose	1 mg / ml
L-Glycine	1 mg / ml
Potassium Dihydrogen Phosphate (KH_2PO_4)	4 mg / ml
Magnesium Sulphate Heptahydrate ($MgSO_4 \cdot 7H_2O$)	0.46 mg / ml
D-Biotin	0.5 µg / ml
Thiamine	0.5 µg / ml
l-3,4-dihydroxyphenylalanine (L-DOPA)	0.2 mg / ml

2.6 Pre-clinical testing

2.6.1 Use of the *Galleria mellonella* infection model to assess *C. neoformans* virulence

A standardised *Galleria mellonella* infection model was used to assess *C. neoformans* virulence, as described previously[275, 276]. *G. mellonella* larvae were ordered from Biosystems Technology (TruLarv™), which were prepared from a breeding colony without feedstuff antibiotic addition. Larvae were sterilised, uniformly aged and approximately 0.35 g. TruLarv™ were stored at 15°C until required. WT (H99) and *Δaox1 C. neoformans* were grown overnight in 5ml of YPD at 30°C with shaking at 180 rpm. The next day, cells were harvested and TruLarv™ *G. mellonella* larvae were inoculated with 1 x 10^6 CFU of wildtype ($H99^{-1}$) and *Δaox1* mutant cultures ($\Delta aox1^{-1}$). A 25µl Hamilton syringe was used to inject 15µl aliquots of either culture inoculum or a PBS control into the hemocoel of each larva via the last left proleg.

Antifungal drugs (ALTOX094, ALTOX102) and appropriate solvent controls were injected using the same technique. For experiments that required multiple injections, such as those with both a cell culture inoculum and a drug inoculum, a different proleg was used for each injection, starting from the left last proleg and rotating left to right and moving proximally as needed. Larvae were then placed into sterile petri dishes containing filter paper and incubated at 37°C. Larvae were assessed every 24 h for 5 days and motility, melanisation and survival using standardised scoring as described previously. A non-injection control set of larvae was also incubated. Larvae were considered dead if there was no motility response to touch.

Kaplan-Meyer survival and melanisation curves were plotted, and significance was calculated using a Log-Rank (Mantel-Cox) test in GraphPad Prism 10. Each inoculum condition contained 10 larvae and was repeated independently three times unless stated otherwise.

2.6.2 Haemolysis assay

A haemolysis assay was carried out using blood agar plates (1 g Peptone, 1 g Sodium Chloride (NaCl), 0.6 g Beef Extract, 3 g Technical Agar, 190 ml sterile mqH_2O, 10 ml defibrinated sheep blood (TCS Biosciences, ref: SB054). Stock concentrations of the drugs listed in Chapter 5 were made,

including the working concentration, a 2x, 5x or 10x working concentration where indicated. 20µl of each drug was pipetted onto filter paper disks placed onto the agar and incubated at 37°C for 24 h. A PBS control and a positive 10% SDS control were also used. At 2 h and 24 h the zone of haemolysis (ZOH) was recorded, and results and statistical significance was plotted in GraphPad Prism 10.

2.7 Recombinant *C. albicans* Aox assay performed by Dr. Luke Young (University of Sussex)

Recombinant *C. albicans* Aox was expressed in *Escherichia coli* strain FN102 and the membranes were harvested as described previously[212]. Dose response curves were generated using a Multiskan SkyHigh (Thermofisher) 96 well plate reader with the following conditions. Aox *E. coli* membrane was diluted to ~ 60 µg ml^{-1} in 65 mM 3-(N-morpholino) propanesulfonic acid (MOPS), pH 7.5 containing 1 mM KCN and 10 mM GMP and left to incubate with the inhibitor for 10 min (3-fold serial dilution). Reaction was initiated with the addition of NADH and followed at 340 nm for 10 min with readings taken every 8 sec. Subsequent dose response curves were plotted in GraphPad Prism 9.

2.8 Rat liver mitochondrial assay performed by Dr. Luke Young (University of Sussex)

Fresh rat liver mitochondria were isolated using previously published methodology[277]. Mitochondrial respiration rates were assessed using an Oroboros Oxygraph-2K oxygen electrode. ~ 600 µg mitochondrial protein was equilibrated in 2ml of assay media (200 mM Sucrose, 25 mM KCl, 11 mM $MgCl_2$, 5 mM KH_2PO_4, 5 mM MOPS pH 7.4) for 10 min at 32°C in the presence of 0.5 µM rotenone, 0.5 µM CCCP and the inhibitor. Respiration was then initiated with the addition of 10 mM succinate and the rate of oxygen consumption was recorded. Dose response curves were plotted using GraphPad Prism 9.

2.9 Statistical Analysis

Statistical analyses were calculated in GraphPad Prism 10, unless stated otherwise. Information on tests for significance is given in each figure. Error bars indicate standard deviation (SD) and asterisks in the figures indicate significant differences, with * <0.05, ** <0.005, *** < 0.0005, **** <0.0001, where P = 0.05.

3. Mitochondrial function of *C. neoformans* and its potential as a novel antifungal drug target

3.1 Introduction

The Aox enzyme has been implicated in pathogenicity among human fungal pathogens, including *C. neoformans*[205]. However, the only published crystal structure for the enzyme is that of *Trypanosoma brucei*[223]. Investigations into Aox activity for fungal pathogens have relied on high levels of conservation between the ETC of multiple fungi[128, 278] although exact roles for Aox in *C. neoformans* remain unclear.

Given the lack of available information we sought to determine how related the Aox of *C. neoformans* is to Aox of other human fungal pathogens at the sequence and predicted structural level. To achieve this, we used the predicted FASTA sequence of *C. neoformans* Aox and compared it to other similar structures using BLAST and aligned the sequence to other enzymes using MEGAX. We then used iTASSER modelling prediction software to generate a predicted structure. Investigations were also carried out to determine whether Aox was actively contributing to respiration and resistance against mitochondrial inhibition through the use of growth and viability analysis, High Resolution Respirometry (HRR), and melanisation assays. Finally, we wanted to identify any putative regulators of mitochondrial function through unbiased kinase knockout screens, and assess the impact of kinase loss on growth, respiration, viability and mitochondrial stress signalling.

3.2 Results

3.2.1 *C. neoformans* Aox shows low sequence similarity to other human fungal pathogens

As studies have shown that Aox is a conserved mediator of alternative respiration across fungi (Section 1.3), we wanted to establish whether the Aox of *C. neoformans* was closely related to that of other human fungal pathogens. Using the predicted amino acid sequence of the enzyme found on UniProt, we used BLAST[279, 280] and MEGAX[281] to compare the predicted sequences of fungal Aox enzymes and generated a phylogenetic tree using the interactive tree of life software (iTOL)[282], which displays and annotates phylogenetic trees using protein sequence alignment data. Sequences with over a 60% percentage identity matrix, generated in Clustal 2.1[283] were considered closely related (Fig. 3.1b). Our data suggests that the closest phylogenetic relations were basidiomycetes found mainly in the order Tremalles, such as *Kwoniella pini* and *Kockovaella imperatae* (Fig. 3.1a), which are associated with growth on plant materials and in everglades[284, 285]. Interestingly, in relation to human fungal pathogens, the Aox of *Aspergillus brasiliensis*, *Aspergillus niger* and *Histoplasma capsulatum* made the top 250 alignments with 53.2%, 52.9%, and 46% similarity, respectively (Appendix 7.1a). None of the Aox enzymes of other human fungal pathogens listed in Section 1.3, including *Candida albicans* and *Candida auris*, showed in the top 250 BLAST alignment results for *C. neoformans* Aox, although amino acid sequences of oleaginous yeasts such as *Cutaneotrichosporon oleaginosum*, *Saitozyma podzolica,* and *Apiotrichum porosum* showed high sequence similarity (Fig. 3.1b). Interestingly, upon assessment of the Aox1 protein sequence alignment in Clustal 2.1, conserved residues could be found across human fungal pathogens (Appendix 7.1b). However, these conserved residues both included and surrounded iron binding sites, which confirmed that Aox1 enzymes from *Cryptococcus neoformans* and *Cryptococcus gattii* have functionality of other heme-cluster enzymes, but that overall enzyme structure was not conserved between *Cryptococcus* species and other human fungal pathogens.

A

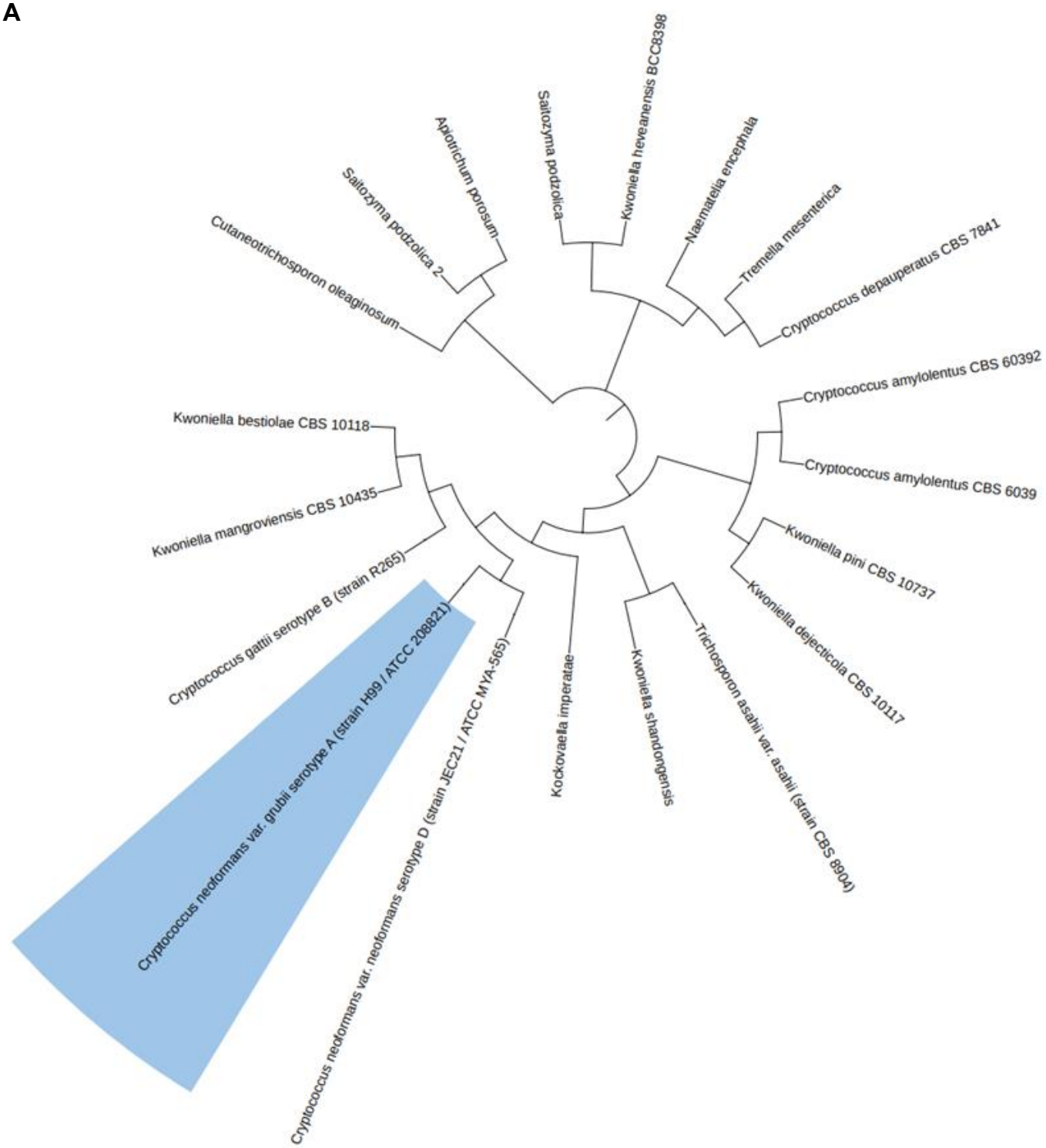
Cutaneotrichosporon oleaginosum
Saitozyma podzolica 2
Apiotrichum porosum
Saitozyma podzolica
Kwoniella heveanensis BCC8398
Naematelia encephala
Tremella mesenterica
Cryptococcus depauperatus CBS 7841
Cryptococcus amylolentus CBS 60392
Cryptococcus amylolentus CBS 6039
Kwoniella pini CBS 10737
Kwoniella dejecticola CBS 10117
Trichosporon asahii var. asahii (strain CBS 8904)
Kwoniella shandongensis
Kockovaella imperatae
Cryptococcus neoformans var. neoformans serotype D (strain JEC21 / ATCC MYA-565)
Cryptococcus neoformans var. grubii serotype A (strain H99 / ATCC 208821)
Cryptococcus gattii serotype B (strain R265)
Kwoniella mangroviensis CBS 10435
Kwoniella bestiolae CBS 10118

B

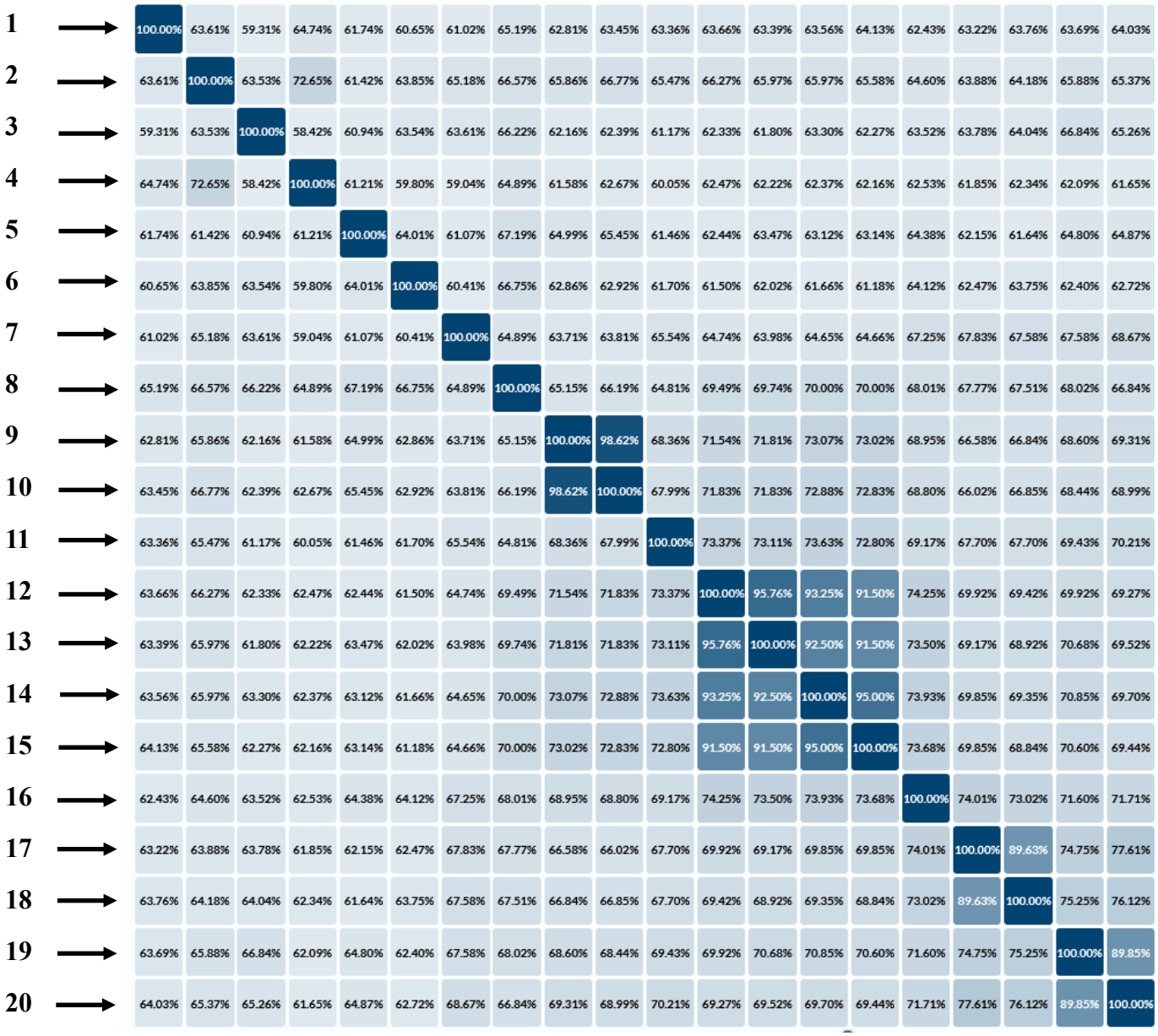

1 →	100.00%	63.61%	59.31%	64.74%	61.74%	60.65%	61.02%	65.19%	62.81%	63.45%	63.36%	63.66%	63.39%	63.56%	64.13%	62.43%	63.22%	63.76%	63.69%	64.03%
2 →	63.61%	100.00%	63.53%	72.65%	61.42%	63.85%	65.18%	66.57%	65.86%	66.77%	65.47%	66.27%	65.97%	65.97%	65.58%	64.60%	63.88%	64.18%	65.88%	65.37%
3 →	59.31%	63.53%	100.00%	58.42%	60.94%	63.54%	63.61%	66.22%	62.16%	62.39%	61.17%	62.33%	61.80%	63.30%	62.27%	63.52%	63.78%	64.04%	66.84%	65.26%
4 →	64.74%	72.65%	58.42%	100.00%	61.21%	59.80%	59.04%	64.89%	61.58%	62.67%	60.05%	62.47%	62.22%	62.37%	62.16%	62.53%	61.85%	62.34%	62.09%	61.65%
5 →	61.74%	61.42%	60.94%	61.21%	100.00%	64.01%	61.07%	67.19%	64.99%	65.45%	61.46%	62.44%	63.47%	63.12%	63.14%	64.38%	62.15%	61.64%	64.80%	64.87%
6 →	60.65%	63.85%	63.54%	59.80%	64.01%	100.00%	60.41%	66.75%	62.86%	62.92%	61.70%	61.50%	62.02%	61.66%	61.18%	64.12%	62.47%	63.75%	62.40%	62.72%
7 →	61.02%	65.18%	63.61%	59.04%	61.07%	60.41%	100.00%	64.89%	63.71%	63.81%	65.54%	64.74%	63.98%	64.65%	64.66%	67.25%	67.83%	67.58%	67.58%	68.67%
8 →	65.19%	66.57%	66.22%	64.89%	67.19%	66.75%	64.89%	100.00%	65.15%	66.19%	64.81%	69.49%	69.74%	70.00%	70.00%	68.01%	67.77%	67.51%	68.02%	66.84%
9 →	62.81%	65.86%	62.16%	61.58%	64.99%	62.86%	63.71%	65.15%	100.00%	98.62%	68.36%	71.54%	71.81%	73.07%	73.02%	68.95%	66.58%	66.84%	68.60%	69.31%
10 →	63.45%	66.77%	62.39%	62.67%	65.45%	62.92%	63.81%	66.19%	98.62%	100.00%	67.99%	71.83%	71.83%	72.88%	72.83%	68.80%	66.02%	66.85%	68.44%	68.99%
11 →	63.36%	65.47%	61.17%	60.05%	61.46%	61.70%	65.54%	64.81%	68.36%	67.99%	100.00%	73.37%	73.11%	73.63%	72.80%	69.17%	67.70%	67.70%	69.43%	70.21%
12 →	63.66%	66.27%	62.33%	62.47%	62.44%	61.50%	64.74%	69.49%	71.54%	71.83%	73.37%	100.00%	95.76%	93.25%	91.50%	74.25%	69.92%	69.42%	69.92%	69.27%
13 →	63.39%	65.97%	61.80%	62.22%	63.47%	62.02%	63.98%	69.74%	71.81%	71.83%	73.11%	95.76%	100.00%	92.50%	91.50%	73.50%	69.17%	68.92%	70.68%	69.52%
14 →	63.56%	65.97%	63.30%	62.37%	63.12%	61.66%	64.65%	70.00%	73.07%	72.88%	73.63%	93.25%	92.50%	100.00%	95.00%	73.93%	69.85%	69.35%	70.85%	69.70%
15 →	64.13%	65.58%	62.27%	62.16%	63.14%	61.18%	64.66%	70.00%	73.02%	72.83%	72.80%	91.50%	91.50%	95.00%	100.00%	73.68%	69.85%	68.84%	70.60%	69.44%
16 →	62.43%	64.60%	63.52%	62.53%	64.38%	64.12%	67.25%	68.01%	68.95%	68.80%	69.17%	74.25%	73.50%	73.93%	73.68%	100.00%	74.01%	73.02%	71.60%	71.71%
17 →	63.22%	63.88%	63.78%	61.85%	62.15%	62.47%	67.83%	67.77%	66.58%	66.02%	67.70%	69.92%	69.17%	69.85%	69.85%	74.01%	100.00%	89.63%	74.75%	77.61%
18 →	63.76%	64.18%	64.04%	62.34%	61.64%	63.75%	67.58%	67.51%	66.84%	66.85%	67.70%	69.42%	68.92%	69.35%	68.84%	73.02%	89.63%	100.00%	75.25%	76.12%
19 →	63.69%	65.88%	66.84%	62.09%	64.80%	62.40%	67.58%	68.02%	68.60%	68.44%	69.43%	69.92%	70.68%	70.85%	70.60%	71.60%	74.75%	75.25%	100.00%	89.85%
20 →	64.03%	65.37%	65.26%	61.65%	64.87%	62.72%	68.67%	66.84%	69.31%	68.99%	70.21%	69.27%	69.52%	69.70%	69.44%	71.71%	77.61%	76.12%	89.85%	100.00%

1. *Trichosporon asahii var. asahii*
2. *Cutaneotrichosporon oleaginosum*
3. *Kockovaella imperatae*
4. *Apiotrichum porosum*
5. *Saitozyma podzolica*
6. *Tremella mesenterica (Jelly fungus)*
7. *Kwoniella heveanensis*
8. *Naematelia encephala*
9. *Cryptococcus amylolentus*
10. *Cryptococcus amylolentus*
11. *Cryptococcus depauperatus*
12. *Cryptococcus neoformans var. grubii serotype A (H99)*
13. *Cryptococcus neoformans var. neoformans serotype D*
14. *Cryptococcus gattii*
15. *Cryptococcus gattii VGII*
16. *Kwoniella shandongensis*
17. *Kwoniella pini*
18. *Kwoniella dejecticola*
19. *Kwoniella bestiolae*
20. *Kwoniella mangroviensis*

Figure 3.1: Predicted phylogeny of an Aox monomer from C. neoformans.
To investigate the phylogeny of cryptococcal Aox, the predicted sequence of the wildtype H99 strain (blue) was compared to other fungal Aox enzymes using BLAST[279] and MEGA-X[281]. (**A**) A phylogenetic tree was generated in iTOL[282] and (**B**) the percent identity matrix of each alignment in the tree was generated in Clustal 2.1[424].

3.2.2 *C. neoformans* Aox prediction modelling

Given that our data showed low sequence homology of *C. neoformans* Aox to other human pathogenic fungi and the only published crystal structure of Aox belongs to *Trypanosoma brucei*[223] (Fig. 3.2a), we wanted to model a possible structure. The predicted FASTA sequence found on UniProt[286] was run through I-TASSER software[287-289], the leading server in the CASP14 experiment (Critical Assessment of Techniques for Protein Structure Prediction). The I-TASSER server tries to retrieve similar protein data bank (PDB) structures to the input FASTA sequence, through the Local Meta-Threading Server (LOMETS), and then generate models through Monte Carlo replica exchange simulations or building models by ab initio modelling (QUARK). The I-TASSER server was able to generate 5 predicted models of *C. neoformans* Aox (Fig. 3.3a). The confidence scores (c-scores) TM-scores (structural similarity) and number of decoys used for modelling can be found in Fig. 3.3b, whereby c-scores ranged from -5 (weak confidence) to 2 (strong confidence) and TM-scores ranged from <0.17 (random similarity) to >0.50 (correct topology). Higher cluster density values mean that the decoys used to simulate the predicted structure 'cluster' and structurally occur more often. Out of the given models, model 1 was shown to be the most likely structure for this enzyme.

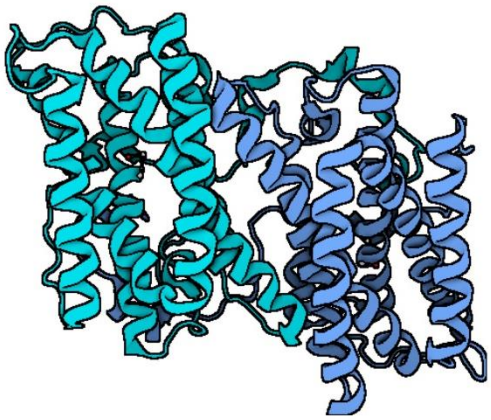

Figure 3.2: The published crystal structure of TAO.

Structure of TAO from *Trypanosoma brucei* (PDB 3VV9)[223]. Created with BioRender.com.

A

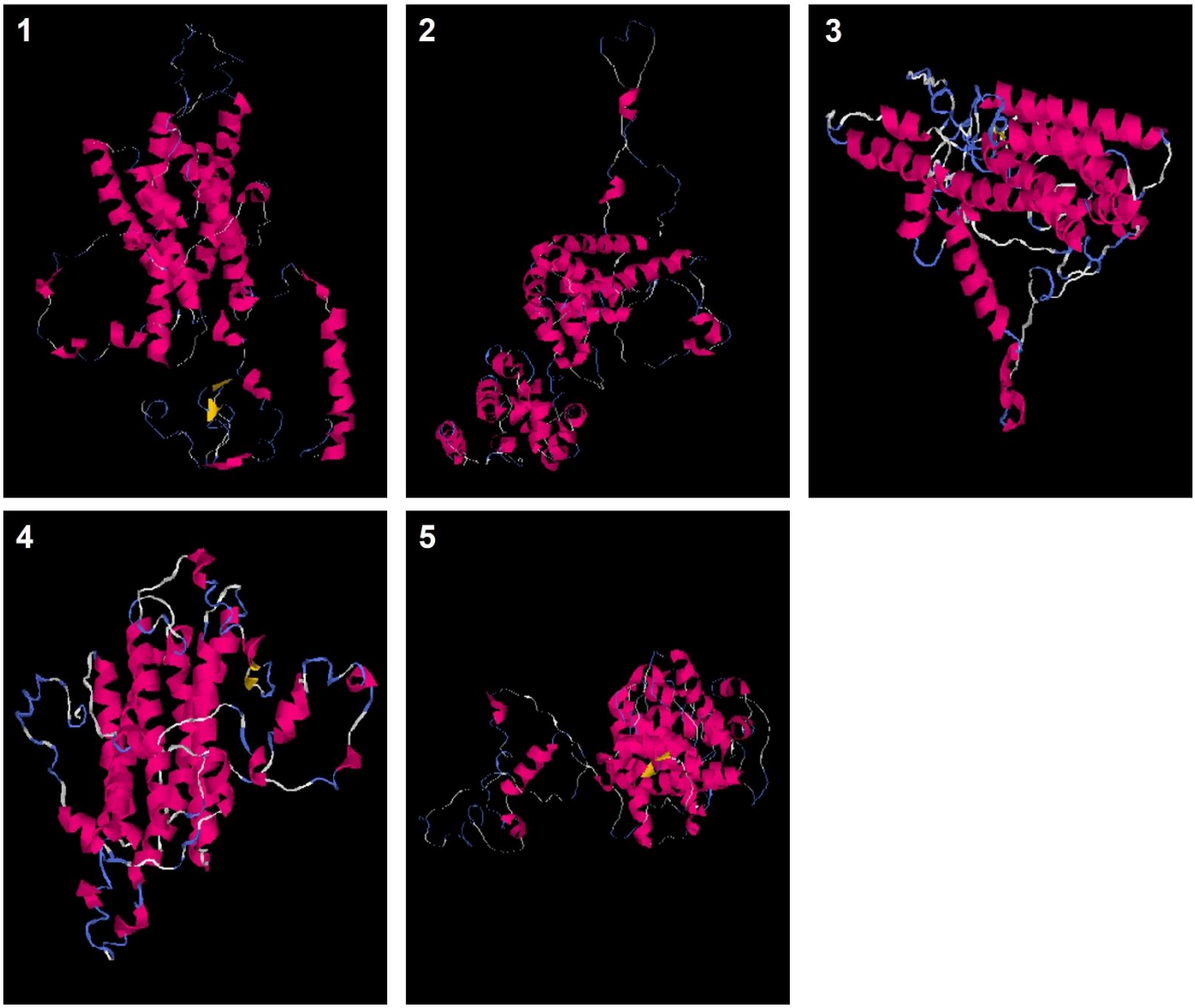

B

Name	C-score	Exp. TM-score	No. of decoys	Cluster density
Model 1	-0.59	0.64 ± 0.13	600	0.1130
Model 2	-0.74		600	0.0971
Model 3	-1.11		600	0.0671
Model 4	-1.56		542	0.0426
Model 5	-3.09		113	0.0093

Figure 3.3: Predicted model of an Aox monomer from C. neoformans.
(**A**) Predicted models of the *C. neoformans* Aox enzyme generated in iTASSER[287-289]. (**B**) Data for each model based on confidence (C-score), sequence similarity (TM-score), number of decoys and a topology score (cluster density).

3.2.3 Confirmation of Aox deletion in *C. neoformans*

To confirm the deletion of Aox in the mutant provided (*Δaox1*), PCR was carried out using generated primers as in Section 2.4.1. Wildtype (H99) and *Δaox1* were harvested after 24 h growth in YPD at 37°C and genomic DNA was extracted as in Section 2.4.2. Samples loaded onto a DNA agarose gel confirmed the deletion of Aox1 in the mutant (Fig. 3.4a) where the fully sized Aox1 gene (around 1000bp) could be seen in the wildtype, but not in *Δaox1.*

In addition, a complementary antibody for the *C. neoformans* Aox structure was created (Section 2.4.7). The complimentary antibody was designed based on the *Cryptococcus*-specific residues FLASEASP identified through Aox1 sequence alignment in Clustal 2.1 (Fig. 3.4a), that were not conserved in other human fungal pathogens such as *Candida albicans*. Following this, a western blot was carried out whereby wildtype (H99) and *Δaox1* were harvested after 24 h growth in YPD and treated with Triethyltin Bromide (TET), Carbonyl Cyanide-p-trifluoromethoxyphenylhydrazone (FCCP) and Antimycin A (AntA), Salicylhydroxamic Acid (SHAM), Sodium Nitroprusside (SNP), potassium cyanide (KCN) and Calcofluor white (CFW) for 2 h at 37°C before lysing the cells. The cell lysate of each sample was loaded onto a western blot where indicated (Fig. 3.4c). We were able to confirm that the generated antibody bound to *C. neoformans* Aox1 and confirmed the *Δaox1* deletion strain (Fig. 3.4c). Interestingly, none of the tested electron transport and cell wall stresses significantly induced expression of Aox (Fig. 3.4d).

A

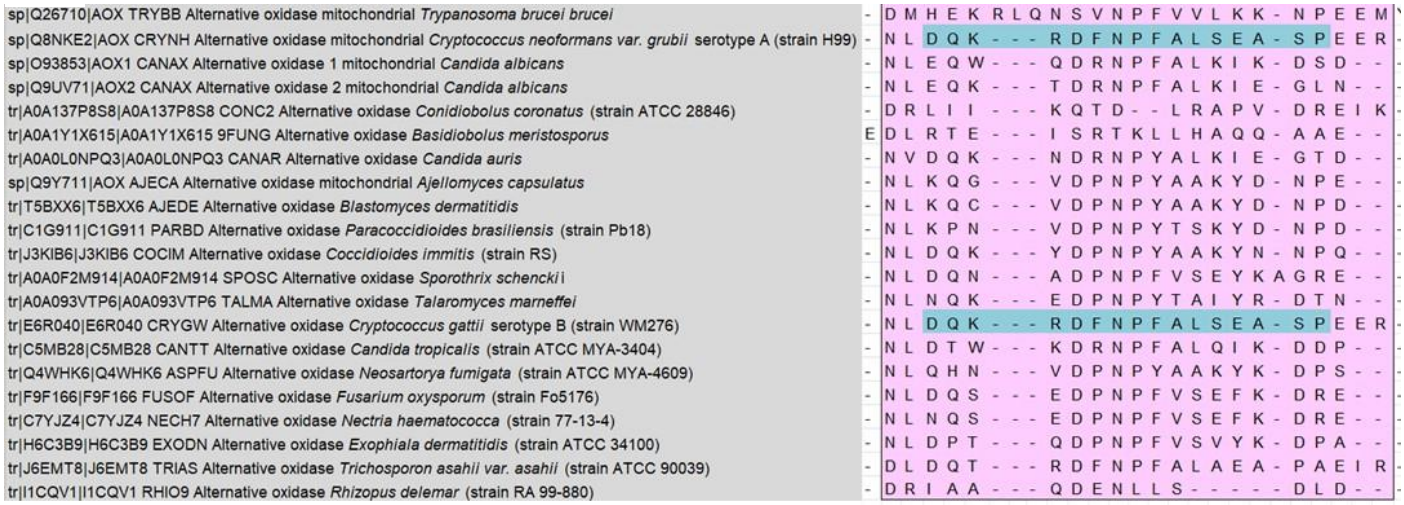

B

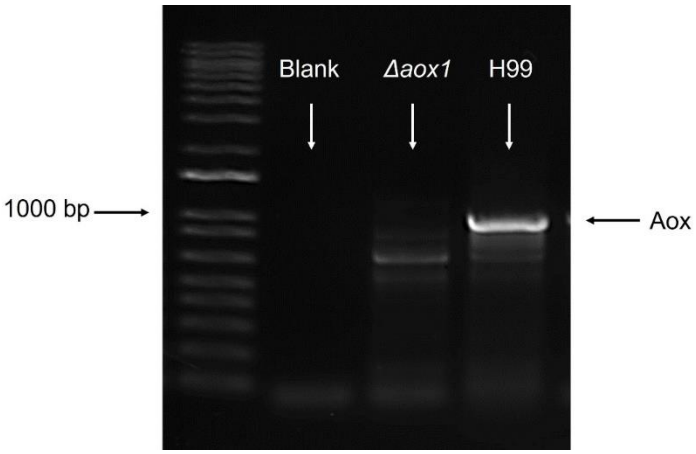
Blank
Δaox1
H99
1000 bp
Aox

C

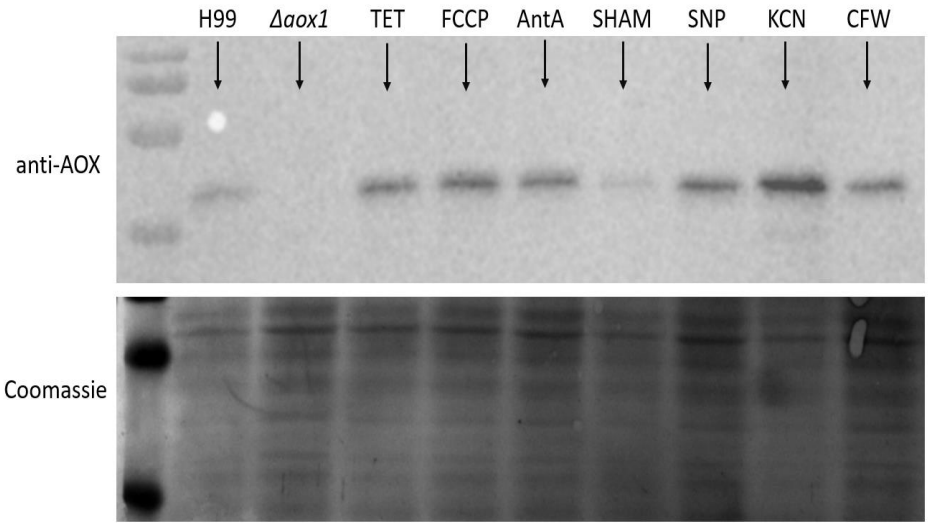
H99
Δaox1
TET
FCCP
AntA
SHAM
SNP
KCN
CFW
anti-AOX
Coomassie

D

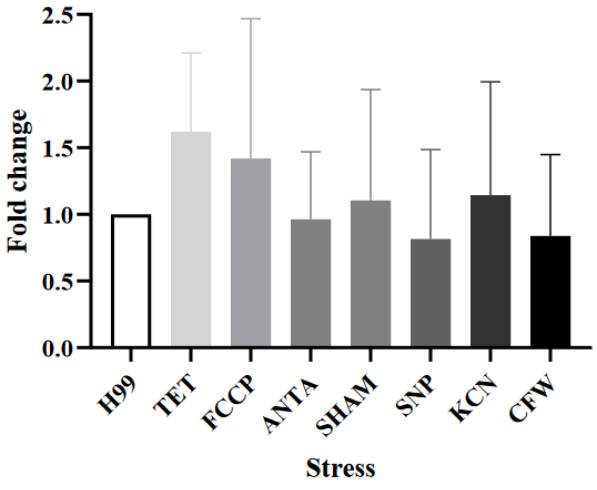
Fold change
2.5
2.0
1.5
1.0
0.5
0.0
H99
TET
FCCP
ANTA
SHAM
SNP
KCN
CFW
Stress

Figure 3.4: Confirmation of the Aox deletion in the Δaox1 C. neoformans mutant
(**A**) Clustal alignment of the *C. neoformans* Aox1 amino acid sequence against other human fungal pathogens, with identification of the peptide sequence used to generate an anti-*aox1* antibody (blue). (**B**) PCR showing the band for the Aox1 gene (Aox) in the wildtype (H99) at around 1000bp, which was not present in the *Δaox1* mutant. (**C**) Representative western blot showing that Aox was present in wildtype *C. neoformans* (H99) but not in the *Δaox1* mutant (*Δaox1).* Wildtype cells were exposed to different mitochondrial stresses for 2 h at 37°C to assess induction of Aox under varying conditions, with a Coomassie loading control. (**D**) Band intensity was recorded using ImageJ and significance was calculated using Dunnett's multiple comparisons test following a one-way ANOVA in GraphPad Prism, where P = 0.05. No significance was recorded. Error bars represent ± Standard Deviation (SD). n =3

3.2.4 *C. neoformans* Aox does not make a significant contribution to respiration during normal growth

As little is known about whether Aox functions within normal growth, we investigated the respiratory profile of the wild type H99 (Fig. 3.5a) and an *Δaox1* mutant *C. neoformans* (Fig. 3.5b) using HRR. Respirometer chambers were inoculated with 1 x 10^6 cells from a culture grown for 24 h at 37°C and treated with TET, FCCP and AntA where indicated. TET inhibits the ATP synthase (complex V) and prevents proton translocation, leading to an accumulation of protons within the intermembrane space that in turn inhibits respiration. Oxygen consumption following TET treatment therefore reflects ATP synthase independent proton movement across the inner mitochondrial membrane, so called, electron 'leak' respiration. FCCP is a proton ionophore which allows random proton movement across the inner mitochondrial membrane that allows respiration to proceed uninhibited and gives a 'maximum respiration' value. The addition of AntA leads to complex III inhibition, which halts classical respiration and provides a 'minimum' value that reflects non-mitochondrial respiration or could also reflect activity of an Aox. Addition of each drug allows a respiratory profile to be generated, which indicates how much each strain utilises the classical ETC, and how coupled this is to ATP synthesis, or indeed if there are alternate routes of respiration. The wildtype H99 respiratory profile (Fig. 3.5a, 3.5c) showed a reduction in respiration after TET addition, a high respiration value after FCCP addition, and a low respiration value after inhibition of the classical ETC through AntA addition, which indicated a normal use of the classical ETC. Interestingly, Aox did not actively

contribute to respiration during normal growth, as a loss of Aox gave rise to a respiratory profile that was similar to the wild type (Fig. 3.5b, 3.5d).

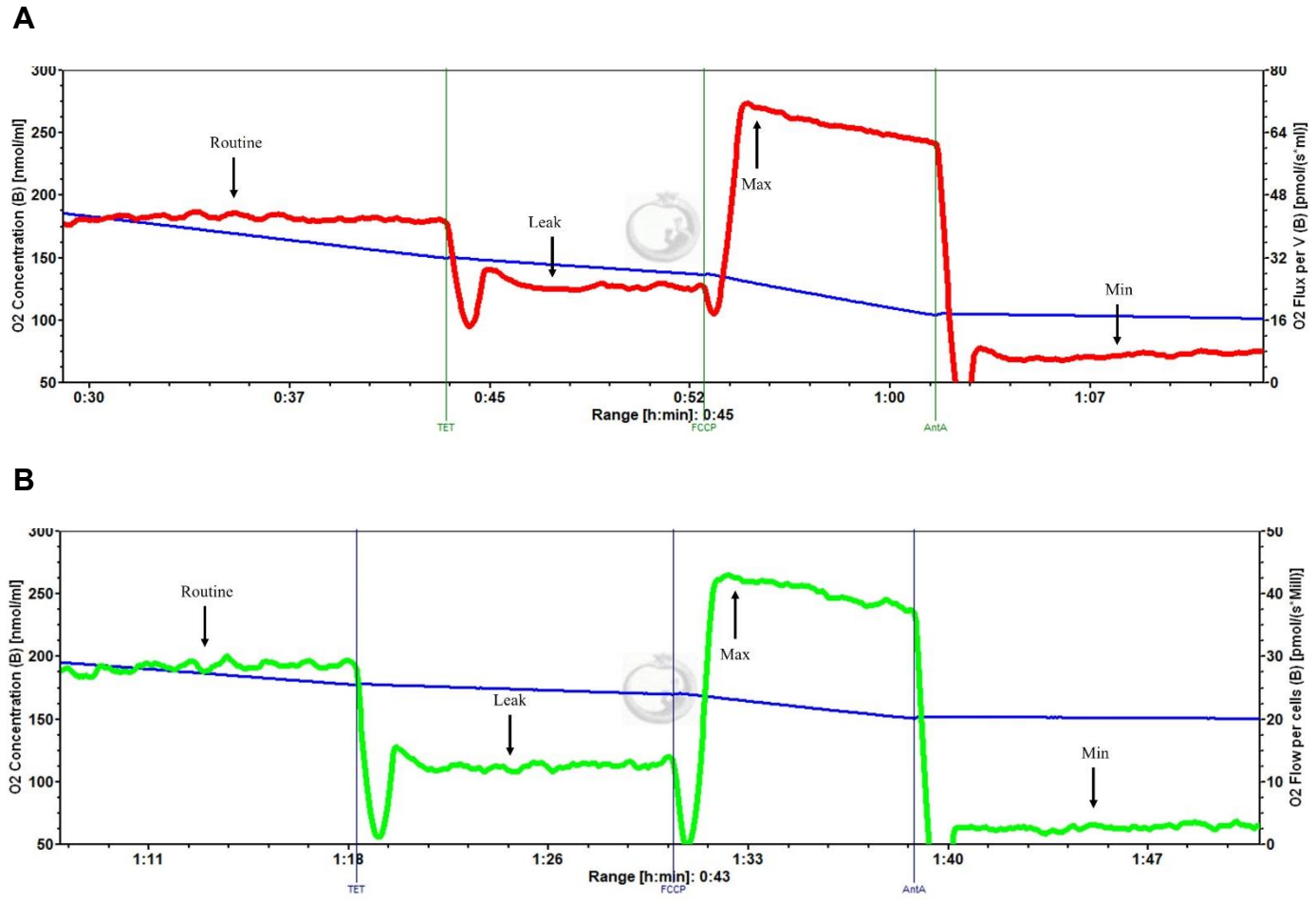

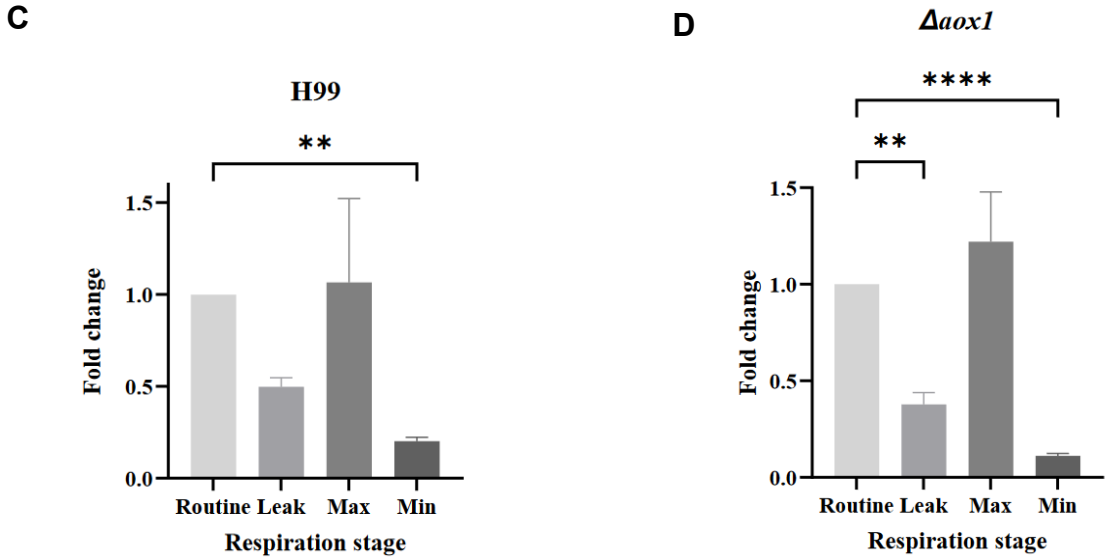

Figure 3.5: Respiratory profiles of C. neoformans strains.
Representative example of respiration in H99 and *Δaox1* determined using HRR. Chambers were inoculated with 1 x 10^6 cells after 24 h growth and treated with TET, FCCP and AntA where indicated. (**A**) H99 (**B**) *Δaox1*. Measurements of Leak (Leak) Maximum (Max) and Minimum (Min) respiration (O2 flow per cells) after drug exposure were taken and compared to the routine level of respiration (Routine) for each strain as indicated. (**E**) H99 (**F**) *Δaox1*. Significance was calculated using Dunnett's multiple comparisons test following a one-way ANOVA in GraphPad Prism. ** <0.005, **** <0.0001, where P = 0.05. n = 3

3.2.5 Aox is required to provide resistance to Complex III inhibition by Azoxystrobin

Aox induction has been attributed to resistance to mitochondrial inhibitors, such as Azoxystrobin, in phytopathogenic fungi (Section 1.3.5), so we tested whether loss of Aox would induce *C. neoformans* sensitivity to mitochondrial inhibitors. We wanted to investigate whether Aox conferred resistance to a broad-spectrum inhibitor of cytochrome bc_1, Azoxystrobin. Wildtype H99 and *Δaox1* mutant *C. neoformans* were screened for Azoxystrobin sensitivity in YPD containing Azoxystrobin ranging from 12.5μM - 100μM in comparison to a methanol solvent control (Fig. 3.6). For H99, no concentrations tested exhibited a strong fungistatic effect (Fig. 3.6a, 3.6d) although 15μM Azoxystrobin led to a mild inhibition of growth. Interestingly, *Δaox1* mutant *C. neoformans* showed sensitivity to 15-20μM Azoxystrobin, however, each biological replicate showed a different phenotype, with lots of variation in the combined data set (Fig. 3.6b). To clarify and assess the variation, the *Δaox1* biological replicates were 'split' into a sensitive phenotype or a non-sensitive phenotype (Fig. 3.6c), whereby the population either displayed complete growth inhibition (sensitive) or robust growth under the same conditions (non-sensitive). *Δaox1* also showed clear sensitivity to Azoxystrobin at 75μM and 100μM (Fig. 3.6e), which indicated that loss of Aox confers sensitivity to Azoxystrobin.

A

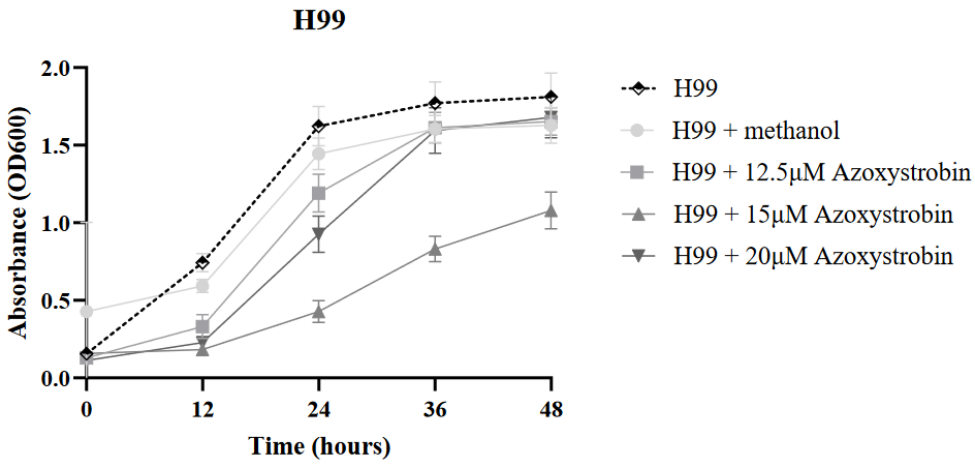
H99
Absorbance (OD600)
2.0
1.5
1.0
0.5
0.0
0
12
24
36
48
Time (hours)
H99
H99 + methanol
H99 + 12.5µM Azoxystrobin
H99 + 15µM Azoxystrobin
H99 + 20µM Azoxystrobin

B

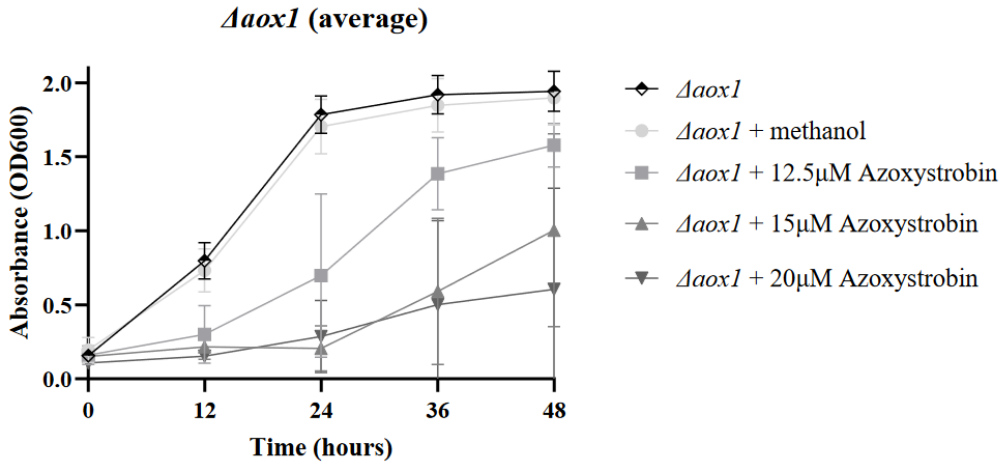
Δaox1 (average)
Absorbance (OD600)
2.0
1.5
1.0
0.5
0.0
0
12
24
36
48
Time (hours)
Δaox1
Δaox1 + methanol
Δaox1 + 12.5µM Azoxystrobin
Δaox1 + 15µM Azoxystrobin
Δaox1 + 20µM Azoxystrobin

C

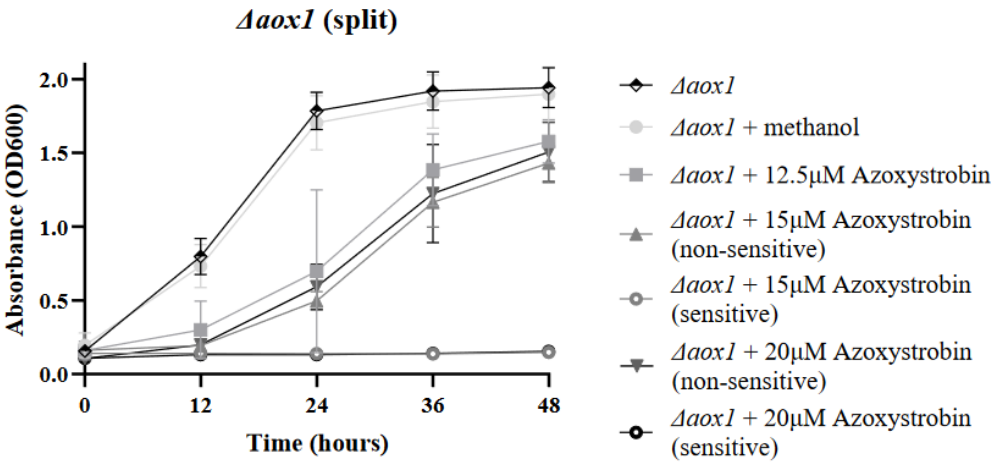
Δaox1 (split)
Absorbance (OD600)
2.0
1.5
1.0
0.5
0.0
0
12
24
36
48
Time (hours)
Δaox1
Δaox1 + methanol
Δaox1 + 12.5µM Azoxystrobin
Δaox1 + 15µM Azoxystrobin (non-sensitive)
Δaox1 + 15µM Azoxystrobin (sensitive)
Δaox1 + 20µM Azoxystrobin (non-sensitive)
Δaox1 + 20µM Azoxystrobin (sensitive)

D

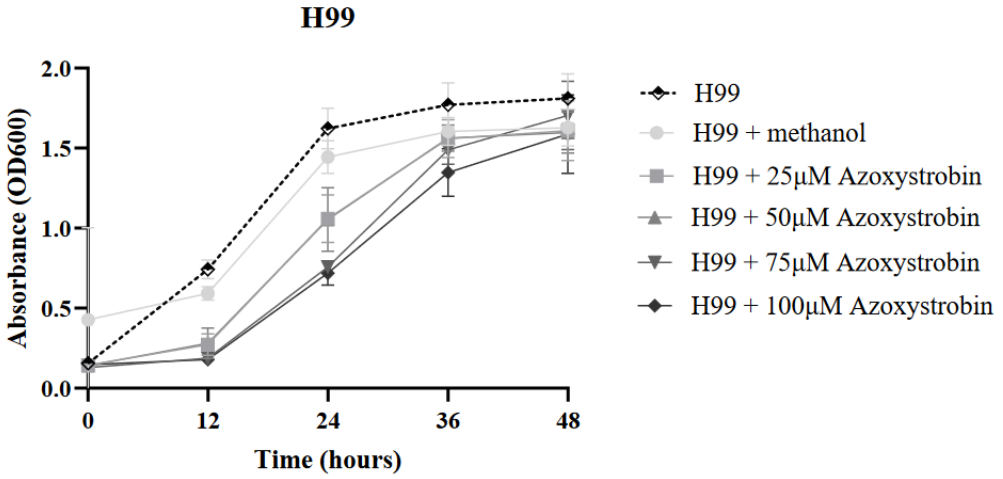

E

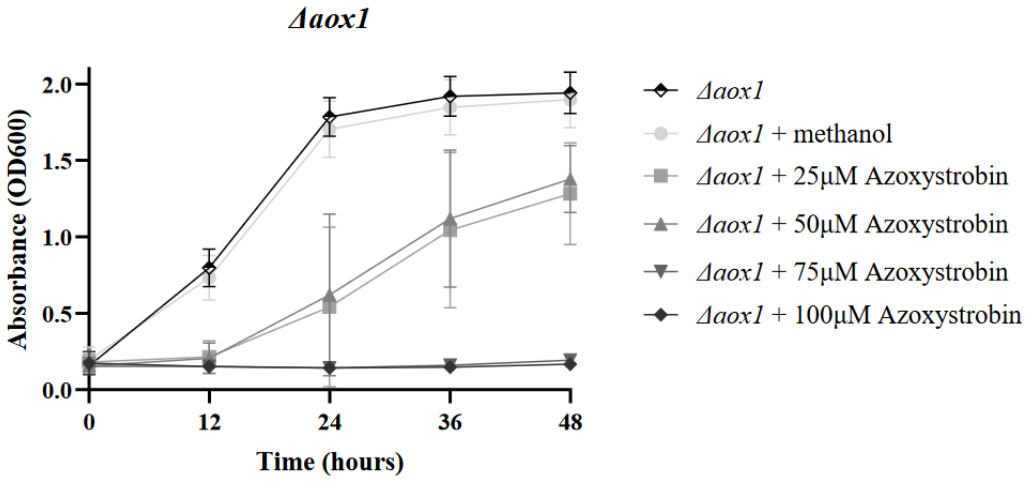

Figure 3.6: Screening the effect of Azoxystrobin on C. neoformans growth.
C. neoformans strains were grown in YPD containing various Azoxystrobin concentrations at 37°C for 48 h. (**A**) H99 + 12.5µM - 20µM Azoxystrobin, (**B**) *Δaox1* + 12.5µM - 20µM Azoxystrobin, (**C**) *Δaox1* + 12.5µM - 20µM Azoxystrobin, where biological replicates were split into a sensitive phenotype 'sensitive' and a non-sensitive phenotype 'non-sensitive' where indicated to assess variation (**D**) H99 + 25µM - 100µM Azoxystrobin, (**E**) *Δaox1* + 25µM - 100µM Azoxystrobin. Graphs were generated in GraphPad Prism. Error bars represent ± SD. n = 9

3.2.6 Azoxystrobin inhibits *Δaox1* mutant *C. neoformans* respiration

To assess whether the inhibition of growth seen in Fig. 3.6 was due to an effect of Azoxystrobin on respiration, the respiratory profiles of H99 and *Δaox1* mutant *C. neoformans* were assessed using HRR. Respirometer chambers were inoculated with 1 x 10^6 cells from a culture grown for 24 h at

37°C and treated with 20μM Azoxystrobin where indicated (Az). Interestingly, an increase in respiration was seen for H99 (Fig. 3.7a), which indicated that Aox was being induced in response to Azoxystrobin addition, leading to an increase in respiration. For *Δaox1,* addition of Azoxystrobin produced either a sensitive phenotype, where complete inhibition was seen (Fig. 3.7c), or a non-sensitive phenotype, where either no observable respiratory effect was seen (Fig. 3.7b), which mirrored the variability shown in growth sensitivity (Fig. 3.7).

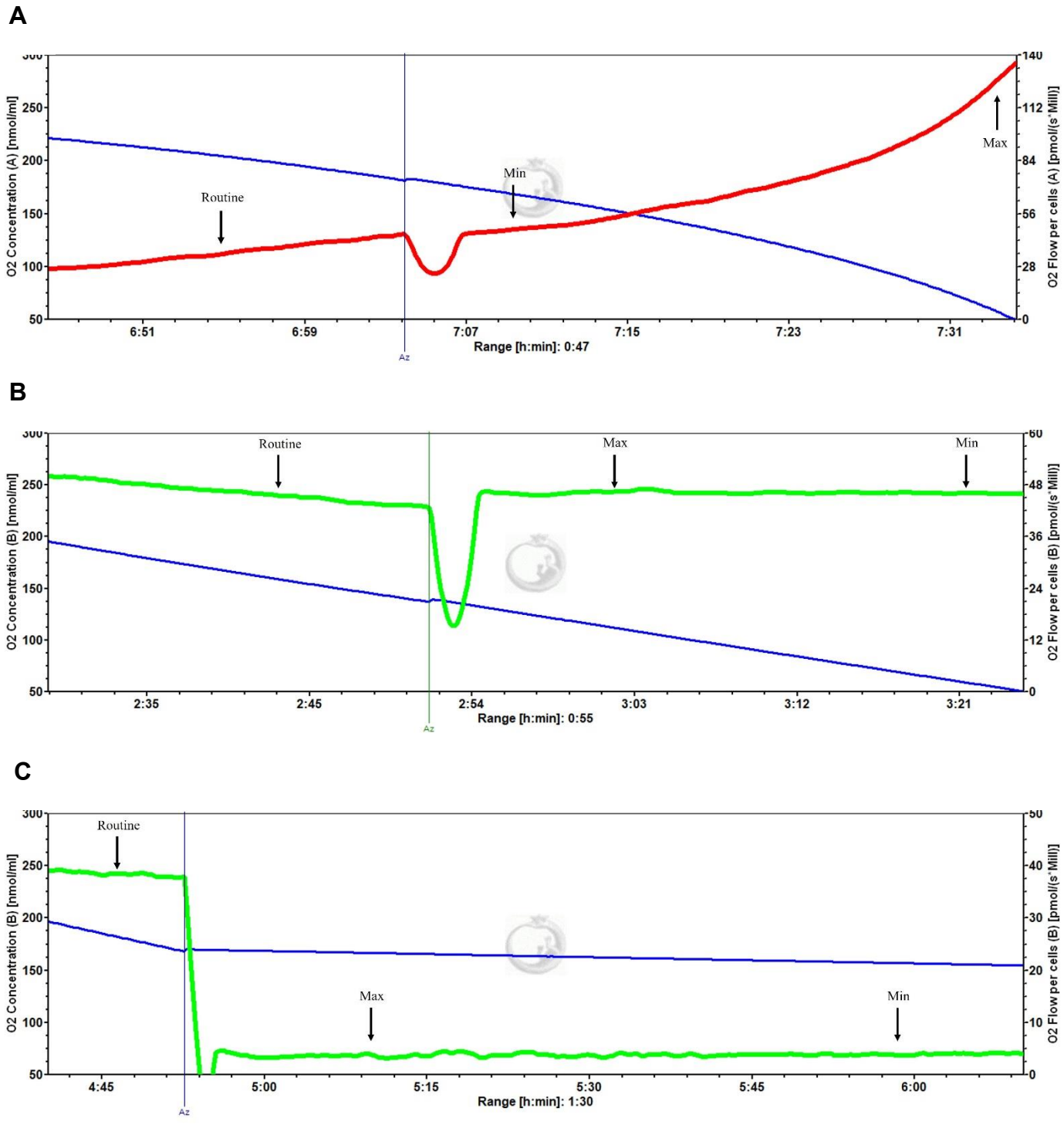

D

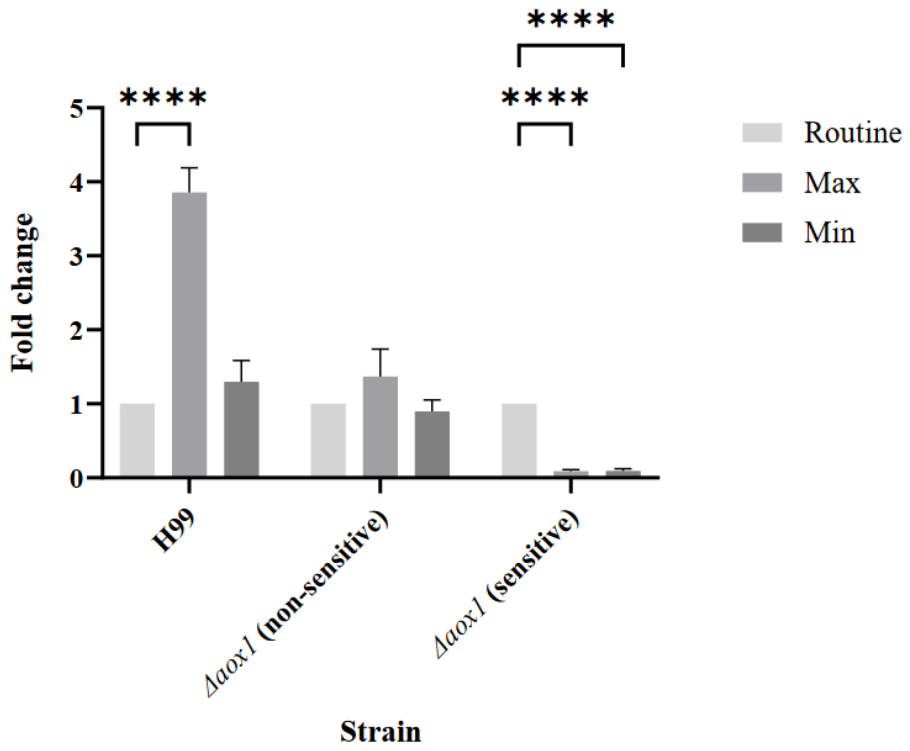

Figure 3.7: Respiratory profiles of C. neoformans exposed to Azoxystrobin.
Representative example of respiration in H99 and *Δaox1* determined using HRR. Chambers were inoculated with 1 x 10^6 cells after 24 h growth and treated with 20μM Azoxystrobin where indicated (Az) (**A**) Respiratory profile of H99 (**B**) Respiratory profile of an *Δaox1* population that is not sensitive to Azoxystrobin, (**C**) Respiratory profile of an *Δaox1* population that is affected by Azoxystrobin. (**D**) Measurements of maximum (Max) and minimum (Min) respiration (O2 flow per cells) after drug exposure were taken and compared to the routine level of respiration (Routine) for each strain as indicated. Significance was calculated using Dunnett's multiple comparisons test following a one-way ANOVA in GraphPad Prism. **** <0.0001, where P = 0.05. Error bars represent ± SD. n = 3

3.2.7 Azoxystrobin exposure does not reduce *C. neoformans* viability

To investigate whether the variable effect of Azoxystrobin on *Δaox1* growth (Fig. 3.6b) and respiration (Fig. 3.7c) was due to a loss of viability, H99 and *Δaox1* mutant cells were plated following a 2 h incubation in YPD containing Azoxystrobin at 20μM and viable colonies were counted after 48 h at 37°C. Surprisingly, although *Δaox1* displayed sensitivity to growth and respiratory inhibition in the presence of Azoxystrobin, no significant loss of viability was observed for either strain (Fig. 3.8), although an increase in viability was seen for H99 after Azoxystrobin addition.

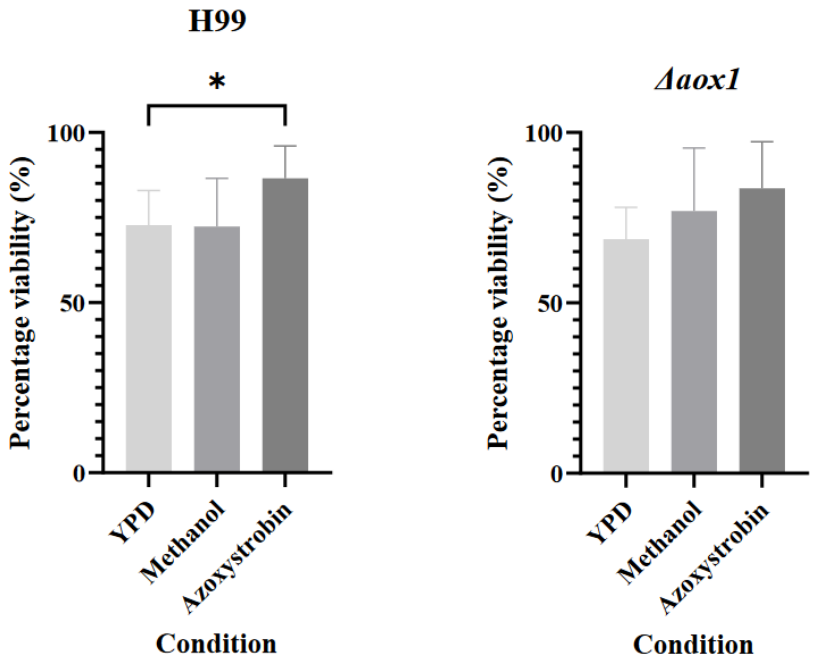

Figure 3.8: Viability assay of C. neoformans exposed to Azoxystrobin treatment.
The viability of wildtype (H99) and *Δaox1* null mutant (*Δaox1*) *C. neoformans* after a 2 h incubation with 20μM Azoxystrobin at 37°C as indicated (Azoxystrobin) in comparison to a YPD control and a methanol solvent control (Methanol). Significance was calculated using Dunnett's multiple comparisons test following a one-way ANOVA in GraphPad Prism. * <0.05. Error bars represent ± SD. n = 9.

3.2.8 *C. neoformans* Aox does not confer resistance to complex IV inhibition

After observing that the deletion of Aox conferred sensitivity to Complex III inhibition during growth and respiration, we wanted to assess whether Aox would confer resistance to Complex IV inhibition as seen in *C. albicans*[142, 213]. Firstly, we investigated the respiratory profile of H99 (Fig. 3.9a) and *Δaox1* mutant *C. neoformans* (Fig. 3.9b) using HRR. Respirometer chambers were inoculated with 1 x 10^6 cells from a culture grown for 24 h at 37°C and treated with 3mM KCN, a complex IV inhibitor, where indicated. Interestingly, addition of KCN did not induce any respiratory activity in either H99 (Fig. 3.9a) or *Δaox1* (Fig. 3.9b), unlike the induction of alternative respiration seen in *C. albicans*, indicating that *C. neoformans* Aox does not confer any KCN resistance.

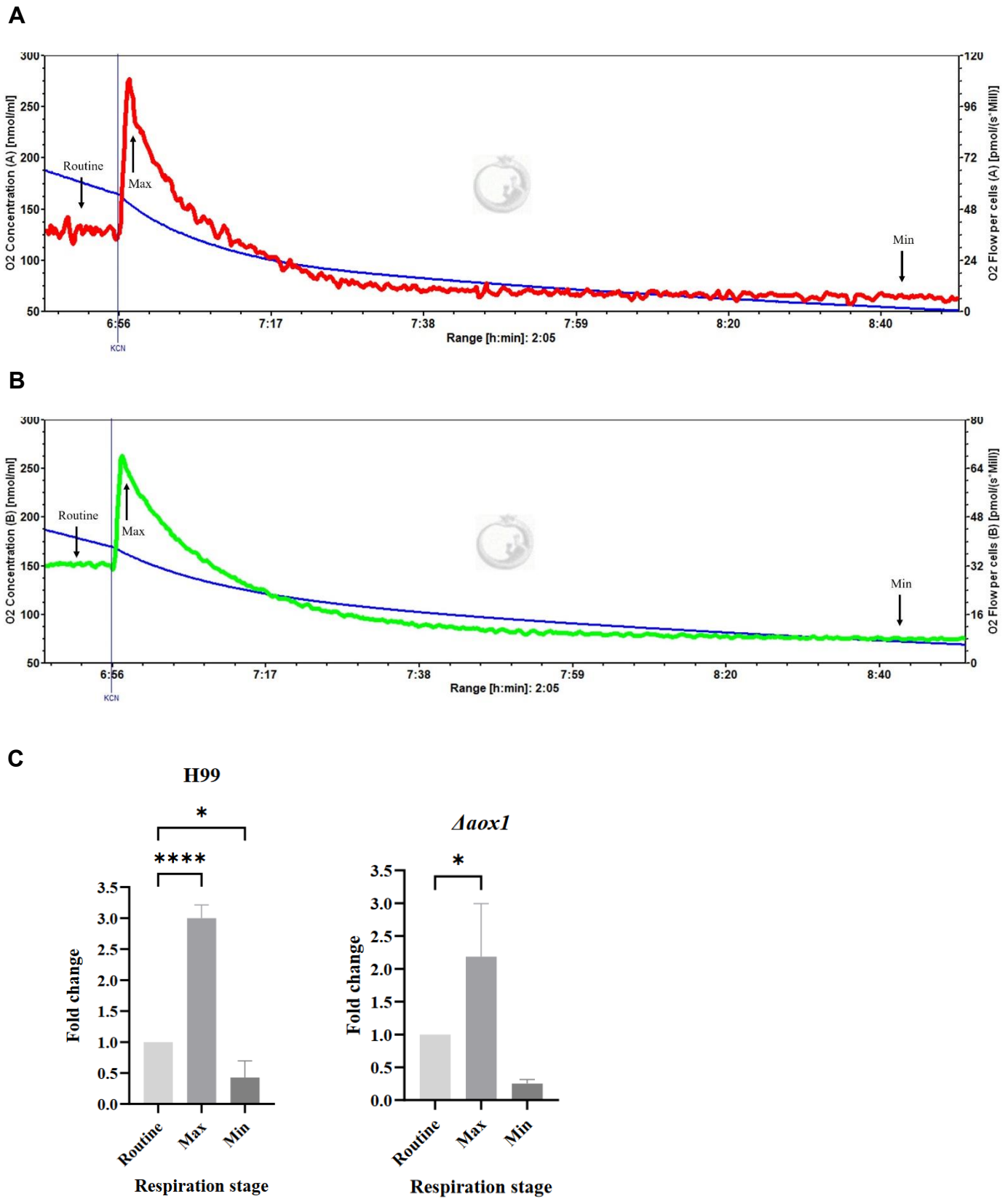

Figure 3.9: Respiratory profiles of C. neoformans strains exposed to KCN.
Representative example of respiration in H99 and *Δaox1* determined using HRR. Chambers were inoculated with 1 x 10^6 cells after 24 h growth and treated with KCN where indicated. (**A**) H99 (**B**) *Δaox1*. (**C**) Measurements of maximum (Max) and minimum (Min) respiration (O2 flow per cells) after drug exposure were taken and compared to the routine level of respiration (Routine) for each strain as indicated. Significance was calculated using Dunnett's multiple comparisons test following a one-way ANOVA in GraphPad Prism. * < 0.05 ** <0.005, **** <0.0001, where P = 0.05. Error bars represent ± SD. n = 3

After observation that Aox did not confer respiratory resistance to KCN (Fig. 3.9) we wanted to assess whether KCN addition affected the viability of *Δaox1*. Wildtype *C. neoformans* (H99) and *Δaox1* mutant cells were plated following a 2 h incubation in YPD containing KCN at 3mM at 37°C and viable colonies were counted after 48 h at 37°C. Interestingly, our data showed that Aox was not activated for respiratory resistance against KCN, but KCN had no significant effect on *Δaox1* viability (Fig. 3.10).

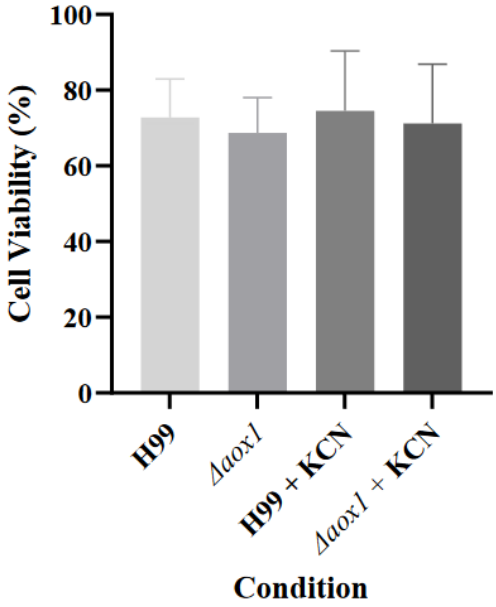

Figure 3.10: Viability assay of C. neoformans exposed to KCN treatment.
The viability of wildtype (H99) and *Δaox1* null mutant (*Δaox1*) *C. neoformans* after a 2 h incubation with 3mM KCN at 37°C as indicated (H99 + KCN, *Δaox1* + KCN) in comparison to a YPD control (H99, *Δaox1*). Significance was calculated using a two-tailed unpaired t-test in GraphPad Prism, where P = 0.05. no significance was recorded. Error bars represent ± SD. n = 9.

3.2.9 Screening a *C. neoformans* kinase knockout library for KCN sensitivity

Given the apparent inherent resistance of *C. neoformans* to KCN with respect to viability, we sought to identify putative regulators using an unbiased screening approach. To achieve this, we made use of a kinase knockout library generated by Kyung-Tae Lee et. al[272], grew each plate overnight in liquid YPD media and plated onto YPD agar containing 3mM KCN for 48 h at 37°C (Fig. 3.11). Plate maps for each knockout series can be found in Appendix 7.2.

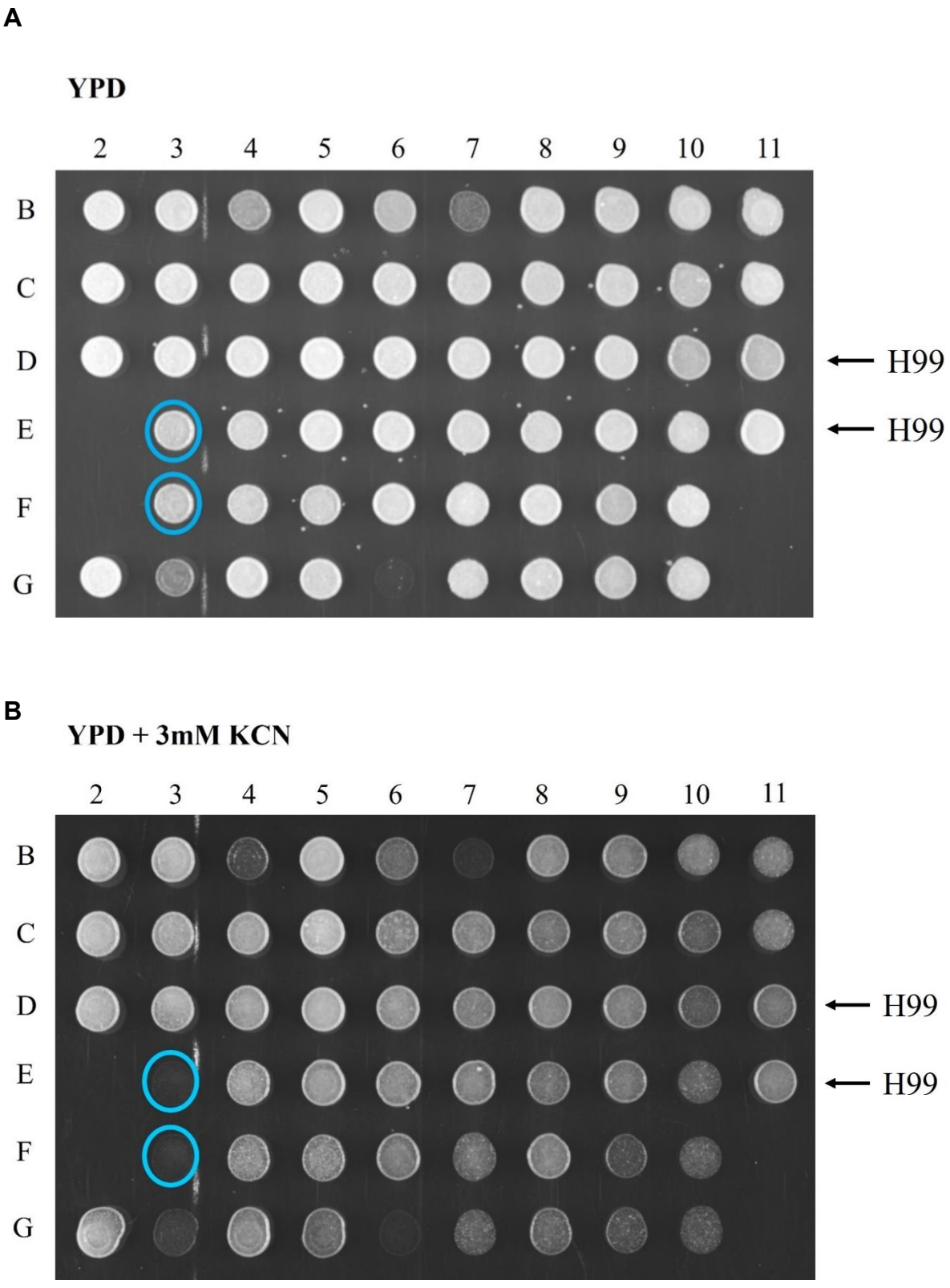

Figure 3.11: Representative example illustrating the determination of KCN sensitive kinase mutants.

(**A**) Kinase knockout mutant *C. neoformans* were grown on YPD plates and (**B**) plates containing YPD + 3mM KCN at 37°C for 48 h. Blue circled stamps show an example of sensitivity to KCN through loss of growth on the plate. Each knockout plate contained wildtype (H99) replicates for comparison where indicated. n = 3

As there were only two clones for each knockout in the screening plates, we performed multiple biological replicates of any knockout strains that showed sensitivity in the initial screen (Fig. 3.11). The initial screen identified a *Δypk1* mutant and a *Δarg5,6* mutant as sensitive to KCN, so we grew cultures of each strain overnight in liquid YPD media and plated onto YPD agar containing 3mM KCN for 48 h at 37°C. We confirmed that the *Δypk1* mutant (Fig. 3.12a), and the *Δarg5,6* mutant (Fig. 3.12b) showed reproducible sensitivity to KCN exposure, with the *Δypk1* mutant showing the strongest sensitivity (Fig. 3.12a). As Ypk1 has been implicated in mitochondrial function, fluconazole tolerance, sphingolipid biosynthesis, membrane maintenance, regulation of mitochondrial generated ROS for actin polarisation and regulated cell death[273, 290-292], we focused on *Δypk1*.

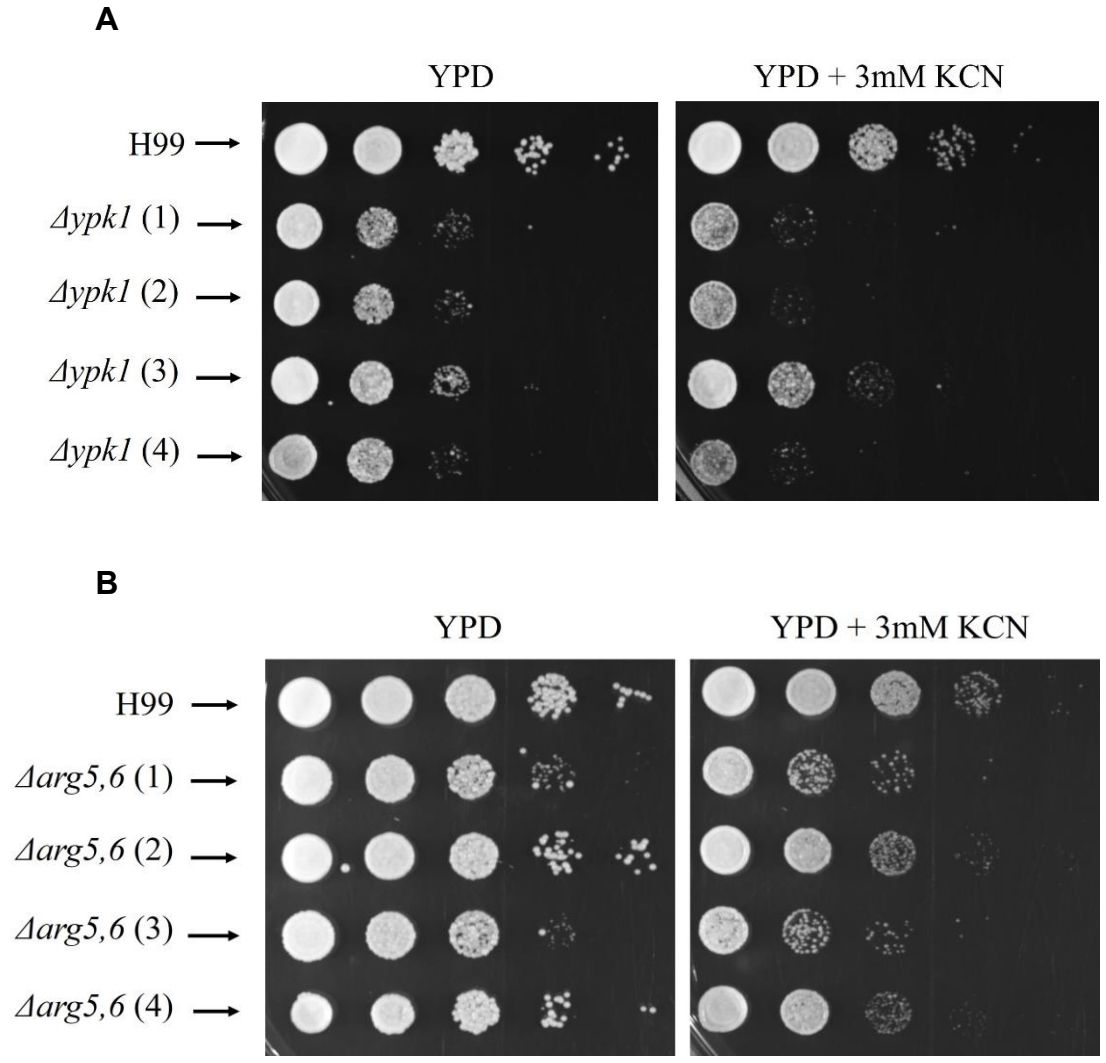

Figure 3.12: Identification of kinase mutant sensitivity to KCN stress
Confirmation of kinase mutant growth sensitivity at 37°C with a *Δypk1* mutant (**A**) and a *Δarg5,6* mutant (**B**) showing sensitivity to KCN at 3mM in comparison to a YPD control. n = 4

To confirm the phenotype seen in the repeated screens (Fig. 3.12a), we repeated the experiment with a strain set from the Chang lab[273] which included the parental strain of the mutant (H99P) *Δypk1* mutant, *Δypk1* mutant + YPK1 flag at the locus, and two kinase-dead mutants, *Δypk1* + YPK-K274A and *Δypk1* + YPK-D386A at both 30°C (Fig. 3.13a) and 37°C (Fig. 3.13b). As expected loss of Ypk1 led to KCN sensitivity that could be rescued by the re-expression of a YPK1-flag but not by either kinase dead mutant at 30°C (Fig. 3.13a), or 37°C (Fig. 3.13b).

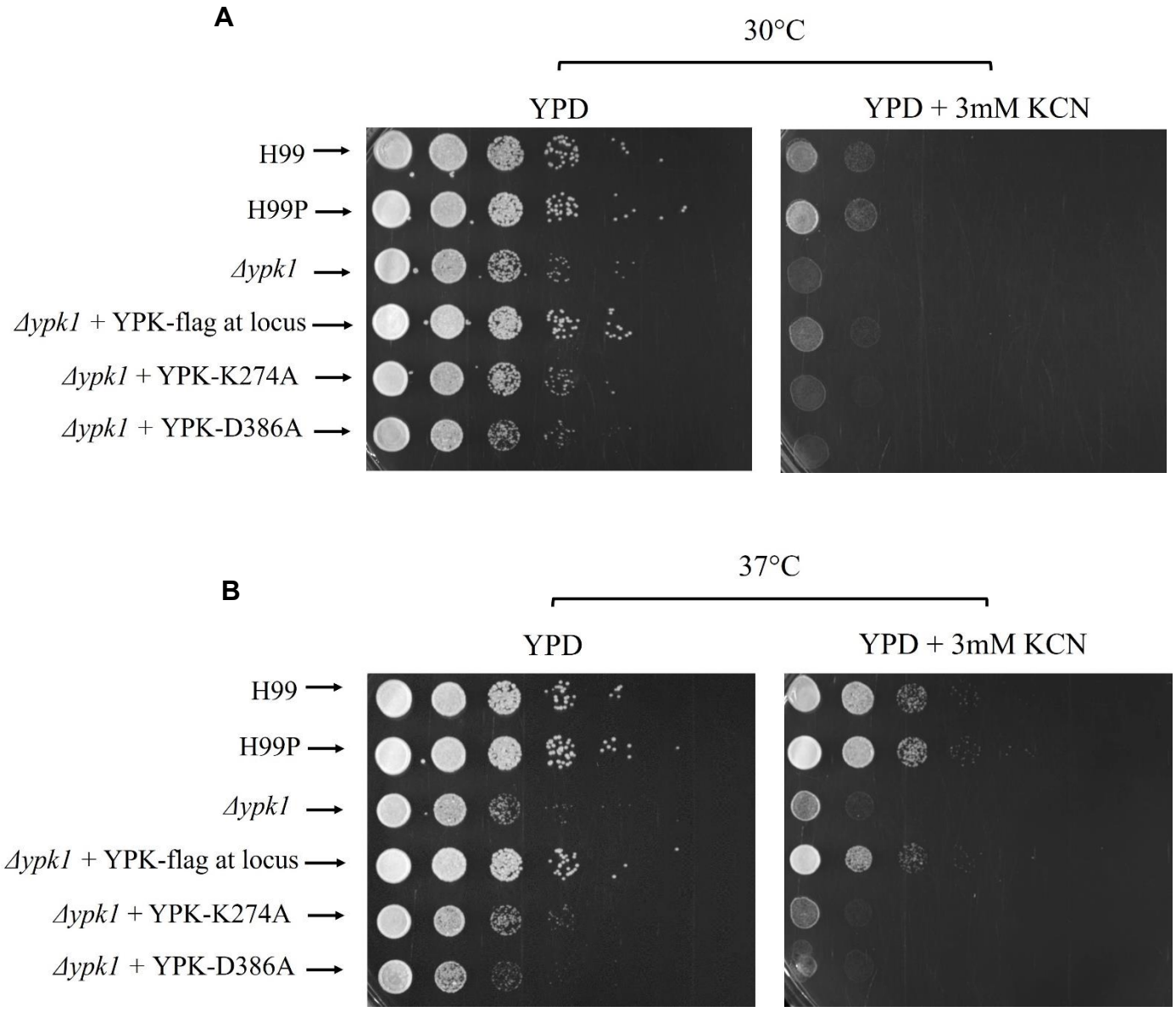

Figure 3.13: Confirmation of Δypk1 mutant sensitivity to KCN stress.
Confirmation of *Δypk1* sensitivity to KCN in reference to a lab wildtype strain (H99), the parental H99 strain (H99P) a *Δypk1* mutant + YPK1 flag at the locus, and two kinase-dead mutants, *Δypk1* + YPK-K274A and *Δypk1* + YPK-D386A was carried out at 30°C (**A**) and 37°C (**B**). n = 3

3.2.10 Ypk1 is required to maintain *C. neoformans* respiration

To assess whether the growth inhibition seen in Fig. 3.13 was due to respiratory disruption, we investigated the respiratory profile of H99 and *Δypk1* mutant *C. neoformans* using HRR. Respirometer chambers were inoculated with 1 x 10^6 cells from a culture grown for 24 h at 37°C and treated with 3mM KCN where indicated (Fig. 3.14). Our data suggested that loss of Ypk1 led to a dramatic reduction in respiration that was only partially rescued by the YPK1-flag re-integration, which was unexpectedly restored by expression of the kinase dead Ypk1 mutants (Fig. 3.14f). We also observed that KCN addition led to a significant spike in oxygen consumption in all strains (Max) followed by a drop to routine levels (Fig. 3.14a), although this spike was not statistically significant in the *Δypk1* mutant (Fig. 3.14g). All of the strains tested mirrored the effect seen in the wildtype (Fig. 3.14a) whereby no induction of alternative respiration was seen. Interestingly, the kinase dead mutant *Δypk1* + YPK-D386A, however, did show a slower decline in respiration rate after the maximum respiratory spike induced by KCN addition (Fig. 3.14e). This data suggests that Ypk1 is required for controlling routine respiration and loss of this kinase may also affect rapid oxygen consumption.

A

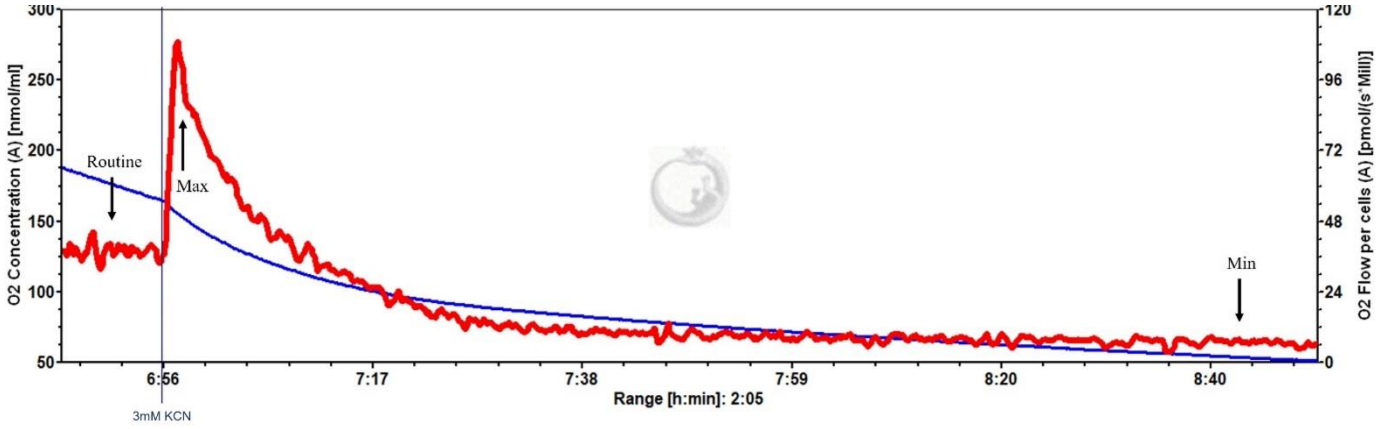

B

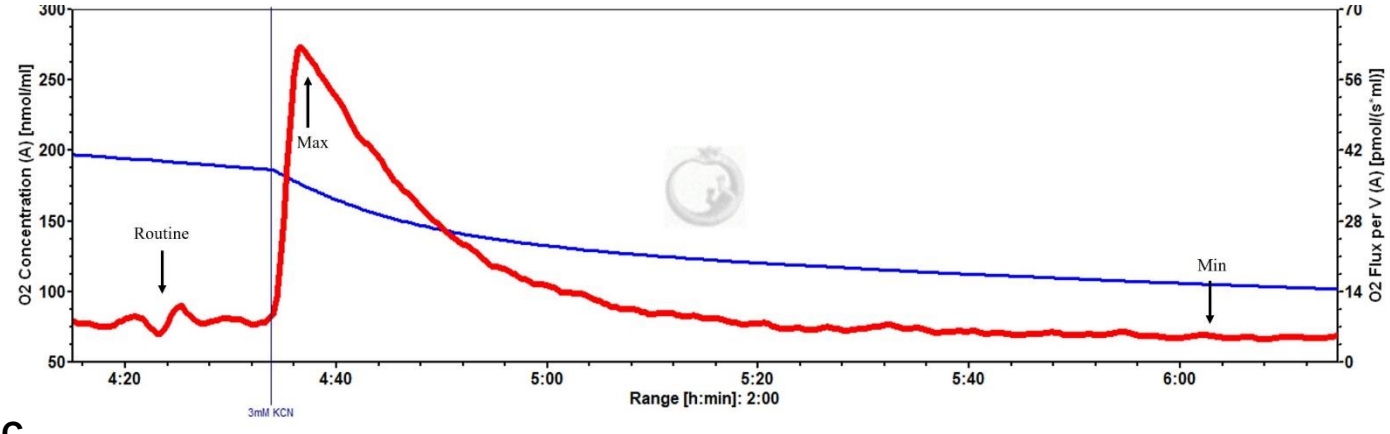
O2 Concentration (A) [nmol/ml]
O2 Flux per V (A) [pmol/(s*ml)]
Max
Routine
Min
3mM KCN
Range [h:min]: 2:00

C

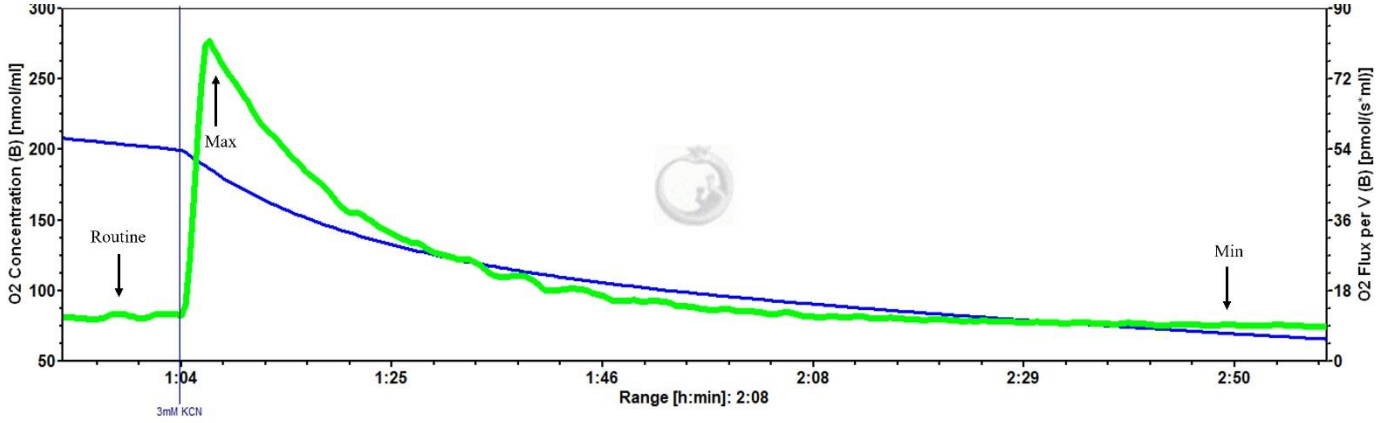
O2 Concentration (B) [nmol/ml]
O2 Flux per V (B) [pmol/(s*ml)]
Max
Routine
Min
3mM KCN
Range [h:min]: 2:08

D

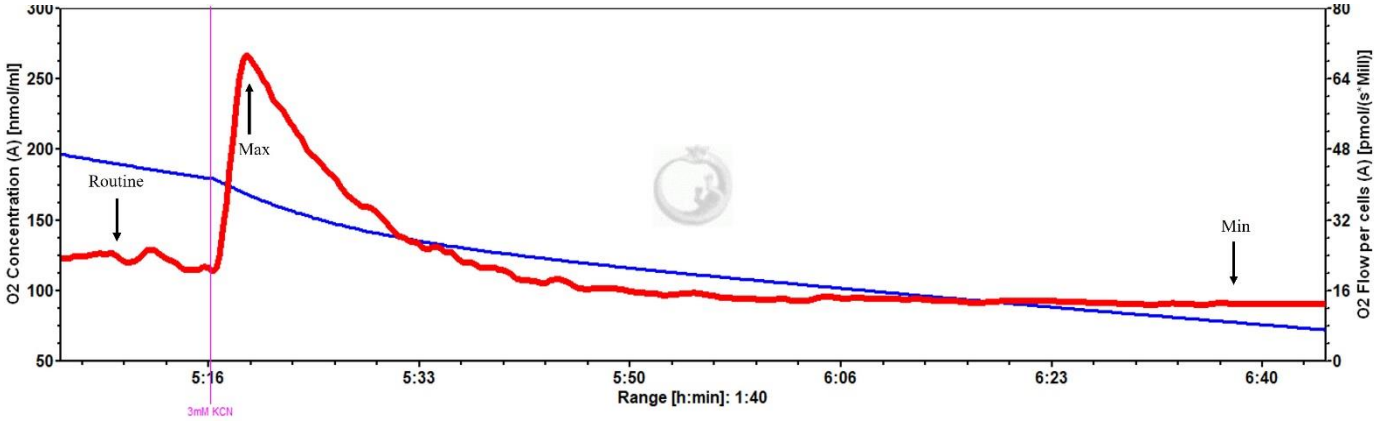
O2 Concentration (A) [nmol/ml]
O2 Flow per cells (A) [pmol/(s*Mill)]
Max
Routine
Min
3mM KCN
Range [h:min]: 1:40

E

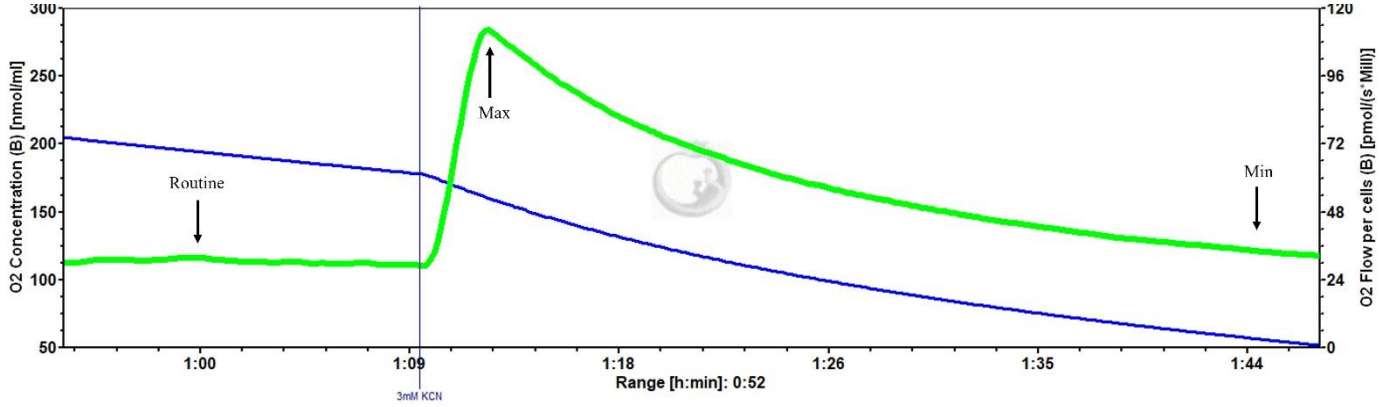
O2 Concentration (B) [nmol/ml]
O2 Flow per cells (B) [pmol/(s*Mill)]
Max
Routine
Min
3mM KCN
Range [h:min]: 0:52

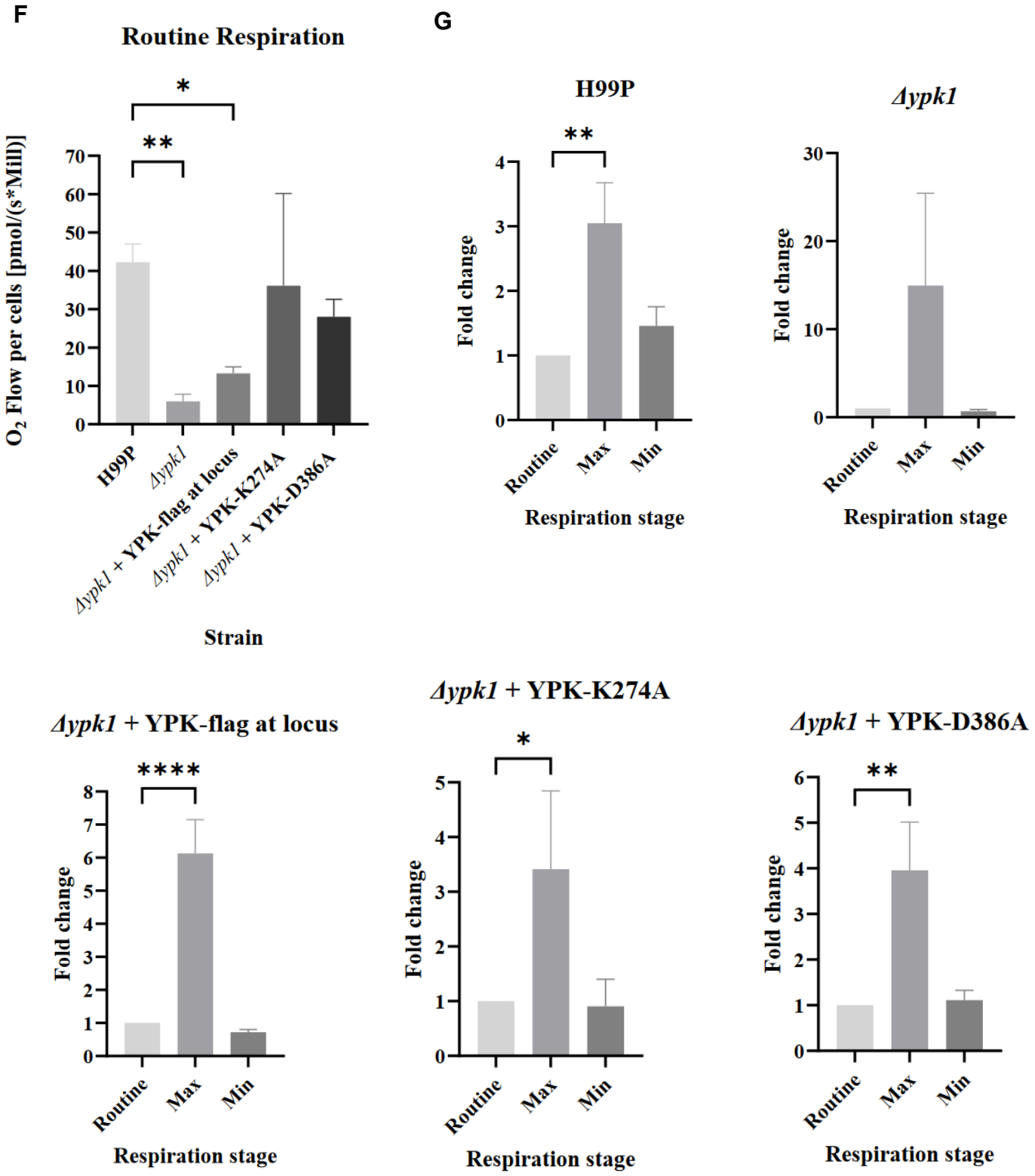

Figure 3.14: Respiratory profiles of Δypk1 mutant C. neoformans exposed to KCN.
Representative example of respiration in H99 and *Δaox1* determined using HRR. Chambers were inoculated with 1 x 10^6 cells after 24 h growth and treated with KCN where indicated (**A**) H99 Parental (H99P) + KCN, (**B**) *Δypk1* + KCN, (**C**) *Δypk1* mutant + YPK1 flag at the locus + KCN, (**D**) *Δypk1* + YPK-K274A + KCN, (**E**) *Δypk1* + YPK-D386A + KCN. Measurements of routine respiration were taken and compared across all strains (**F**) Maximum (Max) and minimum (Min) respiration (O2 flow per cells) after drug exposure were taken and compared to the routine level of respiration (Routine) for each strain as indicated in (**G**). Significance was calculated using Dunnett's multiple comparisons test following a one-way ANOVA in GraphPad Prism. * <0.05, ** <0.005, **** <0.0001, where P = 0.05. Error bars represent ± SD. n = 3

3.2.11 Loss of Ypk1 does not decrease *C. neoformans* melanisation under KCN stress

After assessing that Ypk1 is required for normal respiration and given the known links between mitochondrial function and stress response we wanted to investigate the effects of loss of Ypk1 upon exposure to mitochondrial stress. Parental H99 *C. neoformans* (H99P), a *Δypk1* mutant, a *Δypk1* mutant + YPK1 flag at the locus, and two kinase dead mutants, *Δypk1* + YPK-K274A and *Δypk1* + YPK-D386A, were treated with either YPD or 3mM KCN for 2 h at 37°C. They were then plated onto melanisation agar (Section 2.5.7) for a further incubation at 30°C (Fig. 3.15a) or 37°C (Fig. 3.15b) for 2 or 3 days, respectively. Mean grey values were measured in ImageJ and significance was recorded in GraphPad Prism after background correction, in comparison to a YPD control. Loss of Ypk1 led to a significant increase in melanisation, but this was not rescued by expression of the YPK1-flag. Our data also showed that KCN addition did not affect the *Δypk1* mutant and *Δypk1* mutant + YPK1 flag at the locus melanisation response at 30°C (Fig. 3.15a) or 37°C (Fig. 3.15b) although the kinase dead mutant *Δypk1* + YPK-D386A showed far lower melanisation capacity across all conditions. This indicated that the D386A residue is essential for the melanisation response, but in conjunction with our data from Fig. 3.14 showing that KCN did not inhibit *Δypk1* + YPK-D386A respiration, we can conclude that melanisation is not linked to the classical ETC by Ypk1. However, we cannot rule out the possibility that the strain set used may contain a background mutation that affects melanisation independently of Ypk1.

A

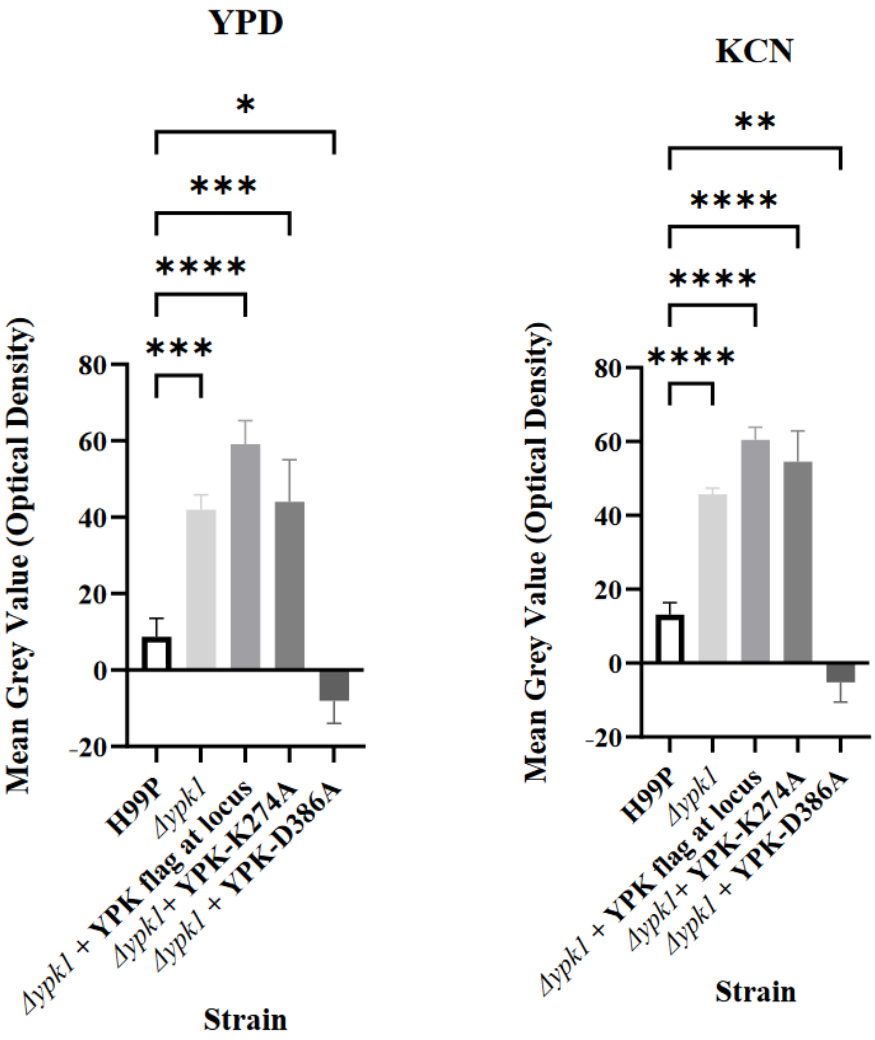
YPD
KCN
Mean Grey Value (Optical Density)
80
60
40
20
0
-20
*
***
****
**
H99P
Δypk1
Δypk1 + YPK flag at locus
Δypk1+ YPK-K274A
Δypk1 + YPK-D386A
Strain

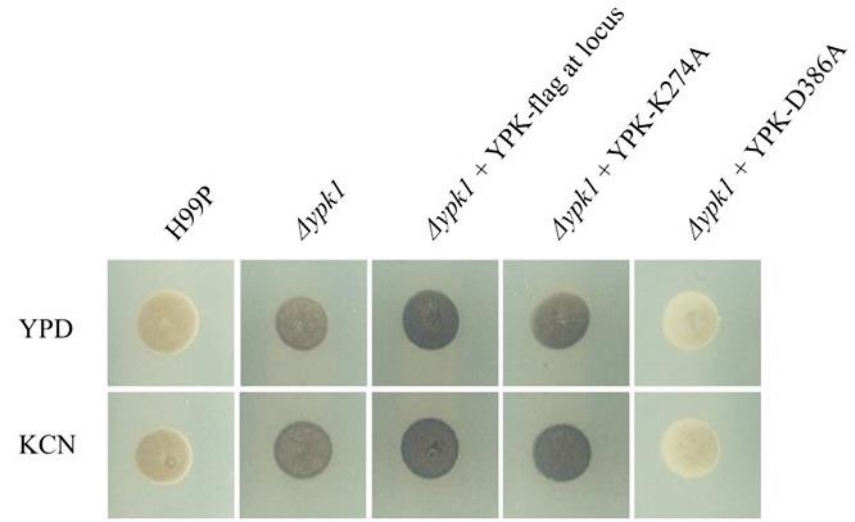
H99P
Δypk1
Δypk1 + YPK-flag at locus
Δypk1 + YPK-K274A
Δypk1 + YPK-D386A
YPD
KCN

B

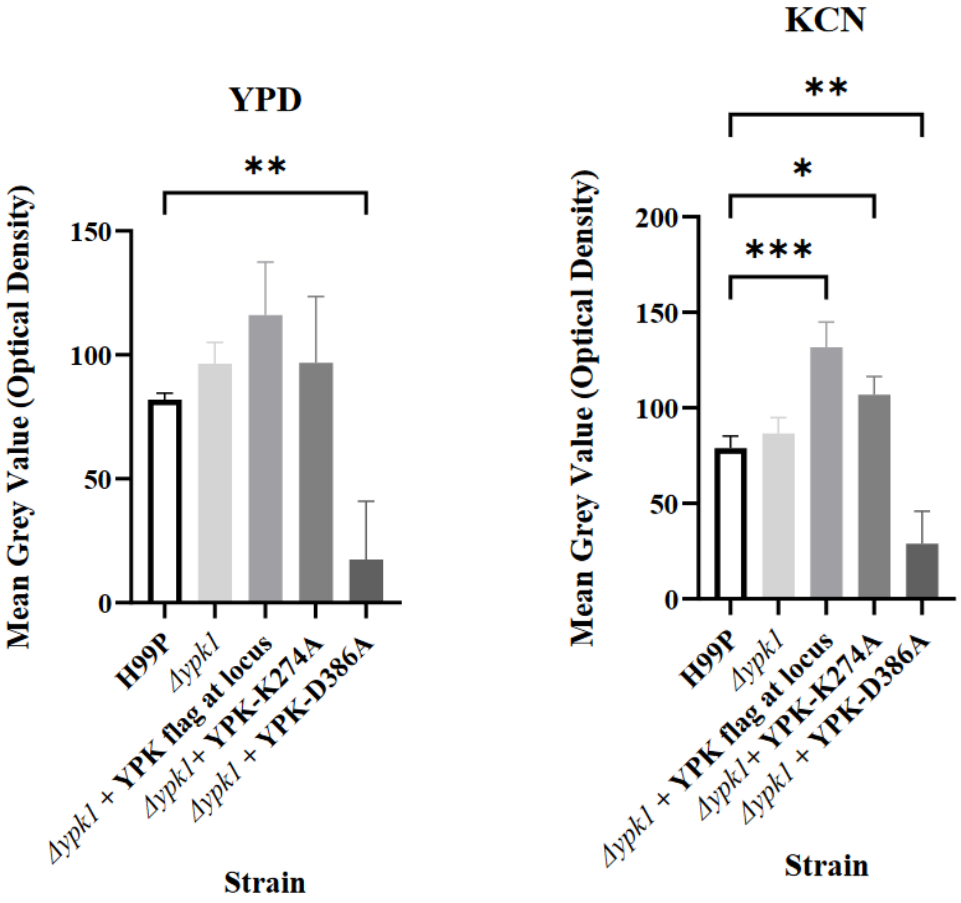

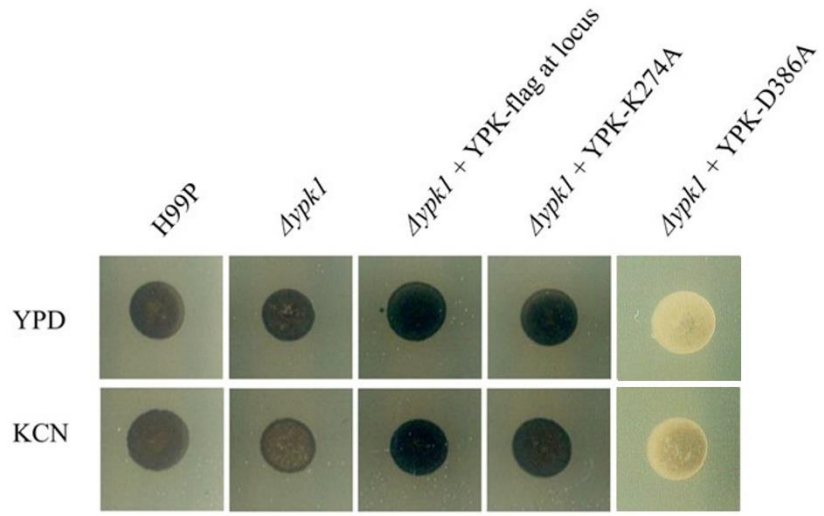

Figure 3.15: Melanisation of Δypk1 mutant C. neoformans treated with KCN.
Parental H99 *C. neoformans* (H99P), *Δypk1* mutant *C. neoformans,* a *Δypk1* mutant + YPK1 flag at the locus, and two kinase dead mutants, *Δypk1* + YPK-K274A and *Δypk1* + YPK-D386A were treated with either YPD or 3mM KCN for 2 h at 37°C. Treated cultures were then plated onto melanisation plates containing L-DOPA and incubated at either 30°C (**A**) or 37°C (**B**). Mean grey values were measured in ImageJ and following background correction, significance was calculated using Dunnett's multiple comparisons test following a one-way ANOVA in GraphPad Prism. * <0.05, ** <0.005, *** < 0.0005, **** <0.0001, where P = 0.05. Error bars represent ± SD. n = 3

3.2.12 Screening for the effect of Azoxystrobin on *Δypk1* mutant *C. neoformans*

As we had observed different responses to mitochondrial stress between Complex III and Complex IV inhibition in relation to Aox, we also tested the effects of Azoxystrobin addition (Complex III inhibition) on cells lacking Ypk1 function. Parental H99 *C. neoformans* (H99P), *Δypk1* mutant *C. neoformans,* a *Δypk1* mutant + YPK1 flag at the locus, and two kinase dead mutants, *Δypk1* + YPK-K274A and *Δypk1* + YPK-D386A were screened for Azoxystrobin sensitivity though plating on YPD containing 20μM Azoxystrobin for 48 h at 30°C (Fig. 3.16a) and 37°C (Fig. 3.16b). Interestingly, *Δypk1*, *Δypk1* + YPK-K274A and *Δypk1* + YPK-D386A all showed sensitivity to Azoxystrobin which was most prominent at 37°C (Fig. 3.16b).

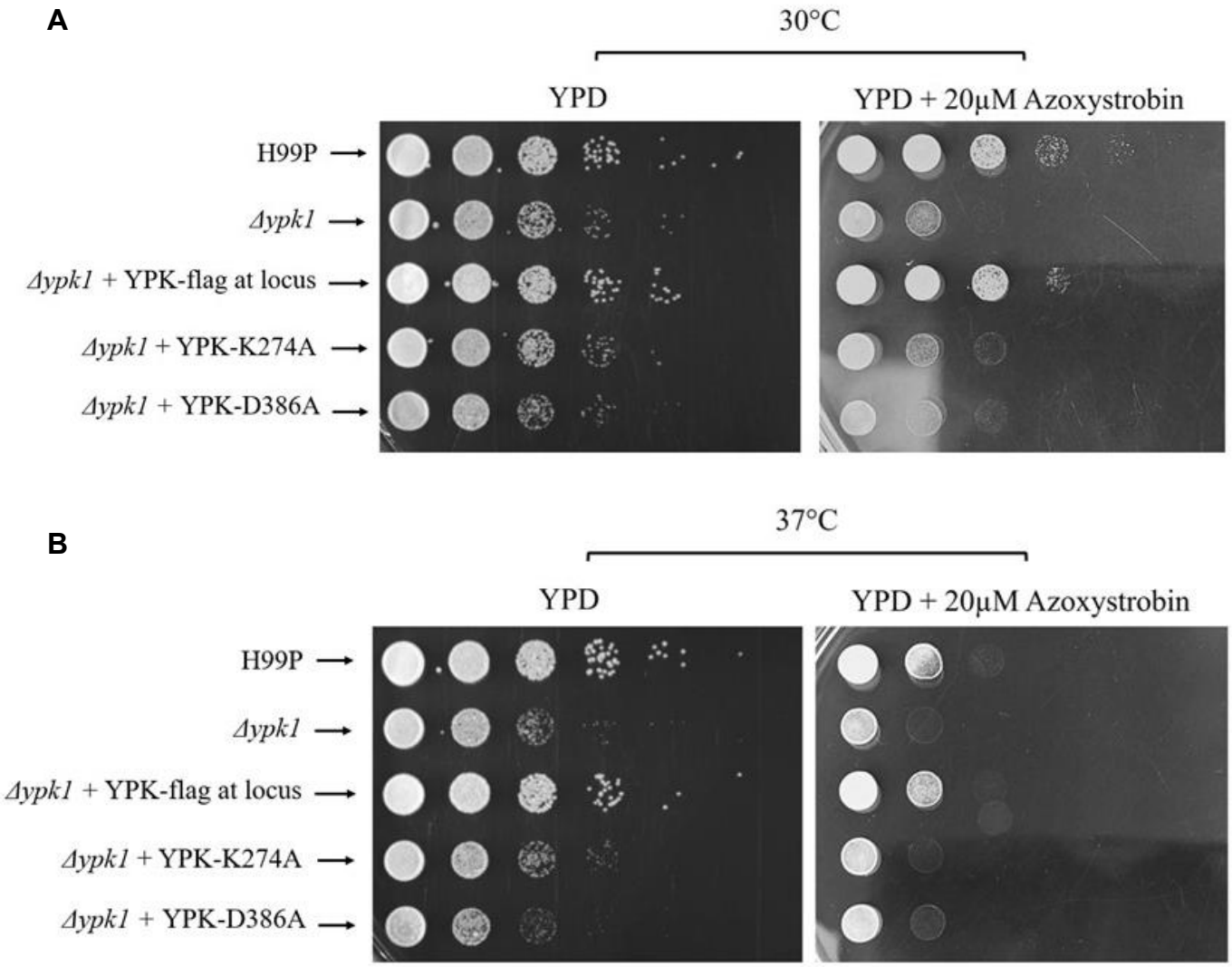

Figure 3.16: Identification of Δypk1 mutant sensitivity to Azoxystrobin stress.
Confirmation of *Δypk1* sensitivity to 20μM Azoxystrobin in reference to the parental H99 strain (H99P) a *Δypk1* mutant + YPK1 flag at the locus, and two kinase-dead mutants, *Δypk1* + YPK-K274A and *Δypk1* + YPK-D386A was carried out at 30°C (**A**) and 37°C (**B**). n = 3.

3.2.13 *Δypk1* mutant *C. neoformans* is sensitive to growth inhibition by Azoxystrobin

To confirm the result of the Azoxystrobin sensitivity (Section 3.2.12) in liquid media, parental H99 *C. neoformans* (H99P), *Δypk1* mutant *C. neoformans,* a *Δypk1* mutant + YPK1 flag at the locus, and two kinase dead mutants, *Δypk1* + YPK-K274A and *Δypk1* + YPK-D386A, were screened for Azoxystrobin sensitivity in comparison to a methanol solvent control (Fig. 3.17b). Interestingly, while *Δypk1* and *Δypk1* + YPK-K274A were sensitive to growth inhibition by both methanol (Fig. 3.17b) and Azoxystrobin (Fig. 3.17c) the kinase dead mutant *Δypk1* + YPK-K274A showed slower growth in the presence of methanol but was more sensitive to Azoxystrobin (Fig. 3.17c). However, the sensitivity of *Δypk1* mutants to Azoxystrobin and methanol could be rescued by expression of a YPK1-flag (Fig. 3.17b, 3.17c).

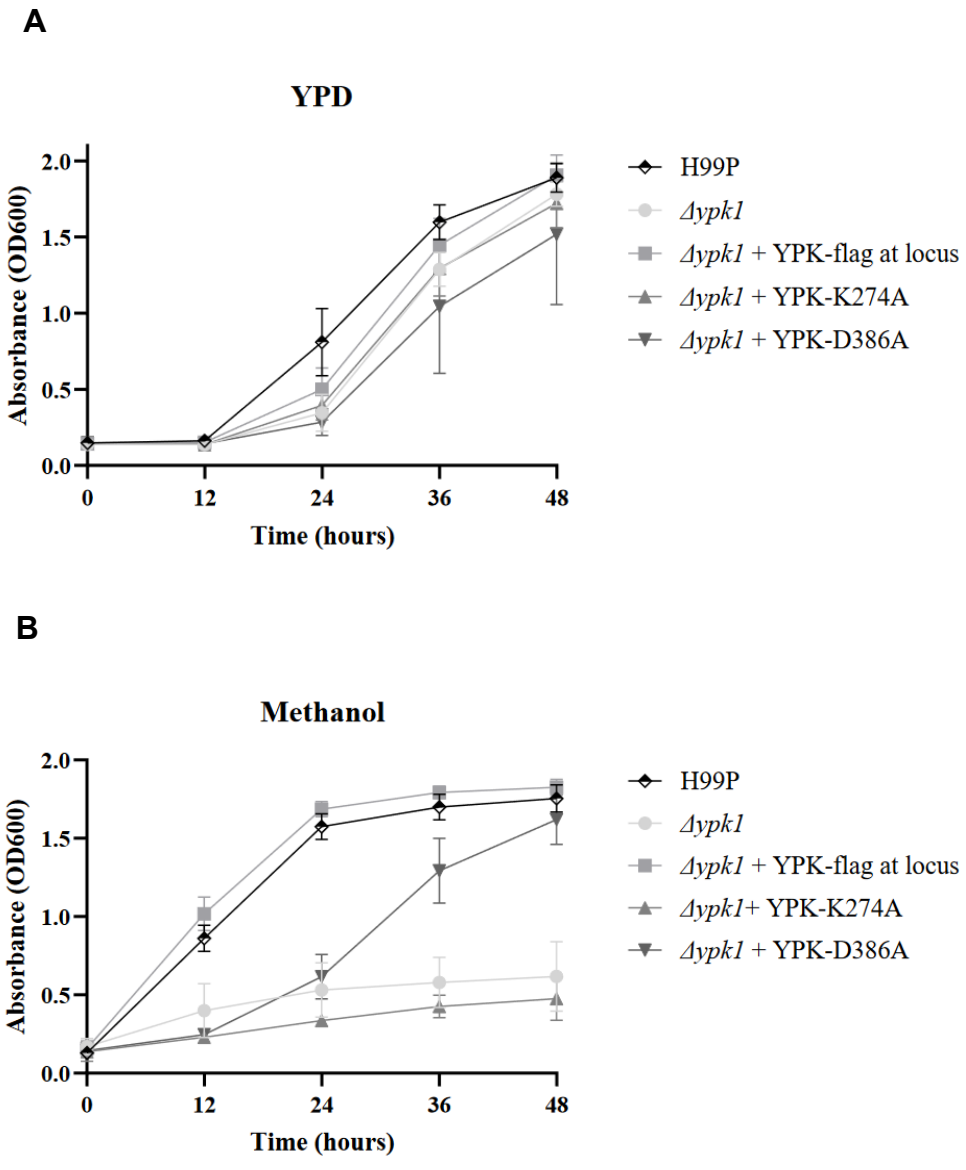

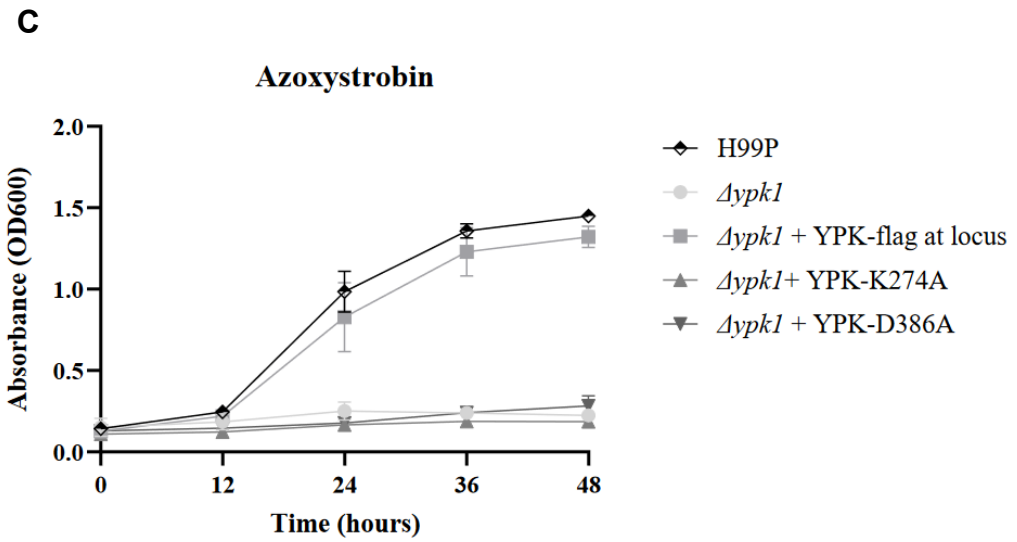

Figure 3.17: Screening for the effect of Azoxystrobin on Δypk1 mutant C. neoformans. Parental H99 *C. neoformans* (H99P), *Δypk1* mutant *C. neoformans,* a *Δypk1* mutant + YPK1 flag at the locus, and two kinase-dead mutants, *Δypk1* + YPK-K274A and *Δypk1* + YPK-D386A cultures were grown in (**A**) YPD, (**B**) YPD + Methanol and (**C**) YPD + 20μM Azoxystrobin for 48 h at 37°C. Graphs were created in GraphPad Prism. Error bars represent ± SD. n=9

3.2.14 *Δypk1* melanisation is not significantly affected by Azoxystrobin

After assessing that *Δypk1* mutant is sensitive to growth inhibition by Azoxystrobin, a melanisation assay was carried out to assess the effect of loss of Ypk1 upon exposure to mitochondrial stress via Complex III inhibition. Parental H99 *C. neoformans* (H99P), *Δypk1* mutant *C. neoformans,* a *Δypk1* mutant + YPK1 flag at the locus, and two kinase dead mutants, *Δypk1* + YPK-K274A and *Δypk1* + YPK-D386A cultures were inoculated with YPD containing 20μM Azoxystrobin for 2h at 37°C. They were then plated onto melanisation agar for a further incubation at 30°C (Fig. 3.18a) or 37°C (Fig. 3.18b) for 2 or 3 days, respectively. Mean grey values were measured in ImageJ and significance was recorded in GraphPad Prism after background correction, in comparison to both a YPD control and a methanol control. Interestingly, Azoxystrobin addition did not seem to significantly affect melanisation of any strain tested at 30°C (Fig. 3.18a) or 37°C (Fig. 3.18b) in comparison to a YPD or methanol control but *Δypk1* + YPK-D386A showed lower melanisation capacity at both 30°C (Fig. 3.18a) and 37°C (Fig. 3.18b), which confirmed the phenotype seen in Fig. 3.15.

A

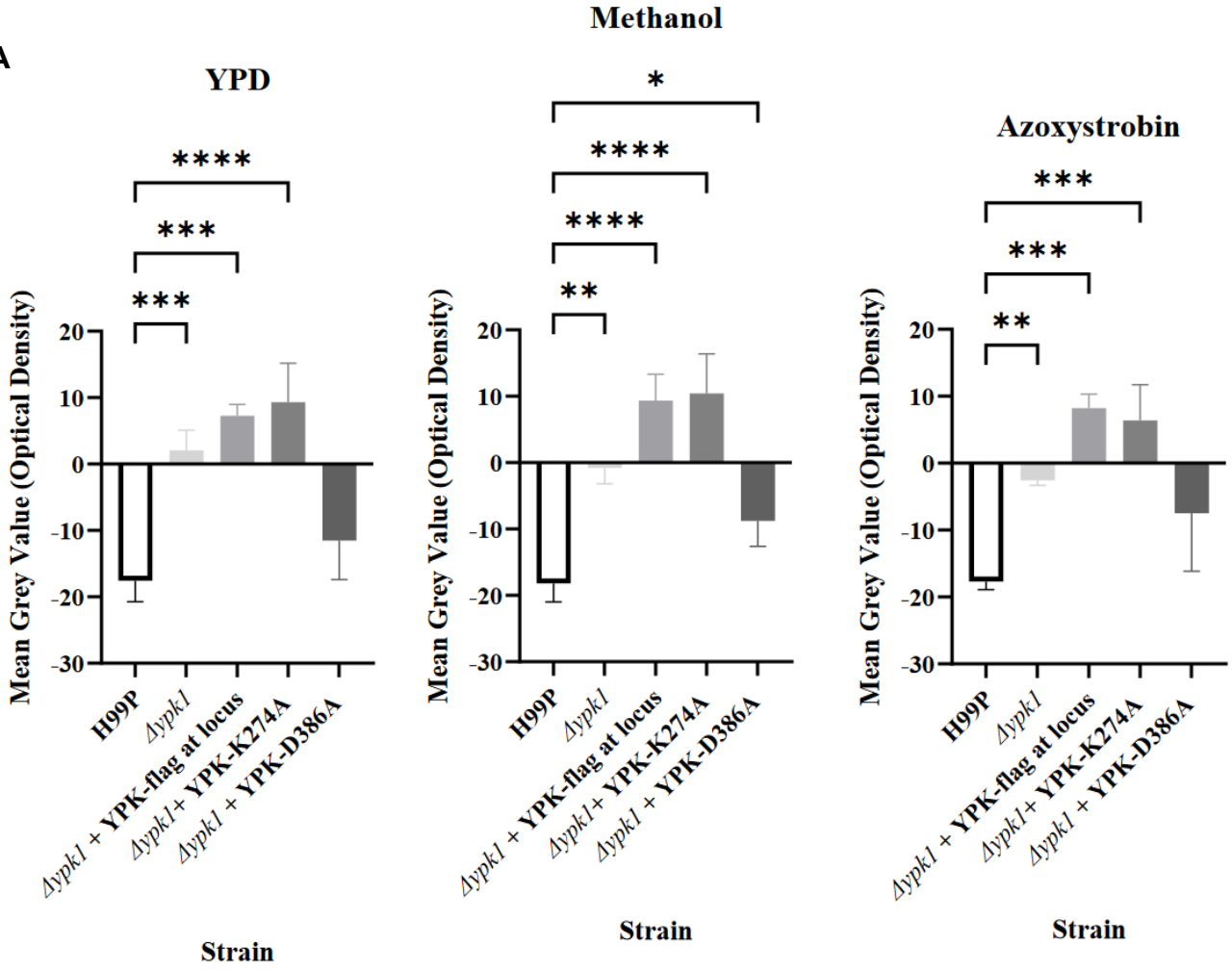
YPD
Methanol
Azoxystrobin
Mean Grey Value (Optical Density)
20
10
0
-10
-20
-30
****
***
**
*
H99P
Δypk1
Δypk1 + YPK-flag at locus
Δypk1+ YPK-K274A
Δypk1 + YPK-D386A
Strain

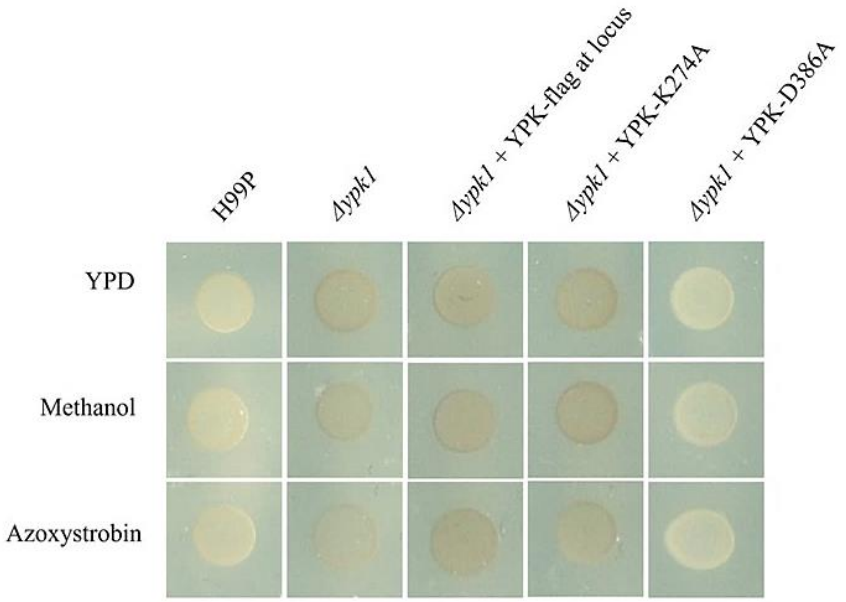
H99P
Δypk1
Δypk1 + YPK-flag at locus
Δypk1 + YPK-K274A
Δypk1 + YPK-D386A
YPD
Methanol
Azoxystrobin

B

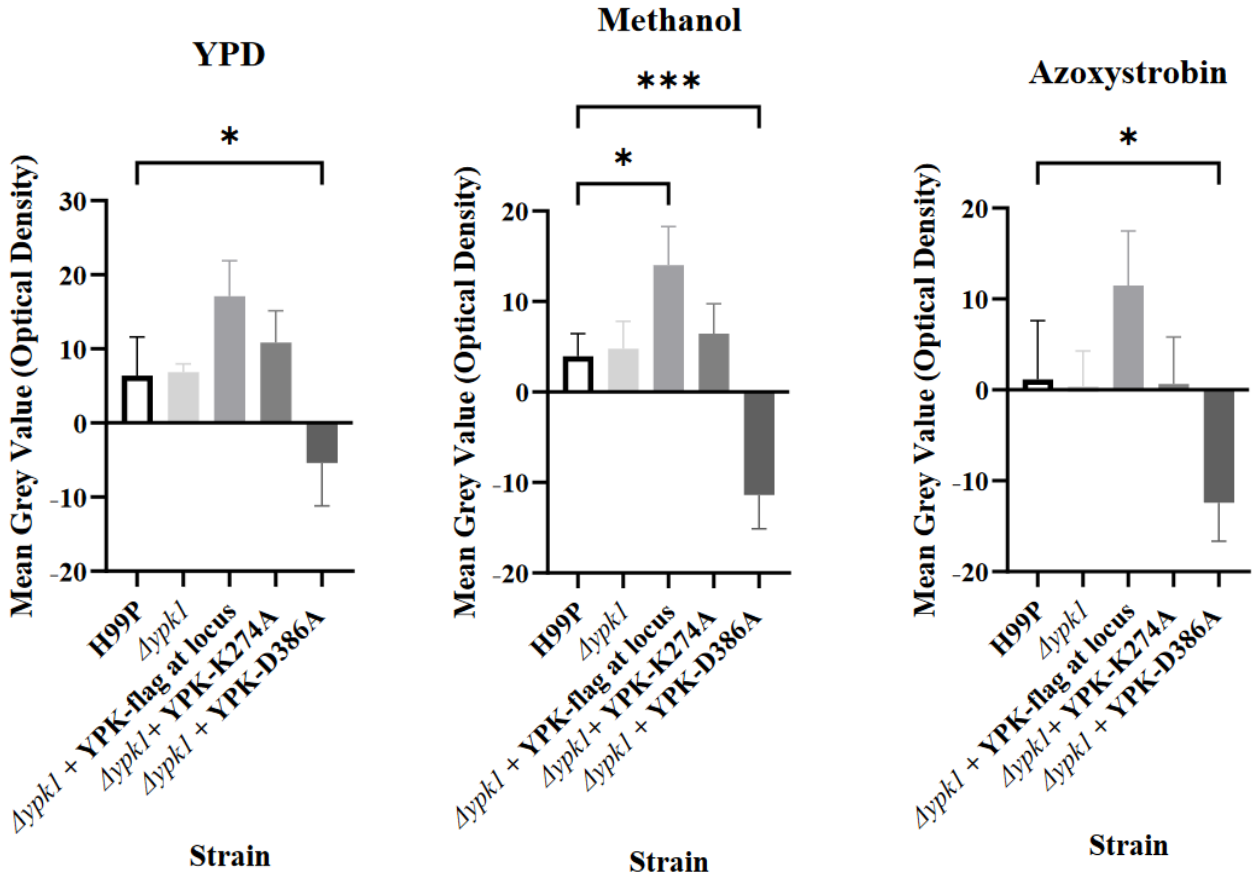

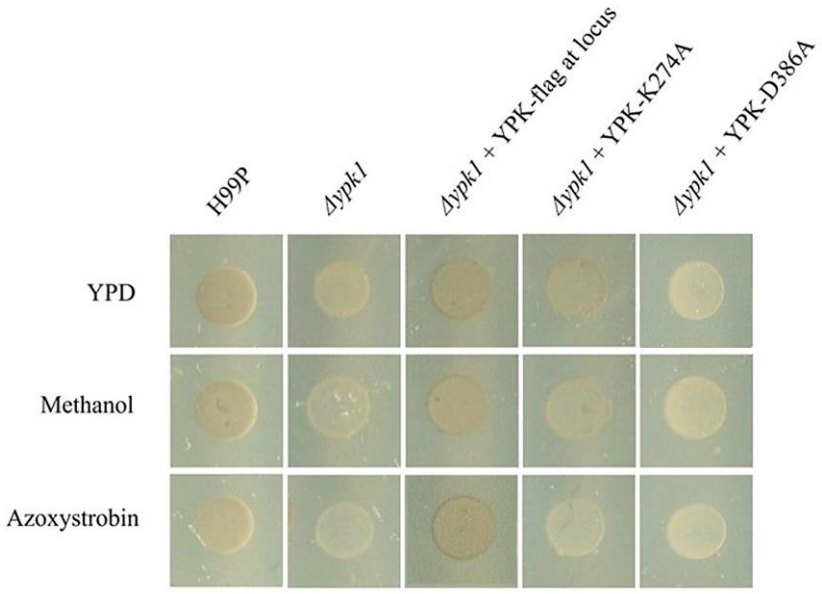

Figure 3.18: Melanisation of Δypk1 mutant C. neoformans treated with Azoxystrobin. Parental H99 *C. neoformans* (H99P), *Δypk1* mutant *C. neoformans,* a *Δypk1* mutant + YPK1 flag at the locus, and two kinase dead mutants, *Δypk1* + YPK-K274A and *Δypk1* + YPK-D386A were treated with YPD, a methanol solvent control, or 20μM Azoxystrobin for 2 h at 37°C. Treated cultures were then plated onto melanisation plates containing L-DOPA and incubated at either 30°C (**A**) or 37°C (**B**). Mean grey values were measured in ImageJ and following background correction, significance was calculated using Dunnett's multiple comparisons test following a one-way ANOVA in GraphPad Prism. * <0.05, ** <0.005, *** < 0.0005, **** <0.0001, where P = 0.05. Error bars represent ± SD. n = 3

3.3 Discussion

3.3.1 *C. neoformans* Aox shows high sequence homology to oleaginous, non-pathogenic yeasts

Our data suggested that *C. neoformans* Aox showed a high sequence homology to Aox enzymes from oleaginous yeasts found in warm, rich soil and water areas like mangroves (Fig. 3.1). However, some *Trichosporon* species that showed high Aox sequence homology such as *Trichosporon asahii* are known for varied clinical manifestations in immunocompromised patients[293]. Oleaginous yeasts are defined as yeasts that have a high number of intracellular and extracellular lipids and triacylglycerides, making up at least 20% of the whole cell mass[294]. However, *Cutaneotrichosporon* species can generate up to 70% of its dry cell mass as lipids when utilising aromatics as a carbon source[295] and as such are of interest to the biotechnology industry for sustainable lipid resources. *C. neoformans* Aox showed high sequence similarity to oleaginous yeasts rather than key human fungal pathogens, but still maintained conserved residues linked to iron binding (Appendix 7.1b). This, along with our data showing that Aox did not actively contribute to normal respiration (Fig. 3.5), indicates that *C. neoformans* may not rely on Aox directly for pathogenicity, but rather regular cellular stress maintenance such as membrane integrity, lipid shuttling and remodelling, which may be a viable target for future therapeutics.

3.3.2 *C. neoformans* Aox is required for resistance to Complex III inhibition

Following our observation that Aox was not actively contributing to respiration during normal growth, we wanted to assess whether Aox activity was inducible under mitochondrial stress. Interestingly, when mitochondrial Complex III was inhibited by Azoxystrobin, a variable-sensitivity phenotype was observed for *Δaox1* in both growth (Fig. 3.6) and respiration (Fig. 3.7) whereby the population either displayed complete sensitivity or robust growth and respiration under the same conditions. For wildtype *C. neoformans*, however, there was little effect of Azoxystrobin availability on growth (Fig.

3.6a) and Azoxystrobin addition led to an increase in respiration (Fig. 3.7a) and viability (Fig. 3.8), which indicates that Azoxystrobin induces Aox activity in the wildtype.

While our data suggested that *C. neoformans* sensitivity to Azoxystrobin was Aox dependent, the variable sensitivity seen by *Δaox1* did not confer a loss of viability (Fig. 3.8). One possibility is that Aox is involved in a switch to a quiescent state under conditions of mitochondrial stress. This induced quiescence, also referred to as dormancy in cryptococcosis, is a well-known phenomenon in which patients undergo latent infection, which can then reactivate upon immunosuppression[114]. It is thought that this dormancy switch is used to resist and survive extreme stresses, resulting in metabolically quiescent cells that are viable, but non-culturable (VBNC)[296]. Studies have shown that VBNC cells have low metabolic activity, but high mitochondrial mass and specific proteomic secretion patterns which are critical for survival within the host[296]. Interestingly, the mitochondrial fatty acid pathway and acetyl-CoA are thought to be involved in VBNC generation and maintenance, so it is tempting to speculate that *C. neoformans* Aox could act as a switch involved in generation of the VBNC phenotype, perhaps through fatty acid signalling.

3.3.3. *C. neoformans* Aox does not confer resistance to Complex IV inhibition

After establishing that Aox was required for resistance to Complex III inhibition, we wanted to investigate the effect of Complex IV inhibition on *C. neoformans* via KCN addition. Interestingly, although Azoxystrobin addition led to a variable phenotype in *Δaox1* mutant populations, addition of KCN did not induce respiration (Fig. 3.9) or a change in viability (Fig. 3.10) in both wildtype and *Δaox1* mutant *C. neoformans.* This, in conjunction with our data showing no reduction in viability after Azoxystrobin treatment (Fig. 3.8), indicated that *C. neoformans* is able to survive under conditions of mitochondrial stress, but this does not seem to require Aox induction.

Our data so far suggests that Aox induction may be linked to the activity of Complex III, while inhibition of Complex IV is not coupled to Aox regulation (at protein level or activity). It is well known that inhibition of Complex III stops electron transfer, leading to a disruption of FET and generating a

build-up of electrons in the UQP which contributes to ROS production[297]. Given that Complex III and Aox share the same source of electrons from the UQP, but Complex IV does not, this data supports the given proposal in Section 1.3.8., where we suggested that an accumulation of electrons in the UQP and loss of FET may induce RET via Aox, and high ΔpH or ROS may act as a signal for VBNC cell induction. We may be able to test for this by investigating the culturability and viability of both wildtype cells and *C. neoformans* cells lacking Aox, using changes in pH and ROS inducing agents such as hydrogen peroxide (H_2O_2), followed by treatment with pantothenic acid. Given that VBNC cells are able to survive stress but reactivate upon treatment with pantothenic acid [298], this would allow us to test whether VBNC is induced and whether this process is reliant on Aox activity.

3.3.4 Ypk1 is required for resistance to Complex III and Complex IV inhibition

Following our findings that Aox is not involved in resistance to Complex IV inhibition, we wanted to identify regulators of mitochondrial function that may contribute to Complex IV stress. Through a kinase knockout library screen for sensitivity to KCN addition we identified that Ypk1 may play a role in this regulation (Fig. 3.12). Ypk1 has been implicated in fluconazole tolerance, which is associated with sphingolipid biosynthesis, mitochondrial dysfunction, and membrane growth and cell wall expansion[273]. In combination with Target of Rapamycin Complex 2 (TORC2), Ypk1 has been shown to regulate actin polarisation and regulated cell death through mitochondrially generated ROS regulation[290-292]. The in-depth signalling interactions of Ypk1 in sphingolipid biosynthesis and mitochondrial function have been discussed in Chapter 6. Interestingly, we observed that *Δypk1* mutant *C. neoformans* had a far lower routine respiration than the wildtype, and KCN addition stopped *Δypk1* respiration (Fig. 3.14) although the kinase dead mutant *Δypk1* + YPK-D386A exhibited a slower decline in respiratory activity (Fig. 3.14e). This indicated that Ypk1 has a role in maintenance of routine respiration.

After establishing *Δypk1* mutant sensitivity to Complex IV inhibition, we wanted to assess the effect of Complex III inhibition via Azoxystrobin addition on cells lacking Ypk1. Interestingly, addition of Azoxystrobin inhibited growth (Fig. 3.17) and viability (Fig. 3.16) of both the *Δypk1* mutant, and the

kinase dead mutants, *Δypk1* + YPK-K274A and *Δypk1* + YPK-D386A (Fig. 3.17c, and Fig. 3.16b, respectively), mirroring the effect of Complex IV inhibition. These results indicate that Ypk1 is involved in mitochondrial respiratory maintenance under stress, and loss of this kinase activity confers sensitivity to mitochondrial inhibition, leading to a loss of growth and viability.

Ypk1 has been implicated with TORC2 in sphingolipid homeostasis[290], which is critical for mitochondrial function and cell membrane remodelling under stress. The downstream targets of Ypk1 include Lac1 and Lag1 ceramide synthases, which through ceramides stimulate the synthesis of complex sphingolipids[290, 292]. Studies have shown that phosphorylation of Lac1 and Lag1 by Ypk1 is essential for cell survival under stress[299], as it is thought that TORC2-Ypk1 activity directs the cell away from autophagy by utilising of long chain base compounds (LCB) like phytosphingosine[300] before phosphorylation (LCBP) to avoid accumulation of toxic LCBPs which are detrimental to yeast growth[299, 301]. As Ypk1 has a role in sphingolipid biosynthesis in response to stress, as well as prevention of metabolite mediated autophagy initiation, loss of this kinase might disrupt membrane lipid integrity, leading to toxic build-up of sphingolipid metabolites and autophagy initiation. This may impact mitochondrial function through the dysregulation of ceramide synthesis, which may control mitochondrial fate under ETC stress. However, further investigations into the role of ceramide in fungal mitochondria are required.

One other possibility given the change in respiration changes observed upon Ypk1 deletion is the involvement of sphingolipid processes in oxygen consumption. As Ypk1 is involved in sphingolipid biosynthesis and signalling, one could propose that off target signalling changes may account for changes to oxygen consumption, such as ceramide desaturase. Membrane-bound lipid desaturases account for changes in oxygen consumption, for example trans 4,5 desaturation of ceramide through DEGS1/2[302, 303]. DEGS 1/2 also acts as a bifunctional sphingolipid *Δ4* desaturase[302, 304], indicating a link between sphingolipid ceramide signalling pathways. Although ceramide signalling has been well documented in mammalian cells[305, 306], further studies are required to fully understand ceramide involvement in *C. neoformans*. However, recent studies of ceramide synthases in *C. neoformans*

pathogenicity[307], and known complex sphingomyelinase signalling for oxygen sensing and hypoxia[303, 308, 309] leads to speculation that similar processes in fungi may be involved in response to oxidative stress, and so the links between ceramide signalling and sphingolipid biosynthesis pathways should be explored. The presence of the membrane bound desaturase, sphingolipid 4-desaturase in *C. neoformans*[310], which is predicted to consume oxygen[311-313], indicates that investigations into sphingolipid control of oxygen consumption should be considered. Observing the respiratory rate and transcriptional response of *Δypk1* mutant and ceramide mutant *C. neoformans* through HRR under hypoxia or H_2O_2 treatment may shed light on the interconnecting signalling pathways that regulate *C. neoformans* oxygen consumption.

Our data suggests that *C. neoformans* resistance to inhibition of mitochondrial complexes III and IV requires functional Ypk1. Loss of this kinase confers reduced growth and culturability, perhaps through disruption of complex sphingolipid production and crosstalk for mitochondrially mediated cell death mechanisms. The speculative roles of Ypk1 in these processes has been discussed further in Chapter 6.

3.3.5 Full kinase activity of Ypk1 is required for melanisation

Given our hypothesis that an active Ypk1-mediated sphingolipid pathway is required for resistance to Complex III and Complex IV inhibition, we wanted to assess the impact of Ypk1 deletion on melanisation. As melanisation is induced under a range of stresses for cellular protection, we wanted to see whether mitochondrial inhibition in the absence of Ypk1 would lead to any defects in melanisation capacity. Interestingly, addition of Azoxystrobin (Fig. 3.18) or KCN (Fig. 3.15) did not induce any changes in melanisation, and so we can conclude that mitochondrial stress at Complex III or Complex IV does not correlate with melanisation. In addition, the *Δypk1* mutant *C. neoformans* did not show a significant reduction in melanisation capacity in comparison to the wildtype when treated with KCN (Fig. 3.15) or Azoxystrobin (Fig. 3.18), although the Ypk1-flag re-integration mutant showed an increase in melanisation across all conditions (Fig 3.15, Fig. 3.18). Although melanisation

was generally lower at 30°C (Fig. 3.15a, Fig.3.18a) than at 37°C (Fig. 3.15b, Fig. 3.18b), this was expected as melanisation in wildtype *C. neoformans* is optimally induced at 37°C [314] and this allowed us to observe any defects in melanisation induction at 37°C. For example, the kinase dead mutant *Δypk1* + YPK-D386A showed a clear reduction in melanisation capacity across all conditions, regardless of temperature (Fig. 3.15, Fig. 3.18). This therefore indicates that Ypk1 is involved in melanisation signalling, and that the D386A residue of Ypk1 is essential for this process.

C. neoformans melanisation is a regulated process which involves multiple transcription factors such as Hob1, Usv101 and Mbs1, all of which play a role in Lac1 induction[88]. Lac1, a laccase enzyme that is involved in eumelanin pigment production under environmental stresses, oxidative damage, and phagocytosis, is also a ceramide synthase subunit[88, 315]. Interestingly, PDK1 and TORC2 can activate Ypk1 through phosphorylation of Thr504 within the activation loop, which spans from residue 341 to 602[88, 316, 317]. Lac1 has been identified as a substrate for activated Ypk1[299], which not only induces ceramide synthesis but catalyses diphenol substrate polymerisation into melanin[318-320]. The clear melanisation defect seen in *Δypk1* + YPK-D386A indicates that mutations within or surrounding the activation loop may disrupt melanisation signalling through the loss of Ypk1-dependent Lac1 activation, which may increase *C. neoformans* sensitivity to oxidative stress imposed by mitochondrial complex inhibition. However, loss of Ypk1 entirely may induce a secondary melanisation pathway to maintain melanisation, which is discussed in Chapter 6.

4. Investigating the metabolic requirements of *C. neoformans*

4.1 Introduction

Survival and adaption of *C. neoformans* is reliant on metabolic flexibility, nutrient scavenging, and sequestration within the human host. As *C. neoformans* transmits from nutrient rich soils to the harsh environment within host macrophages several virulence mechanisms are activated to provide metabolic relief and promote survival[9, 321, 322], including lipid metabolism[323], iron homeostasis[324], and urease utilisation[325]. While our data has shown that *C. neoformans* relies on normal mitochondrial activity to support cell division, studies have identified different genes expressed during multiple stages of infection for adaptive growth within the host[269], and biologically relevant stresses[326]. There is a lack of comprehensive knowledge of the nutrients that can be utilised by, are essential for or can inhibit *C. neoformans* growth. The screen was performed on wildtype and *Δaox1* cells in parallel in the hope that this would reveal additional functions for Aox1.

4.2 Results

4.2.1 BIOLOG metabolite screen for wildtype and *Δaox1 C. neoformans*

We wanted to assess whether cells lacking Aox presented a different ability to utilise nutrients or withstand stressors when added to minimal media that supports a low level of growth. To achieve this, we carried out a BIOLOG system phenotypic microarray™ as described previously[274]. Both WT H99 and *Δaox1* mutant *C. neoformans* were grown in 10 different BIOLOG plates containing a range of metabolites from carbon source utilisation to pH stress adaptability. A summary of each BIOLOG plate tested in this study can be seen in Table 4.1, and the composition of each plate can be found in Section 2.5.5.

Table 4.1: Summary of BIOLOG plates

Plate	Description
PM1	Carbon Source Utilisation
PM2	Carbon Source Utilisation
PM3	Nitrogen Source Utilisation
PM4	Phosphate and Sulphate Source Utilisation
PM5	Nutrient Supplement Utilisation
PM6	Utilisation of Peptides as a Nitrogen Source (Peptide Nitrogen Source Utilisation)
PM7	Utilisation of Peptides as a Nitrogen Source (Peptide Nitrogen Source Utilisation)
PM8	Utilisation of Di- and Tripeptides as a Nitrogen Source (Peptide Nitrogen Source Utilisation)
PM9	Osmolyte Stress Adaption
PM10	pH Stress Adaption

Both WT H99 and *Δaox1* mutant *C. neoformans* were tested in each plate condition in triplicate and analysed using Growthcurver (R Studio) as indicated by the workflow replication in Fig. 4.1, to produce area under the curve (AUC) values. Reproducible conditions from each plate type were generated into heatmaps and significance was determined using a one-way ANOVA in GraphPad Prism.

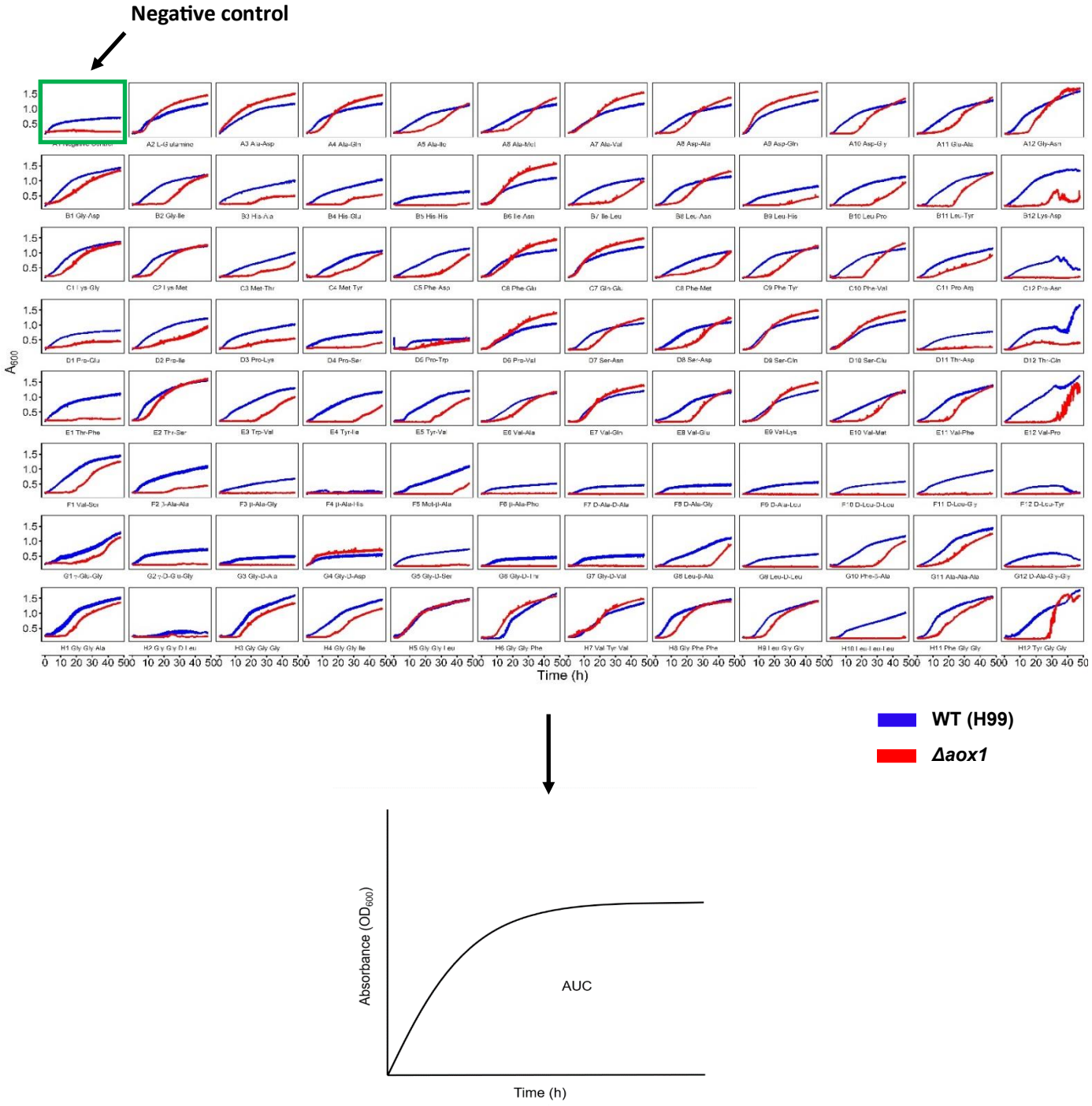

Figure 4.1: Representative schematic illustrating the determination of AUC values.

Representative example of a PM8 plate whereby (**A**) WT H99 (blue) and *Δaox1* mutant (red) *C. neoformans* were grown in 96 wells and analysed using Growthcurver in R Studio to generate area under the curve (AUC) values (**B**). The negative control was located in the well A1, which is highlighted in green.

4.2.2 Wildtype *C. neoformans* can utilise a wider range of carbon sources than cells lacking Aox1

C. neoformans is a Crabtree negative yeast which is reliant on respiration for energy generation, and in doing so is thought to utilise both glucose and alternative carbon sources such as mannose, xylose and mannitol [327]. To investigate whether *C. neoformans* can use a variety of non-glucose carbon sources for growth, both wildtype and *Δaox1* mutant *C. neoformans* cells were inoculated in PM1 (Fig. 4.2a, 4.2b) and PM2 (Fig. 4.2c, 4.2d) carbon source plates as described in 2.5.5. Resultant AUC values were measured in comparison to a negative control composed of minimal media only, to assess the effects of each supplement on growth. Heatmaps representing reproducible changes in AUC were generated in GraphPad Prism.

For PM1 plates, both H99 (Fig. 4.2a) and *Δaox1* (Fig. 4.2b) were able to use D-Mannose, Dulcitol, α-D-Glucose, evidenced by a significant increase in growth, however H99 could also use D-Trehalose and D-Fructose as a carbon source for growth (Fig. 4.2a). Interestingly, when grown in PM2 plates, both H99 and *Δaox1* utilised different additives for growth. H99 was able to use Pectin to significantly increase the AUC value, but growth was inhibited by Caproic Acid (Fig. 4.2c) while *Δaox1* mutant *C. neoformans* cells showed a significantly increased AUC in the presence of Gelatin and β-Hydroxy Butyric Acid, but Caproic Acid had no significant effect (Fig. 4.2d). A summary of all of the carbon sources that significantly affected *C. neoformans* growth can be found in Fig. 4.2e for PM1 and Fig. 4.2f for PM2.

A

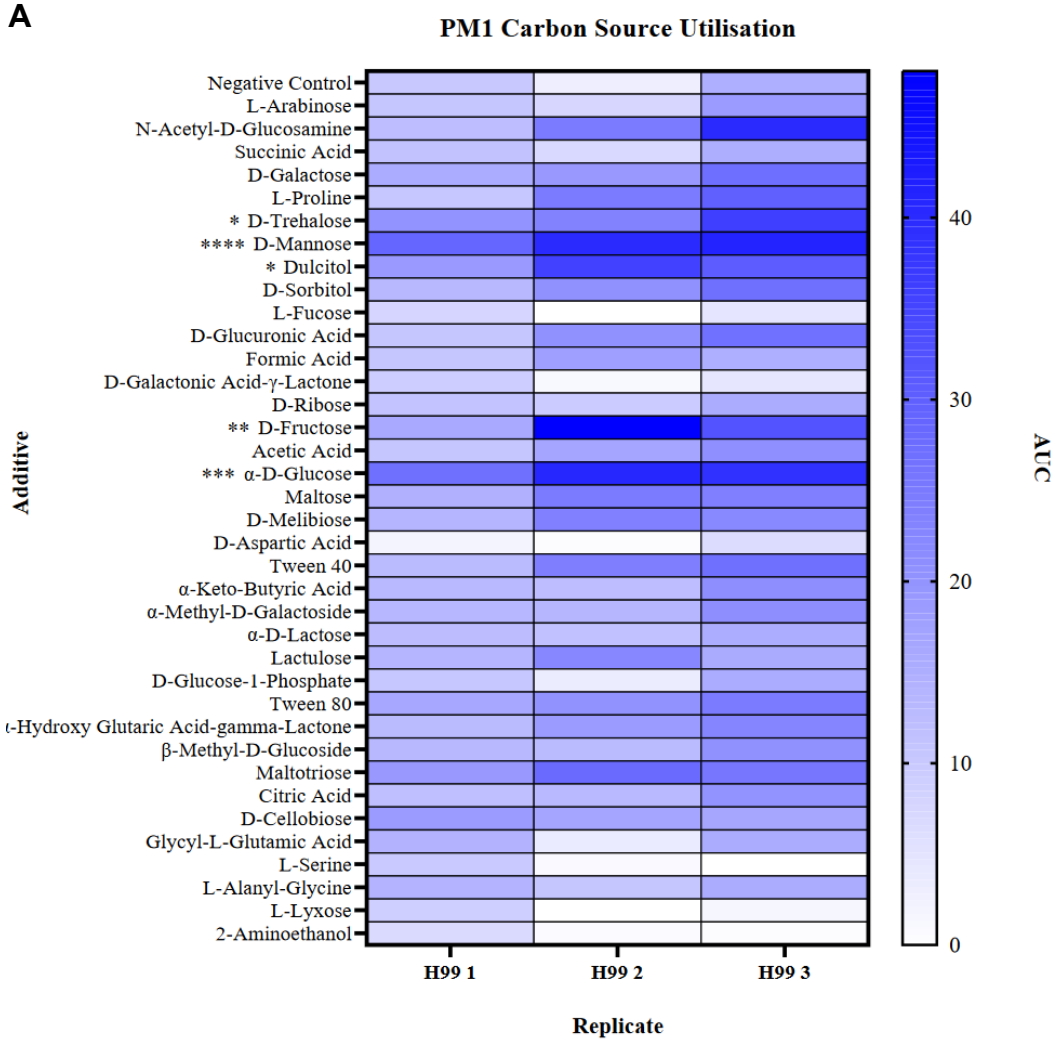
PM1 Carbon Source Utilisation
Negative Control
L-Arabinose
N-Acetyl-D-Glucosamine
Succinic Acid
D-Galactose
L-Proline
* D-Trehalose
**** D-Mannose
* Dulcitol
D-Sorbitol
L-Fucose
D-Glucuronic Acid
Formic Acid
D-Galactonic Acid-γ-Lactone
D-Ribose
** D-Fructose
Acetic Acid
*** α-D-Glucose
Maltose
D-Melibiose
D-Aspartic Acid
Tween 40
α-Keto-Butyric Acid
α-Methyl-D-Galactoside
α-D-Lactose
Lactulose
D-Glucose-1-Phosphate
Tween 80
ι-Hydroxy Glutaric Acid-gamma-Lactone
β-Methyl-D-Glucoside
Maltotriose
Citric Acid
D-Cellobiose
Glycyl-L-Glutamic Acid
L-Serine
L-Alanyl-Glycine
L-Lyxose
2-Aminoethanol
Additive
H99 1
H99 2
H99 3
Replicate
40
30
20
10
0
AUC

B

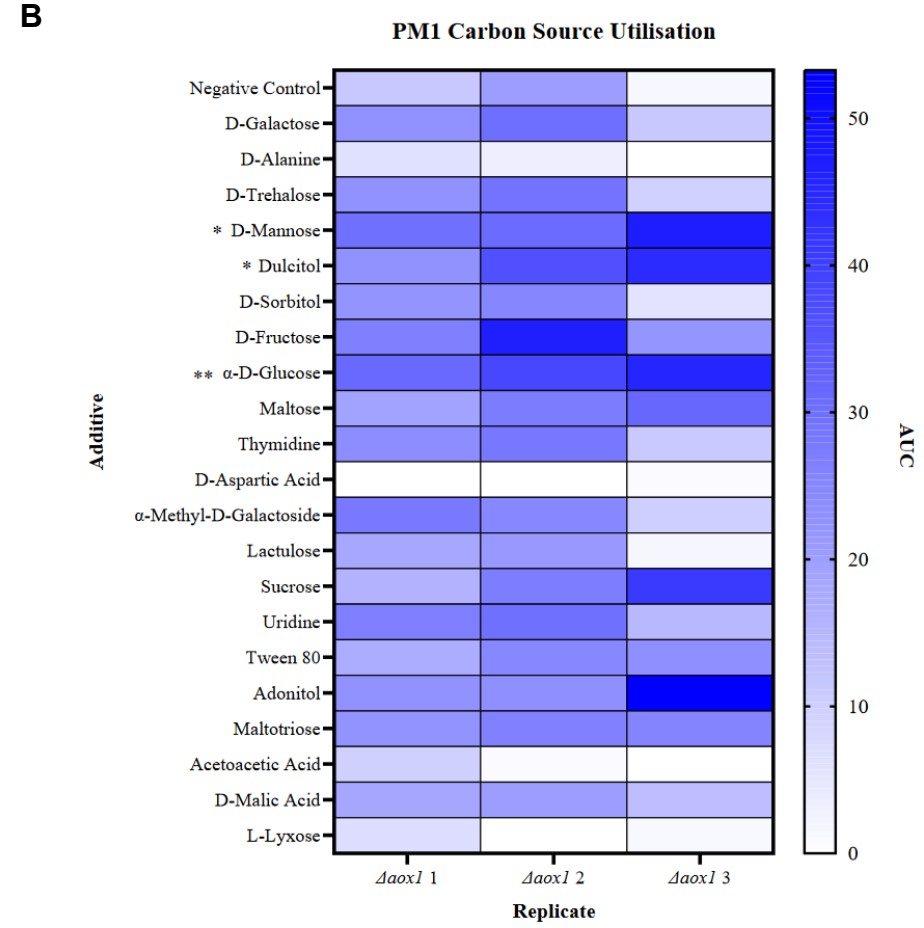
PM1 Carbon Source Utilisation
Negative Control
D-Galactose
D-Alanine
D-Trehalose
* D-Mannose
* Dulcitol
D-Sorbitol
D-Fructose
** α-D-Glucose
Maltose
Thymidine
D-Aspartic Acid
α-Methyl-D-Galactoside
Lactulose
Sucrose
Uridine
Tween 80
Adonitol
Maltotriose
Acetoacetic Acid
D-Malic Acid
L-Lyxose
Additive
Δaox1 1
Δaox1 2
Δaox1 3
Replicate
50
40
30
20
10
0
AUC

C

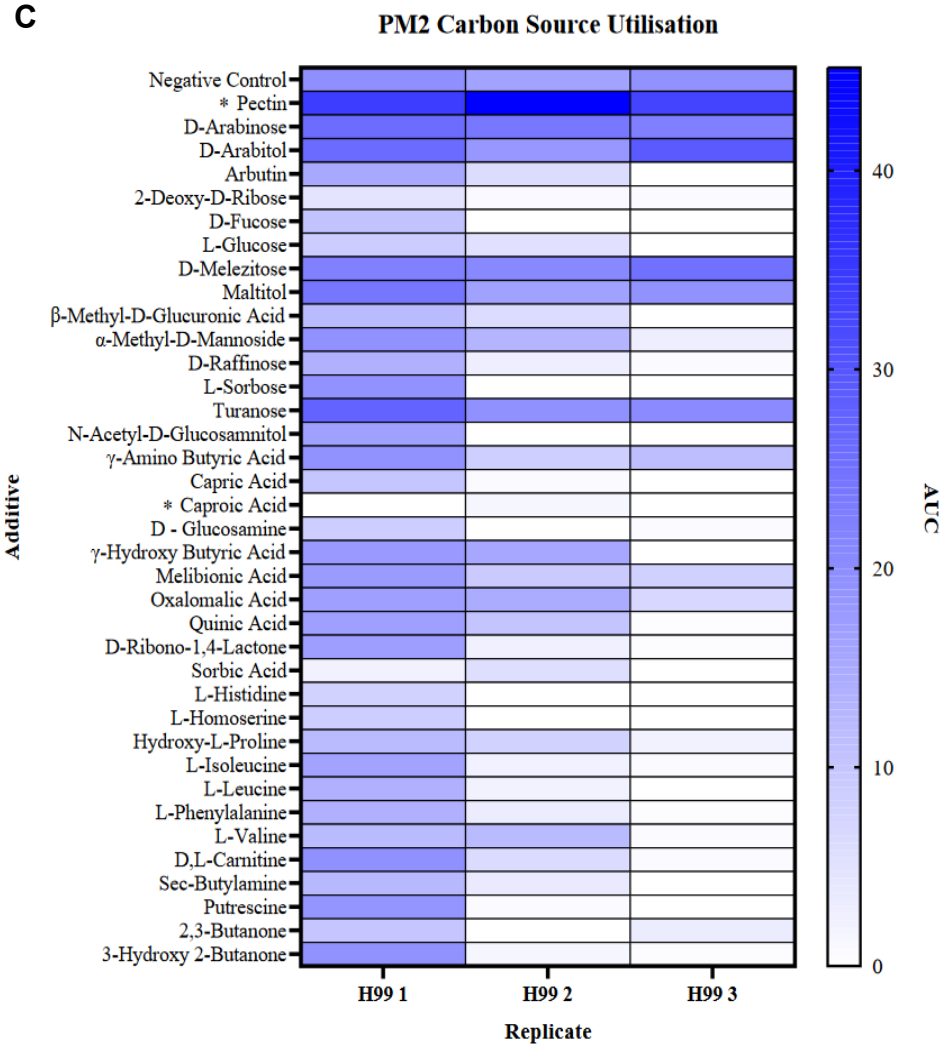
PM2 Carbon Source Utilisation
Negative Control
* Pectin
D-Arabinose
D-Arabitol
Arbutin
2-Deoxy-D-Ribose
D-Fucose
L-Glucose
D-Melezitose
Maltitol
β-Methyl-D-Glucuronic Acid
α-Methyl-D-Mannoside
D-Raffinose
L-Sorbose
Turanose
N-Acetyl-D-Glucosamnitol
γ-Amino Butyric Acid
Capric Acid
* Caproic Acid
D - Glucosamine
γ-Hydroxy Butyric Acid
Melibionic Acid
Oxalomalic Acid
Quinic Acid
D-Ribono-1,4-Lactone
Sorbic Acid
L-Histidine
L-Homoserine
Hydroxy-L-Proline
L-Isoleucine
L-Leucine
L-Phenylalanine
L-Valine
D,L-Carnitine
Sec-Butylamine
Putrescine
2,3-Butanone
3-Hydroxy 2-Butanone
Additive
H99 1
H99 2
H99 3
Replicate
40
30
20
10
0
AUC

D

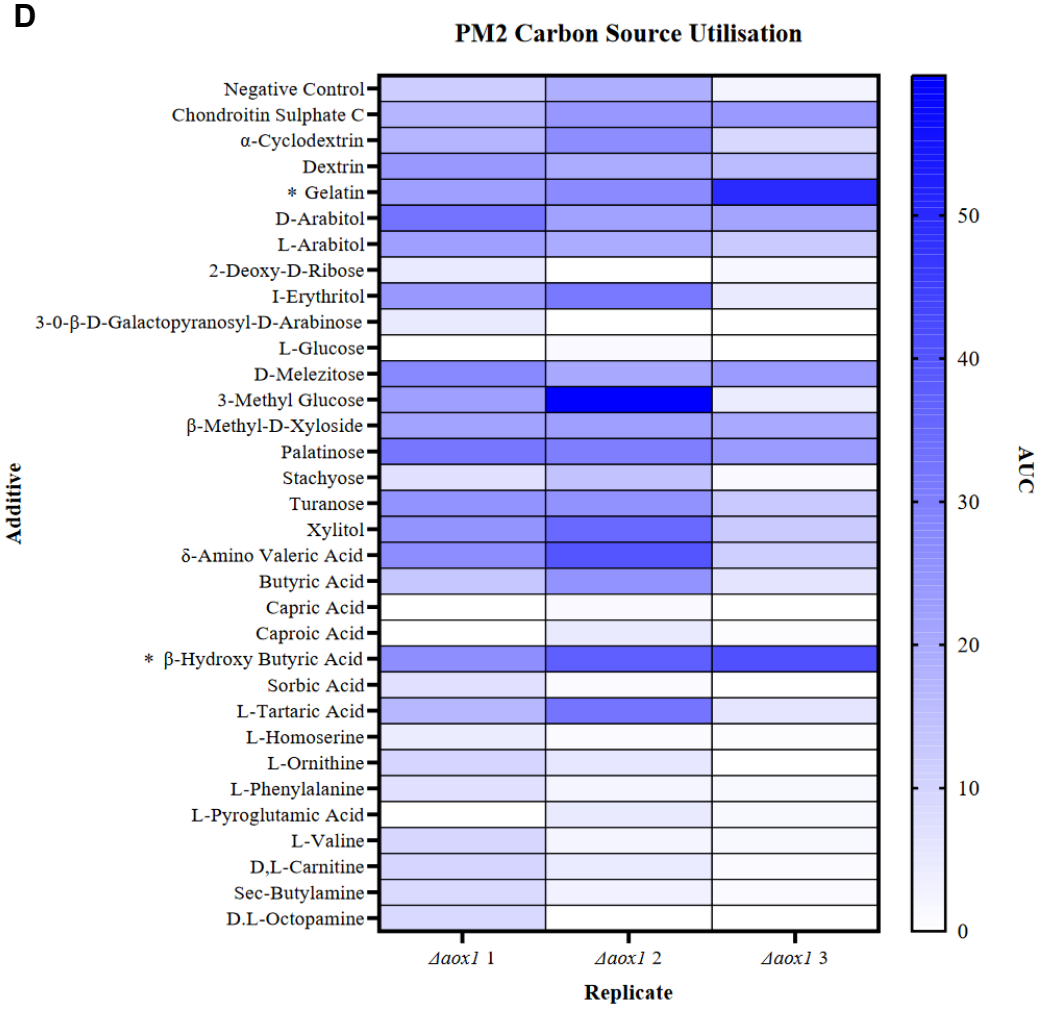
PM2 Carbon Source Utilisation
Negative Control
Chondroitin Sulphate C
α-Cyclodextrin
Dextrin
* Gelatin
D-Arabitol
L-Arabitol
2-Deoxy-D-Ribose
I-Erythritol
3-0-β-D-Galactopyranosyl-D-Arabinose
L-Glucose
D-Melezitose
3-Methyl Glucose
β-Methyl-D-Xyloside
Palatinose
Stachyose
Turanose
Xylitol
δ-Amino Valeric Acid
Butyric Acid
Capric Acid
Caproic Acid
* β-Hydroxy Butyric Acid
Sorbic Acid
L-Tartaric Acid
L-Homoserine
L-Ornithine
L-Phenylalanine
L-Pyroglutamic Acid
L-Valine
D,L-Carnitine
Sec-Butylamine
D,L-Octopamine
Additive
Δaox1 1
Δaox1 2
Δaox1 3
Replicate
AUC
0
10
20
30
40
50

E

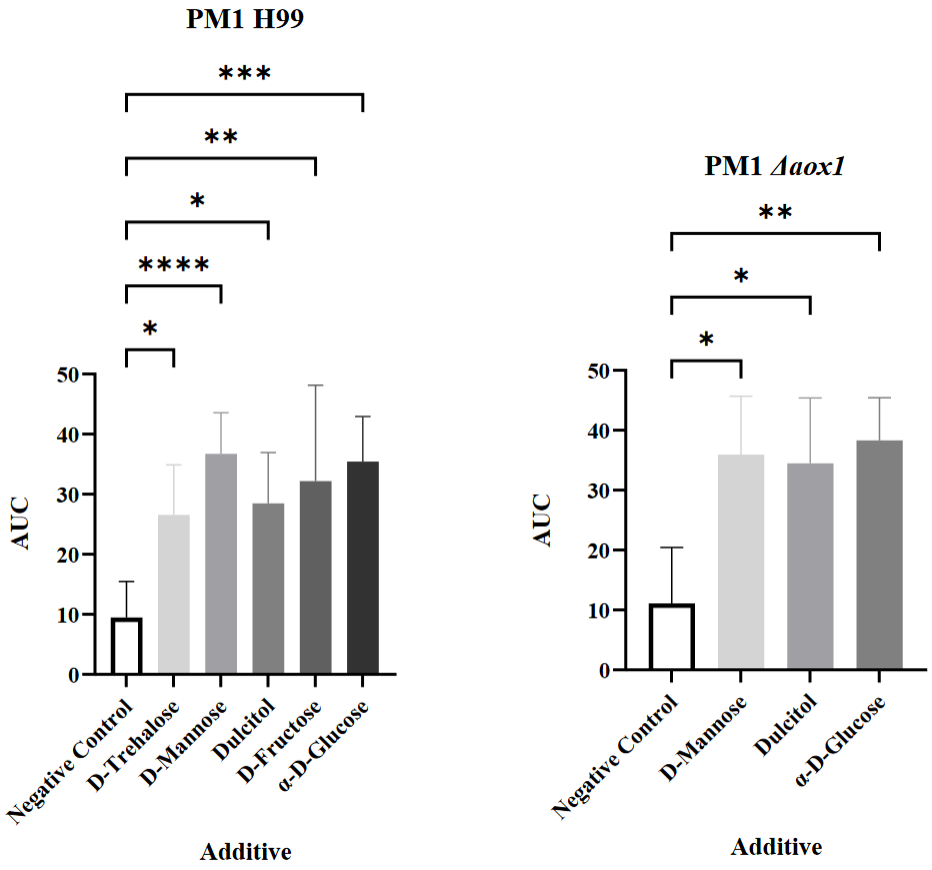
PM1 H99
***
**
*
****
*
AUC
0
10
20
30
40
50
Negative Control
D-Trehalose
D-Mannose
Dulcitol
D-Fructose
α-D-Glucose
Additive
PM1 Δaox1
**
*
*
AUC
0
10
20
30
40
50
Negative Control
D-Mannose
Dulcitol
α-D-Glucose
Additive

F

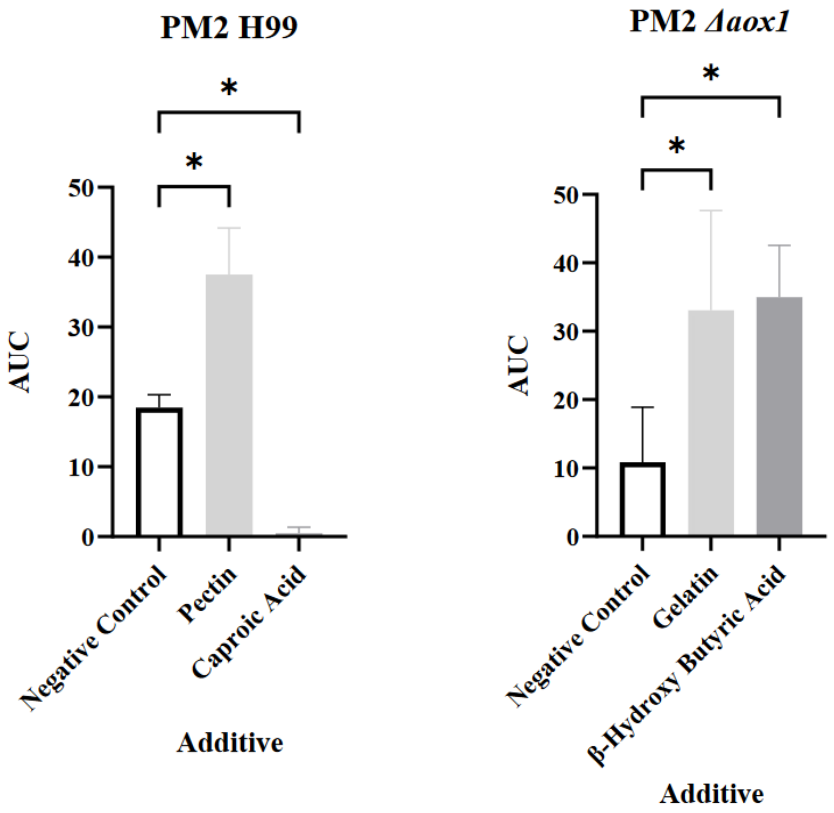

Figure 4.2: C. neoformans carbon source utilisation.
Biological triplicates of WT (H99) and *Δaox1* were grown in the presence of different carbon source additives (Additive) using the BIOLOG system and the area under the curve was recorded (AUC). (**A**) PM1 / H99, (**B**) PM1 / *Δaox1*, (**C**) PM2 / H99, (**D**) PM2 / *Δaox1,* with a summary of statistically significant hits for (**E**) PM1 and (**F**) PM2. Significance was calculated using Dunnett's multiple comparisons test following a one-way ANOVA in GraphPad Prism. * < 0.05, ** < 0.005, *** < 0.0005, **** <0.0001, where P = 0.05. Error bars represent ± SD. n = 3

4.2.3 *C. neoformans* can utilise peptides as a nitrogen source

Accumulation and regulation of nitrogen sources is essential for fungal pathogenicity in the nutrient-scarce host [328], so we wanted to investigate whether *C. neoformans* could utilise a variety of nitrogen sources for growth. Both wildtype and *Δaox1* mutant *C. neoformans* were inoculated in PM3 (Fig. 4.3) nitrogen source plates as described and resultant AUC values were measured in comparison to a negative control to assess additive impact on cellular growth. Interestingly, while an increased AUC was observed for some replicates, no statistical significance was observed in the PM3 plates

for either H99 (Fig. 4.3a) or *Δaox1* (Fig. 4.3b) in comparison to a negative control, which may be in part attributed to disparities in reproducibility in the PM3 plate set.

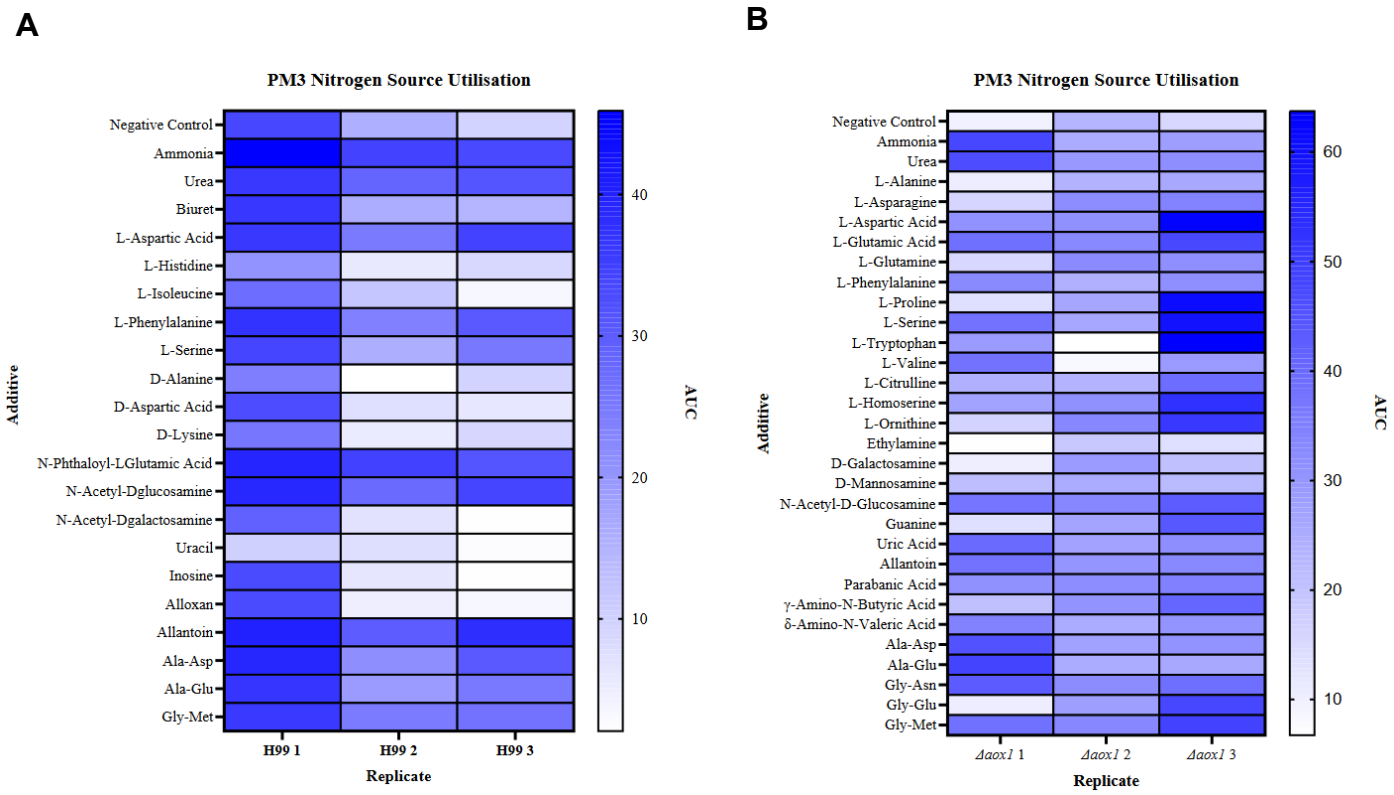

Figure 4.3: C. neoformans utilisation of nitrogen sources for growth in PM3.
Biological triplicates of WT (H99) and *Δaox1* mutant *C. neoformans* cells were grown in the presence of different nitrogen source additives (Additive) using the BIOLOG system and the area under the curve was recorded (AUC). (**A**) PM3 / H99, (**B**) PM3 / *Δaox1*. Significance was calculated using Dunnett's multiple comparisons test following a one-way ANOVA in GraphPad Prism. No significance was observed. n = 3.

However, *C. neoformans* cultures were also inoculated into other nitrogen source plates (PM6, PM7 and PM8) from the BIOLOG system as described (Section 2.5.5) and the calculated AUC values were compared to a negative control for each replicate. Interestingly, additives across PM6, PM7 and PM8 significantly affected the growth of wildtype cells, and summaries of significant hits from each plate can be found in Fig. 4.4e. 4.4f, and 4.4i, respectively. Ala-Asn, Ala-Lys, Ala-Pro, Arg-Ile, Arg-Lys, Arg-Met, Arg-Trp, Asp-Leu, Asp-Lys, Asp-Phe, Asp-Val, Gln-Gln, Glu-Ser, Glu-Tyr, Gly-Ala, Gly-Arg, Gly-Gly, Gly-Phe, Gly-Ser, Gly-Val and Ile-Gln all significantly increased growth of H99 in the PM6 plate (Fig. 4.4a, 4.4e). For PM7, addition of Leu-Ser, Lys-Leu, Lys-Pro, Met-Gln, Phe-Gly and Ser-Phe dipeptides showed an increased AUC value for H99 (Fig. 4.4c, 4.4f). The dipeptides

Ala-Gln, Asp-Ala, Asp-Gln, Asp-Gly, Glu-Ala, Gly-Asn, Gly-Asp, Ile-Asn, Leu-Asn, Lys-Gly, Lys-Met, Gln-Glu, Phe-Tyr, Ser-Asn, Ser-Gln, Ser-Glu, Thr-Ser, Val-Gln, Val-Phe, Val-Ser, Ala-Ala-Ala, and the tripeptides Gly-Gly-Ala, Gly-Gly-Gly, Gly-Gly-Ile, Gly-Gly-Leu, Gly-Gly-Phe, Leu-Gly-Gly, Phe-Gly-Gly, Tyr-Gly-Gly from PM8 also significantly increased growth of H99 (Fig. 4.4g, 4.4i).

Interestingly, *Δaox1* cells in both PM6 (Fig. 4.4b) and PM7 (Fig. 4.4d) showed no significant growth changes in these plates, which mirrored the result for PM3 (Fig. 4.3b). However, for PM8, which included tripeptides, addition of the dipeptides Ala-Asp, Ala-Gln, Ala-Val, Asp-Gln, Asp-Gly, Gly-Asn, Gly-Asp, Ile-Asn, Lys-Gly, Lys-Met, Gln-Glu, Ser-Gln, Ser-Glu, Thr-Ser, Val-Gln, Val-Lys, and addition of the tripeptides Gly-Gly-Ala, Gly-Gly-Leu, Gly-Gly-Phe, Gly-Phe-Phe, Leu-Gly-Gly, Phe-Gly-Gly, and Tyr-Gly-Gly all significantly increased *Δaox1* cell growth (Fig. 4.4f). A summary of additives that significantly affected *Δaox1* cell growth in the PM8 plate can be found in Fig. 4.4i.

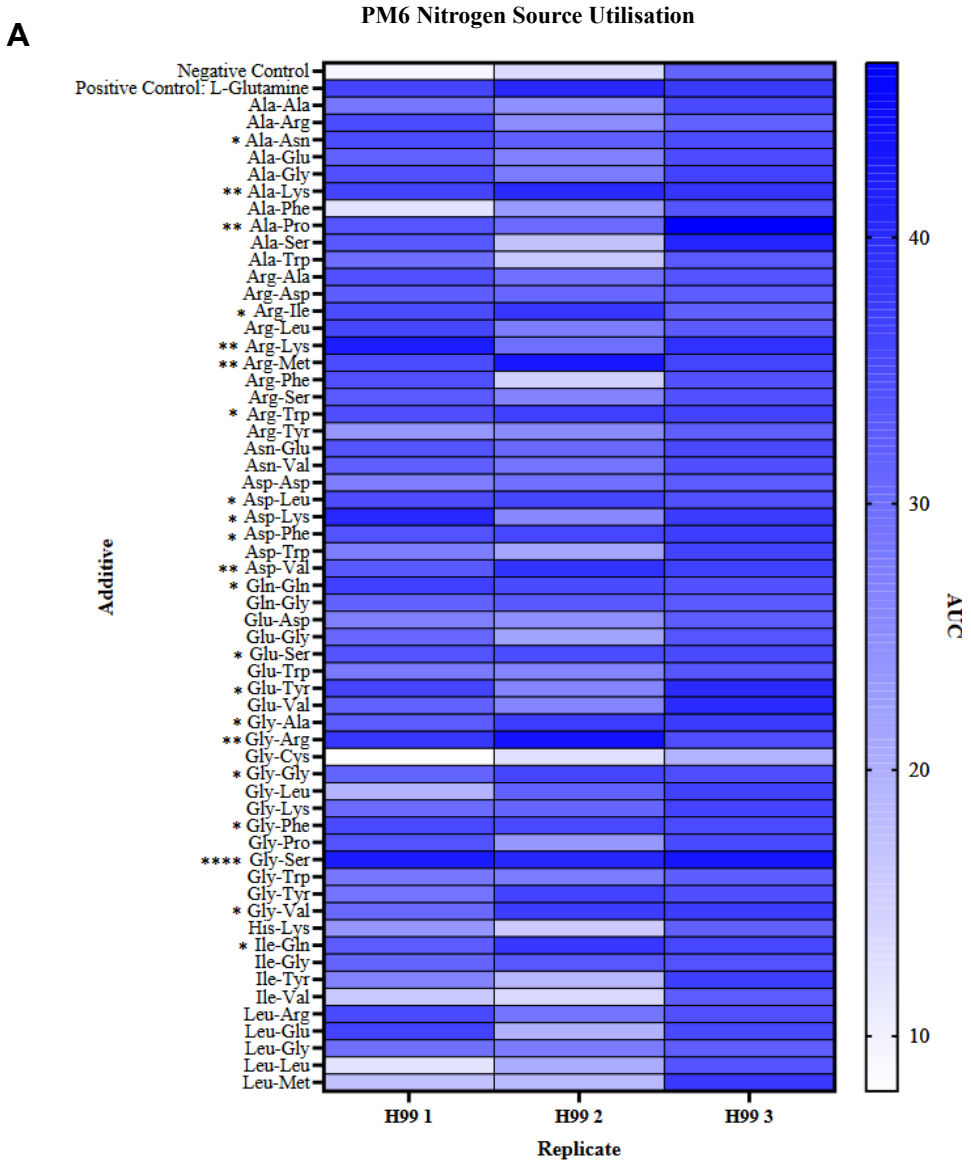

B

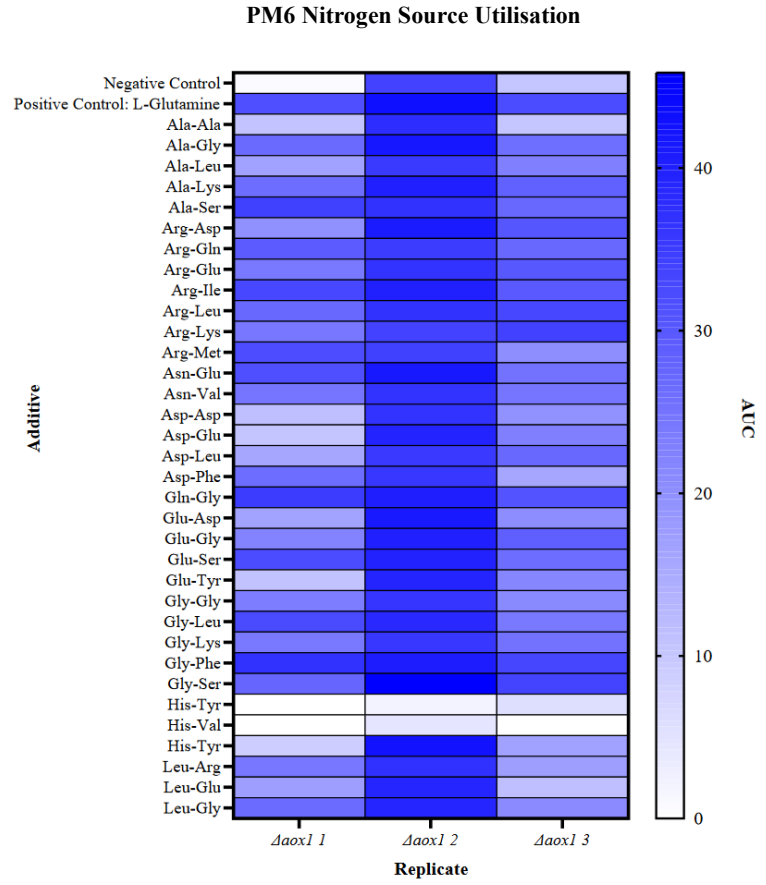
PM6 Nitrogen Source Utilisation
Negative Control
Positive Control: L-Glutamine
Ala-Ala
Ala-Gly
Ala-Leu
Ala-Lys
Ala-Ser
Arg-Asp
Arg-Gln
Arg-Glu
Arg-Ile
Arg-Leu
Arg-Lys
Arg-Met
Asn-Glu
Asn-Val
Asp-Asp
Asp-Glu
Asp-Leu
Asp-Phe
Gln-Gly
Glu-Asp
Glu-Gly
Glu-Ser
Glu-Tyr
Gly-Gly
Gly-Leu
Gly-Lys
Gly-Phe
Gly-Ser
His-Tyr
His-Val
His-Tyr
Leu-Arg
Leu-Glu
Leu-Gly
Additive
Δaox1 1
Δaox1 2
Δaox1 3
Replicate
40
30
20
10
0
AUC

C

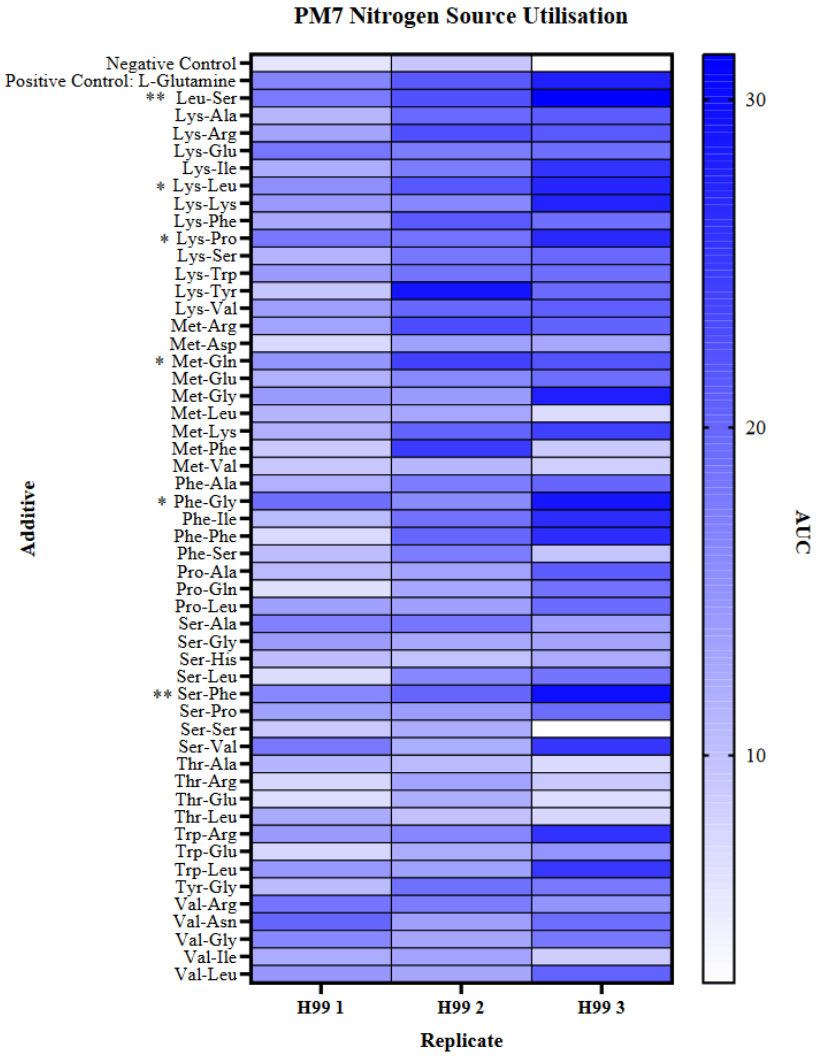
PM7 Nitrogen Source Utilisation
Negative Control
Positive Control: L-Glutamine
** Leu-Ser
Lys-Ala
Lys-Arg
Lys-Glu
Lys-Ile
* Lys-Leu
Lys-Lys
Lys-Phe
* Lys-Pro
Lys-Ser
Lys-Trp
Lys-Tyr
Lys-Val
Met-Arg
Met-Asp
* Met-Gln
Met-Glu
Met-Gly
Met-Leu
Met-Lys
Met-Phe
Met-Val
Phe-Ala
* Phe-Gly
Phe-Ile
Phe-Phe
Phe-Ser
Pro-Ala
Pro-Gln
Pro-Leu
Ser-Ala
Ser-Gly
Ser-His
Ser-Leu
** Ser-Phe
Ser-Pro
Ser-Ser
Ser-Val
Thr-Ala
Thr-Arg
Thr-Glu
Thr-Leu
Trp-Arg
Trp-Glu
Trp-Leu
Tyr-Gly
Val-Arg
Val-Asn
Val-Gly
Val-Ile
Val-Leu
Additive
H99 1
H99 2
H99 3
Replicate
30
20
10
AUC

D

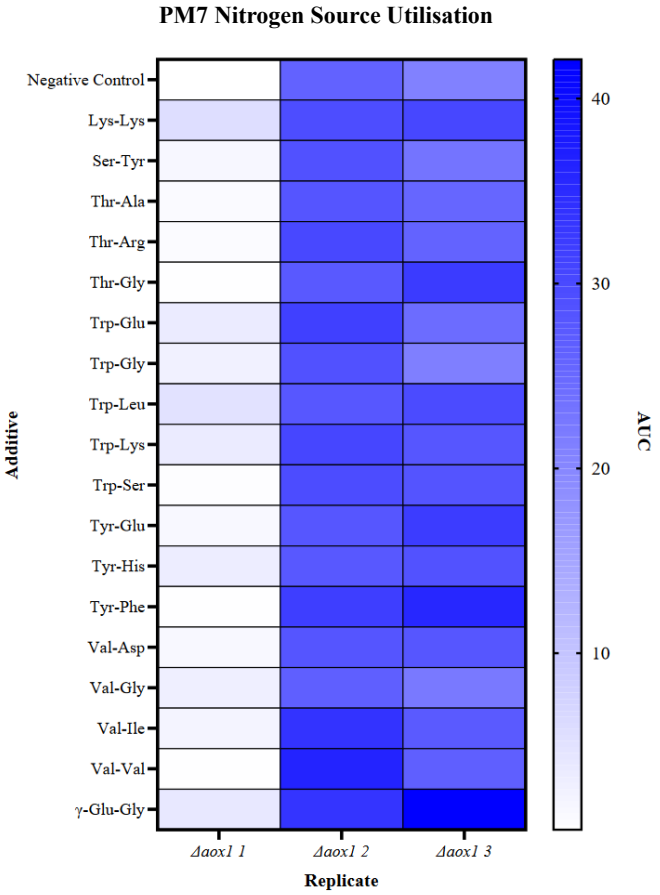
PM7 Nitrogen Source Utilisation
Negative Control
Lys-Lys
Ser-Tyr
Thr-Ala
Thr-Arg
Thr-Gly
Trp-Glu
Trp-Gly
Trp-Leu
Trp-Lys
Trp-Ser
Tyr-Glu
Tyr-His
Tyr-Phe
Val-Asp
Val-Gly
Val-Ile
Val-Val
γ-Glu-Gly
Additive
Δaox1 1
Δaox1 2
Δaox1 3
Replicate
40
30
20
10
AUC

E

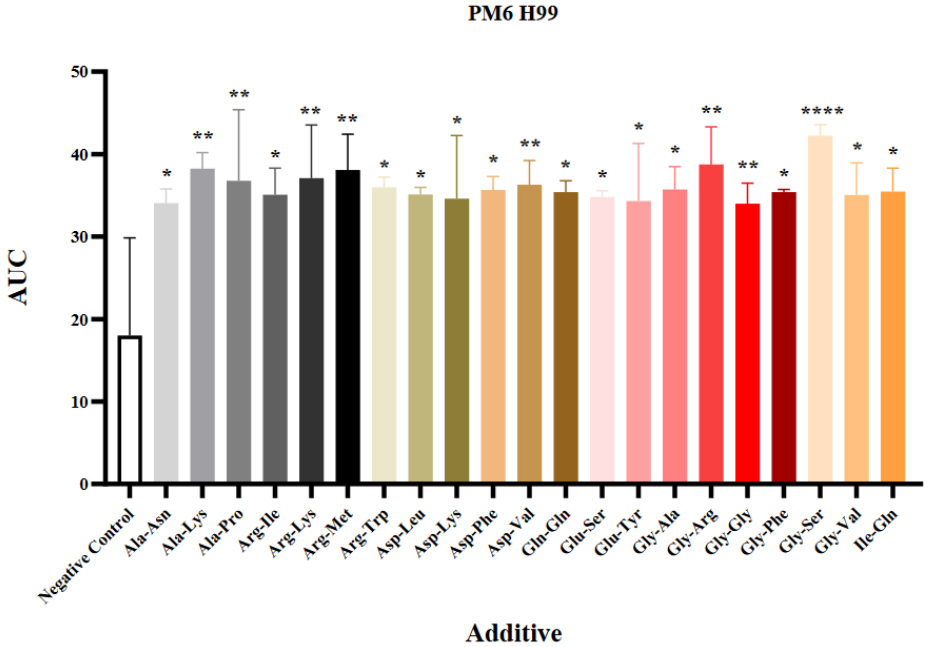
PM6 H99
AUC
50
40
30
20
10
0
Negative Control
Ala-Asn
Ala-Lys
Ala-Pro
Arg-Ile
Arg-Lys
Arg-Met
Arg-Trp
Asp-Leu
Asp-Lys
Asp-Phe
Asp-Val
Gln-Gln
Glu-Ser
Glu-Tyr
Gly-Ala
Gly-Arg
Gly-Gly
Gly-Phe
Gly-Ser
Gly-Val
Ile-Gln
Additive

F

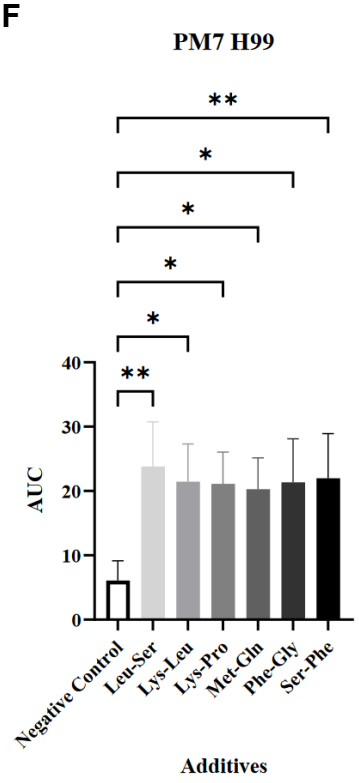
PM7 H99
AUC
40
30
20
10
0
Negative Control
Leu-Ser
Lys-Leu
Lys-Pro
Met-Gln
Phe-Gly
Ser-Phe
Additives

G

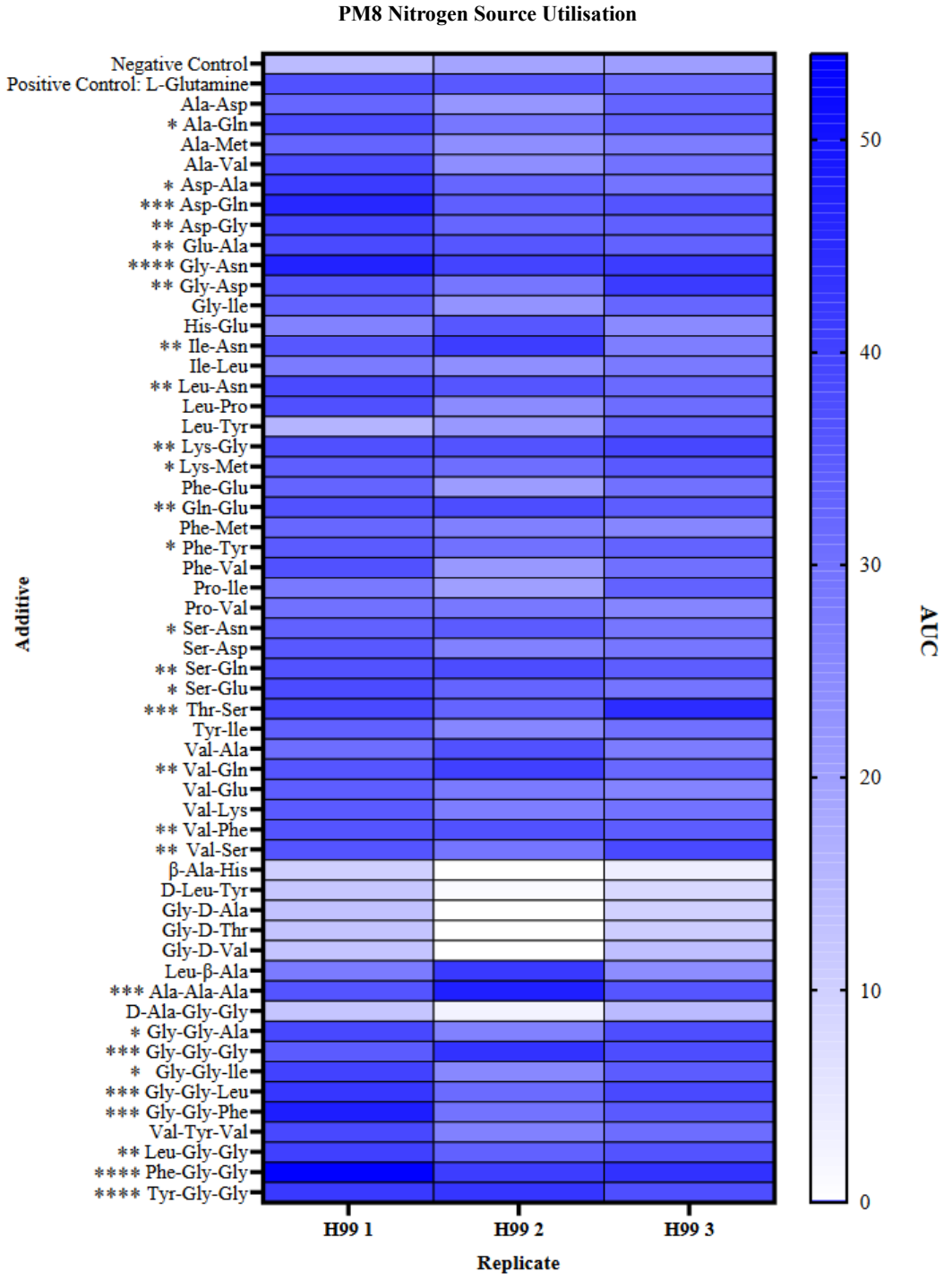
PM8 Nitrogen Source Utilisation
Negative Control
Positive Control: L-Glutamine
Ala-Asp
* Ala-Gln
Ala-Met
Ala-Val
* Asp-Ala
*** Asp-Gln
** Asp-Gly
** Glu-Ala
**** Gly-Asn
** Gly-Asp
Gly-Ile
His-Glu
** Ile-Asn
Ile-Leu
** Leu-Asn
Leu-Pro
Leu-Tyr
** Lys-Gly
* Lys-Met
Phe-Glu
** Gln-Glu
Phe-Met
* Phe-Tyr
Phe-Val
Pro-Ile
Pro-Val
* Ser-Asn
Ser-Asp
** Ser-Gln
* Ser-Glu
*** Thr-Ser
Tyr-Ile
Val-Ala
** Val-Gln
Val-Glu
Val-Lys
** Val-Phe
** Val-Ser
β-Ala-His
D-Leu-Tyr
Gly-D-Ala
Gly-D-Thr
Gly-D-Val
Leu-β-Ala
*** Ala-Ala-Ala
D-Ala-Gly-Gly
* Gly-Gly-Ala
*** Gly-Gly-Gly
* Gly-Gly-Ile
*** Gly-Gly-Leu
*** Gly-Gly-Phe
Val-Tyr-Val
** Leu-Gly-Gly
**** Phe-Gly-Gly
**** Tyr-Gly-Gly
Additive
H99 1
H99 2
H99 3
Replicate
50
40
30
20
10
0
AUC

H

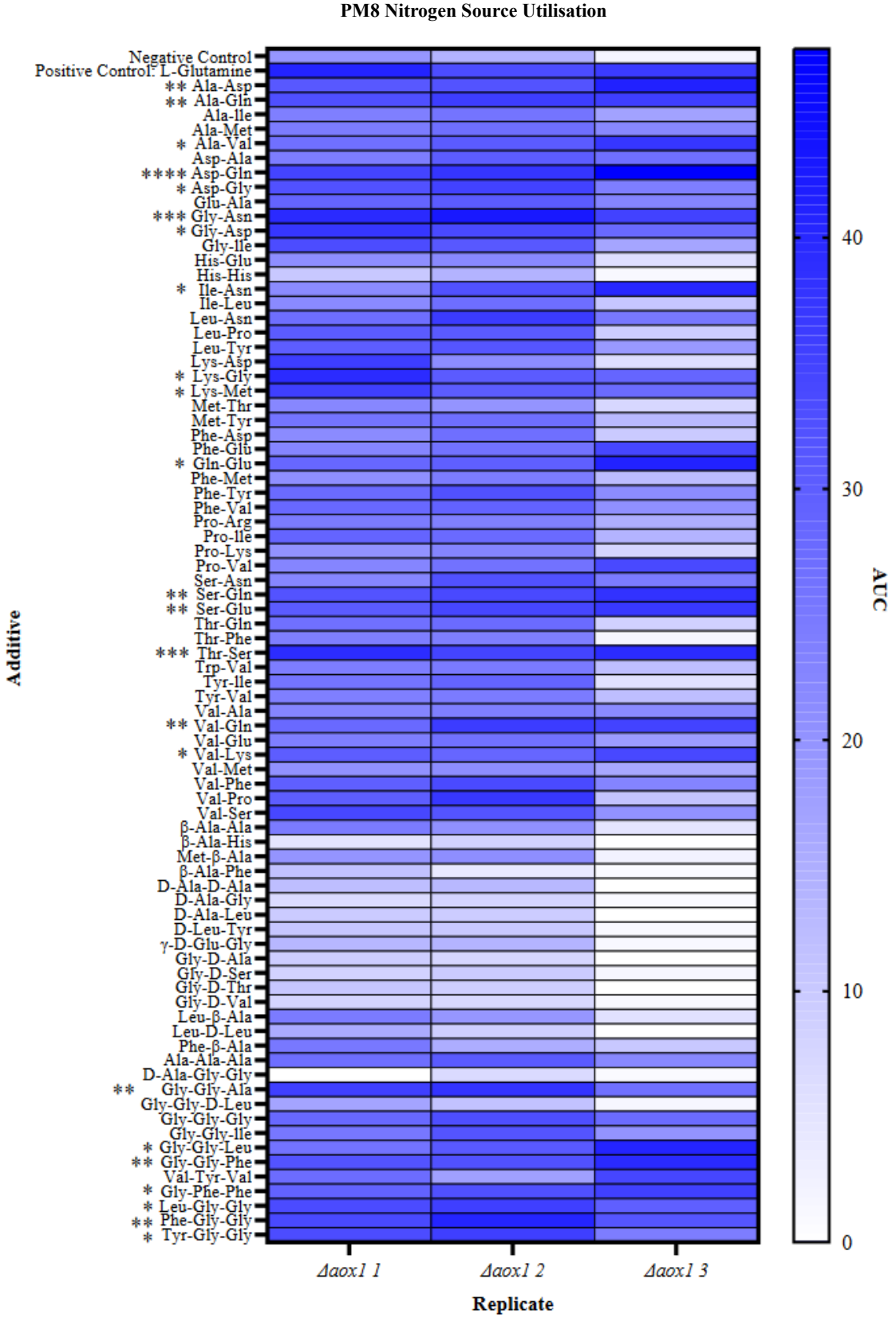
PM8 Nitrogen Source Utilisation
Negative Control
Positive Control: L-Glutamine
** Ala-Asp
** Ala-Gln
Ala-Ile
Ala-Met
* Ala-Val
Asp-Ala
**** Asp-Gln
* Asp-Gly
Glu-Ala
*** Gly-Asn
* Gly-Asp
Gly-Ile
His-Glu
His-His
* Ile-Asn
Ile-Leu
Leu-Asn
Leu-Pro
Leu-Tyr
Lys-Asp
* Lys-Gly
* Lys-Met
Met-Thr
Met-Tyr
Phe-Asp
Phe-Glu
* Gln-Glu
Phe-Met
Phe-Tyr
Phe-Val
Pro-Arg
Pro-Ile
Pro-Lys
Pro-Val
Ser-Asn
** Ser-Gln
** Ser-Glu
Thr-Gln
Thr-Phe
*** Thr-Ser
Trp-Val
Tyr-Ile
Tyr-Val
Val-Ala
** Val-Gln
Val-Glu
* Val-Lys
Val-Met
Val-Phe
Val-Pro
Val-Ser
β-Ala-Ala
β-Ala-His
Met-β-Ala
β-Ala-Phe
D-Ala-D-Ala
D-Ala-Gly
D-Ala-Leu
D-Leu-Tyr
γ-D-Glu-Gly
Gly-D-Ala
Gly-D-Ser
Gly-D-Thr
Gly-D-Val
Leu-β-Ala
Leu-D-Leu
Phe-β-Ala
Ala-Ala-Ala
D-Ala-Gly-Gly
** Gly-Gly-Ala
Gly-Gly-D-Leu
Gly-Gly-Gly
Gly-Gly-Ile
* Gly-Gly-Leu
** Gly-Gly-Phe
Val-Tyr-Val
* Gly-Phe-Phe
* Leu-Gly-Gly
** Phe-Gly-Gly
* Tyr-Gly-Gly
Additive
Δaox1 1
Δaox1 2
Δaox1 3
Replicate
AUC
40
30
20
10
0

I

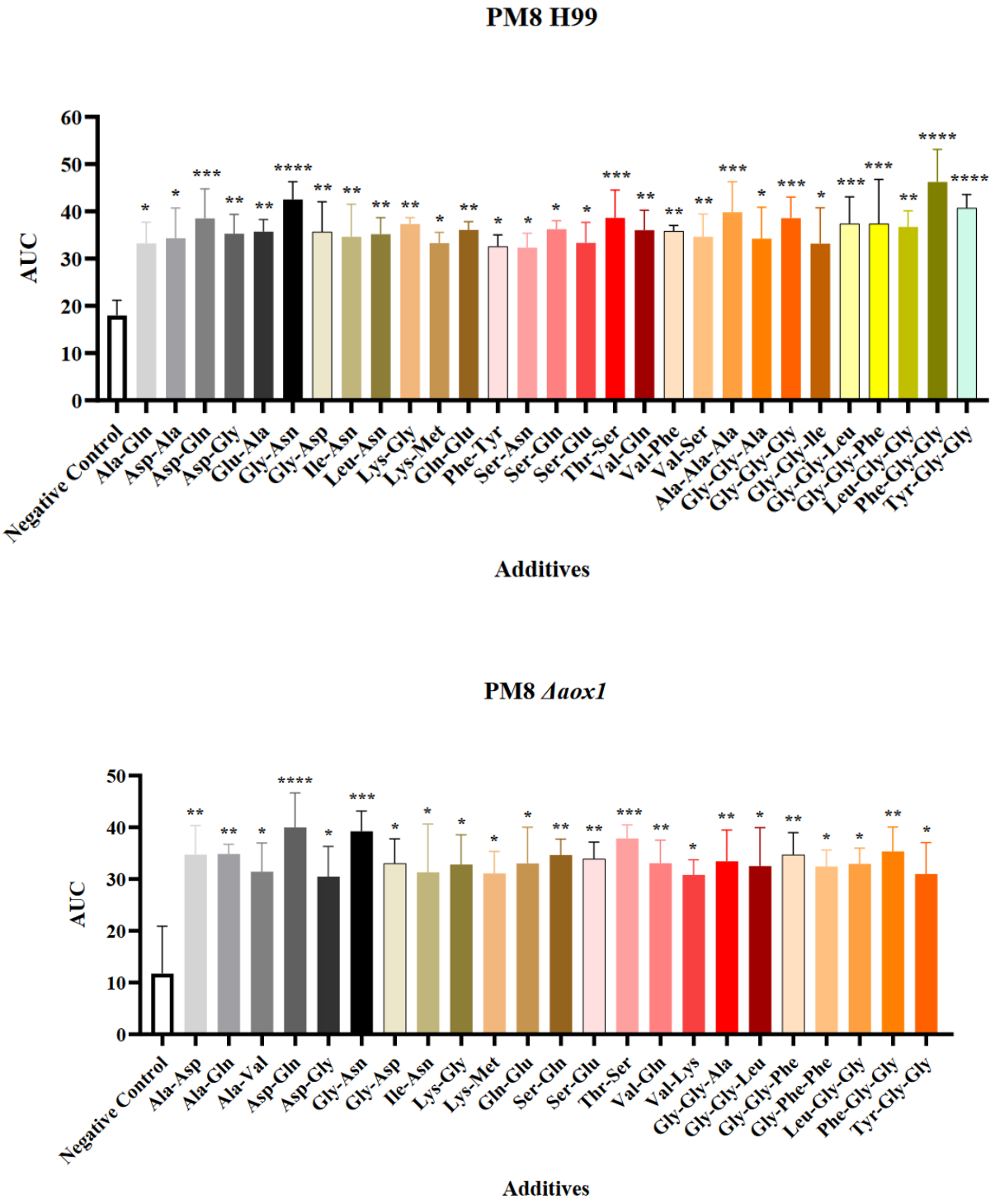

Figure 4.4: C. neoformans utilisation of nitrogen sources for growth in PM6, PM7, and PM8 plates.

Biological triplicates of WT (H99) and *Δaox1* mutant *C. neoformans* cells were grown in the presence of different peptides as a nitrogen source (Additive) using the BIOLOG system and the area under the curve was recorded (AUC). (**A**) PM6 / H99, (**B**) PM6 / *Δaox1* (**C**) PM7 / H99, (**D**) PM7 / *Δaox1* (**E**) Summary of significant hits from PM6 / H99, (**F**) Summary of significant hits from PM7 / H99, (**G**) PM8 / H99, (**H**) PM8 / *Δaox1*, (**I**) Summary of significant hits from PM8 / H99 and PM8 / *Δaox1*. Significance was calculated using Dunnett's multiple comparisons test following a one-way ANOVA in GraphPad Prism. * < 0.05, ** < 0.005, *** < 0.0005, **** <0.0001, where P = 0.05. Error bars represent ± SD. n = 3.

4.2.4 Phosphorus and sulphur sources significantly increase *Δaox1* mutant *C. neoformans* growth

Following the assessment of carbon and nitrogen source availability on *C. neoformans* growth, phosphorus and sulphur source utilisation by WT and *Δaox1* mutant cells was investigated. *C. neoformans* cultures were inoculated into PM4 plates from the BIOLOG system containing phosphorus and sulphur sources and the calculated AUC values were compared to a negative control. Interestingly, although a higher number of repeatable hits were found for H99 (Fig. 4.5a), only Adenosine- 2',3', -cyclic monophosphate significantly increased growth. However, for PM4 plates inoculated with *Δaox1* cells, Phosphate, Tripoly-phosphate, Adenosine- 2',3', -cyclic monophosphate, Phosphoenol Pyruvate, D-Glucose-6-Phosphate, D-Mannose-1-Phosphate, Cysteamine-S-Phosphate, Uridine-3'-monophosphate, O-Phospho-L-Tyrosine, O-Phosphoryl-Ethanolamine, Thymidine-5'-monophosphate, Inositol Hexaphosphate, Sulfate and Glutathione all significantly increased growth in comparison to a negative control (Fig. 4.5b). The summary of additives that increased growth of *Δaox1* cells in the PM4 plate can be found in Fig. 4.5c.

A

PM4 Phosphorous and Sulphur Source Utilisation

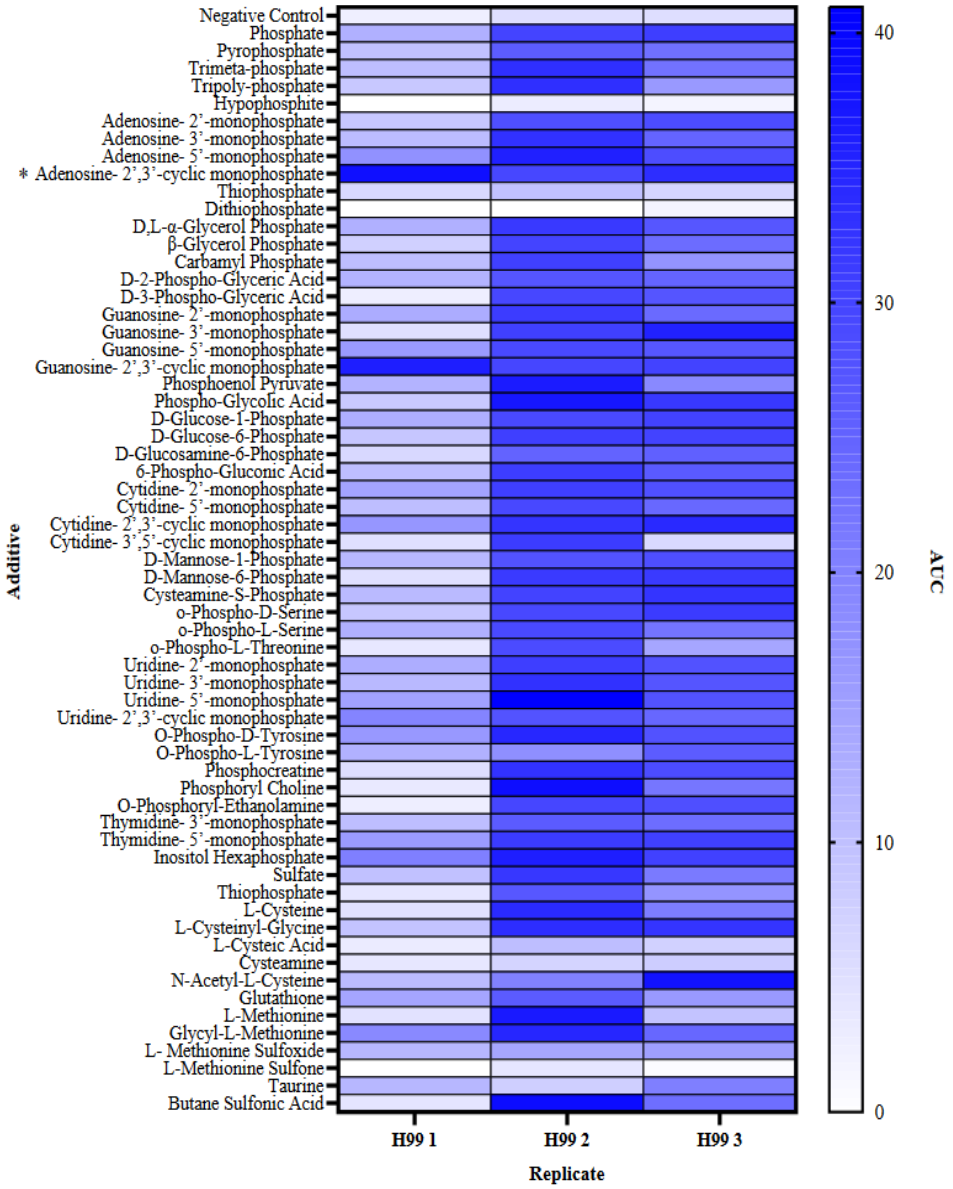

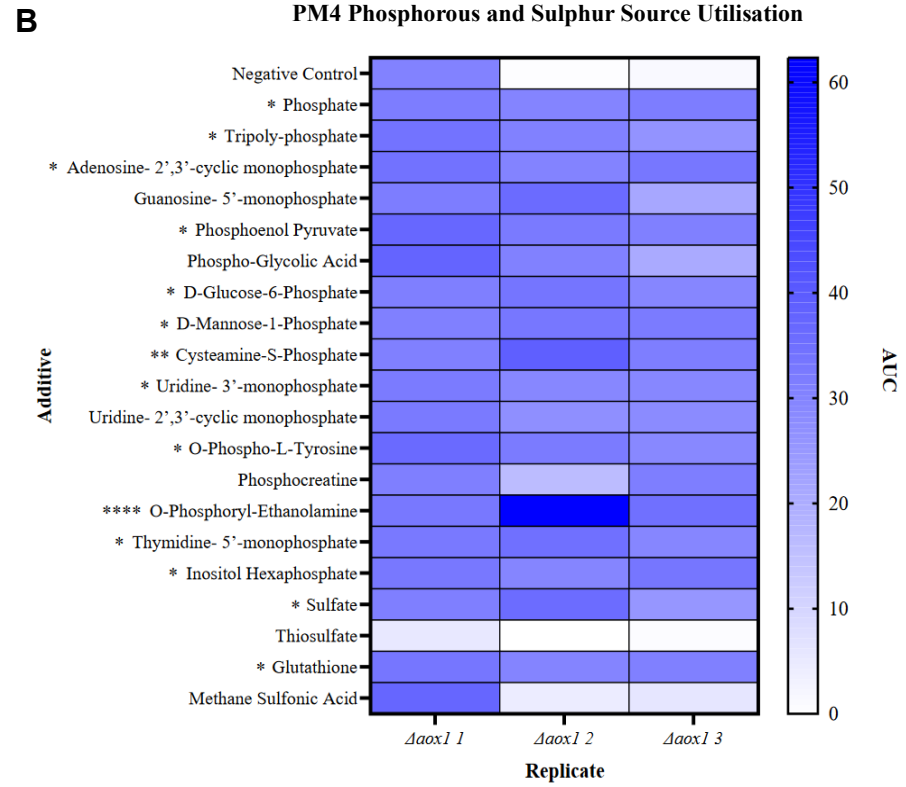

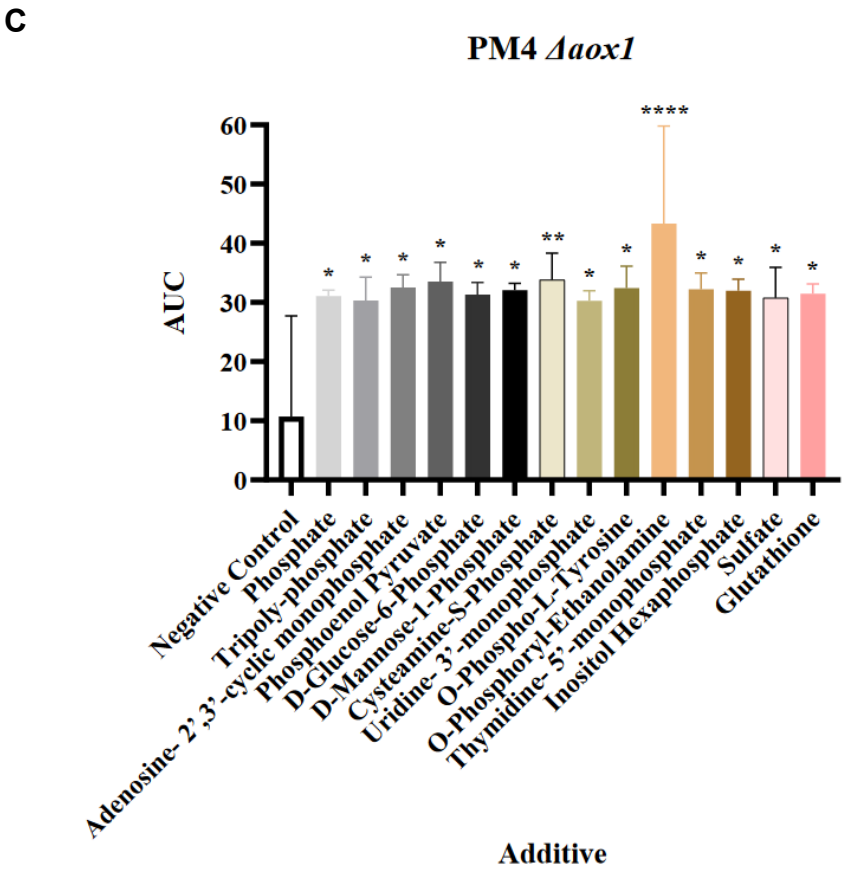

Figure 4.5: C. neoformans phosphorous and sulphur source utilisation.
Biological triplicates of WT (H99) and *Δaox1* were grown in the presence of different phosphorous and sulphur source additives (Additive) using the BIOLOG system and the area under the curve was recorded (AUC). (**A**) PM4 / H99, (**B**) PM4 / *Δaox1*, (**C**) Summary of significant hits from PM4 / *Δaox1.* Significance was calculated using Dunnett's multiple comparisons test following a one-way ANOVA in GraphPad Prism. * < 0.05, ** < 0.005, **** <0.0001, where P = 0.05. Error bars represent ± SD. n = 3

4.2.5 Addition of key biosynthetic pathway substrates does not significantly affect *C. neoformans* growth

We wanted to investigate how well *C. neoformans* could utilise biosynthetic pathway substrates in minimal media, as creation of multiple complex intermediates from simpler substrates enables rapid cellular signalling and remodelling in a limiting environment such as the nutrient scarce host, which could enhance pathogenicity. To assess biosynthetic pathway substrate addition on *C. neoformans* growth, wildtype H99 and *Δaox1* cultures were inoculated into PM5 plates from the BIOLOG system and the calculated AUC values were compared to a negative control (Fig. 4.6). Interestingly, none of the substrate additives provided significantly affected growth of H99 (Fig. 4.6a) or *Δaox1* (Fig. 4.6b), with *Δaox1* cells grown in the PM5 plate producing very few repeatable hits.

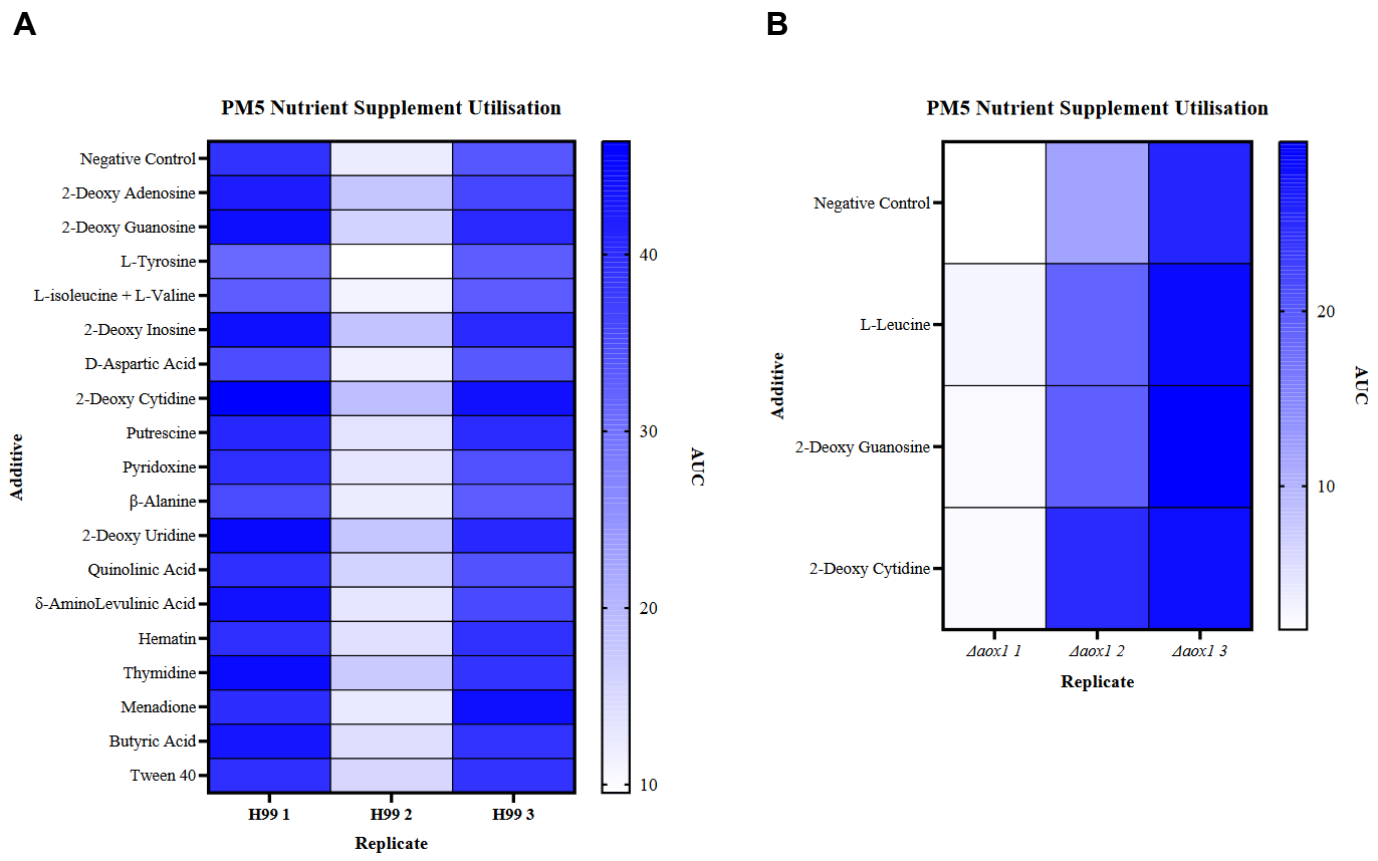

Figure 4.6: C. neoformans BIOLOG nutrient supplement utilisation.
Biological triplicates of WT (H99) and *Δaox1* were grown in the presence of different BIOLOG nutrient supplements (Additive) using the BIOLOG system and the area under the curve was recorded (AUC). (**A**) PM5 / H99, (**B**) PM5 / *Δaox1*. Significance was calculated using Dunnett's multiple comparisons test following a one-way ANOVA in GraphPad Prism. No significance was observed. n = 3.

4.2.6 Effects of pH on *C. neoformans* growth

One key virulence factor observed in *C. neoformans* is its ability to survive the harsh, acidic phagolysosome of macrophages[27], which is thought to heavily contribute to host dissemination and dragotcytosis. We therefore wanted to assess whether loss of Aox would change sensitivity to pH stress. Wildtype H99 and *Δaox1* cultures were inoculated into PM10 plates from the BIOLOG system that contained different pH conditions and the calculated AUC values were compared to a negative control (Fig. 4.7). Our data showed that pH values ranging from pH 5 – 7 displayed an increase in AUC value for both H99 (Fig. 4.7a) and *Δaox1* cells (Fig. 4.7b), although both strains were sensitive to pH 9.5 and pH 10. A summary of significant hits for pH effect on growth for both strains can be found in Fig. 4.7c.

While pH 4.5 alone had no significant effect on growth of H99 (Fig. 4.7a) or *Δaox1* (Fig. 4.7b), pH 4.5 supplemented with all given additives apart from L-Glutamic Acid, L-Isoleucine, L-Leucine, L-Threonine, and L-Homoserine also showed an increase in growth for H99 (Fig. 4.7a). PM10 plates containing *Δaox1* cells showed a similar result, whereby pH 4.5 supplemented with L-Glutamine, Glycine, L-Histidine, L-Lysine, L-Phenylalanine, L-Threonine, L-Tyrosine, L-Valine, Hydroxy- L-Proline, L-Ornithine, L-Homoarginine, L-Norleucine, β-Hydroxy Glutamate, 5-Hydroxy Lysine, 5-Hydroxy Tryptophan, D,L-Diamino pimelic acid and Trimethyl amine-N-oxide showed an increase in AUC value (Fig. 4.7b). Interestingly, pH 4.5 + α-Amino malonate displayed a reproducible inhibition of both H99 and *Δaox1* growth. Significant loss of wildtype (Fig. 4.7a) and *Δaox1* (Fig. 4.7b) growth at pH 9.5 and pH 10 could not be rescued by supplement addition, and both strains showed sensitivity to X-Caprylate, X-α-D-Glucoside, X-β-D-Galactoside, X-α-D-Glucuronide, X-β-D-Glucuronide, X-β-D-Glucosaminide, X-β-D-Galactosaminide and X-SO4 (Fig. 4.7a, 4.7b). A summary of both pH 4.5 with additives that significantly affected growth of H99 and *Δaox1* can be found in Fig. 4.7d, while statistically significant hits for pH 9.5 with additives can be found in Fig. 4.7e for both strains.

A

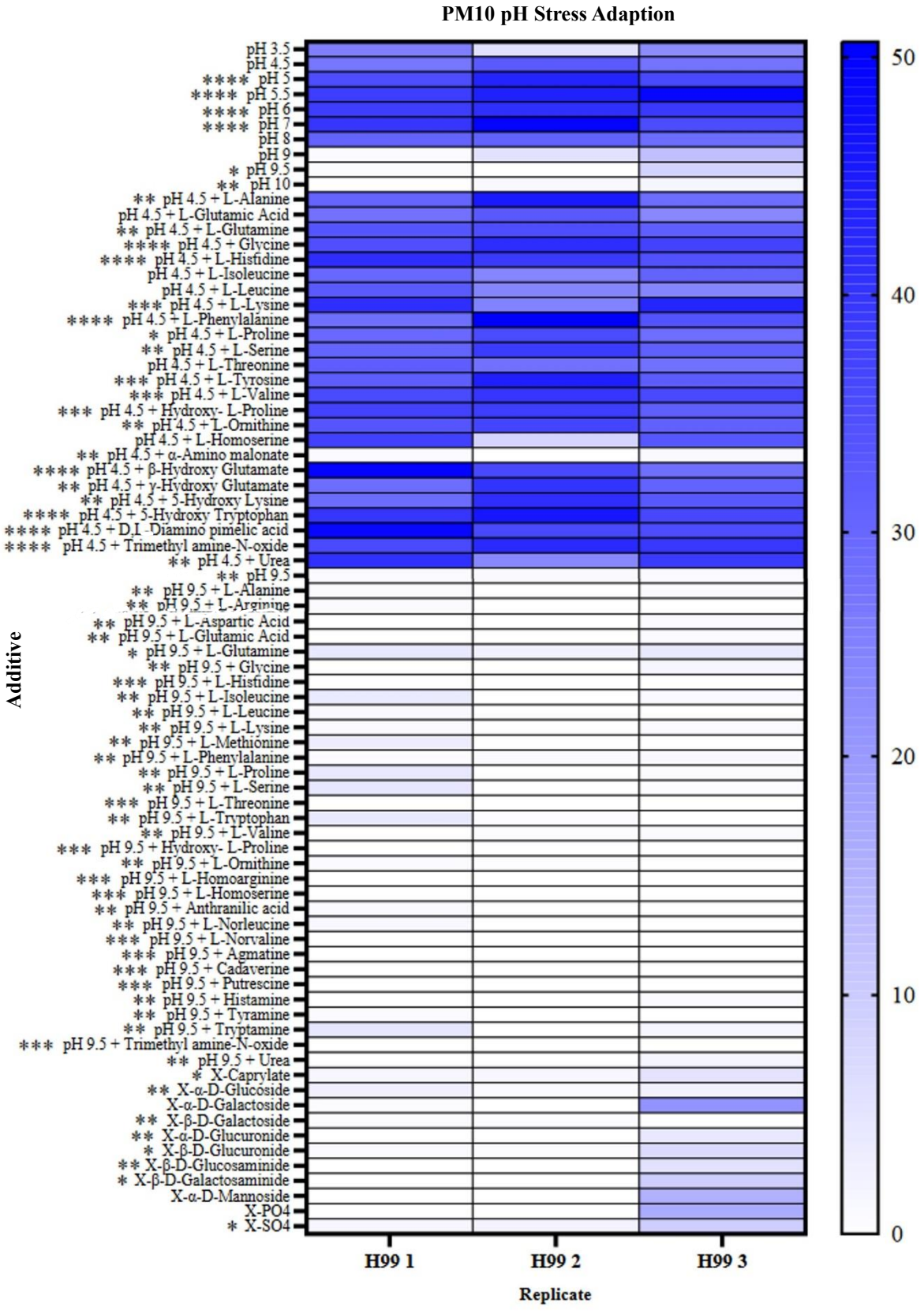
PM10 pH Stress Adaption
pH 3.5
pH 4.5
**** pH 5
**** pH 5.5
**** pH 6
**** pH 7
pH 8
pH 9
* pH 9.5
** pH 10
** pH 4.5 + L-Alanine
pH 4.5 + L-Glutamic Acid
** pH 4.5 + L-Glutamine
**** pH 4.5 + Glycine
**** pH 4.5 + L-Histidine
pH 4.5 + L-Isoleucine
pH 4.5 + L-Leucine
*** pH 4.5 + L-Lysine
**** pH 4.5 + L-Phenylalanine
* pH 4.5 + L-Proline
** pH 4.5 + L-Serine
pH 4.5 + L-Threonine
*** pH 4.5 + L-Tyrosine
*** pH 4.5 + L-Valine
*** pH 4.5 + Hydroxy- L-Proline
** pH 4.5 + L-Ornithine
pH 4.5 + L-Homoserine
** pH 4.5 + α-Amino malonate
**** pH 4.5 + β-Hydroxy Glutamate
** pH 4.5 + γ-Hydroxy Glutamate
** pH 4.5 + 5-Hydroxy Lysine
**** pH 4.5 + 5-Hydroxy Tryptophan
**** pH 4.5 + D,L -Diamino pimelic acid
**** pH 4.5 + Trimethyl amine-N-oxide
** pH 4.5 + Urea
** pH 9.5
** pH 9.5 + L-Alanine
** pH 9.5 + L-Arginine
** pH 9.5 + L-Aspartic Acid
** pH 9.5 + L-Glutamic Acid
* pH 9.5 + L-Glutamine
** pH 9.5 + Glycine
*** pH 9.5 + L-Histidine
** pH 9.5 + L-Isoleucine
** pH 9.5 + L-Leucine
** pH 9.5 + L-Lysine
** pH 9.5 + L-Methionine
** pH 9.5 + L-Phenylalanine
** pH 9.5 + L-Proline
** pH 9.5 + L-Serine
*** pH 9.5 + L-Threonine
** pH 9.5 + L-Tryptophan
** pH 9.5 + L-Valine
*** pH 9.5 + Hydroxy- L-Proline
** pH 9.5 + L-Ornithine
*** pH 9.5 + L-Homoarginine
*** pH 9.5 + L-Homoserine
** pH 9.5 + Anthranilic acid
** pH 9.5 + L-Norleucine
*** pH 9.5 + L-Norvaline
*** pH 9.5 + Agmatine
*** pH 9.5 + Cadaverine
*** pH 9.5 + Putrescine
** pH 9.5 + Histamine
** pH 9.5 + Tyramine
** pH 9.5 + Tryptamine
*** pH 9.5 + Trimethyl amine-N-oxide
** pH 9.5 + Urea
* X-Caprylate
** X-α-D-Glucoside
X-α-D-Galactoside
** X-β-D-Galactoside
** X-α-D-Glucuronide
* X-β-D-Glucuronide
** X-β-D-Glucosaminide
* X-β-D-Galactosaminide
X-α-D-Mannoside
X-PO4
* X-SO4
Additive
H99 1
H99 2
H99 3
Replicate
50
40
30
20
10
0

B

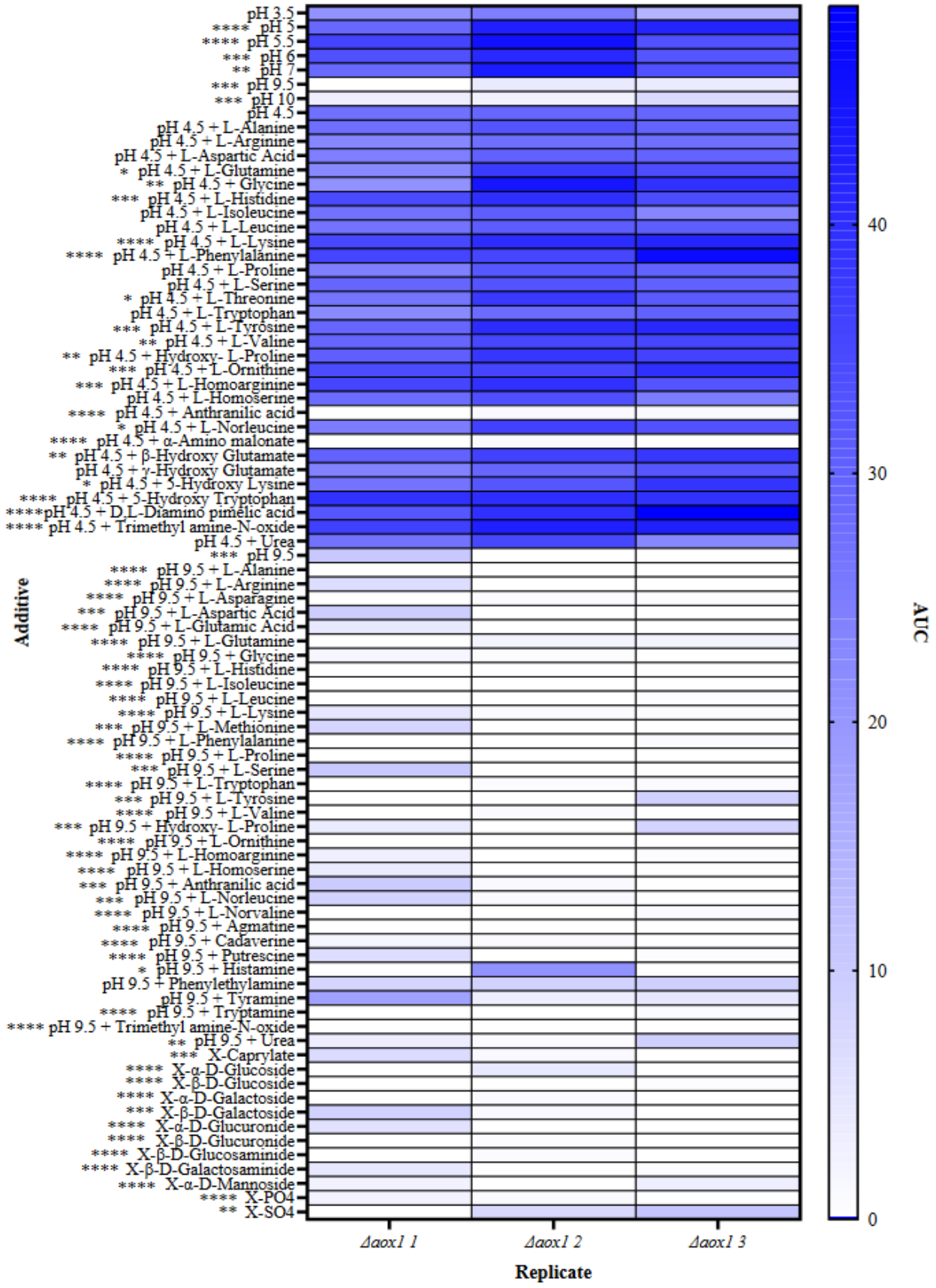
PM10 pH Stress Adaption
pH 3.5
**** pH 5
**** pH 5.5
*** pH 6
** pH 7
*** pH 9.5
*** pH 10
pH 4.5
pH 4.5 + L-Alanine
pH 4.5 + L-Arginine
pH 4.5 + L-Aspartic Acid
* pH 4.5 + L-Glutamine
** pH 4.5 + Glycine
*** pH 4.5 + L-Histidine
pH 4.5 + L-Isoleucine
pH 4.5 + L-Leucine
**** pH 4.5 + L-Lysine
**** pH 4.5 + L-Phenylalanine
pH 4.5 + L-Proline
pH 4.5 + L-Serine
* pH 4.5 + L-Threonine
pH 4.5 + L-Tryptophan
*** pH 4.5 + L-Tyrosine
** pH 4.5 + L-Valine
** pH 4.5 + Hydroxy- L-Proline
*** pH 4.5 + L-Ornithine
*** pH 4.5 + L-Homoarginine
pH 4.5 + L-Homoserine
**** pH 4.5 + Anthranilic acid
* pH 4.5 + L-Norleucine
**** pH 4.5 + α-Amino malonate
** pH 4.5 + β-Hydroxy Glutamate
pH 4.5 + γ-Hydroxy Glutamate
* pH 4.5 + 5-Hydroxy Lysine
**** pH 4.5 + 5-Hydroxy Tryptophan
****pH 4.5 + D,L-Diamino pimelic acid
**** pH 4.5 + Trimethyl amine-N-oxide
pH 4.5 + Urea
*** pH 9.5
**** pH 9.5 + L-Alanine
**** pH 9.5 + L-Arginine
**** pH 9.5 + L-Asparagine
*** pH 9.5 + L-Aspartic Acid
**** pH 9.5 + L-Glutamic Acid
**** pH 9.5 + L-Glutamine
**** pH 9.5 + Glycine
**** pH 9.5 + L-Histidine
**** pH 9.5 + L-Isoleucine
**** pH 9.5 + L-Leucine
**** pH 9.5 + L-Lysine
*** pH 9.5 + L-Methionine
**** pH 9.5 + L-Phenylalanine
**** pH 9.5 + L-Proline
*** pH 9.5 + L-Serine
**** pH 9.5 + L-Tryptophan
*** pH 9.5 + L-Tyrosine
**** pH 9.5 + L-Valine
*** pH 9.5 + Hydroxy- L-Proline
**** pH 9.5 + L-Ornithine
**** pH 9.5 + L-Homoarginine
**** pH 9.5 + L-Homoserine
*** pH 9.5 + Anthranilic acid
*** pH 9.5 + L-Norleucine
**** pH 9.5 + L-Norvaline
**** pH 9.5 + Agmatine
**** pH 9.5 + Cadaverine
**** pH 9.5 + Putrescine
* pH 9.5 + Histamine
pH 9.5 + Phenylethylamine
pH 9.5 + Tyramine
**** pH 9.5 + Tryptamine
**** pH 9.5 + Trimethyl amine-N-oxide
** pH 9.5 + Urea
*** X-Caprylate
**** X-α-D-Glucoside
**** X-β-D-Glucoside
**** X-α-D-Galactoside
*** X-β-D-Galactoside
**** X-α-D-Glucuronide
**** X-β-D-Glucuronide
**** X-β-D-Glucosaminide
**** X-β-D-Galactosaminide
**** X-α-D-Mannoside
**** X-PO4
** X-SO4
Additive
Δaox1 1
Δaox1 2
Δaox1 3
Replicate
AUC
40
30
20
10
0

C

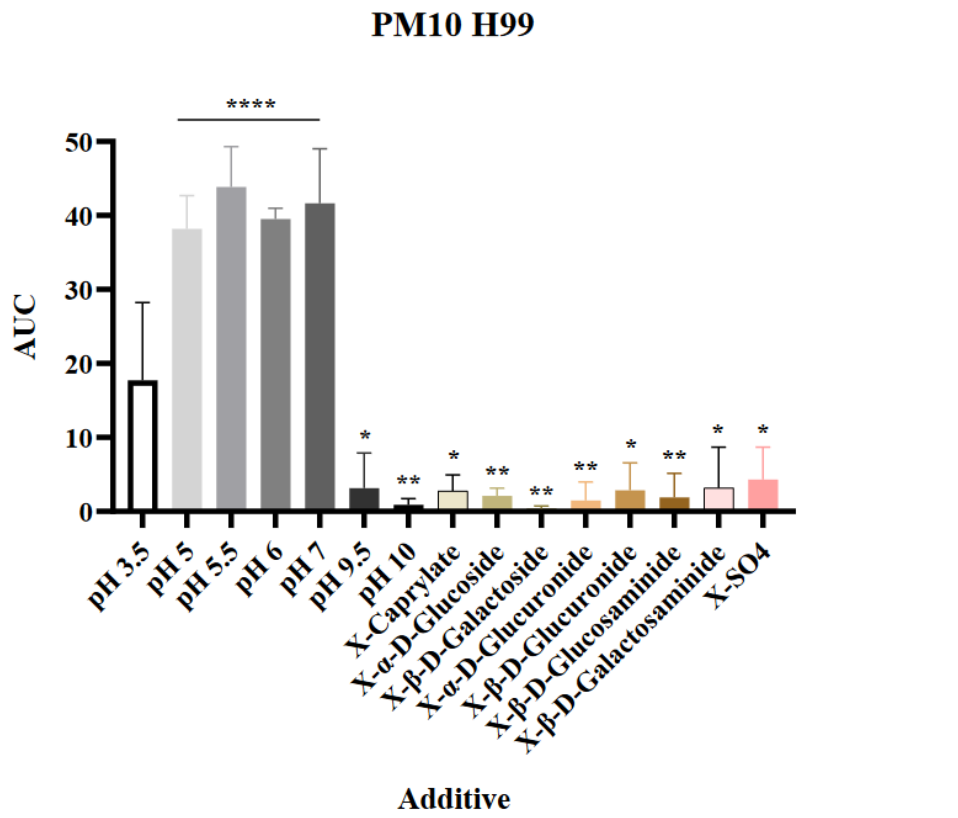
PM10 H99
AUC
Additive
pH 3.5
pH 5
pH 5.5
pH 6
pH 7
pH 9.5
pH 10
X-Caprylate
X-α-D-Glucoside
X-β-D-Galactoside
X-α-D-Glucuronide
X-β-D-Glucuronide
X-β-D-Glucosaminide
X-β-D-Galactosaminide
X-SO4

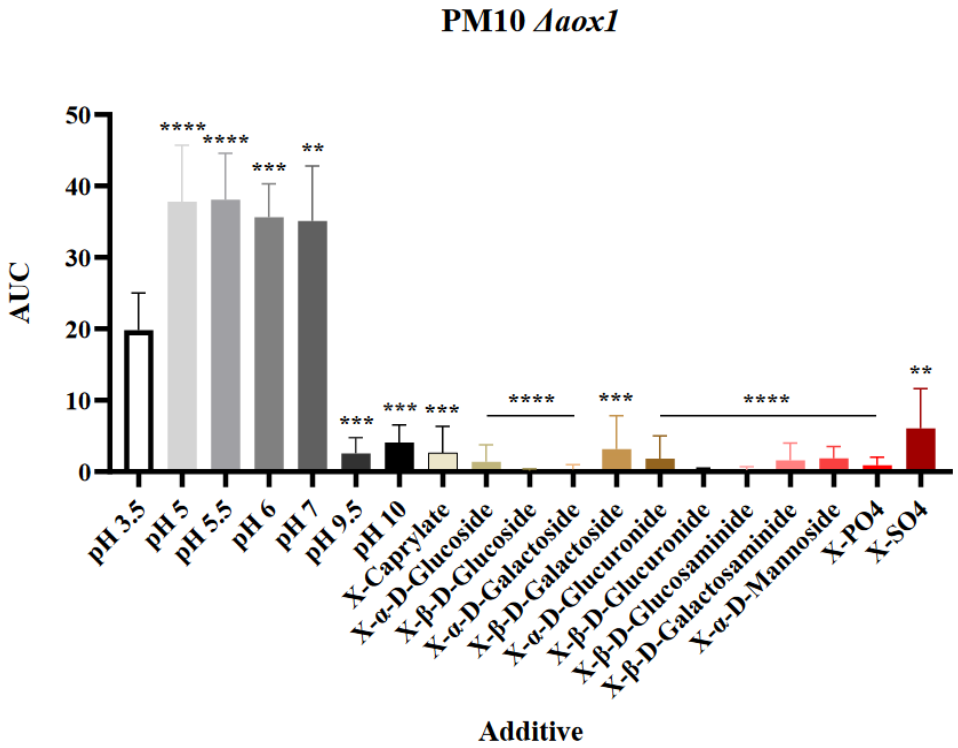
PM10 Δaox1
AUC
Additive
pH 3.5
pH 5
pH 5.5
pH 6
pH 7
pH 9.5
pH 10
X-Caprylate
X-α-D-Glucoside
X-β-D-Glucoside
X-α-D-Galactoside
X-β-D-Galactoside
X-α-D-Glucuronide
X-β-D-Glucuronide
X-β-D-Glucosaminide
X-β-D-Galactosaminide
X-α-D-Mannoside
X-PO4
X-SO4

D

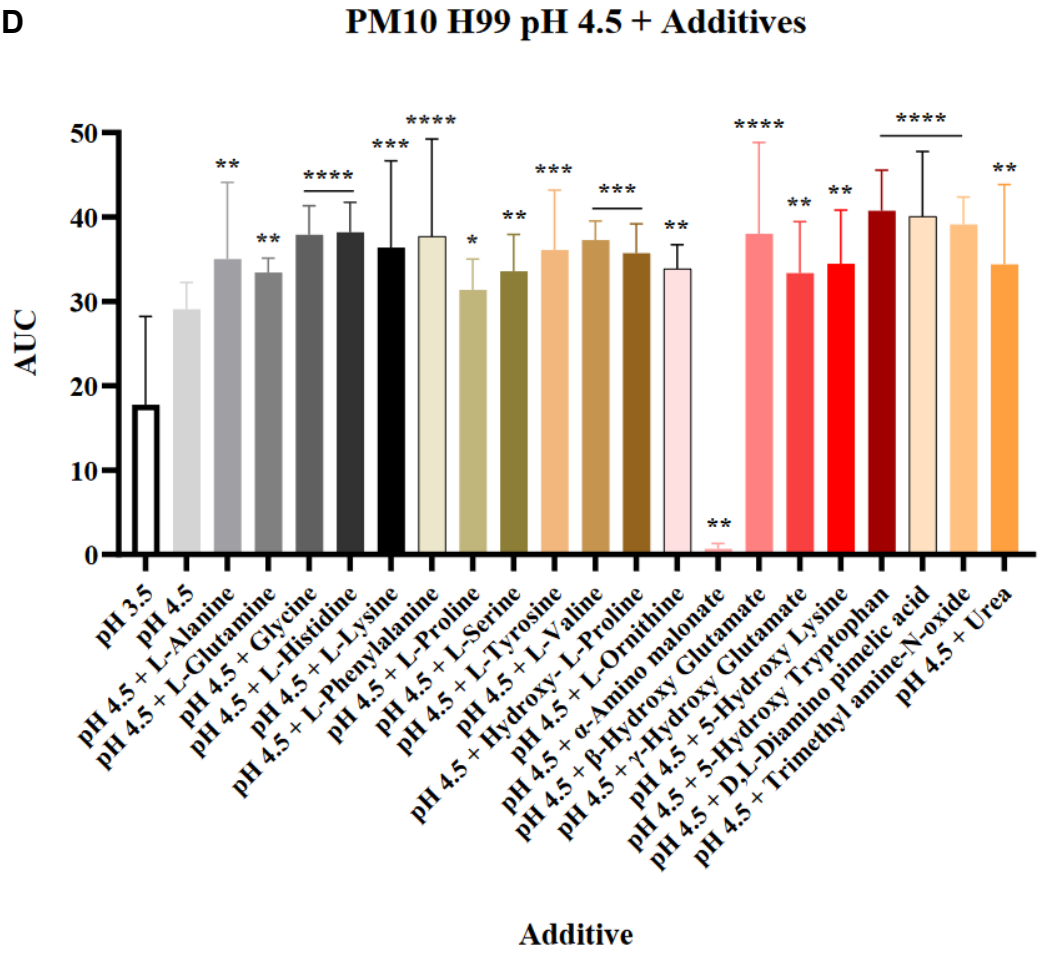
PM10 H99 pH 4.5 + Additives
AUC
Additive
pH 3.5
pH 4.5
pH 4.5 + L-Alanine
pH 4.5 + L-Glutamine
pH 4.5 + Glycine
pH 4.5 + L-Histidine
pH 4.5 + L-Lysine
pH 4.5 + L-Phenylalanine
pH 4.5 + L-Proline
pH 4.5 + L-Serine
pH 4.5 + L-Tyrosine
pH 4.5 + L-Valine
pH 4.5 + Hydroxy- L-Proline
pH 4.5 + L-Ornithine
pH 4.5 + α-Amino malonate
pH 4.5 + β-Hydroxy Glutamate
pH 4.5 + γ-Hydroxy Glutamate
pH 4.5 + 5-Hydroxy Lysine
pH 4.5 + 5-Hydroxy Tryptophan
pH 4.5 + D,L-Diamino pimelic acid
pH 4.5 + Trimethyl amine-N-oxide
pH 4.5 + Urea

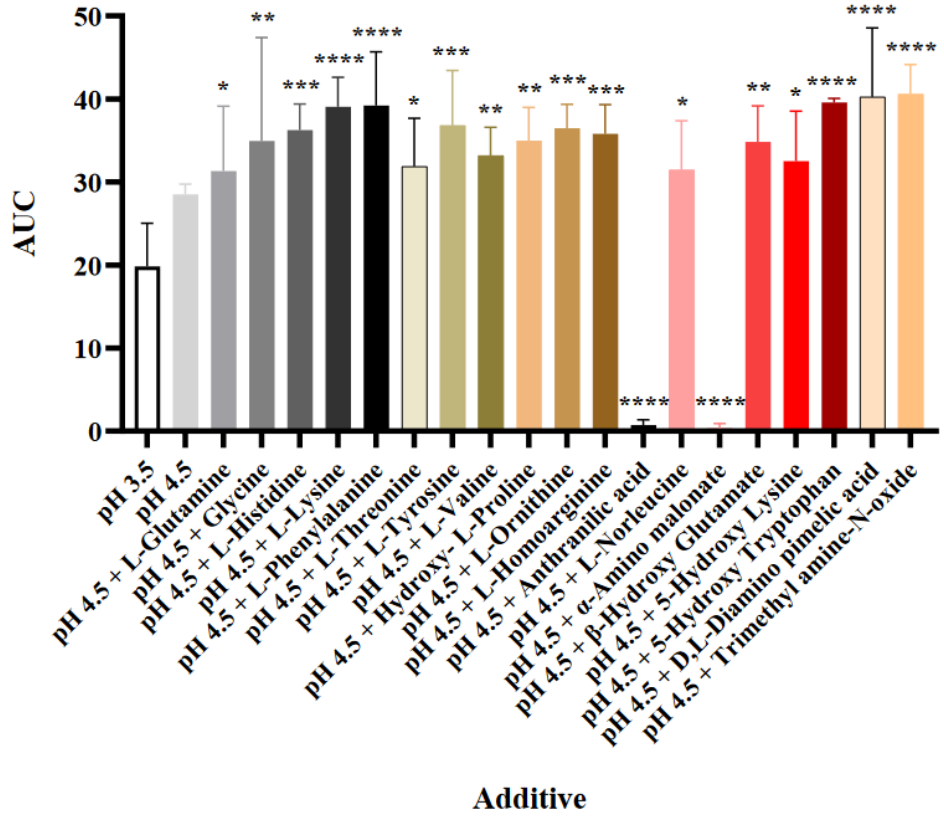
PM10 Δaox1 pH 4.5 + Additives
AUC
Additive
pH 3.5
pH 4.5
pH 4.5 + L-Glutamine
pH 4.5 + Glycine
pH 4.5 + L-Histidine
pH 4.5 + L-Lysine
pH 4.5 + L-Phenylalanine
pH 4.5 + L-Threonine
pH 4.5 + L-Tyrosine
pH 4.5 + L-Valine
pH 4.5 + Hydroxy- L-Proline
pH 4.5 + L-Ornithine
pH 4.5 + L-Homoarginine
pH 4.5 + Anthranilic acid
pH 4.5 + L-Norleucine
pH 4.5 + α-Amino malonate
pH 4.5 + β-Hydroxy Glutamate
pH 4.5 + 5-Hydroxy Lysine
pH 4.5 + 5-Hydroxy Tryptophan
pH 4.5 + D,L-Diamino pimelic acid
pH 4.5 + Trimethyl amine-N-oxide

E

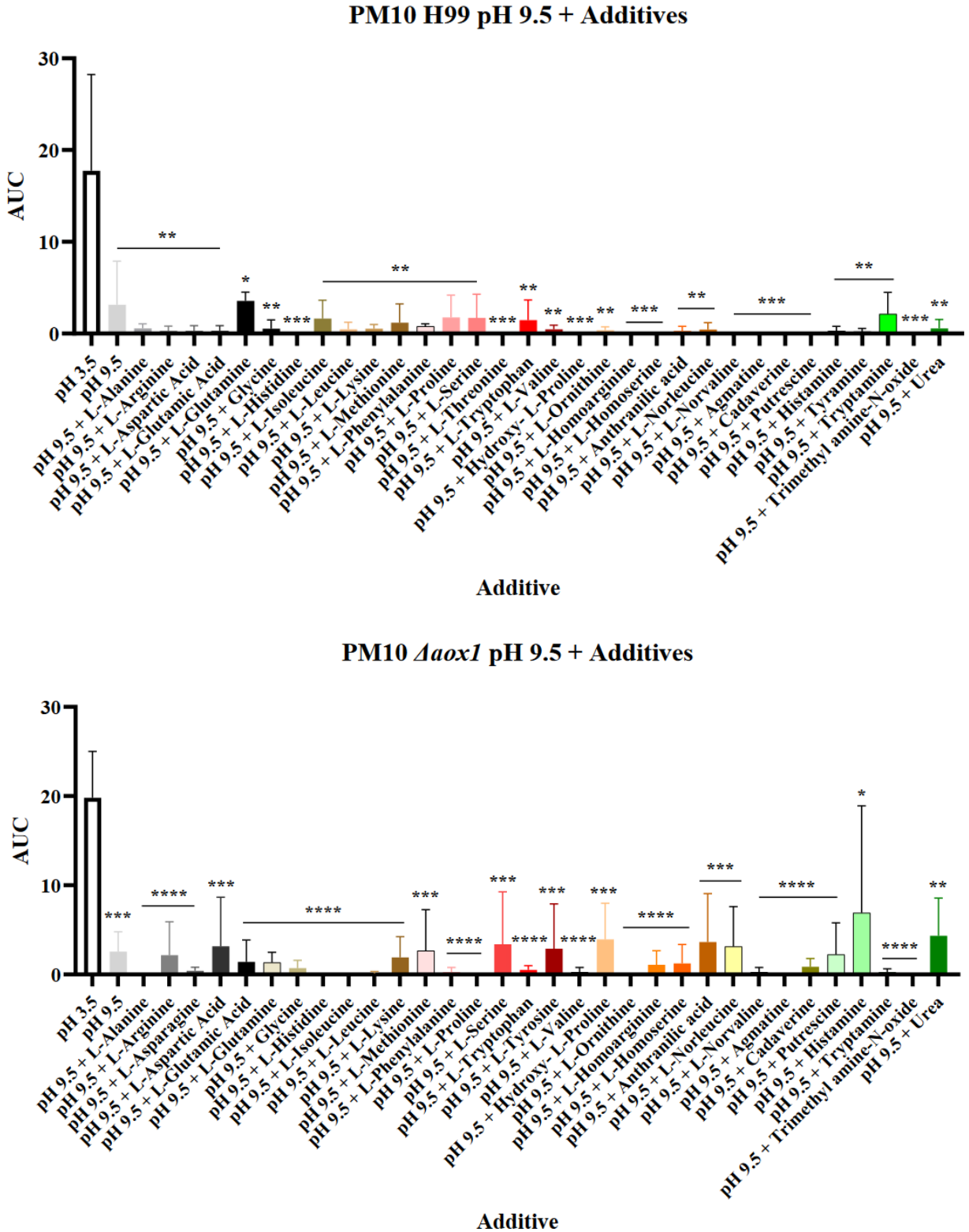

Figure 4.7: C. neoformans pH stress adaption.
Biological triplicates of WT (H99) and *Δaox1* were grown in the presence of different pH stresses (Additive) using the BIOLOG system and the area under the curve was recorded (AUC). (**A**) PM10 / H99, (**B**) PM10 / *Δaox1*. (**C**) Summaries of statistically significant pH conditions affecting both H99 and *Δaox1* cell growth. (**D**) Summaries of statistically significant additives at pH 4.5 affecting both H99 and *Δaox1* cell growth. (**E**) Summaries of statistically significant additives at pH 9.5 affecting both H99 and *Δaox1* cell growth. Significance was calculated using Dunnett's multiple comparisons test following a one-way ANOVA in GraphPad Prism. * < 0.05, ** < 0.005, ** < 0.0005, **** <0.0001, where P = 0.05. Error bars represent ± SD. n = 3

4.2.7 *C. neoformans* is sensitive to osmotic stress

After investigation of supplement additives on *C. neoformans* strain growth in minimal media, we wanted to assess whether loss of Aox would confer more sensitivity to osmotic stress. Wildtype H99 and *Δaox1* cultures were inoculated into PM9 plates from the BIOLOG system and the calculated AUC values were compared to a negative control (Fig. 4.8). Interestingly, our data shows that H99 appeared to be sensitive to osmolyte addition, with all additives apart from Sodium Sulfate (211mM), Sodium Formate (147mM), Sodium Lactate (178mM), Sodium Phosphate (pH 7, 50mM), Ammonium Sulfate (pH 8, up to 50mM) and Sodium Nitrate (80mM and 100mM, respectively) showing significantly lower AUC values (Fig. 4.8a). The full summary of osmolytes that significantly affected H99 cell growth can be found in Fig. 4.8c. However, for *Δaox1*, some additional additives significantly inhibited growth such as NaCl (1026mM – NaCl 1710mM), NaCl 1026mM + L-Carnitine, NaCl 1026mM + Trimethylamine-N-oxide, NaCl 1026mM + Trigonelline, Urea 1169mM, Sodium Lactate (979mM and 1068mM), Sodium Benzoate pH 5.2 (20mM – 200mM), and Sodium Nitrite (20mM-100mM), although interestingly Ethylene glycol (805mM and 1610mM) and Sodium Phosphate (pH 7, 20mM) additives showed an increase in growth for *Δaox1* (Fig. 4.8b). The summary of osmolyte additives that significantly impacted *Δaox1* cell growth can be found in Fig. 4.8d. Overall summary tables for statistically significant results from the entire BIOLOG screen can be found in Appendix Table 7.1.

Interestingly, both wildtype and *Δaox1* mutant cell growth was greatly inhibited by various concentrations of sodium nitrite (Fig. 4.8e). Given that sodium nitrite is known to inhibit fungal respiration and induce ROS generation, this was of interest for this thesis, and we decided to investigate this further.

A

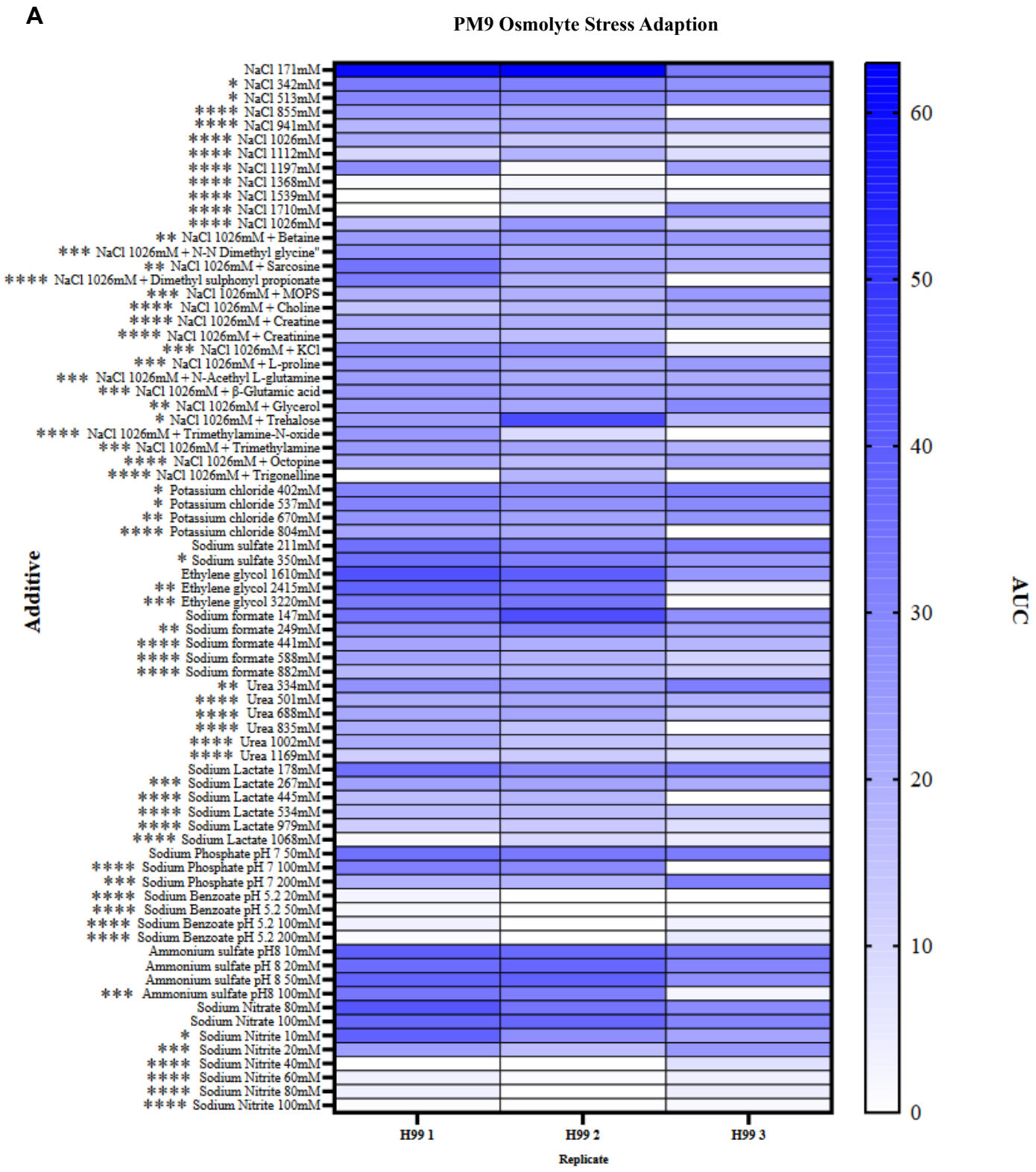
PM9 Osmolyte Stress Adaption
Additive
NaCl 171mM
* NaCl 342mM
* NaCl 513mM
**** NaCl 855mM
**** NaCl 941mM
**** NaCl 1026mM
**** NaCl 1112mM
**** NaCl 1197mM
**** NaCl 1368mM
**** NaCl 1539mM
**** NaCl 1710mM
**** NaCl 1026mM
** NaCl 1026mM + Betaine
*** NaCl 1026mM + N-N Dimethyl glycine"
** NaCl 1026mM + Sarcosine
**** NaCl 1026mM + Dimethyl sulphonyl propionate
*** NaCl 1026mM + MOPS
**** NaCl 1026mM + Choline
**** NaCl 1026mM + Creatine
**** NaCl 1026mM + Creatinine
*** NaCl 1026mM + KCl
*** NaCl 1026mM + L-proline
*** NaCl 1026mM + N-Acethyl L-glutamine
*** NaCl 1026mM + β-Glutamic acid
** NaCl 1026mM + Glycerol
* NaCl 1026mM + Trehalose
**** NaCl 1026mM + Trimethylamine-N-oxide
*** NaCl 1026mM + Trimethylamine
**** NaCl 1026mM + Octopine
**** NaCl 1026mM + Trigonelline
* Potassium chloride 402mM
* Potassium chloride 537mM
** Potassium chloride 670mM
**** Potassium chloride 804mM
Sodium sulfate 211mM
* Sodium sulfate 350mM
Ethylene glycol 1610mM
** Ethylene glycol 2415mM
*** Ethylene glycol 3220mM
Sodium formate 147mM
** Sodium formate 249mM
**** Sodium formate 441mM
**** Sodium formate 588mM
**** Sodium formate 882mM
** Urea 334mM
**** Urea 501mM
**** Urea 688mM
**** Urea 835mM
**** Urea 1002mM
**** Urea 1169mM
Sodium Lactate 178mM
*** Sodium Lactate 267mM
**** Sodium Lactate 445mM
**** Sodium Lactate 534mM
**** Sodium Lactate 979mM
**** Sodium Lactate 1068mM
Sodium Phosphate pH 7 50mM
**** Sodium Phosphate pH 7 100mM
*** Sodium Phosphate pH 7 200mM
**** Sodium Benzoate pH 5.2 20mM
**** Sodium Benzoate pH 5.2 50mM
**** Sodium Benzoate pH 5.2 100mM
**** Sodium Benzoate pH 5.2 200mM
Ammonium sulfate pH8 10mM
Ammonium sulfate pH 8 20mM
Ammonium sulfate pH 8 50mM
*** Ammonium sulfate pH8 100mM
Sodium Nitrate 80mM
Sodium Nitrate 100mM
* Sodium Nitrite 10mM
*** Sodium Nitrite 20mM
**** Sodium Nitrite 40mM
**** Sodium Nitrite 60mM
**** Sodium Nitrite 80mM
**** Sodium Nitrite 100mM
H99 1
H99 2
H99 3
Replicate
AUC
60
50
40
30
20
10
0

B

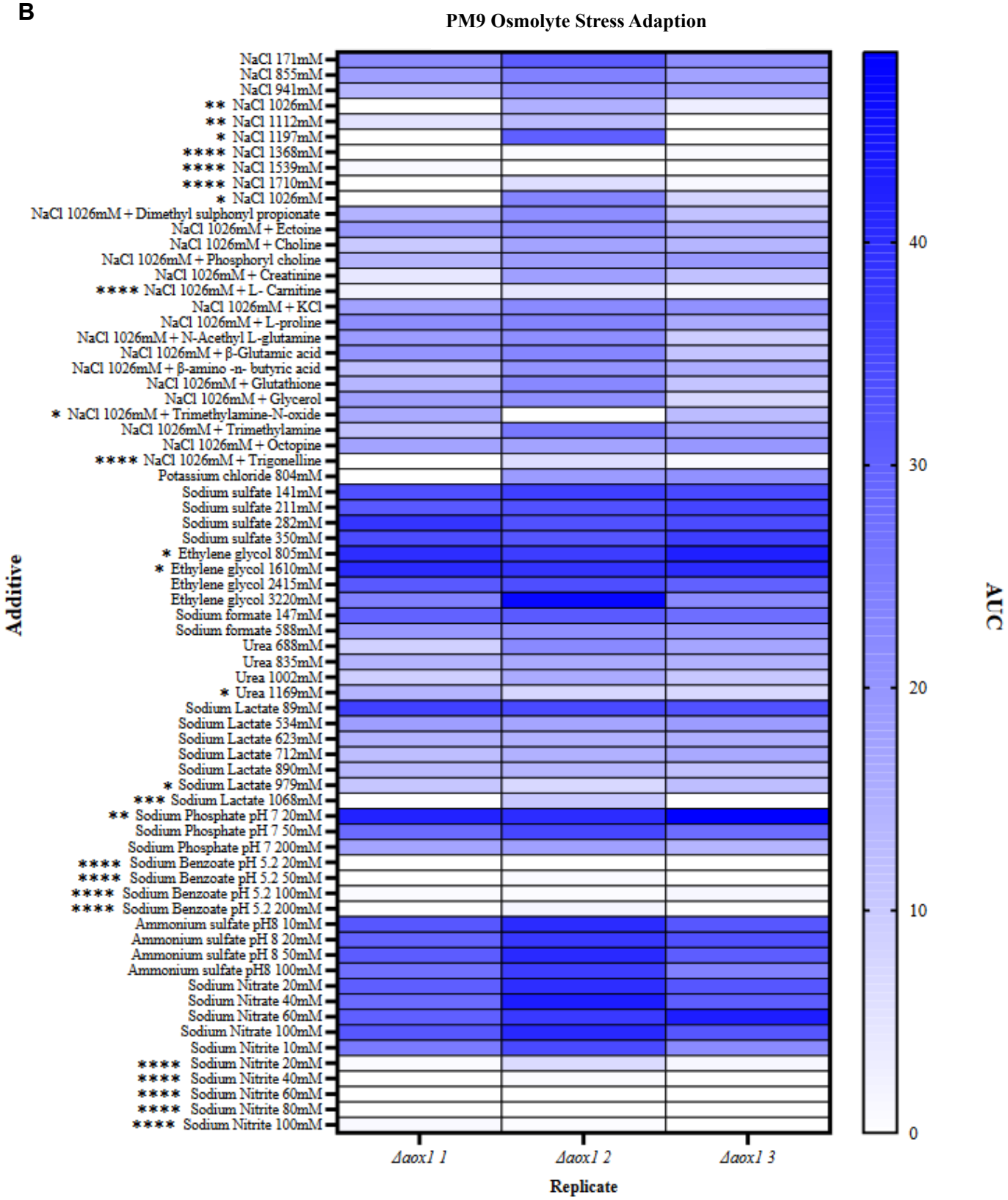
PM9 Osmolyte Stress Adaption
NaCl 171mM
NaCl 855mM
NaCl 941mM
** NaCl 1026mM
** NaCl 1112mM
* NaCl 1197mM
**** NaCl 1368mM
**** NaCl 1539mM
**** NaCl 1710mM
* NaCl 1026mM
NaCl 1026mM + Dimethyl sulphonyl propionate
NaCl 1026mM + Ectoine
NaCl 1026mM + Choline
NaCl 1026mM + Phosphoryl choline
NaCl 1026mM + Creatinine
**** NaCl 1026mM + L- Carnitine
NaCl 1026mM + KCl
NaCl 1026mM + L-proline
NaCl 1026mM + N-Acethyl L-glutamine
NaCl 1026mM + β-Glutamic acid
NaCl 1026mM + β-amino -n- butyric acid
NaCl 1026mM + Glutathione
NaCl 1026mM + Glycerol
* NaCl 1026mM + Trimethylamine-N-oxide
NaCl 1026mM + Trimethylamine
NaCl 1026mM + Octopine
**** NaCl 1026mM + Trigonelline
Potassium chloride 804mM
Sodium sulfate 141mM
Sodium sulfate 211mM
Sodium sulfate 282mM
Sodium sulfate 350mM
* Ethylene glycol 805mM
* Ethylene glycol 1610mM
Ethylene glycol 2415mM
Ethylene glycol 3220mM
Sodium formate 147mM
Sodium formate 588mM
Urea 688mM
Urea 835mM
Urea 1002mM
* Urea 1169mM
Sodium Lactate 89mM
Sodium Lactate 534mM
Sodium Lactate 623mM
Sodium Lactate 712mM
Sodium Lactate 890mM
* Sodium Lactate 979mM
*** Sodium Lactate 1068mM
** Sodium Phosphate pH 7 20mM
Sodium Phosphate pH 7 50mM
Sodium Phosphate pH 7 200mM
**** Sodium Benzoate pH 5.2 20mM
**** Sodium Benzoate pH 5.2 50mM
**** Sodium Benzoate pH 5.2 100mM
**** Sodium Benzoate pH 5.2 200mM
Ammonium sulfate pH8 10mM
Ammonium sulfate pH 8 20mM
Ammonium sulfate pH 8 50mM
Ammonium sulfate pH8 100mM
Sodium Nitrate 20mM
Sodium Nitrate 40mM
Sodium Nitrate 60mM
Sodium Nitrate 100mM
Sodium Nitrite 10mM
**** Sodium Nitrite 20mM
**** Sodium Nitrite 40mM
**** Sodium Nitrite 60mM
**** Sodium Nitrite 80mM
**** Sodium Nitrite 100mM
Additive
Δaox1 1
Δaox1 2
Δaox1 3
Replicate
AUC
40
30
20
10
0

c

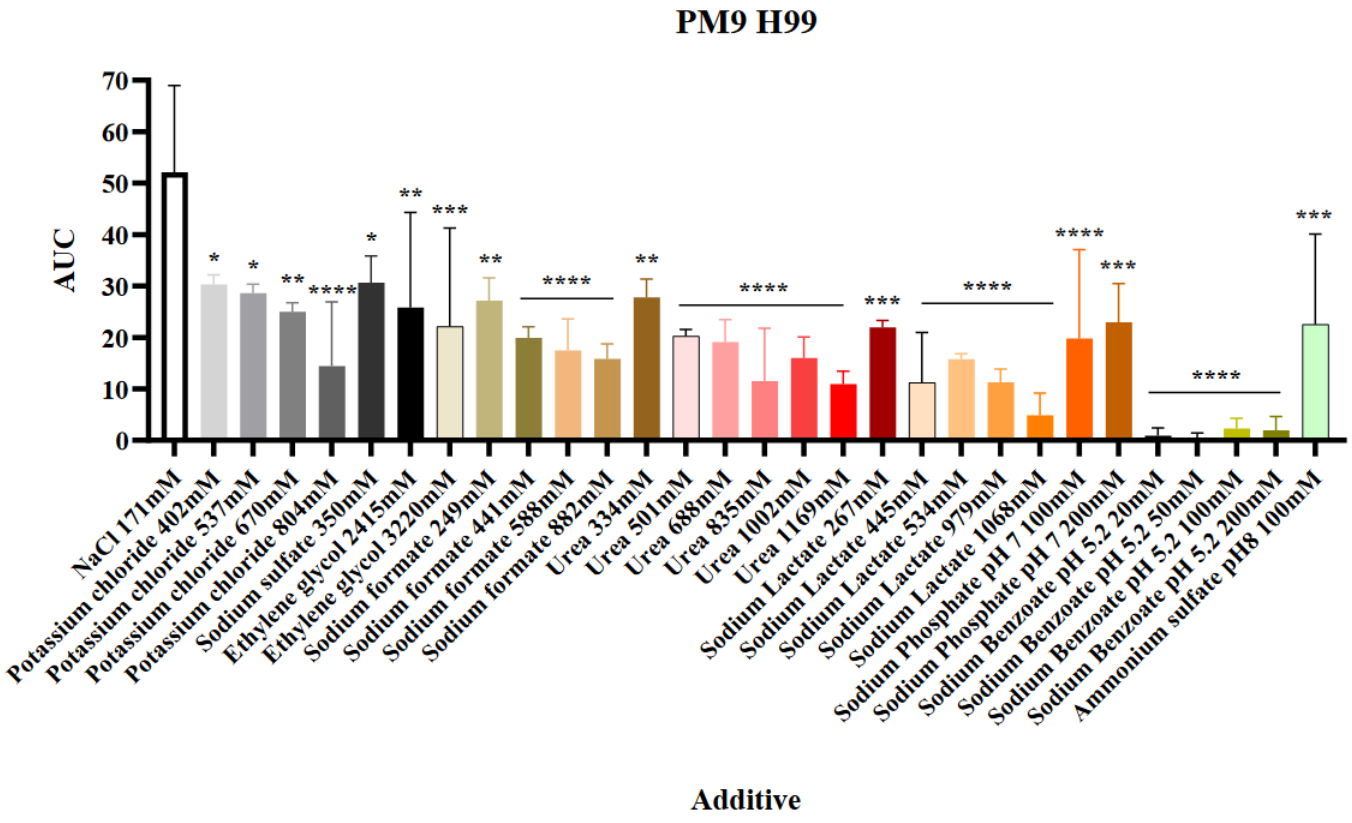
PM9 H99
AUC
70
60
50
40
30
20
10
0
NaCl 171mM
Potassium chloride 402mM
Potassium chloride 537mM
Potassium chloride 670mM
Potassium chloride 804mM
Sodium sulfate 350mM
Ethylene glycol 2415mM
Ethylene glycol 3220mM
Sodium formate 249mM
Sodium formate 441mM
Sodium formate 588mM
Sodium formate 882mM
Urea 334mM
Urea 501mM
Urea 688mM
Urea 835mM
Urea 1002mM
Urea 1169mM
Sodium Lactate 267mM
Sodium Lactate 445mM
Sodium Lactate 534mM
Sodium Lactate 979mM
Sodium Lactate 1068mM
Sodium Phosphate pH 7 100mM
Sodium Phosphate pH 7 200mM
Sodium Benzoate pH 5.2 20mM
Sodium Benzoate pH 5.2 50mM
Sodium Benzoate pH 5.2 100mM
Sodium Benzoate pH 5.2 200mM
Ammonium sulfate pH8 100mM
Additive

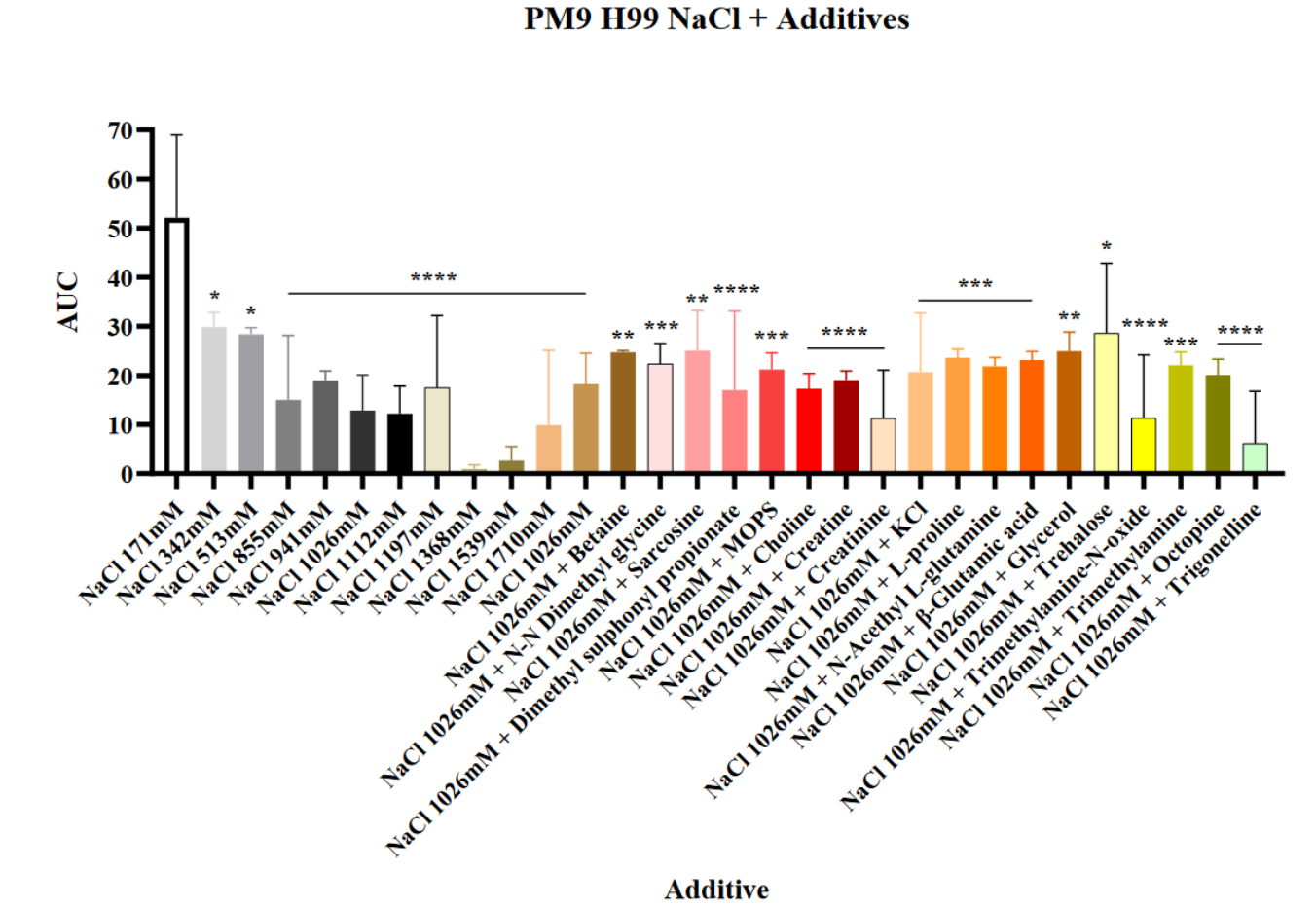
PM9 H99 NaCl + Additives
AUC
70
60
50
40
30
20
10
0
NaCl 171mM
NaCl 342mM
NaCl 513mM
NaCl 855mM
NaCl 941mM
NaCl 1026mM
NaCl 1112mM
NaCl 1197mM
NaCl 1368mM
NaCl 1539mM
NaCl 1710mM
NaCl 1026mM
NaCl 1026mM + Betaine
NaCl 1026mM + N-N Dimethyl glycine
NaCl 1026mM + Sarcosine
NaCl 1026mM + Dimethyl sulphonyl propionate
NaCl 1026mM + MOPS
NaCl 1026mM + Choline
NaCl 1026mM + Creatine
NaCl 1026mM + Creatinine
NaCl 1026mM + KCl
NaCl 1026mM + L-proline
NaCl 1026mM + N-Acethyl L-glutamine
NaCl 1026mM + β-Glutamic acid
NaCl 1026mM + Glycerol
NaCl 1026mM + Trehalose
NaCl 1026mM + Trimethylamine-N-oxide
NaCl 1026mM + Trimethylamine
NaCl 1026mM + Octopine
NaCl 1026mM + Trigonelline
Additive

D

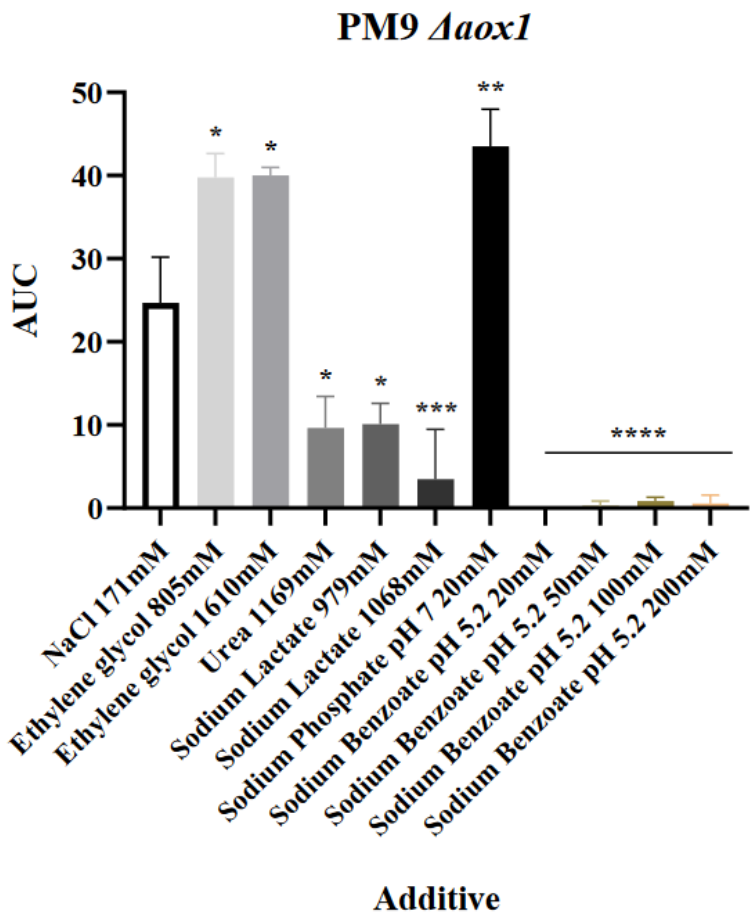
PM9 Δaox1
AUC
50
40
30
20
10
0
*
*
*
*
***
**
****
NaCl 171mM
Ethylene glycol 805mM
Ethylene glycol 1610mM
Urea 1169mM
Sodium Lactate 979mM
Sodium Lactate 1068mM
Sodium Phosphate pH 7 20mM
Sodium Benzoate pH 5.2 20mM
Sodium Benzoate pH 5.2 50mM
Sodium Benzoate pH 5.2 100mM
Sodium Benzoate pH 5.2 200mM
Additive

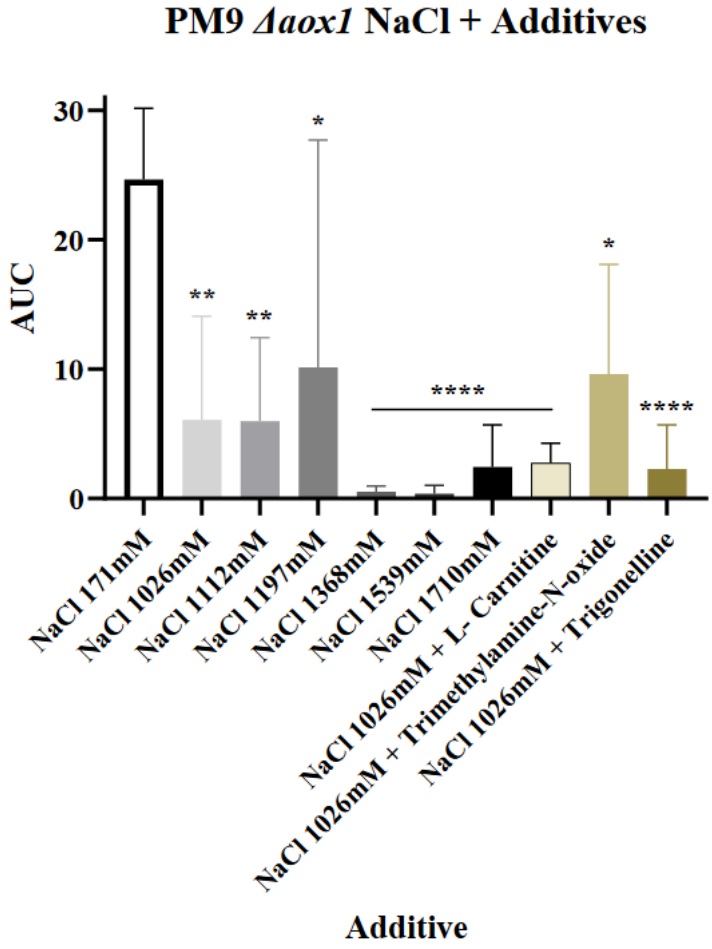
PM9 Δaox1 NaCl + Additives
AUC
30
20
10
0
**
**
*
****
*
****
NaCl 171mM
NaCl 1026mM
NaCl 1112mM
NaCl 1197mM
NaCl 1368mM
NaCl 1539mM
NaCl 1710mM
NaCl 1026mM + L- Carnitine
NaCl 1026mM + Trimethylamine-N-oxide
NaCl 1026mM + Trigonelline
Additive

E

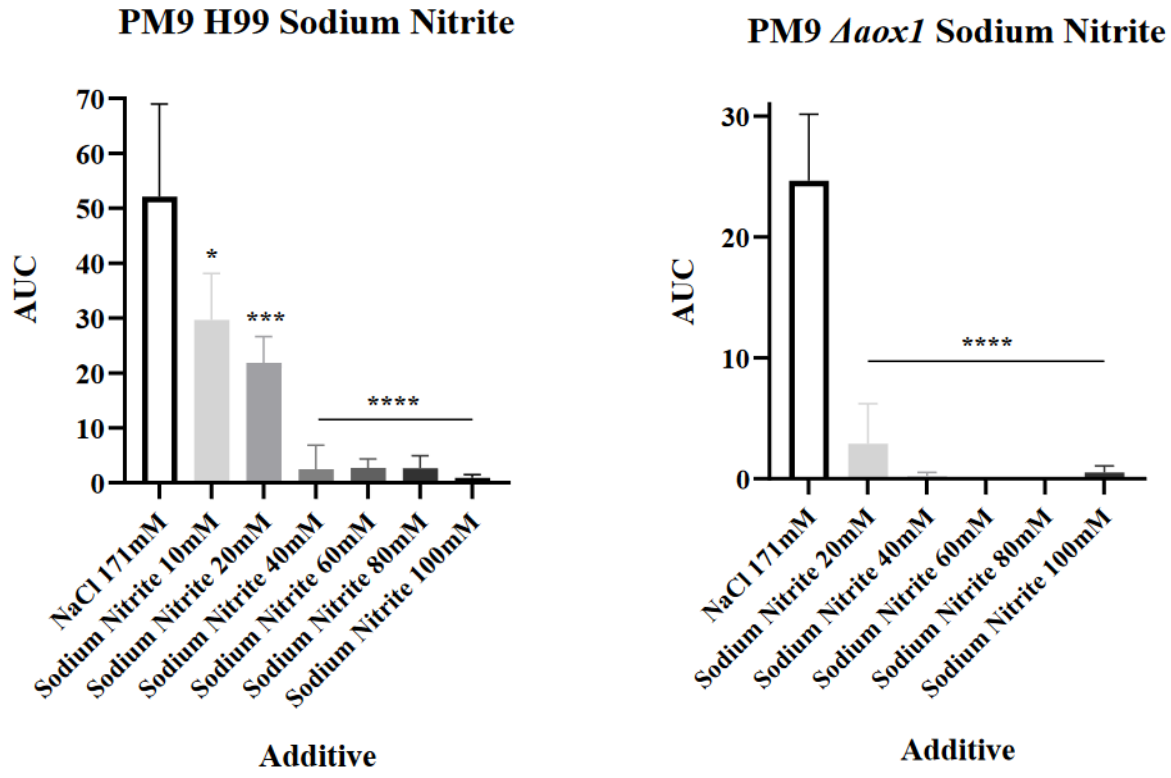

Figure 4.8: C. neoformans osmotic stress adaption.
Biological triplicates of WT (H99) and *Δaox1* were grown in the presence of different osmolyte stresses (Additive) using the BIOLOG system and the area under the curve was recorded (AUC). (**A**) PM9 / H99, (**B**) PM9 / *Δaox1*. (**C**) Summary of PM9 additives that significantly affected growth of H99 cells. (**D**) Summary of PM9 additives that significantly affected growth of *Δaox1* cells. (**E**) summary graphs highlighting the significance of sodium nitrite on growth of both H99 and *Δaox1* cells. Significance was calculated using Dunnett's multiple comparisons test following a one-way ANOVA in GraphPad Prism. * < 0.05, ** < 0.005, *** < 0.0005, **** <0.0001, where P = 0.05. Error bars represent ± SD. n = 3

4.2.8 Sodium nitrite inhibits the growth of *C. neoformans*

The BIOLOG screen highlighted different sensitivities of *C. neoformans* to additives, including sodium nitrite (Fig. 4.8). We wanted to investigate sodium nitrite as it is a well-known antimicrobial additive for food products[329], where it can increase oxidative damage of bacteria and fungi through inhibition of respiration, leading to ROS generation. To confirm that the results seen in the BIOLOG plates were reproducible outside of the pre-fabricated plate system, wildtype (H99) and *aox1* null mutant *C. neoformans* (*Δaox1*) cells were grown in minimal IFY-0 media in the presence of sodium nitrite within a concentration range of 20mM – 100mM for 48 h at 37°C. We found that sodium nitrite addition at all tested concentrations inhibited the growth of both H99 (Fig. 4.9a) and *Δaox1* mutant cells (Fig. 4.9b).

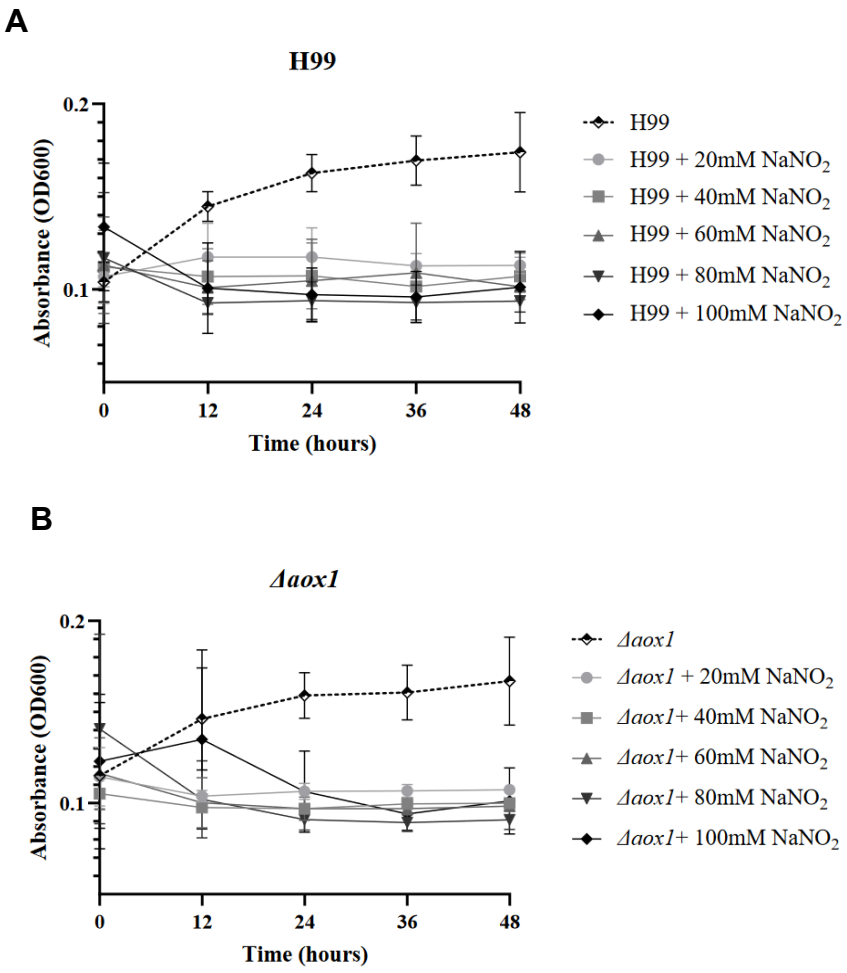

Figure 4.9: Confirmation of the effect of sodium nitrite on C. neoformans growth.

Wildtype H99 (**A**) and *Δaox1* mutant *C. neoformans* cells (**B**) were grown in YPD containing sodium nitrite ($NaNO_2$) in the concentration range 20mM-100mM for 48 h at 37°C. Graphs were created in GraphPad Prism. Error bars represent ± SD. n=9

4.2.9 Investigation of sodium nitrite on *C. neoformans* viability

We decided to investigate the effects of sodium nitrite on cell viability, as it significantly inhibited growth of both H99 and *Δaox1* in the BIOLOG screen (Fig. 4.8), which was reproducible under lab conditions (Fig. 4.9). H99 and *Δaox1* mutant cells were plated following a 2 h incubation in minimal IFY-0 media containing sodium nitrite at 20mM, 40mM, 60mM, 80mM, or 100mM, and viable colonies were counted. Interestingly, while all doses of sodium nitrite between 20mM – 100mM significantly inhibited growth of both H99 (Fig. 4.9a) and *Δaox1* (Fig. 4.9b), 20mM sodium nitrite significantly increased viability of H99 (Fig. 4.10a) and 40mM sodium nitrite increased viability of both H99 and *Δaox1* (Fig. 4.10b). However, both the 80mM and 100mM concentrations significantly reduced viability of both strains (Fig. 4.10).

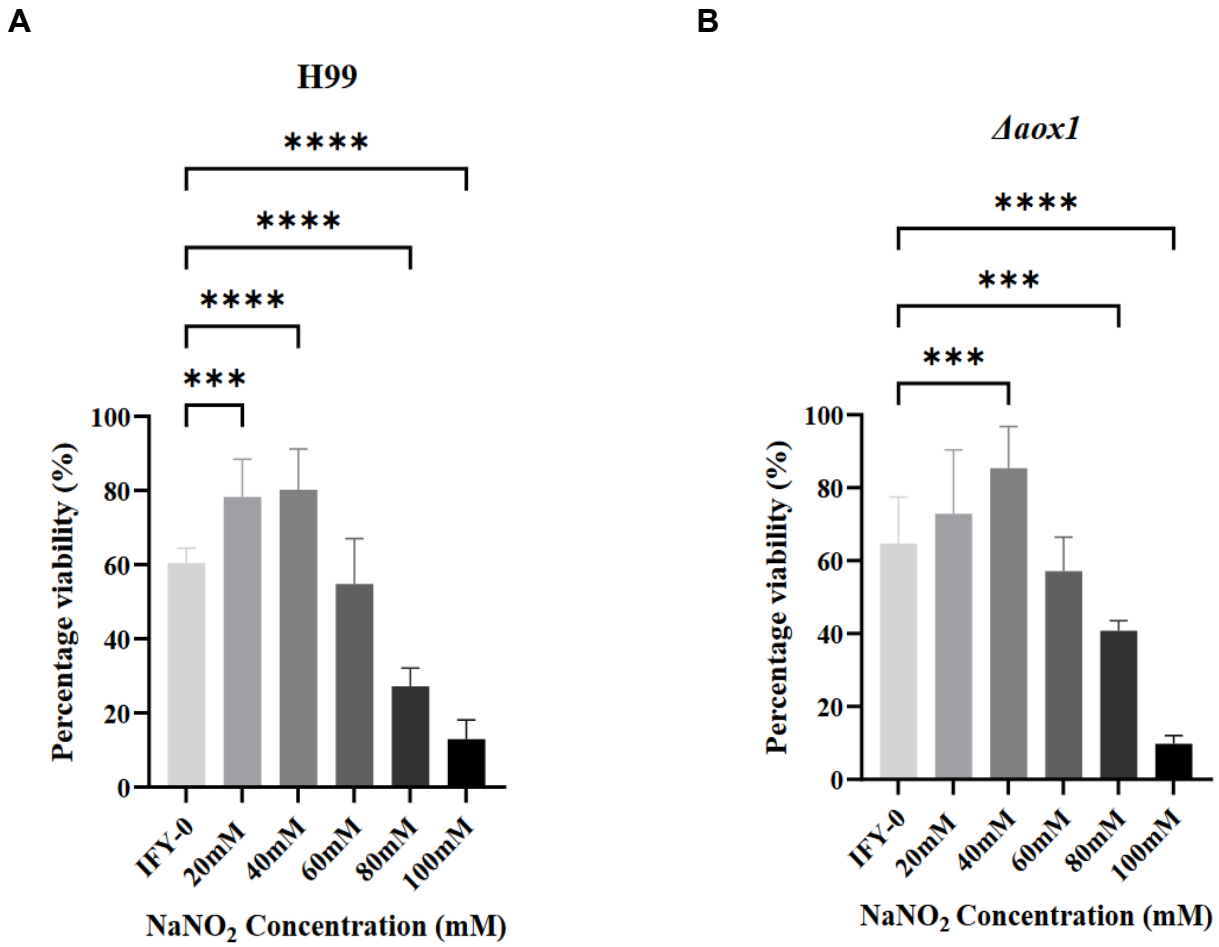

Figure 4.10: Viability assay of C. neoformans exposed to sodium nitrite treatment.
The viability of wildtype (H99) (**A**) and *Δaox1* null mutant (*Δaox1*) (**B**) *C. neoformans* after a 2 h incubation with different concentrations of sodium nitrite as indicated, in comparison to an IFY-0 minimal media control. Significance was calculated using Dunnett's multiple comparisons test following a one-way ANOVA in GraphPad Prism. *** < 0.0005, **** <0.0001, where P = 0.05. Error bars represent ± SD. n = 9

4.2.10 Sodium nitrite affects *C. neoformans* respiration

We wanted to investigate whether the loss of viability observed after addition of sodium nitrite at 80mM and 100mM was due to an effect on respiration. The respiratory profile of H99 and *Δaox1* mutant *C. neoformans* using HRR. Respirometer chambers were inoculated with 1 x 10^6 cells after 24 h growth at 37°C and treated with either 80mM (Fig. 4.11a, 4.11b) or 100mM sodium nitrite (Fig. 4.11c, 4.11d) where indicated. Our data showed that addition of sodium nitrite at either concentration led to a rapid increase in respiration. The effects of sodium nitrite on respiration were Aox independent, as respiratory traces of *Δaox1* treated with 80mM (Fig. 4.11b) and 100mM sodium nitrite (Fig. 4.11d) mirrored that of the wildtype treatment.

A

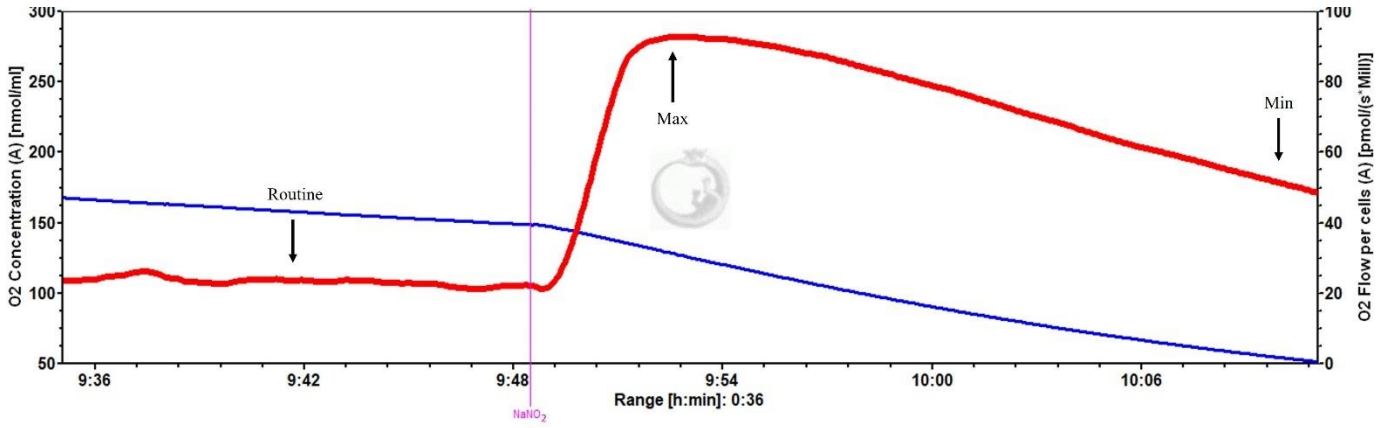

B

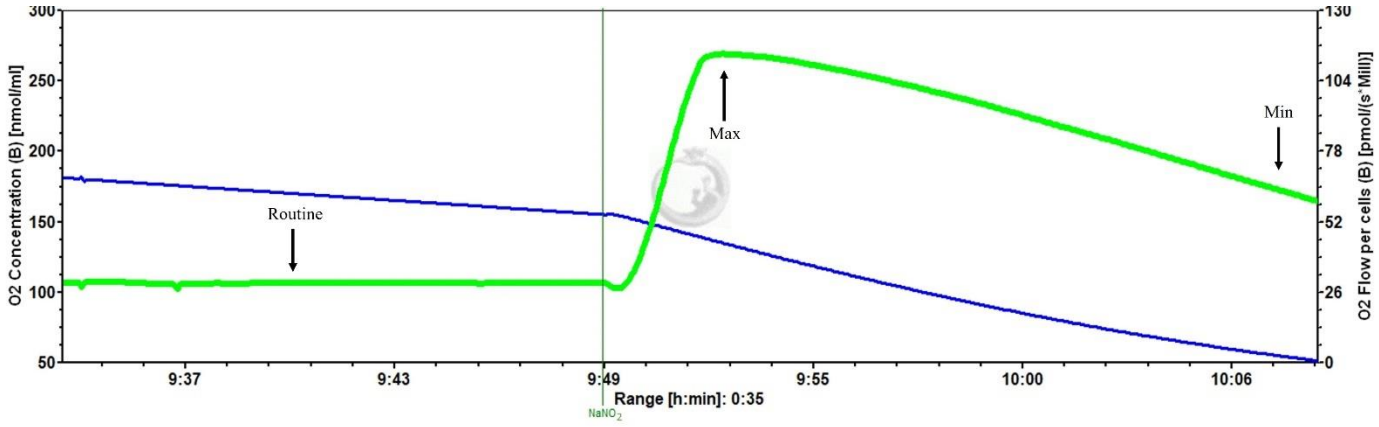

C

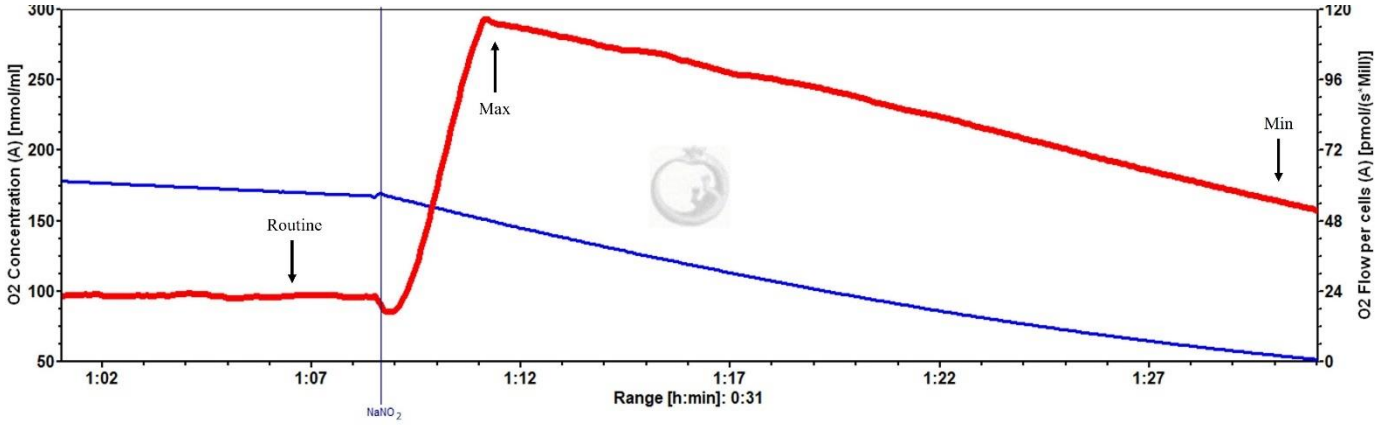
O2 Concentration (A) [nmol/ml]
O2 Flow per cells (A) [pmol/(s*Mill)]
Routine
Max
Min
NaNO2
Range [h:min]: 0:31

D

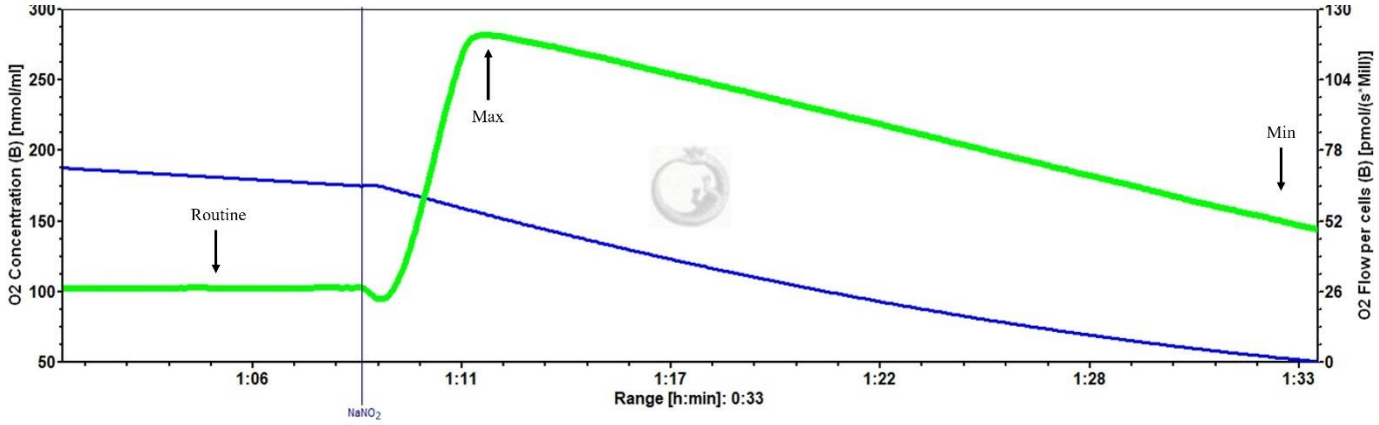
O2 Concentration (B) [nmol/ml]
O2 Flow per cells (B) [pmol/(s*Mill)]
Routine
Max
Min
NaNO2
Range [h:min]: 0:33

E

F

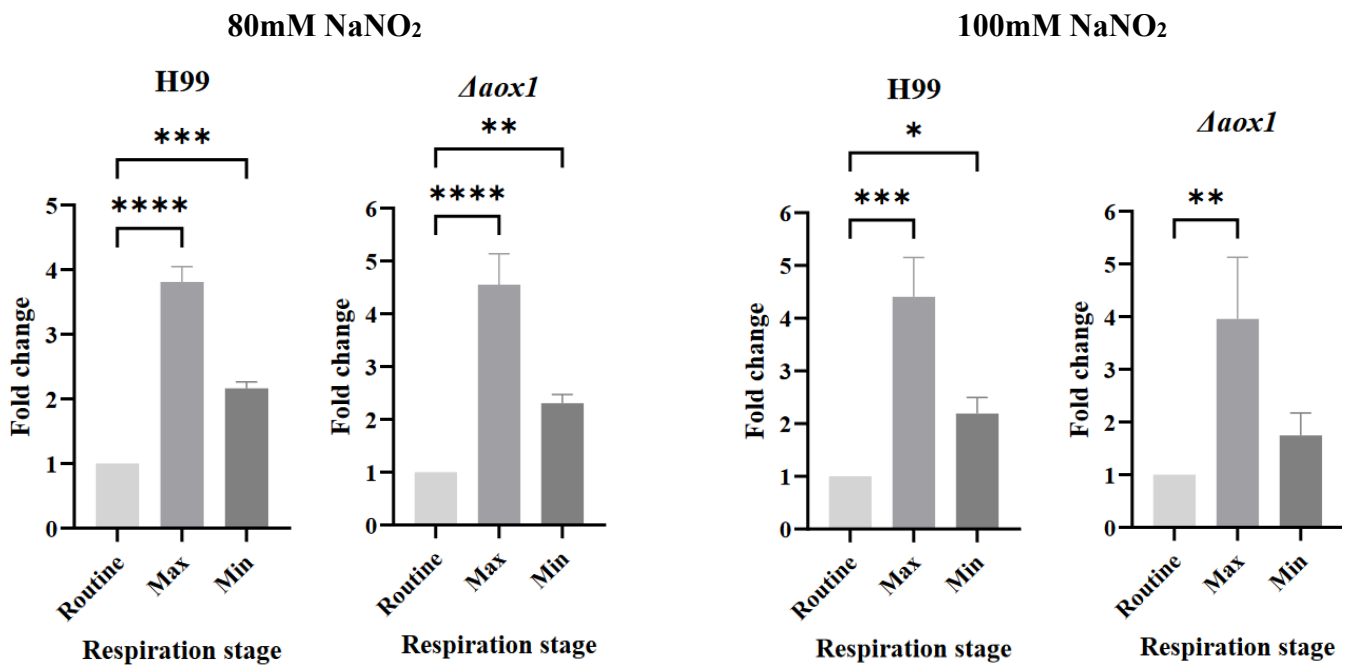
80mM NaNO2
100mM NaNO2
H99
Δaox1
Fold change
Routine
Max
Min
Respiration stage

Figure 4.11: Respiratory profiles of C. neoformans exposed to sodium nitrite.
Representative example of respiration in H99 and *Δaox1* determined using HRR. Chambers were inoculated with 1 x 10^6 cells after 24 h growth and treated with sodium nitrite ($NaNO_2$) where indicated (**A**) H99 and 80mM sodium nitrite, (**B**) *Δaox1* and 80mM sodium nitrite, (**C**) H99 and 100mM sodium nitrite, (**D**) *Δaox1* and 100mM sodium nitrite. Measurements of Maximum (Max) and Minimum (Min) respiration (O2 flow per cells) after drug exposure were taken and compared to the routine level of respiration (Routine) for each strain as indicated. (**E**) 80mM sodium nitrite, (**F**) 100mM sodium nitrite. Significance was calculated using Dunnett's multiple comparisons test following a one-way ANOVA in GraphPad Prism. * <0.05, ** <0.005, *** < 0.0005, **** <0.0001, where P = 0.05. Error bars represent ± SD. n = 3

4.2.11 Sodium nitrite affects the melanisation ability of *C. neoformans*

After establishing that sodium nitrite induces an increase in respiration, we wanted to investigate whether the addition of sodium nitrite affected the melanisation capacity of *C. neoformans*, as mitochondrial function has been linked to this process[88, 89]. Both H99 and *Δaox1* cells were treated with sodium nitrite for 2 h at 37°C and then plated onto melanisation agar for a further incubation at 30°C (Fig. 4.12a) or 37°C (Fig. 4.12b) for 2 or 3 days, respectively. Mean grey values were measured in ImageJ and significance was recorded in GraphPad Prism after background correction and compared to an IFY-0 minimal media control. Interestingly, at 30°C, a significant increase in melanisation was observed after sodium nitrite treatment at 40mM and 60mM for both strains (Fig. 4.12a). H99 also showed an increase in melanisation after sodium nitrite treatment at 20mM, although *Δaox1* treated with 20mM sodium nitrite showed a melanisation level similar to that of untreated *Δaox1* cells (Fig. 4.12a). At 37°C, while no significant effect was seen on melanisation of either strain after treatment with 20mM sodium nitrite (Fig. 4.12b), 40mM and 60mM concentrations led to a loss of melanisation which was Aox independent. Across all conditions, treatment at 80mM and 100mM resulted in a loss of colony formation for both strains (Fig. 4.12).

A

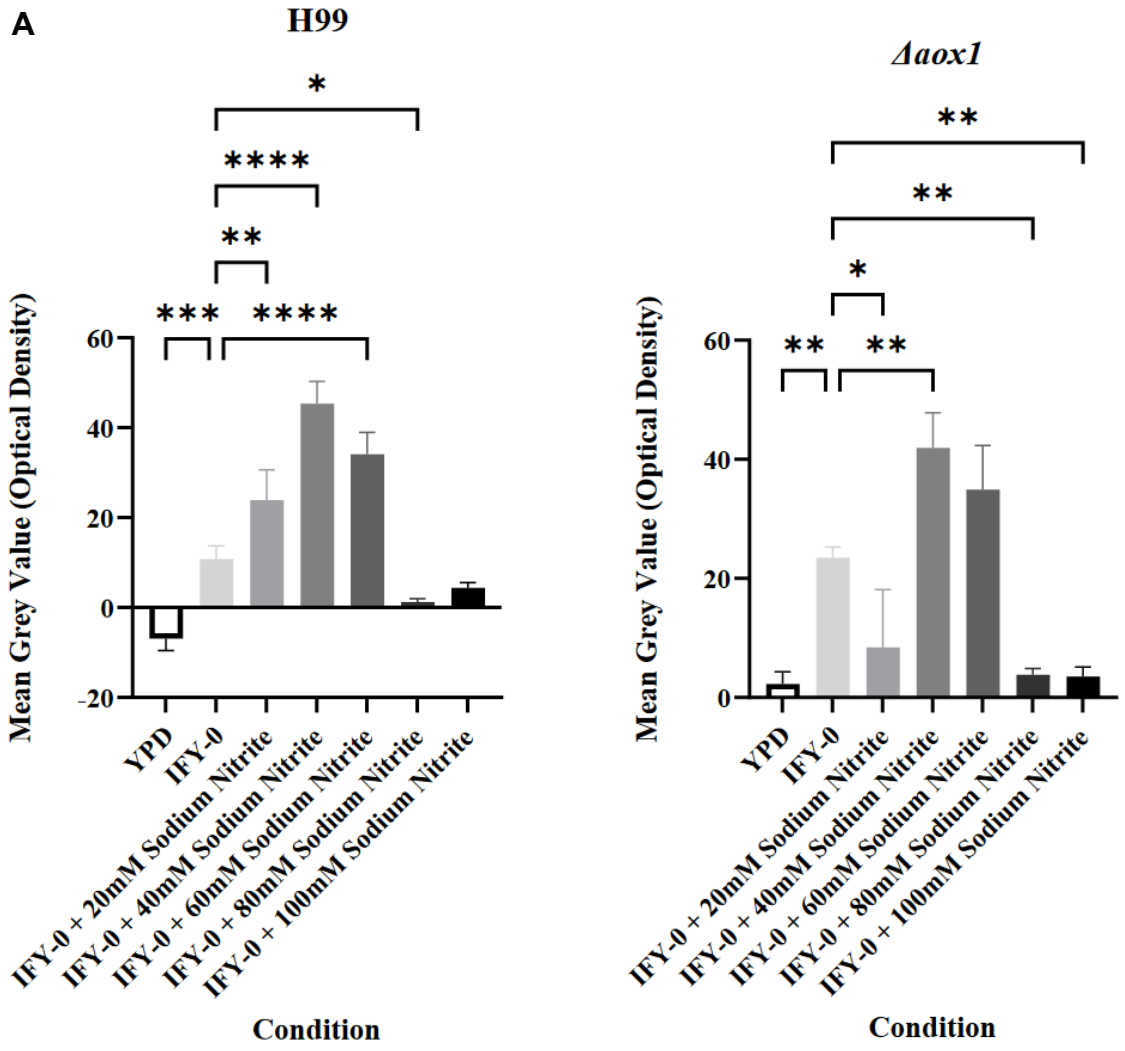
H99
*
****
**
***
****
Mean Grey Value (Optical Density)
60
40
20
0
-20
YPD
IFY-0
IFY-0 + 20mM Sodium Nitrite
IFY-0 + 40mM Sodium Nitrite
IFY-0 + 60mM Sodium Nitrite
IFY-0 + 80mM Sodium Nitrite
IFY-0 + 100mM Sodium Nitrite
Condition
Δaox1
**
**
*
**
**
Mean Grey Value (Optical Density)
60
40
20
0
YPD
IFY-0
IFY-0 + 20mM Sodium Nitrite
IFY-0 + 40mM Sodium Nitrite
IFY-0 + 60mM Sodium Nitrite
IFY-0 + 80mM Sodium Nitrite
IFY-0 + 100mM Sodium Nitrite
Condition

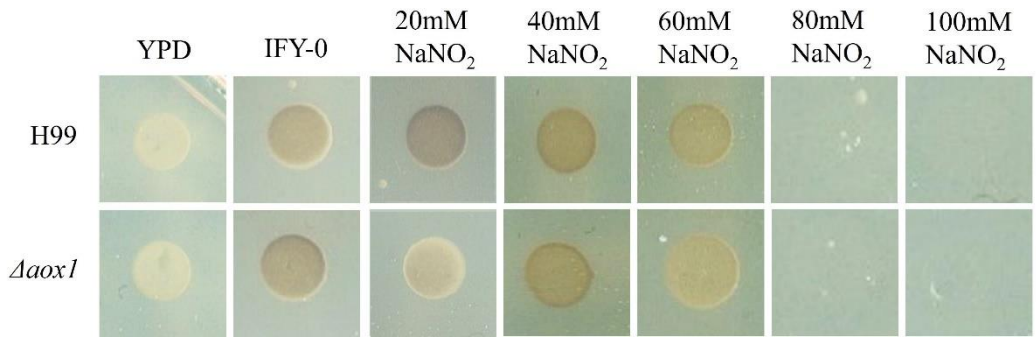
YPD
IFY-0
20mM NaNO2
40mM NaNO2
60mM NaNO2
80mM NaNO2
100mM NaNO2
H99
Δaox1

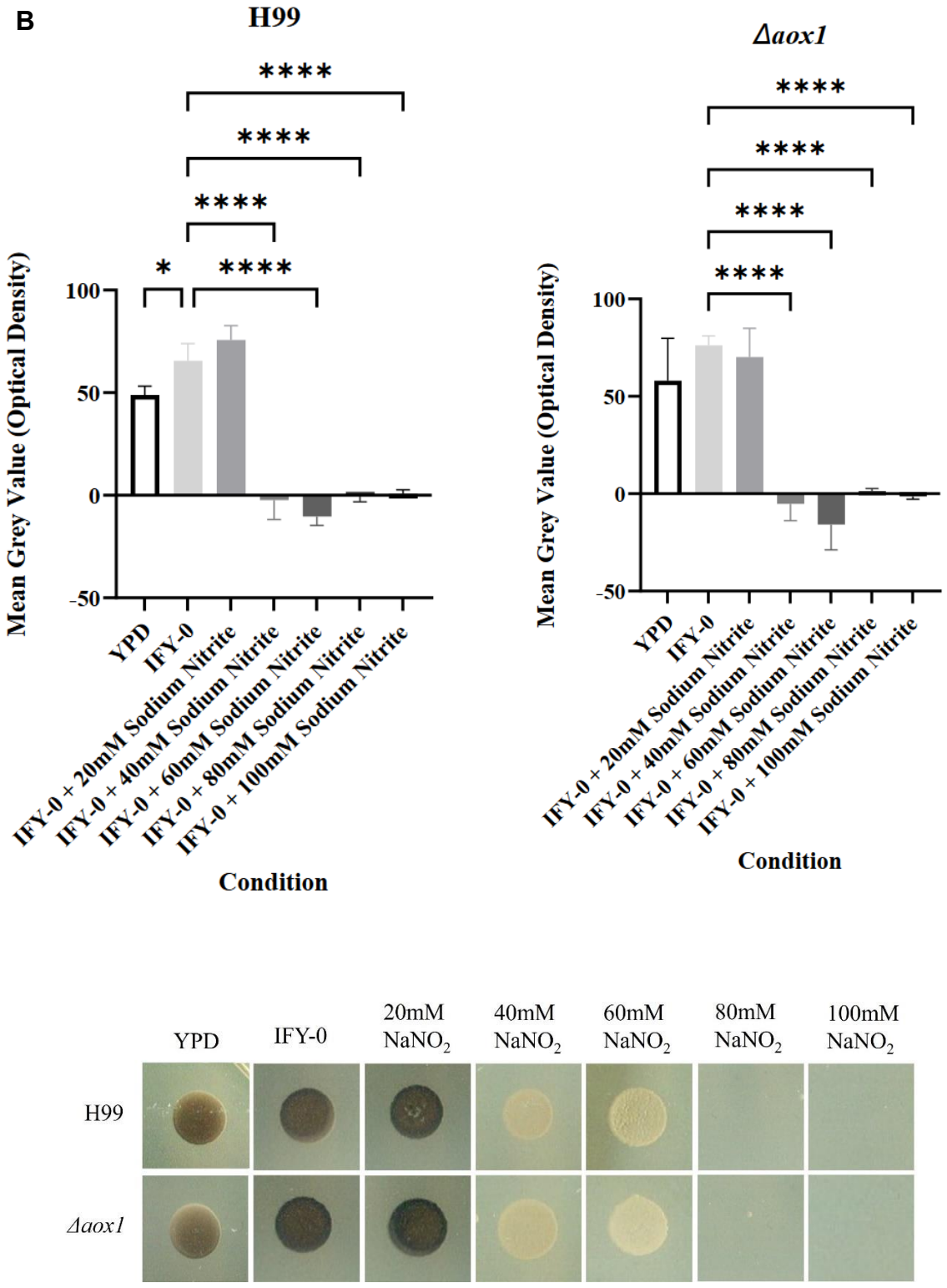

Figure 4.12: Melanisation of C. neoformans treated with sodium nitrite.
Wildtype (H99) and *Δaox1* mutant (*Δaox1*) *C. neoformans* were treated with sodium nitrite ($NaNO_2$) in the concentration range 20mM-100mM or an IFY-0 minimal media control for 2 h at 37°C. Treated cultures were then plated onto melanisation plates containing L-DOPA and incubated at either 30°C (**A**) or 37°C (**B**). Mean grey values were measured in ImageJ and following background correction, significance was calculated using Dunnett's multiple comparisons test following a one-way ANOVA in GraphPad Prism. * <0.05, ** <0.005, *** < 0.0005, **** <0.0001, where P = 0.05. Error bars represent ± SD. n = 3

4.3 Discussion

4.3.1 *C. neoformans* can make use of a variety of nutritional sources to support growth

Carbon sources

Our data suggests that *C. neoformans* was capable of using multiple carbon sources for growth, including D-Mannose, Dulcitol and α-D-Glucose (Fig. 4.2). However, we observed some disparities between the carbon sources that affected the growth of wildtype and *Δaox1* mutant *C. neoformans.* For example, wildtype cells could use D- Trehalose, D-Fructose and Pectin to significantly increase growth, but cells lacking Aox did not. However, *Δaox1* could utilise both β-Hydroxy Butyric Acid and Gelatin for growth. The ability of *C. neoformans* to utilise multiple carbon sources has been shown as advantageous in murine pulmonary infection [330], of which trehalose biosynthesis has a key role in thermotolerance and protein protection from stress (discussed below). Interestingly, while not much is known about the role of pectin in fungi, mutations in the pectin-lyase like domain of *C. neoformans* produces a mutant with a defect in capsule integrity [52]. While Pectin function has mainly been attributed to plant cell wall maintenance [331], one could speculate that Pectin may play a role in capsule and cell wall integrity, which wildtype cells are able to utilise for growth.

For the use of carbon sources in *Δaox1* mutant cell growth, precise signalling roles remain ambiguous. For example, β-Hydroxy Butyric Acid is often found as a carbon source in bacteria such as *Ralstonia eutropha*, but common soil dwelling fungi such as *Aspergillus* are able to degrade it [332]. The mechanisms behind this degradation in *C. neoformans* are largely unknown. However, the use of Gelatin has been linked to proteinase activity in *C. neoformans*, where it can degrade several host proteins via proteolytic activity [333]. One could speculate that loss of Aox in *C. neoformans* may upregulate scavenging pathways and extracellular proteinase secretion for carbon source acquisition. This would perhaps indicate that Aox is not able to synthesise carbon source intermediates as effectively as the wildtype and thus relies on scavenging to support growth.

Nitrogen sources

Interestingly, while the presence of some nitrogen sources yielded no significant change in growth (Fig. 4.3), providing multiple di- and tripeptides as a nitrogen source significantly increased the growth of *C. neoformans* cells, which seemed independent of Aox (Fig. 4.4). Uptake of dipeptides, through amino acid permeases, and processes like Nitrogen Catabolite Repression (NCR), the Target of Rapamycin (TOR) and SPS-sensing is thought to contribute to *C. neoformans* growth at elevated temperatures and virulence[334, 335], although the regulatory mechanisms behind amino acid uptake and metabolism remain unclear. Interestingly, several studies have highlighted cyclic dipeptides show antimicrobial action against pathogenic fungi, presenting a new potential antifungal strategy[336-340]. It could be postulated that the enhanced uptake of di- and tripeptides by *C. neoformans*, which our data showed to be independent of Aox, may provide a role for these peptides in antifungal uptake and transport.

Phosphate sources

While phosphorus and sulphur source availability did not greatly impact wildtype growth, multiple significant hits were observed for *Δaox1* growth (Fig. 4.5b). Phosphate acquisition has been attributed to preservation of membrane integrity, lipid remodelling and maintenance of a small 'seeding' morphotype that enhances cryptococcal dissemination in the host[68, 341]. One other key role of phosphate sources, such as D-Glucose-6-Phosphate, is for trehalose biosynthesis, an integral component in membrane and protein protection from host-induced stresses[342-348]. For example, trehalose-6-phosphate synthase (TPS1) and trehalose-6-phosphate phosphatase (TPS2) have been implicated in growth and survival at high temperatures, which is indispensable for *C. neoformans* dissemination within the host [349]. One notable observation is that wildtype *C. neoformans* could utilise trehalose itself for increased growth (Fig. 4.2a) but little significance was shown for growth in the presence of phosphorus and sulphur sources (Fig. 4.5a). However, while *Δaox1* could utilise multiple phosphate sources for increased growth (Fig. 4.5b) there was no significant growth changes in the presence of trehalose (Fig. 4.2b). This data suggests that Aox may

have a role in mitochondrial membrane maintenance and thermotolerance under stress, and so one could speculate loss of this enzyme induces increased uptake of phosphate sources for growth.

4.3.2 *C. neoformans* growth is sensitive to pH and osmolarity

Our data suggests that the metabolic responses of *C. neoformans* are varied, with strong hits for peptide utilisation and clear sensitivities to both pH and osmolyte addition. We were able to confirm an optimum range for *C. neoformans* growth of pH 5-7 (Fig. 4.7), which has also been implicated in other studies[350]. It is interesting to note that wildtype growth at pH 4.5 was significantly increased through the addition of multiple amino acids (Fig. 4.7a, 4.7d). This ability to grow in an acidic pH range, including the use of amino acid additives to aid growth in acidic conditions, supports studies which suggest that *C. neoformans* replication within the macrophages of the host is dependent on acidification of the phagolysosome lumen and modulation of acidity through chemical modulation[27, 351, 352]. One notable exception to the utilisation of amino acids during acidic growth is α-Amino Malonate, which completely inhibited the growth of both H99 (Fig. 4.7a) and *Δaox1* mutant cells (Fig. 4.7b).

4.3.3 *C. neoformans* is sensitive to sodium nitrite

The BIOLOG microarray allowed us to investigate *C. neoformans* sensitivity to osmotic stress (Fig. 4.8). These screens allowed us to isolate a particular osmolyte of interest, sodium nitrite, which is already in circulation as an antimicrobial for the food preservation industry[353-355]. Our data show that addition of sodium nitrite leads to an inhibition of growth (Fig. 4.9), and loss of viability at 80mM (Fig. 4.10), which is Aox independent. While further work to establish a Minimum Inhibitory Concentration (MIC) and mechanism of cell death is required, we have shown that sodium nitrite at fungicidal concentrations affected mitochondrial membranes and induced a strong uncoupling effect (Fig. 4.11). Alternatively, the increase in oxygen consumption observed upon sodium nitrite addition could be a result of increasing activity of other enzymes, for example Catalase, which rapidly decomposes

superoxide species to oxygen for relief of oxidative stress [356], although further respirometry analysis is required to substantiate this. Interestingly, sodium nitrite has been proven to enhance healthy vascular ageing and endothelial function in patients through decreasing mitochondria – derived ROS and restoration of NO homeostasis[357, 358]. It has also been implemented as a KCN antidote due to its oxidising ability, which inhibits oxidative phosphorylation in *P. aeruginosa*[359, 360]. Our data showing sensitivity of *C. neoformans* to sodium nitrite could indicate therefore that *C. neoformans* is sensitive to mitochondrial inhibition, disruption of oxidative species production and homeostasis and could indicate that these processes are reliant on mitochondrial membrane integrity.

Studies have also implicated sodium nitrite in ROS control, whereby it can induce a flux of high ROS which is disruptive to membrane integrity and oxidative stress redox responses [361]. Our studies suggest that while sodium nitrite increased respiratory activity (Fig. 4.11), lower levels of sodium nitrite increased cellular viability (Fig. 4.10). This indicates that a redox imbalance generated by sodium nitrite at low levels may allow generated ROS to act a signalling component for increased cell fitness, but high levels of rapidly generated ROS induces cell death. This is of interest as activated macrophages elevate levels of ROS and NO stresses, including nitrites, for killing of fungal pathogens via oxidative bursts [362, 363]. One could speculate that rapid generation of ROS via sodium nitrite may mimic the oxidative bursts of macrophages that interact with *C. neoformans* in the host environment, leading to cell death.

4.3.4 Sodium nitrite reduces *C. neoformans* melanisation

Melanisation of *C. neoformans* is a tightly regulated response to host-induced stress, relying on both the PKA-cAMP pathway and the HOG pathway[364]. The loss of melanisation seen at 37°C after sodium nitrite treatment (Fig. 4.12) indicates that sodium nitrite may affect the HOG pathway through alteration of osmolarity levels, which may partially develop from membrane disruption seen in Fig. 4.11. Melanin regulation may also include signalling mechanisms involving mitochondria[88, 89], and mutated NADH dehydrogenase has been shown to increase melanisation and virulence in the

murine model [172]. It is tempting to speculate that disruption to mitochondrial function, including ROS and NO homeostasis, may affect melanin production and accumulation through disruption of stress signalling components and cell membrane remodelling pathways that allow for melanin coats to form. However, further investigations into both sodium nitrite roles in redox disruption and melanin signalling in *C. neoformans* are required.

5. A search for novel mitochondrial inhibitors reveals a fungal specific role for Decylalkyl in inducing necrosis in *C. neoformans*

Elizabeth SM Edrich[1], Luke Young[2], John Spencer[2], Andrew McGown[2], Anthony Moore[2] and Campbell W Gourlay[1*]

[1]Kent Fungal Group, School of Biosciences, University of Kent, Kent, CT2 9HY, UK.

[2]Biochemistry & Biomedicine, School of Life Sciences, University of Sussex, Brighton BN1 9QG, U.K.

[*]Author for correspondence

All experimental work herein was conducted by me, besides the synthesis and rationale pertaining to compound synthesis, carried out by John Spencer, Andrew McGown, Tony Moore and Luke Young and *in vitro* testing of compounds, conducted by Luke Young, where stated.

5.1 Introduction

The roles of mitochondria in cryptococcal pathogenesis have been implicated in multiple studies[149, 365]. Many of the ETC components are well-conserved among both fungi and humans, which poses a problem for finding new anti-fungal targets. Fungal specific enzymes such as Aox provide an alternative respiratory pathway that are not coupled to ATP generation but may play a role in metabolic adaptability under stress[128, 140, 205, 366]. As Aox has been shown to be required for pathogenesis in *C. neoformans*, and is not found in mammalian mitochondria, it provides a therapeutic target. Unfortunately, there are no current Aox inhibitors with high specificity, and those currently available exhibit off target effects, so are not considered as compounds with therapeutic potential. In this work we sought to develop new Aox inhibitors with improved specificity and more therapeutic prospects.

Previous work has demonstrated that the natural product Colletochlorin B is an effective inhibitor of the Aox from plant[367], fungal[368] and protozoan species[369], with a typical IC_{50} in the 6-20 nm range *in vitro*. However, *in vitro* findings could not be replicated *in vivo*, indicating a need to improve the *in vivo* efficacy. The Triphenyl phosphonium cation (TPP+) has been shown to increase mitochondrial targeting of compounds[370-372], increasing the mitochondrial accumulation up to 1000-fold by utilising the electrochemical difference across the inner mitochondrial membrane[373]. Here we describe the development and testing of TPP+ targeted derivatives of Colletochlorin B against *C. neoformans.*

We investigated the efficacy of the TPP+ targeted Colletochlorin B derivatives, termed ALTOX compounds, against *C. neoformans* by assessing drug effects on growth, respiration, and viability. This was coupled with drug toxicity assays measuring the effect of ALTOX drugs in the *Galleria mellonella* model and haemolysis assays. This project was conducted in collaboration with the laboratory of Professor Anthony Moore (University of Sussex) who specialise in the development of Aox inhibitors.

5.2 Results

5.2.1 Inhibitor synthesis and rationale (conducted by Luke Young, University of Sussex)

Following on from our previous work conducted in the Moore laboratory where it was determined that the natural product Colletochlorin B was a potent inhibitor of *C. albicans* Aox[212], we set out to improve the mitochondrial targeting of the compound. To this end, the isoprene tail was replaced by an alkyl chain of variable length (12-Carbon for **ALTOX094** and 8-Carbon **ALTOX102**) capped with the TPP+ moiety. The Chlorine found at R1 of Colletochlorin B and Colletochlorin D (Table 5.1) was replaced with Bromine to yield **ISSF31** and **ISSF33**, respectively. This change was made to allow for assessment of the potential design space around the head group, as successful inhibition with the larger halide would allow for further manipulation around this side of the molecule.

Table 5.1: Structures for natural products Colletochlorin B and D, and the analogues synthesised for this study

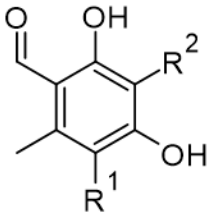

Compound	R1	R2
Colletochlorin B	Cl	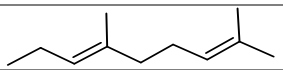
Colletochlorin D	Cl	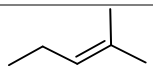
ISSF31	Br	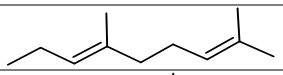
ISSF33	Br	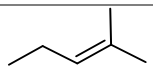
ALTOX094	Br	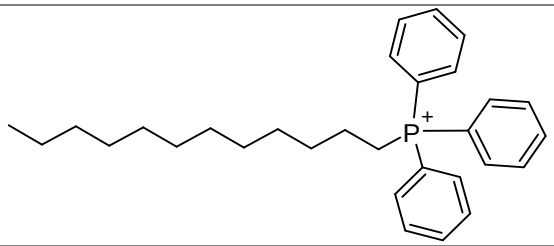
ALTOX102	Br	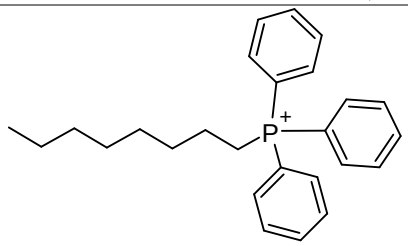

5.2.2 Recombinant Aox and cytochrome *bc₁* complex inhibition screening (conducted by Luke Young, University of Sussex)

The newly synthesized compounds were assessed for inhibitory activity against membrane bound recombinant Aox (rAox) expressed in *E. coli* utilising the same methodology as described previously[374]. The half-maximal inhibitory concentration (IC_{50}) was calculated, which indicates how much of each drug was required to inhibit enzyme activity by 50%, and the negative log value of the

IC_{50} (pIC_{50}) was also given for comparison of drug potency. Substitution of the chlorine for bromine (**Colletochlorin B** to **ISSF31**) did not lead to a significant reduction in potency (Fig. 5.1), reducing the pIC_{50} from 8.2 ± 0.1 to 7.7 ± 0.2. Addition of the alkyl TPP^+, however, led to a significant reduction in inhibition, with both **ALTOX094** and **ALTOX102** being reduced to 4.8 ± 0.1 and 4.9 ± 0.1, respectively.

Mitochondrial samples were extracted from rat liver to assess the impact of the compounds on the complex II through complex IV pathway. As can be seen in Fig. 5.1, none of the compounds demonstrated a significant inhibitory increase over that of **Colletochlorin B** (pIC_{50} = 6.0 ± 0.05), with the shorter chain compounds **Colletochlorin D** and **ISSF33** showing a marked decrease to 4.3 ± 0.2 and 4.4 ± 0.1, respectively. The LogP values, which indicates how lipophilic each compound is in relation to Absorption, Distribution, Metabolism and Excretion (ADME) can be found for each compound in Appendix Table 7.3.

Although the given pIC50 values for ALTOX094 and ALTOX102 were lower than that of Colletochlorin B, the values for both Aox2 and cytochrome bc_1 inhibition were relatively equal, whereas other compounds tested showed a larger disparity in inhibitory ability of both targets. This indicated that ALTOX094 and ALTOX102 showed potential as dual inhibitors of both Aox2 and cytochrome bc_1.

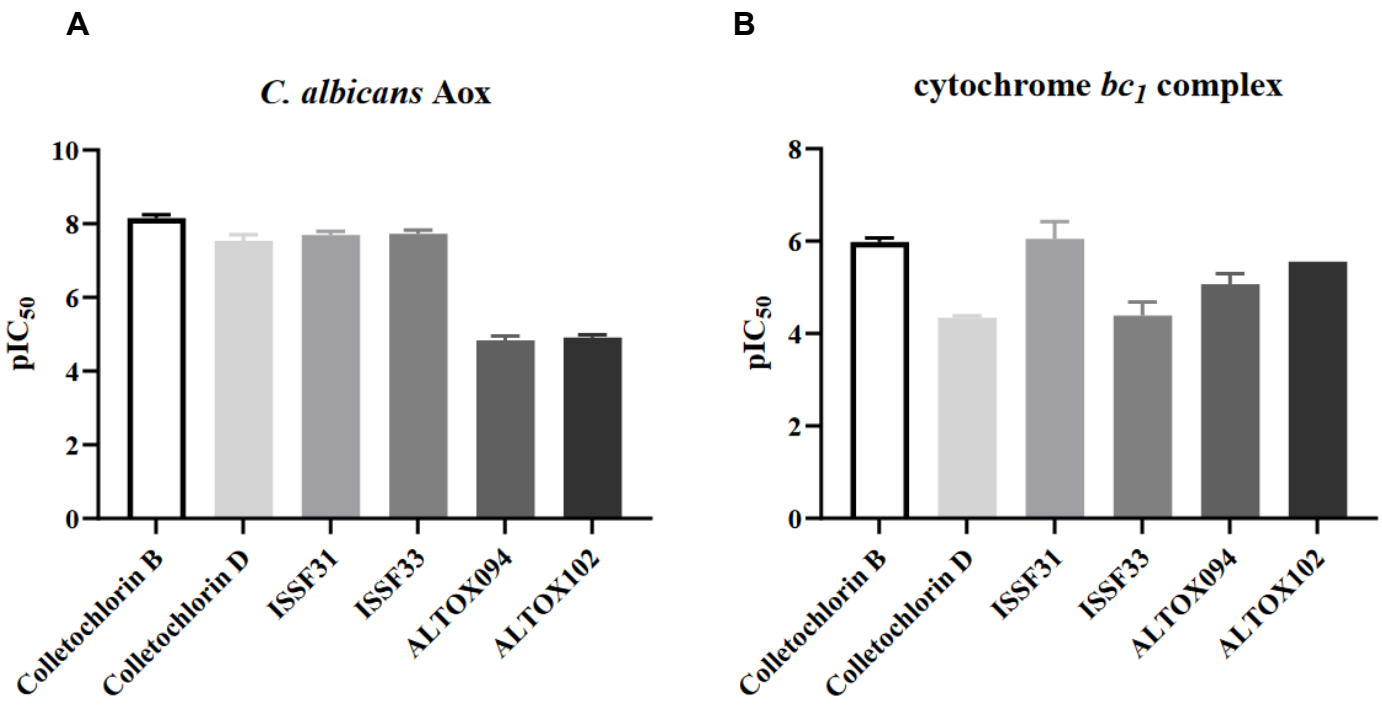

Table 5.2: pIC_{50} value table

Compound	*C. albicans* Aox2	Cytochrome *bc₁*
Colletochlorin B	8.2 ± 0.1	5.9 ± 0.05
Colletochlorin D	7.8 ± 0.02	4.3 ± 0.02
ISSF31	7.7 ± 0.1	6.0 ± 0.2
ISSF33	7.7 ± 0.1	4.4 ± 0.2
ALTOX094	4.8 ± 0.1	5.1 ± 0.1
ALTOX102	4.9 ± 0.1	5.4 ± 0.2

Table 5.3: IC_{50} value table

Compound	*C. albicans* Aox2	Cytochrome *bc₁*
Colletochlorin B	7.3 nM ± 2.4	1.1 µM ± 0.1
Colletochlorin D	15.9 nM ± 1.4	45.8 µM ± 2.2
ISSF31	21.1 nM ± 8.0	1.2 µM ± 0.6
ISSF33	19.6 nM ± 7.1	47.1 µM ± 1.7
ALTOX094	15.0 µM ± 1	9.1 µM ± 1.2
ALTOX102	11.1 µM ± 1	5.8 µM ± 1.4

Figure 5.1: pIC_{50} values for synthesised compounds against C. albicans.
pIC_{50} values (Table 5.2) from inhibitor dose response curves against (**A**) *C. albicans* Aox2 and (**B**) *cytochrome bc₁* complex, where the pIC_{50} value is the calculated negative log of the IC_{50} value in molar. The IC_{50} values for each drug can be found in Table 5.3. All results plotted in triplicate ± SEM in GraphPad Prism. n = 3.

The second string of our synthetic strategy was to improve the drug-like properties of the compounds. The highly substituted pharmacophore had several problematic metabolic hotspots, with 2 phenols and an aldehyde. The ‘greasy’ isoprenoid tail of Colletochlorin B also gave undesirable log P values (cLogP = 7.3), and while Colletochlorin D had a more favourable LogP (cLogP = 5.25) it lacked inhibitory efficacy against mitochondrial samples (Fig. 5.1). In order to reduce these problematic areas, we synthesised a series of benzofuranones based off the **ISSF31** structure (Table. 5.4), reducing both the chain length and removing one of the phenolic groups.

Table 5.4: Modified Benzofuranone structures used for this study

Compound	Structure
ISSF338-A	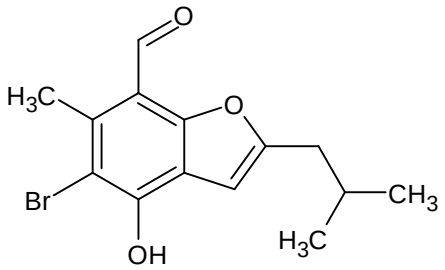
ISSF338-B	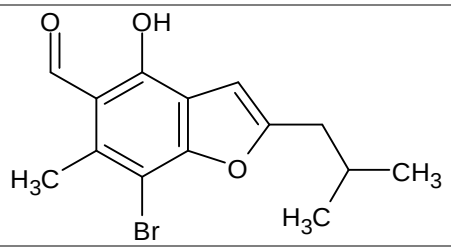
ISSF342	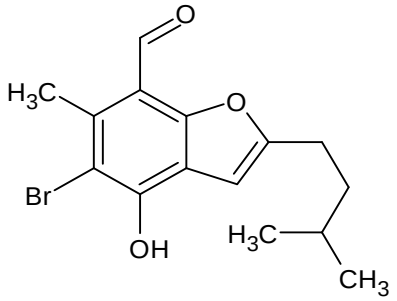

5.2.3 Identification of novel fungistatic compounds that effect *C. neoformans* growth

Our data suggested that the *C. neoformans* Aox1 sequence was not closely related to that of other human fungal pathogens such as *C. albicans* (Fig. 3.1). The data gathered by the Moore laboratory showed potential of ALTOX094 and ALTOX102 for dual inhibitor activity against *C. albicans* recombinant Aox2 and cytochrome bc_1. We wanted to assess whether ALTOX094 and ALTOX102 would also have a higher inhibitory activity against *C. neoformans* Aox1 and cytochrome bc_1 *in vivo,* in comparison to the modified benzofuranones in Table 5.4.

Wildtype (H99) and *aox1* null mutant *C. neoformans* (*Δaox1*) cells were grown in YPD containing ALTOX compounds (ALTOX094, ALTOX102, ISSF338 A, ISSF338 B, ISSF342) within a concentration range of 50μM - 200μM for 48 h at 37°C. Compounds ALTOX094 and ALTOX102 showed clear inhibition of both wildtype (Fig. 5.2a) and *Δaox1* mutant growth (Fig. 5.2b). However, ISSF338 A (Fig. 5.2c, 5.2d), ISSF338 B (Fig. 5.2e, 5.2f) and ISSF342 (Fig. 5.2g, 5.2h) had a more limited effect on the growth of both wildtype and *Δaox1* mutant cells.

A

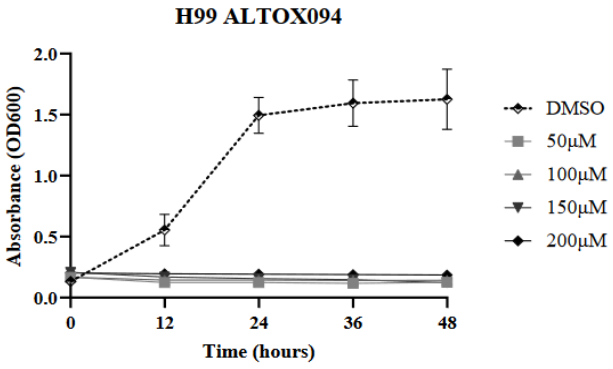
H99 ALTOX094
Absorbance (OD600)
2.0
1.5
1.0
0.5
0.0
0
12
24
36
48
Time (hours)
DMSO
50μM
100μM
150μM
200μM

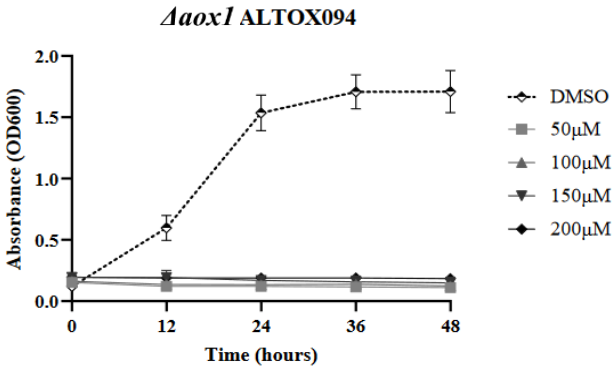
Δaox1 ALTOX094
Absorbance (OD600)
2.0
1.5
1.0
0.5
0.0
0
12
24
36
48
Time (hours)
DMSO
50μM
100μM
150μM
200μM

B

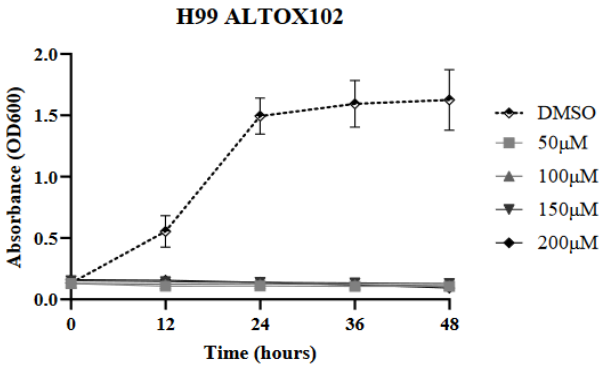
H99 ALTOX102
Absorbance (OD600)
2.0
1.5
1.0
0.5
0.0
0
12
24
36
48
Time (hours)
DMSO
50μM
100μM
150μM
200μM

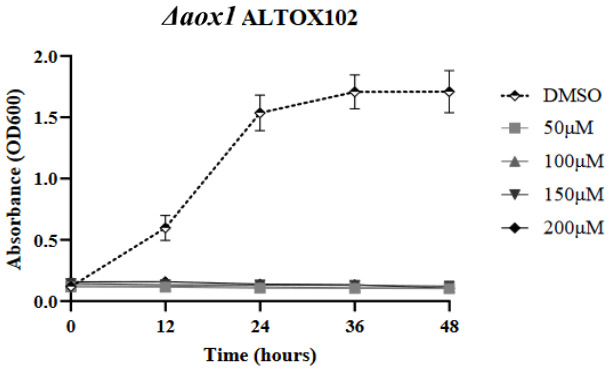
Δaox1 ALTOX102
Absorbance (OD600)
2.0
1.5
1.0
0.5
0.0
0
12
24
36
48
Time (hours)
DMSO
50μM
100μM
150μM
200μM

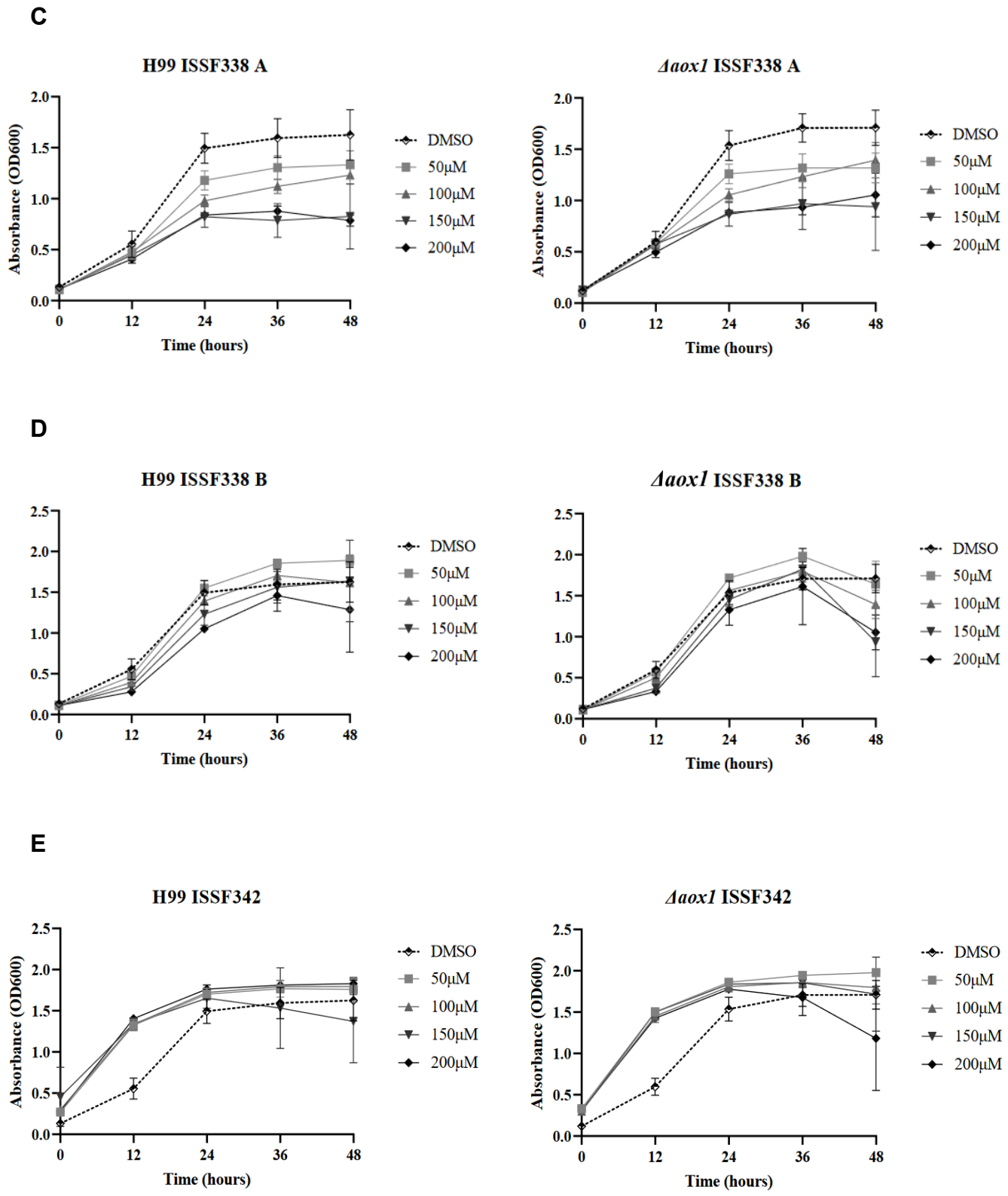

Figure 5.2: Screening of ALTOX compounds and their effect on C. neoformans growth. Wildtype (H99) and *Δaox1* null mutant (*Δaox1*) *C. neoformans* were grown in YPD containing ALTOX094 (**A**), ALTOX102 (**B**), ISSF338 A (**C**), ISSF338 B (**D**) and ISSF342 (**E**) for 48 h at 37°C. Graphs were plotted in GraphPad Prism. Error bars represent ± SD. n = 9

5.2.4 ALTOX094 and ALTOX102 show fungistatic activity even at low concentrations

Following the initial screening indicating ALTOX094 and ALTOX102 were effective against *C. neoformans* growth at broad-range concentrations (Fig. 5.2a, 5.2b), we sought to identify the Minimum Inhibitory Concentration (MIC90) and Non- Inhibitory Concentration (NIC) of ALTOX094 and ALTOX102 against *C. neoformans*. The NIC value shows the lowest drug concentration required to slow growth. The MIC90 value shows the drug concentration required to inhibit the growth by 90%. The NIC values for ALTOX094 were 6.181μM and 7.5μM for cultures of H99 and *Δaox1,* respectively (Fig. 5.3a) while the NIC values for ALTOX102 were 3.207μM for H99 and 5.896μM for *Δaox1* (Fig 5.3b). The MIC90 values for ALTOX094 were 14.52μM for H99 and 14.12μM for *Δaox1* (Fig. 5.3a) and so were rounded to 15 μM, while for ALTOX102 the MIC90 values were 6.587μM for H99 and 10.94μM for *Δaox1* mutant cultures (Fig. 5.3b), and so these values were rounded to 7μM and 11μM, respectively. For all further experiments, the active MIC90 concentration of ALTOX094 used was 15μM and the concentration of ALTOX102 used was 7μM and 11μM, respectively.

A

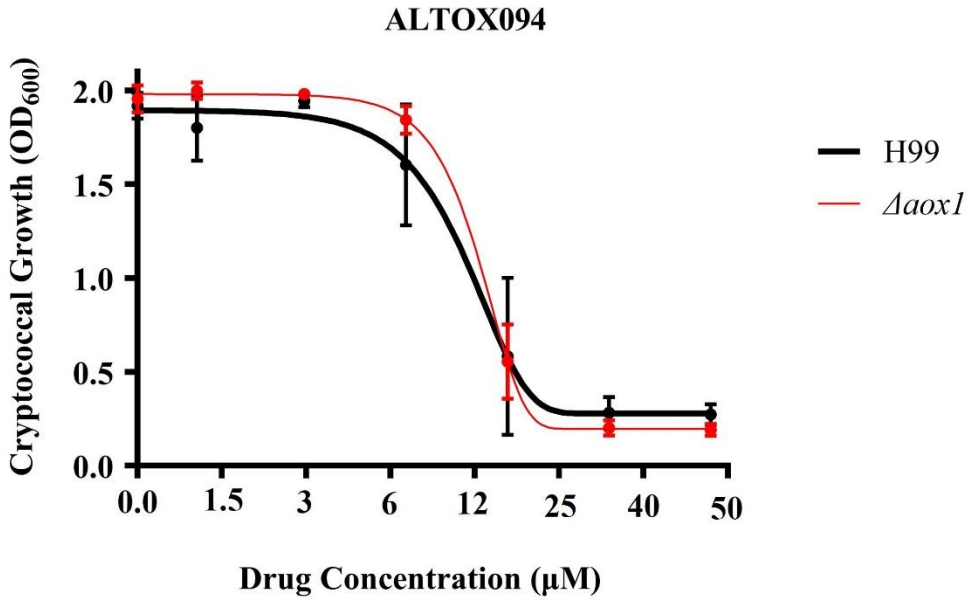

	H99	*Δaox1*
Best-fit values		
logNIC	**0.7910**	**0.8775**
Slope	**7.316**	**9.985**
Bottom	**0.2784**	**0.1974**
Span	**1.617**	**1.784**
NIC	**6.181**	**7.543**

	H99	*Δaox1*
Best-fit values		
logMIC	**1.163**	**1.150**
Slope	**7.316**	**9.985**
Bottom	**0.2784**	**0.1974**
Span	**1.617**	**1.784**
MIC	**14.54**	**14.12**

	H99	*Δaox1*
Std. Error		
logNIC	0.04838	0.01239

	H99	*Δaox1*
Std. Error		
logMIC	0.02869	0.005142

B

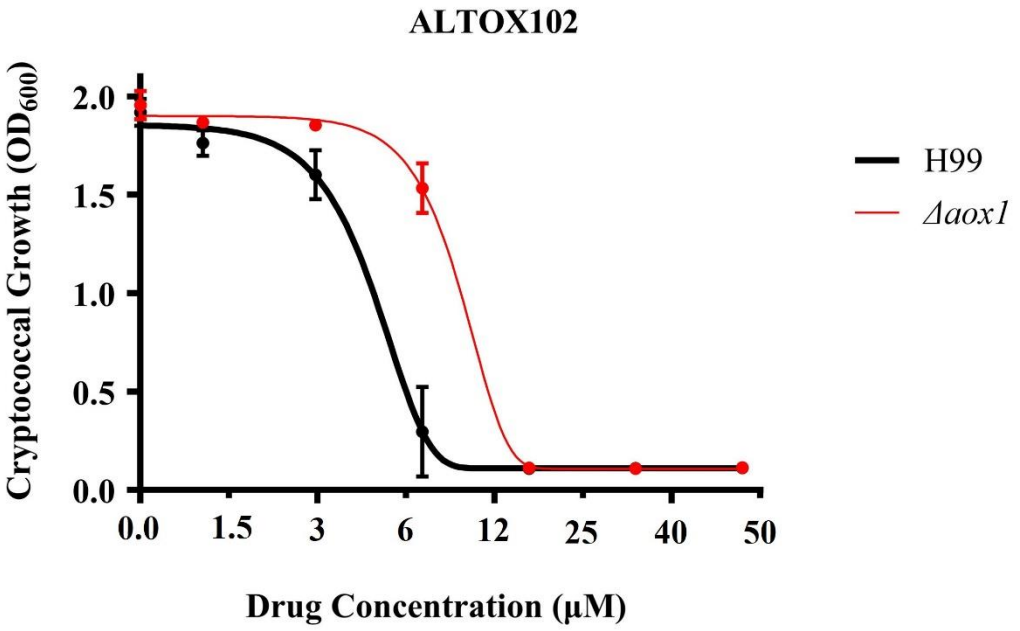

	H99	*Δaox1*
Best-fit values		
logNIC	**0.5061**	**0.7706**
Slope	**8.696**	**10.12**
Bottom	**0.1105**	**0.1081**
Span	**1.746**	**1.793**
NIC	**3.207**	**5.896**

	H99	*Δaox1*
Best-fit values		
logMIC	**0.8187**	**1.039**
Slope	**8.696**	**10.12**
Bottom	**0.1105**	**0.1081**
Span	**1.746**	**1.793**
MIC	**6.587**	**10.94**

	H99	*Δaox1*
Std. Error		
logNIC	0.03387	0.01606

	H99	*Δaox1*
Std. Error		
logMIC	0.01935	0.05701

Figure 5.3: Minimum Inhibitory Concentration (MIC90) values of ALTOX094 and ALTOX102.

The Non-Inhibitory Concentration (NIC) and Minimum Inhibitory Concentration (MIC90) values of wildtype (H99) and *Δaox1* null mutant (*Δaox1*) *C. neoformans* treated with ALTOX094 (**A**) and ALTOX102 (**B**) calculated using the Gompertz equation for NIC/MIC90 determination in GraphPad Prism. The MIC90 of ALTOX094 is 14.54µM for H99 and 14.12µM for *Δaox1,* while the MIC90 of ALTOX102 is 6.587µM and 10.94µM for H99 and *Δaox1,* respectively. MIC90 values were rounded to 15µM for ALTOX094 and 7µM and 11µM for ALTOX102. Error bars represent ± SD. n = 9

5.2.5 ALTOX drugs exhibit fungicidal activity

To assess whether the disruption to growth observed in Fig. 5.2 and Figure 5.3 was due to a reduction in viability, H99 and *Δaox1* mutant cells were plated following a 2 h incubation in YPD containing ALTOX094 or ALTOX102 at the calculated MIC for each compound. Interestingly, addition of ALTOX094 at the MIC90 showed a strong effect on viability for both wildtype and *Δaox1* mutant cells (Fig. 5.5a). Addition of ALTOX102 at the MIC90 of 11µM also led to a decrease in viability for both strains (Fig. 5.5b). However, while the viability of *Δaox1* mutant *C. neoformans* was affected

by both calculated MIC90 values for ALTOX102, there was no significant fungicidal effect on wild-type H99 at the fungistatic MIC90 of 7μM (Fig. 5.5b). While the data for ALTOX094 showed a strong fungicidal activity at the given MIC90, the data for ALTOX102 exhibited dose-dependent fungicidal activity, with lower dose providing a fungistatic effect.

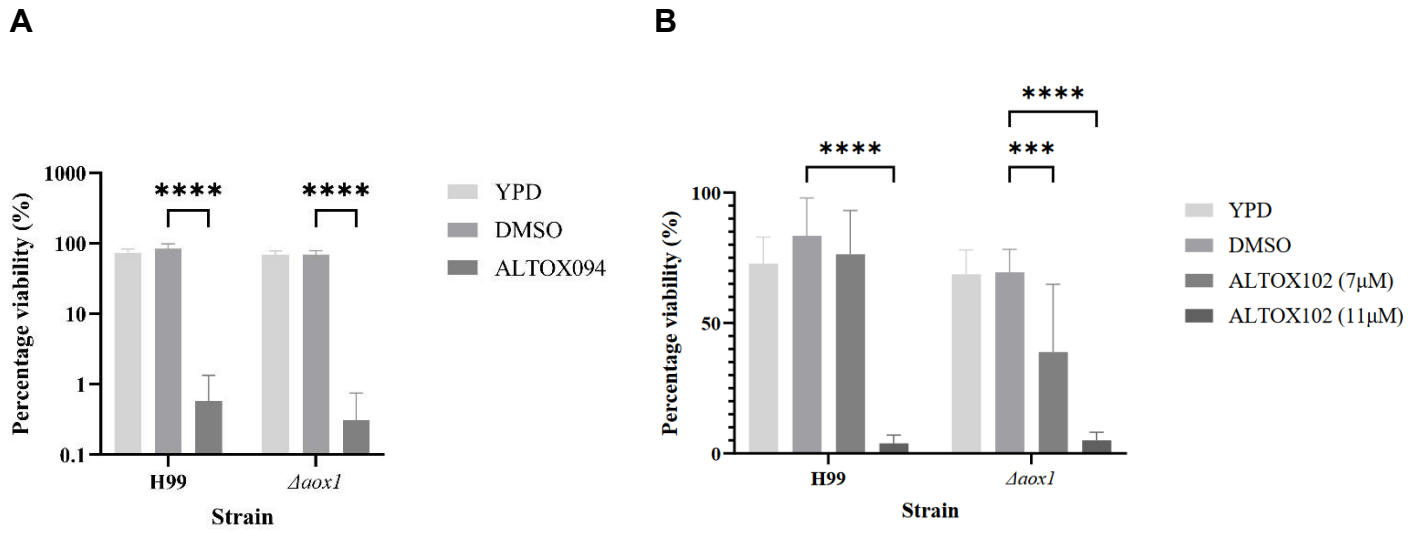

Figure 5.4: Viability assay of C. neoformans exposed to ALTOX094 and ALTOX102 treatment.
The viability of wildtype (H99) and *Δaox1* null mutant (*Δaox1*) *C. neoformans* after a 2 h incubation in YPD containing ALTOX094 (**A**) and ALTOX102 (**B**) in comparison to a DMSO control. Significance was calculated using Dunnett's multiple comparisons test following a one-way ANOVA in GraphPad Prism. *** < 0.0005, **** <0.0001, where P = 0.05. Error bars represent ± SD. n = 9

5.2.6 ALTOX094 treatment induces necrosis

As ALTOX094 and ALTOX102 exposure led to a dramatic loss of viability we sought to assess the mechanism of cell death. *C. neoformans* were treated with ALTOX094 at the given MIC90 value and following a 2 h incubation at 37°C, the cultures were assessed for Propidium Iodide (PI) uptake, a marker of necrosis. Interestingly, treatment with ALTOX094 induced necrosis in 99% of H99 (Fig. 5.5a) and 98% of *Δaox1* mutant *C. neoformans* cells (Fig. 5.5b). In contrast, treatment with 7μM ALTOX102 resulted in minimal necrosis, with only 2% of wildtype (Fig. 5.5c) and 3% of *Δaox1* (Fig. 5.5d) showing PI uptake. This figure did not increase with treatment at 11μM ALTOX102. Interestingly, while average necrosis levels after ALTOX102 treatment were far lower than

ALTOX094, ALTOX102 did significantly induce necrosis in *Δaox1* populations at both MIC90s (Fig. 5.5d).

A

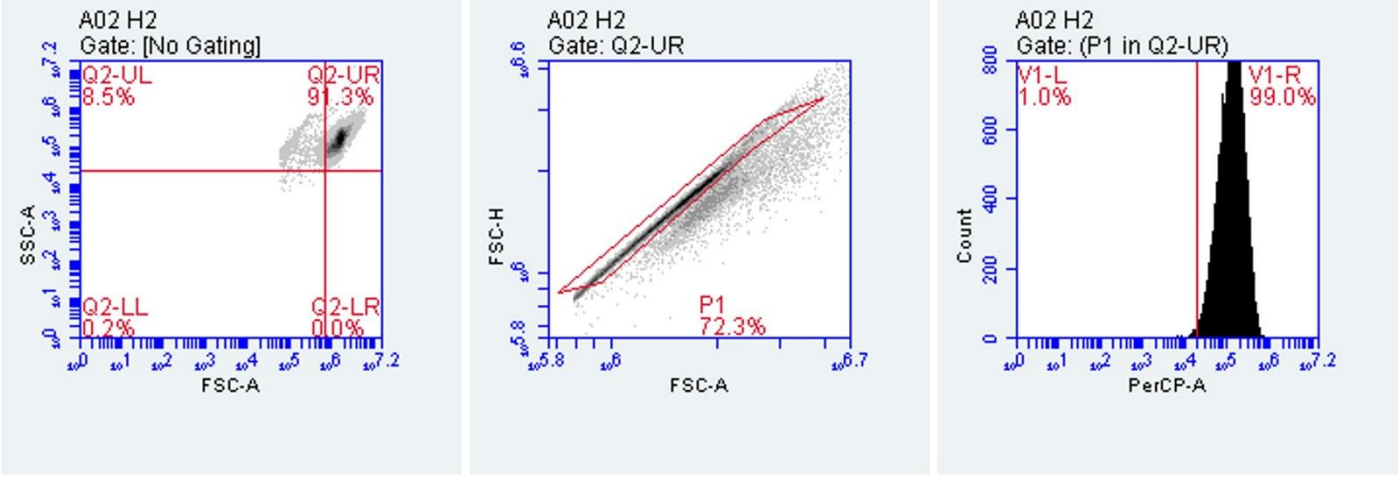

B

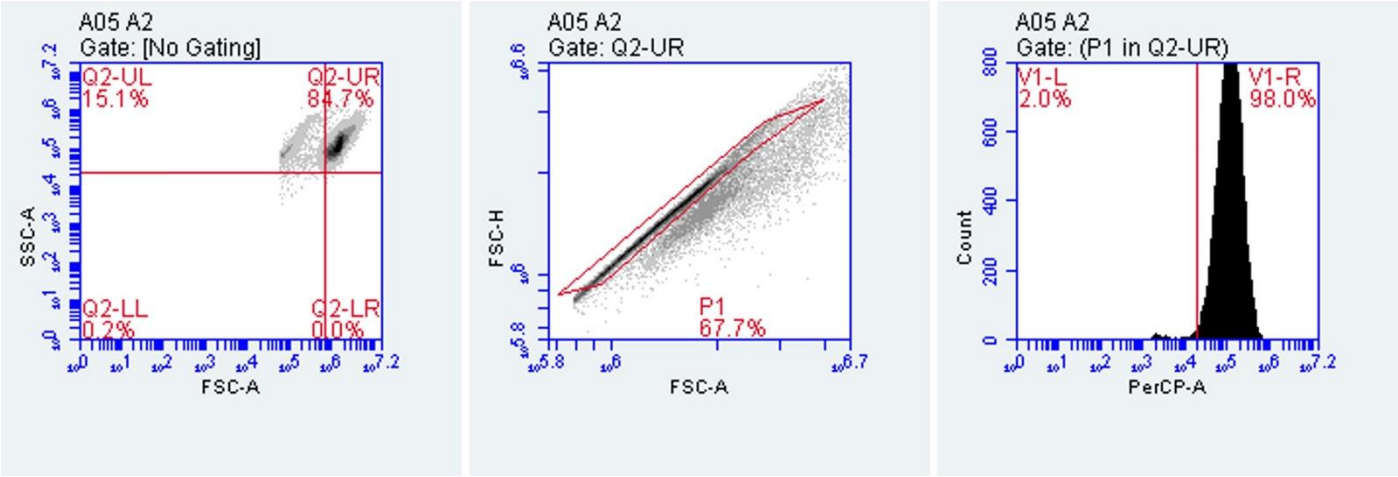

C

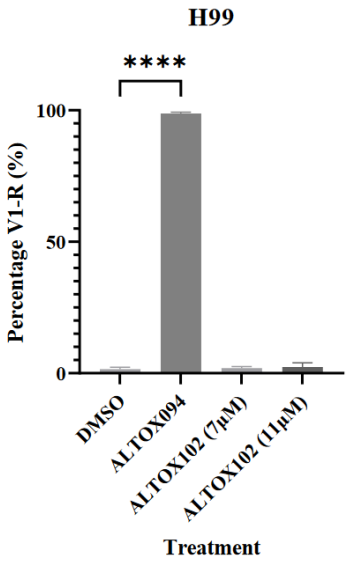

D

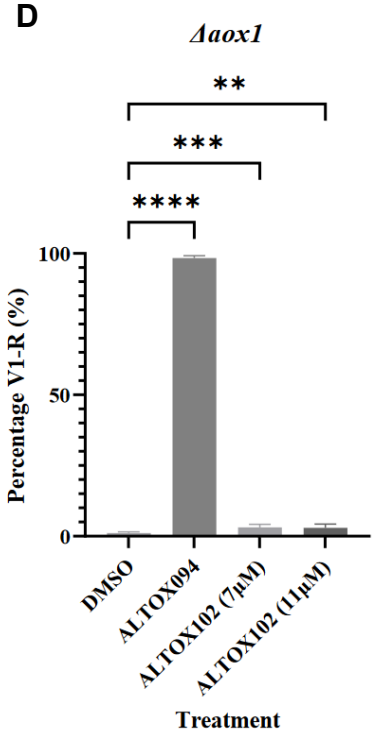

Figure 5.5: Flow cytometry assay of C. neoformans exposed to ALTOX094 and ALTOX102 treatment.
C. neoformans strains were stained with PI and analysed via Flow Cytometry after a 2 h incubation with ALTOX094 or ALTOX102 at the given MIC90. Percentage necrosis was measured via fluorescence in V1-R for H99 (**A**) and *Δaox1* (**B**) including a representative histogram of the population percentage found in V1-R after ALTOX094 treatment. Percentage necrosis of strains treated with ALTOX094 and ALTOX102 in comparison to a DMSO control were calculated. (**C**) H99, (**D**) *Δaox1* Significance was calculated using Dunnett's multiple comparisons test following a one-way ANOVA in GraphPad Prism. ** <0.005, *** <0.0005, **** <0.0001, where P = 0.05. Error bars represent ± SD. n = 9

5.2.7 ALTOX102 treatment does not induce ROS production

After establishing that ALTOX102 treatment did not induce high levels of necrosis, we wanted to establish whether *C. neoformans* strains treated with ALTOX102 at the given MIC90 values induced ROS production, a common occurrence when respiratory inhibition is applied to cells. Following a 2 h incubation at 37°C, wildtype and *Δaox1* cultures were stained with 2',7'-Dichlorodihydrofluorescein diacetate (H_2DCF-DA) and analysed using Flow Cytometry. However, after treatment with 7μM ALTOX102, 86% of wildtype (Fig. 5.6a) and 96% of *Δaox1* (Fig. 5.6b) showed low levels of ROS, while addition of 11μM ALTOX102 maintained low ROS in 97% of H99 (Fig. 5.6c) and 97% of *Δaox1* populations (Fig. 5.6d). These data suggest that the reduction in viability associated with ALTOX102 exposure at 11μM is not accompanied by ROS accumulation as assessed by H_2DCF-DA.

A

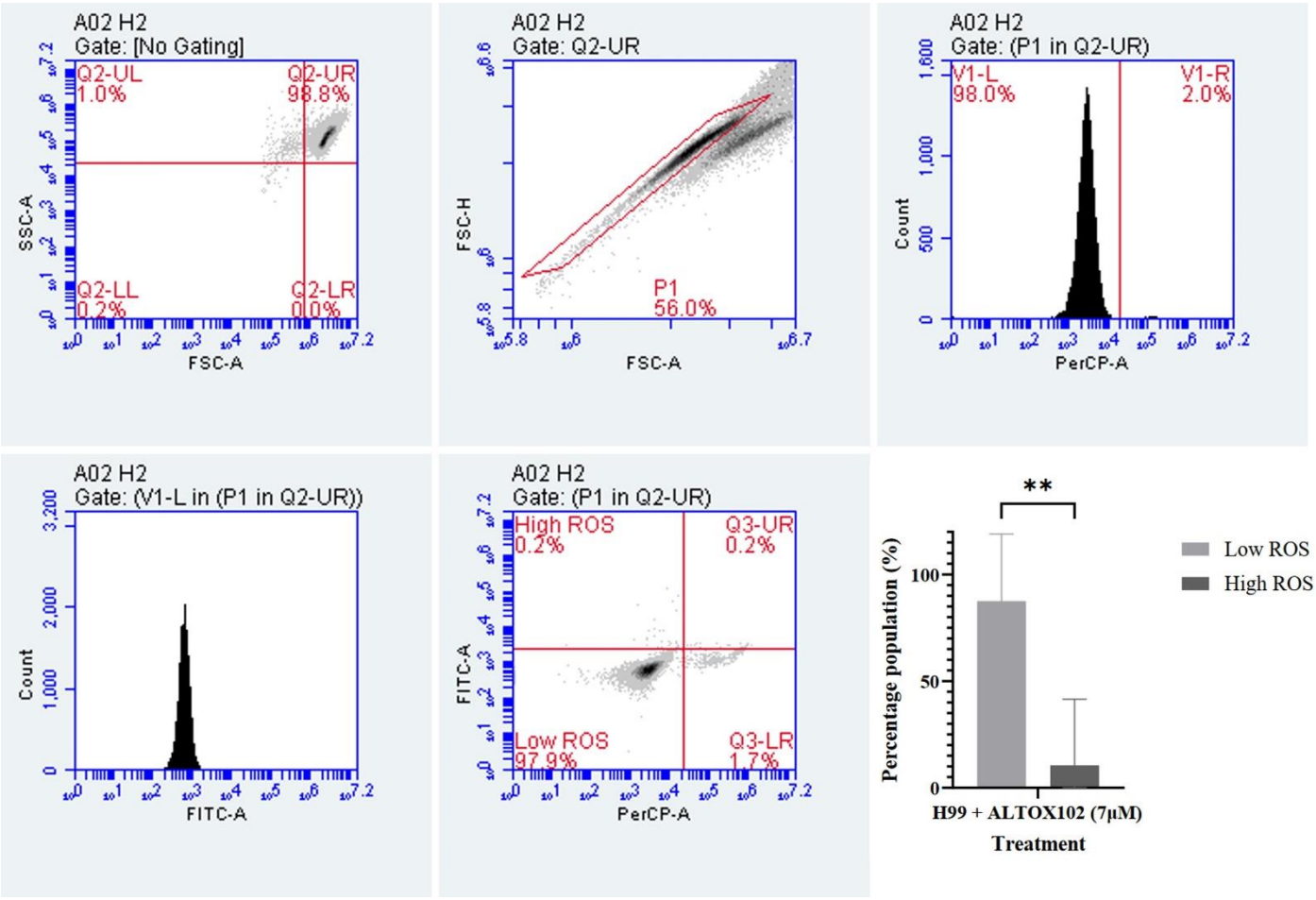
A02 H2
Gate: [No Gating]
Q2-UL
1.0%
Q2-UR
98.8%
Q2-LL
0.2%
Q2-LR
0.0%
SSC-A
FSC-A
A02 H2
Gate: Q2-UR
FSC-H
FSC-A
P1
56.0%
A02 H2
Gate: (P1 in Q2-UR)
V1-L
98.0%
V1-R
2.0%
Count
PerCP-A
A02 H2
Gate: (V1-L in (P1 in Q2-UR))
Count
FITC-A
A02 H2
Gate: (P1 in Q2-UR)
High ROS
0.2%
Q3-UR
0.2%
Low ROS
97.9%
Q3-LR
1.7%
FITC-A
PerCP-A
**
Percentage population (%)
Low ROS
High ROS
H99 + ALTOX102 (7μM)
Treatment

B

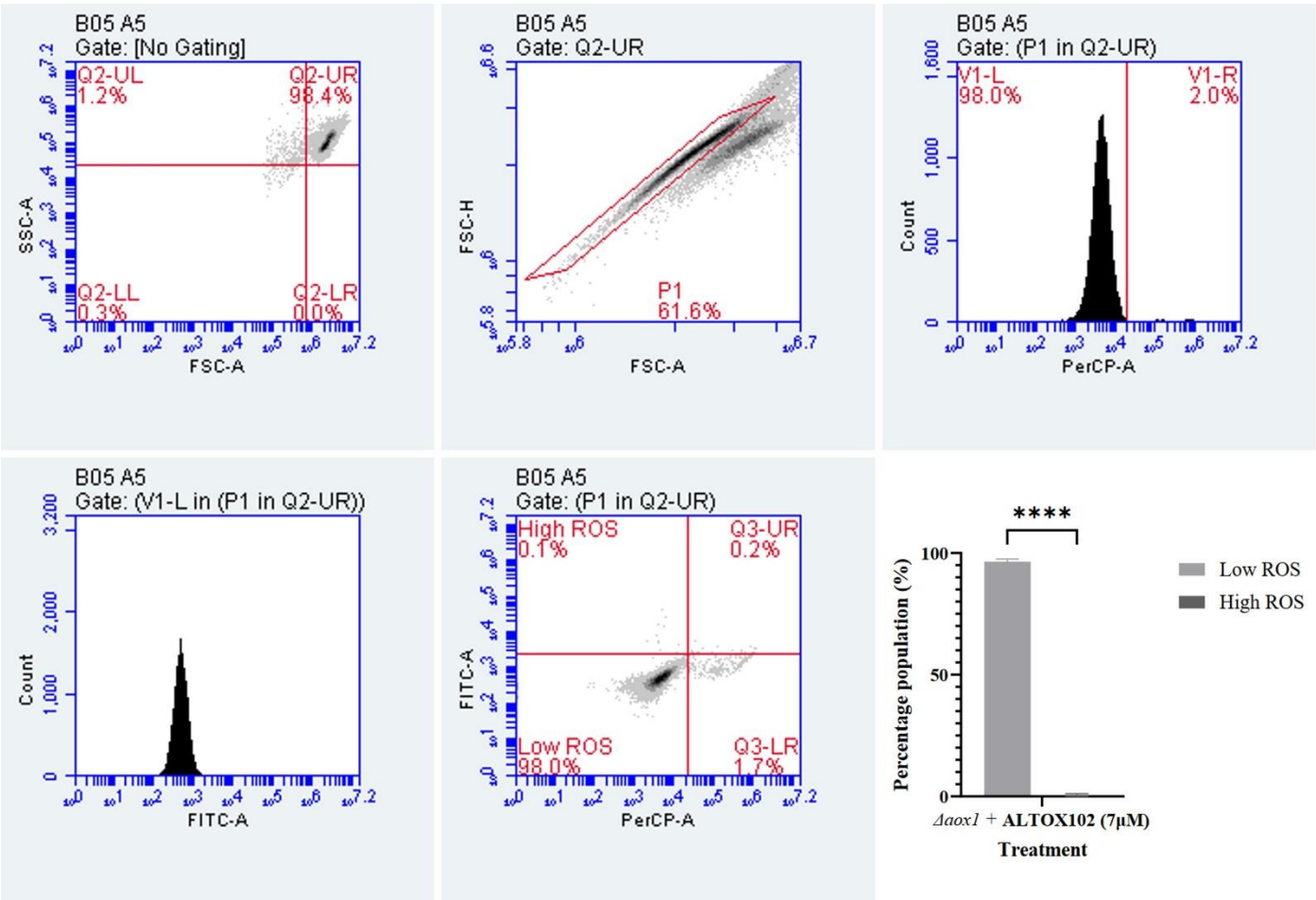
B05 A5
Gate: [No Gating]
Q2-UL
1.2%
Q2-UR
98.4%
Q2-LL
0.3%
Q2-LR
0.0%
SSC-A
FSC-A
B05 A5
Gate: Q2-UR
FSC-H
FSC-A
P1
61.6%
B05 A5
Gate: (P1 in Q2-UR)
V1-L
98.0%
V1-R
2.0%
Count
PerCP-A
B05 A5
Gate: (V1-L in (P1 in Q2-UR))
Count
FITC-A
B05 A5
Gate: (P1 in Q2-UR)
High ROS
0.1%
Q3-UR
0.2%
Low ROS
98.0%
Q3-LR
1.7%
FITC-A
PerCP-A
****
Percentage population (%)
Low ROS
High ROS
Δaox1 + ALTOX102 (7μM)
Treatment

C

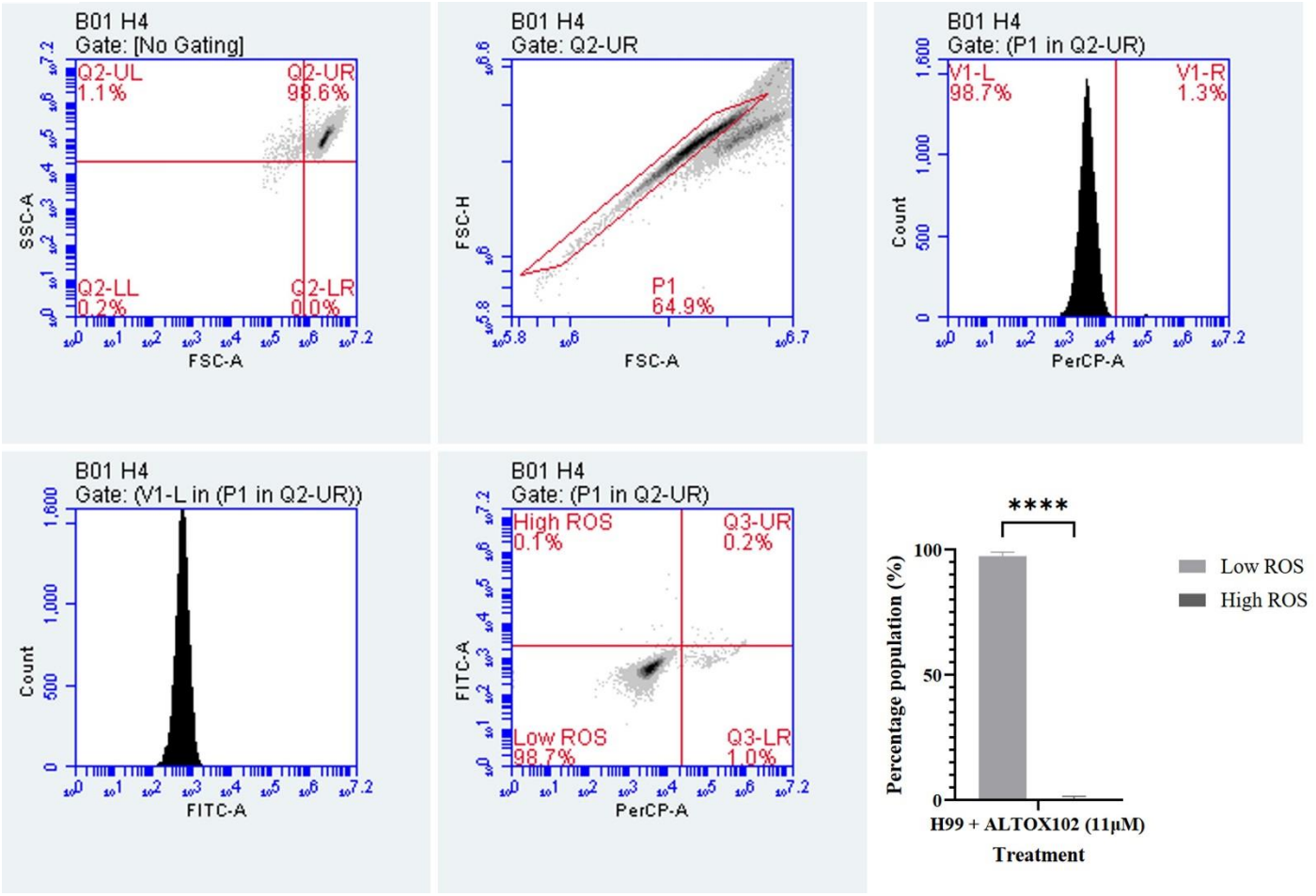
B01 H4
Gate: [No Gating]
Q2-UL
1.1%
Q2-UR
98.6%
Q2-LL
0.2%
Q2-LR
0.0%
SSC-A
FSC-A
B01 H4
Gate: Q2-UR
P1
64.9%
FSC-H
FSC-A
B01 H4
Gate: (P1 in Q2-UR)
V1-L
98.7%
V1-R
1.3%
Count
PerCP-A
B01 H4
Gate: (V1-L in (P1 in Q2-UR))
Count
FITC-A
B01 H4
Gate: (P1 in Q2-UR)
High ROS
0.1%
Q3-UR
0.2%
Low ROS
98.7%
Q3-LR
1.0%
FITC-A
PerCP-A
****
Percentage population (%)
100
50
0
H99 + ALTOX102 (11μM)
Treatment
Low ROS
High ROS

D

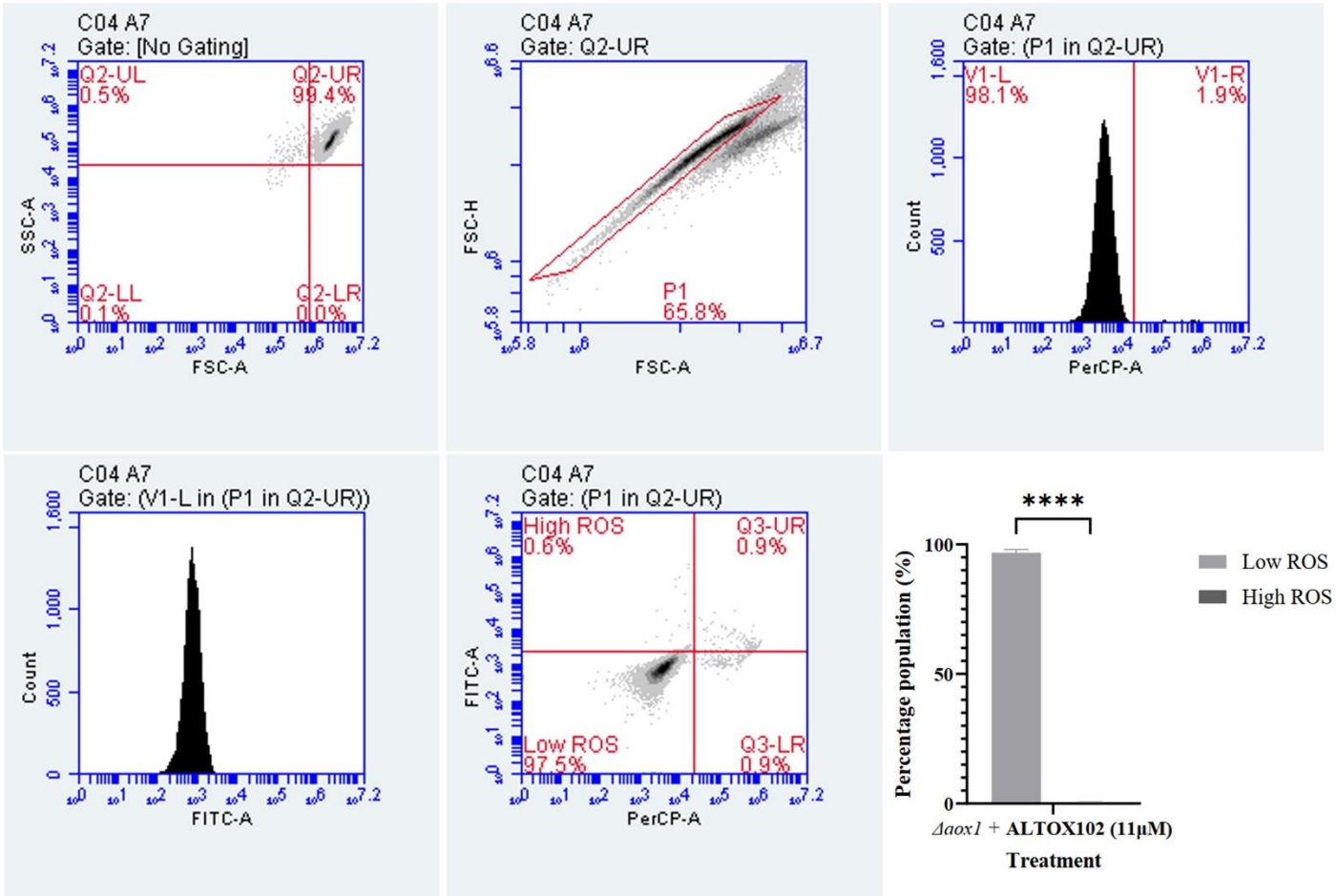
C04 A7
Gate: [No Gating]
Q2-UL
0.5%
Q2-UR
99.4%
Q2-LL
0.1%
Q2-LR
0.0%
SSC-A
FSC-A
C04 A7
Gate: Q2-UR
P1
65.8%
FSC-H
FSC-A
C04 A7
Gate: (P1 in Q2-UR)
V1-L
98.1%
V1-R
1.9%
Count
PerCP-A
C04 A7
Gate: (V1-L in (P1 in Q2-UR))
Count
FITC-A
C04 A7
Gate: (P1 in Q2-UR)
High ROS
0.6%
Q3-UR
0.9%
Low ROS
97.5%
Q3-LR
0.9%
FITC-A
PerCP-A
****
Percentage population (%)
100
50
0
Δaox1 + ALTOX102 (11μM)
Treatment
Low ROS
High ROS

Figure 5.6: Flow cytometry assay of C. neoformans exposed to ALTOX102 treatment. *C. neoformans* strains were stained with H_2DCF-DA and analysed via Flow Cytometry after a 2 h incubation with ALTOX102 at the given MIC90. Percentage necrosis was measured via fluorescence in V1-R. Panels: (**A**) H99 + 7µM ALTOX102, (**B**) *Δaox1* + 7µM ALTOX102, (**C**) H99 + 11µM ALTOX102, (**D**) *Δaox1* + 11µM ALTOX102 including a representative histogram of the population percentage found in V1-L after ALTOX102 treatment. Percentage population of strains with low ROS and high ROS after ALTOX102 treatment were calculated. Significance was calculated using Dunnett's multiple comparisons test following a one-way ANOVA in GraphPad Prism. ** <0.005, *** <0.0005, **** <0.0001, where P = 0.05. Error bars represent ± SD. n = 9

5.2.8 ALTOX treatment affects cellular respiration

Following the initial assessment of ALTOX drugs on growth and viability, we investigated the respiratory profile of H99 and *Δaox1* mutant *C. neoformans* using HRR. Respirometer chambers were inoculated with 1 x 10^6 cells after 24 h growth at 37°C and treated with either ALTOX094 or ALTOX102 where indicated to a final concentration of the MIC90 for both drugs. Addition of ALTOX094 had a biphasic effect whereby addition of ALTOX094 at 7.5 µM induced an increase in respiration, but addition of the full MIC90 led to a significant loss of respiration in both H99 (Fig. 5.7a) and *Δaox1* (Fig. 5.7b). Addition of ALTOX102, however, led to an increase in respiration in both H99 (Fig. 5.7c) and a significant increase in *Δaox1* (Fig. 5.7d) cells. Measurements of maximum and minimum respiration after exposure to ALTOX094 (Fig. 5.7e) and ALTOX102 (Fig. 5.7f) were taken and compared to the routine level of respiration for each strain.

A

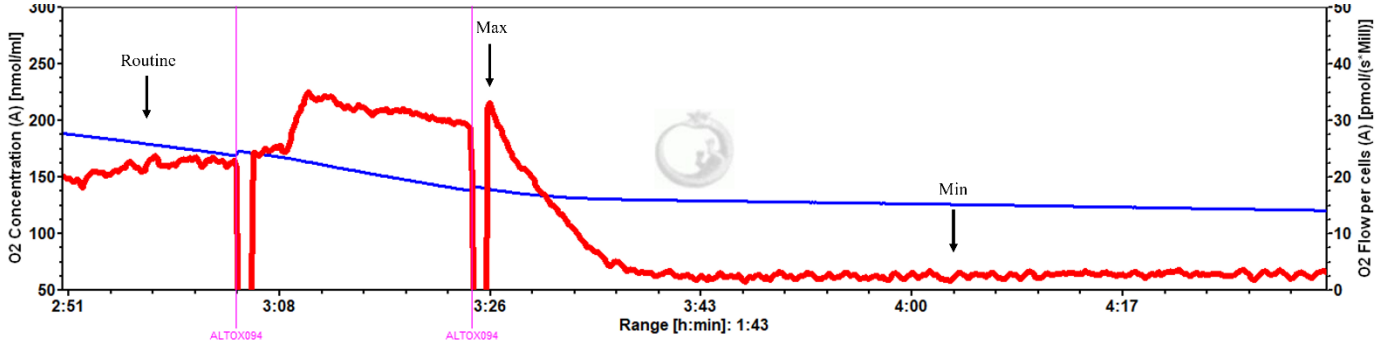

B

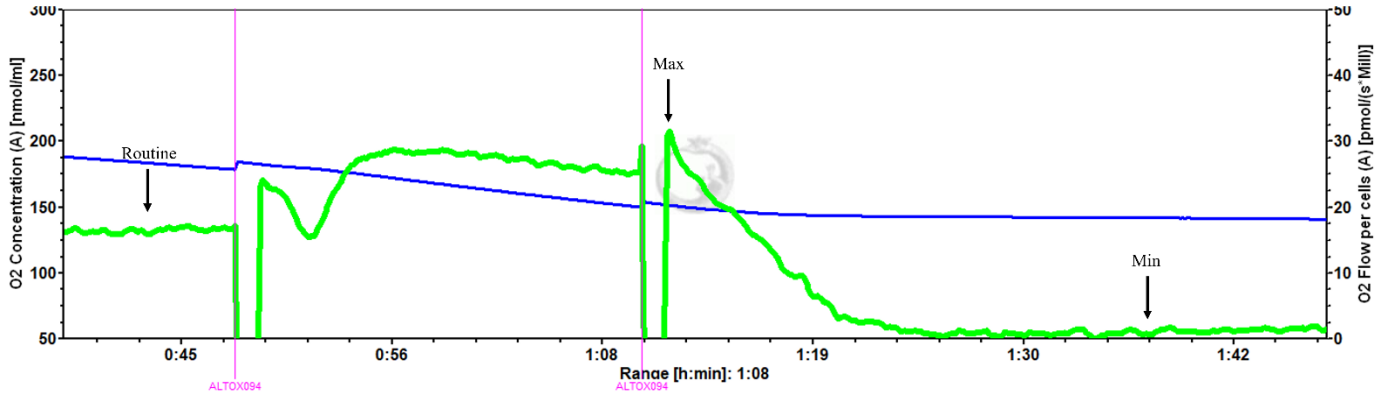
O2 Concentration (A) [nmol/ml]
O2 Flow per cells (A) [pmol/(s*Mill)]
Routine
Max
Min
0:45
0:56
1:08
1:19
1:30
1:42
Range [h:min]: 1:08
ALTOX094

C

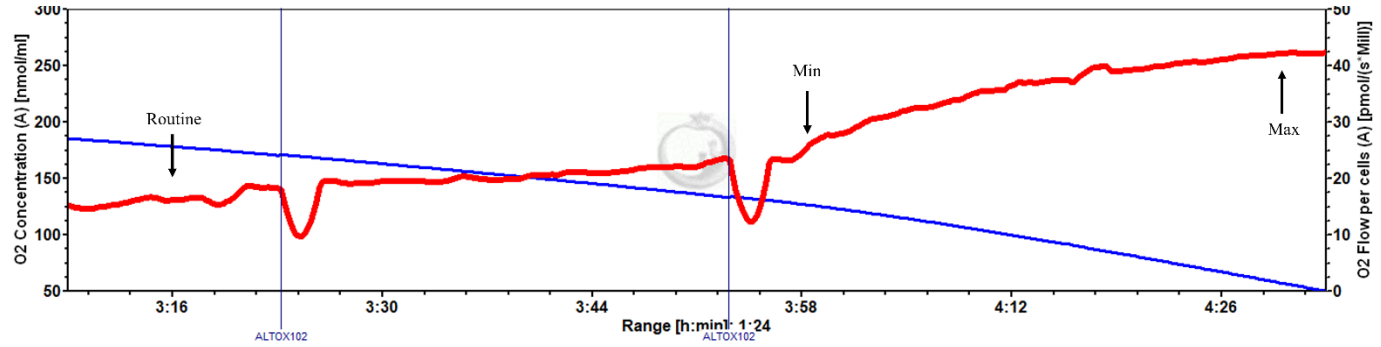
O2 Concentration (A) [nmol/ml]
O2 Flow per cells (A) [pmol/(s*Mill)]
Routine
Min
Max
3:16
3:30
3:44
3:58
4:12
4:26
Range [h:min]: 1:24
ALTOX102

D

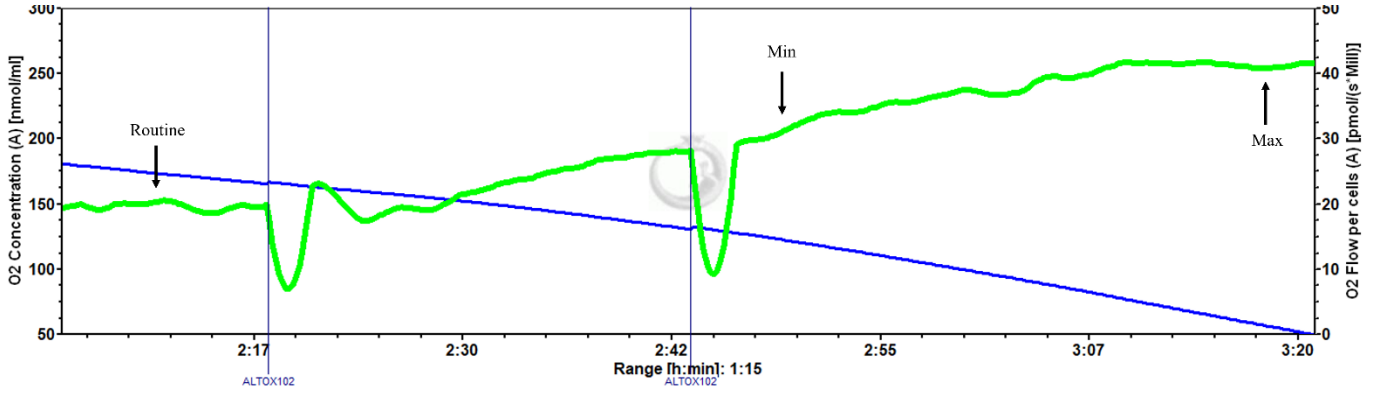
O2 Concentration (A) [nmol/ml]
O2 Flow per cells (A) [pmol/(s*Mill)]
Routine
Min
Max
2:17
2:30
2:42
2:55
3:07
3:20
Range [h:min]: 1:15
ALTOX102

E

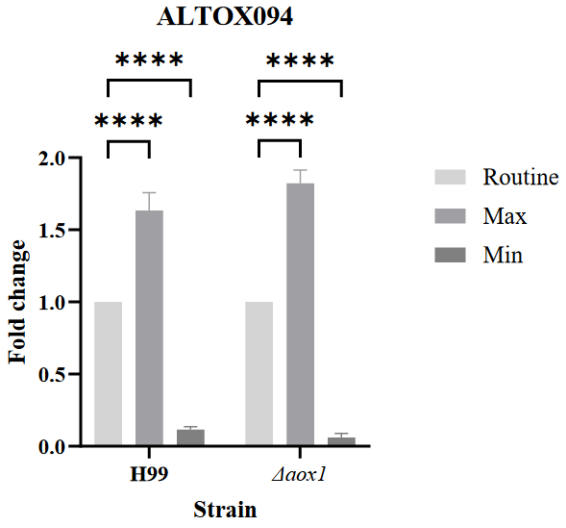
ALTOX094
****
****
****
****
Fold change
2.0
1.5
1.0
0.5
0.0
H99
Δaox1
Strain
Routine
Max
Min

F

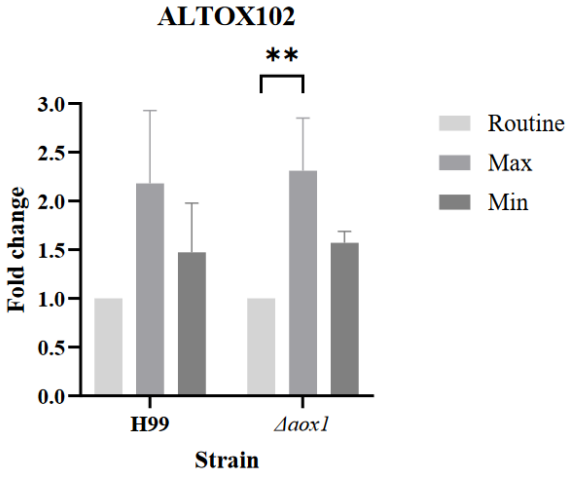
ALTOX102
**
Fold change
3.0
2.5
2.0
1.5
1.0
0.5
0.0
H99
Δaox1
Strain
Routine
Max
Min

Figure 5.7: Respiratory profiles of C. neoformans exposed to ALTOX drugs.
Representative example of respiration in H99 and *Δaox1* determined using HRR. Chambers were inoculated with 1 x 10^6 cells after 24 h growth and treated with either ALTOX094 or ALTOX102 where indicated to a final concentration of the MIC90 for both drugs. (**A**) H99 and ALTOX094, (**B**) *Δaox1* and ALTOX094, (**C**) H99 and ALTOX102, (**D**) *Δaox1* and ALTOX102. Measurements of Maximum (Max) and Minimum (Min) respiration (O2 flow per cells) after drug exposure were taken and compared to the routine level of respiration (Routine) for each strain as indicated. (**E**) ALTOX094, (**F**) ALTOX102. Significance was calculated using Dunnett's multiple comparisons test following a one-way ANOVA in GraphPad Prism. Error bars represent ± SD. * <0.05, ** <0.005, **** <0.0001, where P = 0.05. n = 3

5.2.9 Effects of ALTOX drug application on *C. neoformans* virulence

To investigate whether the presence of ALTOX094 and ALTOX102 reduced *C. neoformans* virulence in an animal we made use of the *Galleria mellonella* infection model. TruLarv™ *G. mellonella* larvae were inoculated with 1 x 10^6 CFU of wildtype (H99^{-1}) and *Δaox1* mutant cultures (*Δaox1*$^{-1}$) in the lower left proleg, followed by injection with 15μM ALTOX094, 11μM ALTOX102 or a DMSO control where indicated in the lower right proleg. Larvae were then incubated at 37°C and scored for survival (Fig. 5.8) and melanisation (Fig. 5.9) every 24 h for 5 days. Interestingly, the addition of ALTOX094 showed no significant effect *in vivo* for either H99 (Fig. 5.8a) or *Δaox1*$^{-1}$ (Fig. 5.8b) either alone or following injection with H99 or *Δaox1* cells. However, pre-treatment of cells with ALTOX094 (H99 / *Δaox1* treated) via incubation for 2 h at 37°C before injection significantly decreased larval mortality (Fig. 5.8a, 5.8b). Interestingly, pre-treatment of cells with ALTOX102 did not show the same effect, with no significant effect on larval survival (Fig. 5.8c, 5.8d). The addition of ALTOX102 alone significantly increased mortality by day 5 (Fig. 5.8c, 5.8d) and showed an increased toxicity to Galleria larvae following injection with *Δaox1* (Fig. 5.8d). In contrast to a previous report[205] we did not observe a significant difference between H99 and *Δaox1* virulence in *the G. mellonella* infection model at the infection titres used (Appendix 7.3).

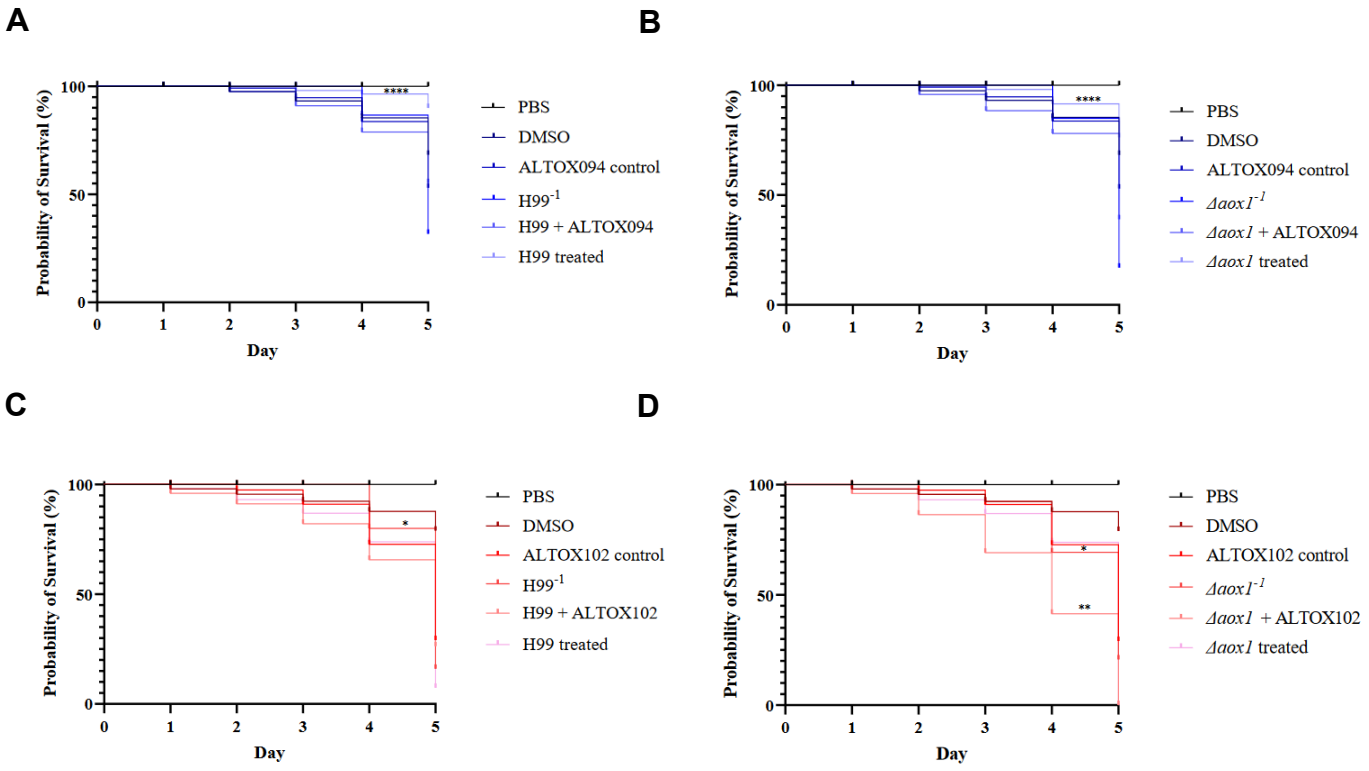

Figure 5.8: Mortality of Galleria mellonella exposed to ALTOX drugs.

TruLarv™ G. mellonella larvae were infected with 1 x 10^6 CFU *C. neoformans* and were inoculated with either ALTOX094 (n = 30) or ALTOX102 (n = 10) at the MIC90 and incubated at 37°C for 5 days. Larvae were injected through the lower left proleg with either (**A**) H99/ALTOX094, (**B**) *Δaox1*/ALTOX094, (**C**) H99/ALTOX102, or (**D**) *Δaox1*/ALTOX102. Kaplan-Meyer curves were plotted, and significance was calculated using a Log-Rank (Mantel-Cox) test in GraphPad Prism. * <0.05, **<0.005, *** <0.0010, **** < 0.0001 where P = 0.05.

5.2.10 ALTOX102 induces melanisation in *Galleria mellonella* larvae

To determine whether *G. mellonella* showed an increased immune response in response to ALTOX102 exposure melanisation was scored in conjunction with survival analyses every 24 h. The Prophenoloxidase (PPO) cascade system in *G. mellonella* induces the production of melanin as part of the immune response[375] and can be quantified using a standardised scoring system[275, 276] to assess larval melanisation from 0 (complete, systemic melanisation) to 4 (no melanisation). Interestingly, addition of ALTOX094 at the MIC90 had no significant impact on melanisation of larvae infected with H99 (Fig. 5.9a) although larvae infected with *Δaox1* both with and without ALTOX094 inoculation showed significant melanisation on day 5 (Fig. 5.9b) in comparison to a DMSO control. However, by day 5 data for ALTOX102 showed increased melanisation after inoculation with

ALTOX102 alone, as well as larvae inoculated with ALTOX102 after infection with H99, and H99 pre-treated with ALTOX102 for 2 h prior to infection (Fig. 5.9c). Addition of ALTOX102 after infection with *Δaox1* showed significant larval melanisation after day 1, which increased until day 5, where strong melanisation of *Δaox1* pre-treated larvae were also observed (Fig. 5.9d).

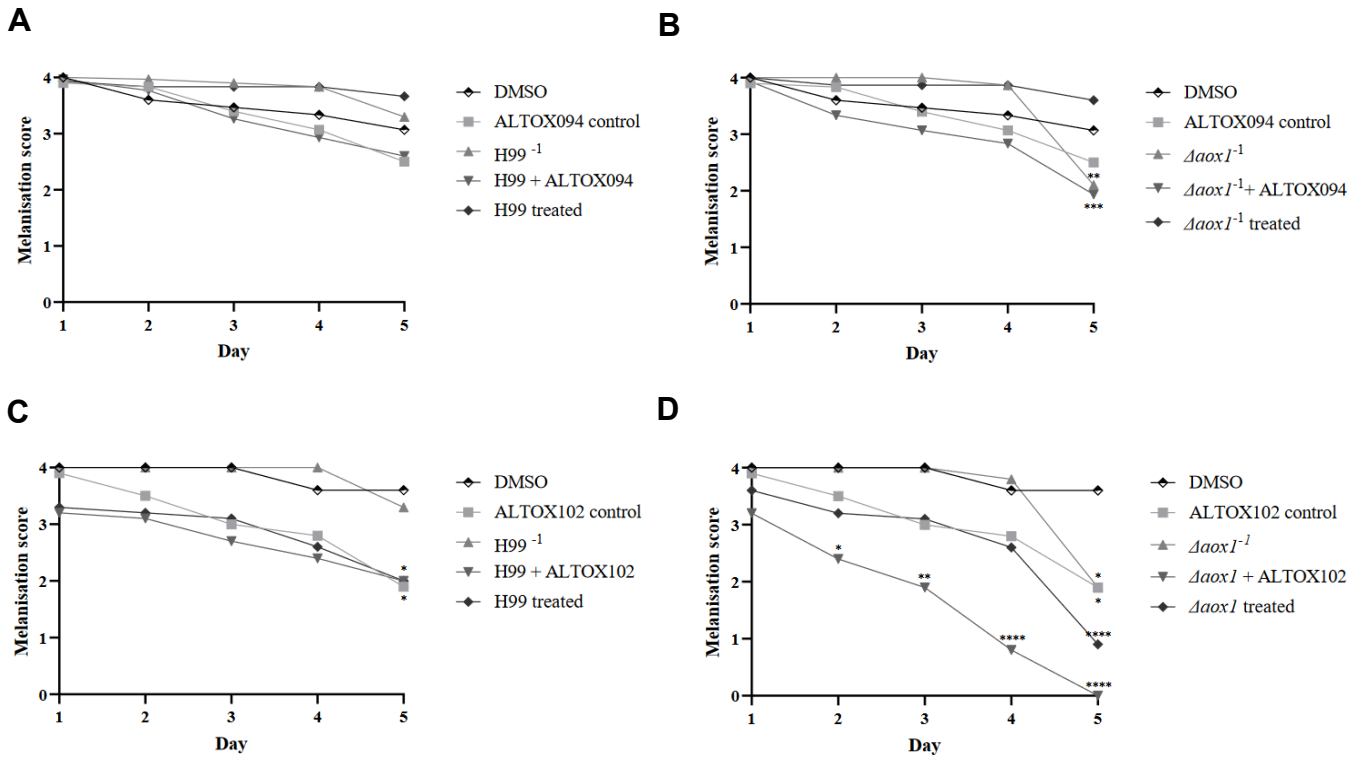

Figure 5.9: Melanisation of Galleria mellonella exposed to ALTOX drugs.

TruLarv™ *G. mellonella* larvae were infected with 1 x 10^6 CFU *C. neoformans* and were inoculated with either ALTOX094 (n = 30) or ALTOX102 (n = 10) at the MIC90 and incubated at 37°C for 5 days. Larvae were injected through the lower left proleg with either (**A**) H99/ALTOX094, (**B**) *Δaox1*/ALTOX094, (**C**) H99/ALTOX102, or (**D**) *Δaox1*/ALTOX102 and melanisation was recorded via standardised scoring from 0 (complete melanisation) to 4 (no melanisation). Significance was calculated using Dunnett's multiple comparisons test following a two-way ANOVA in GraphPad Prism. * <0.05, **<0.005, *** <0.0005, **** < 0.0001 where P = 0.05.

5.2.11 ALTOX drugs do not lead to haemolysis

Although the application of ALTOX094 or ALTOX102 at MIC90 concentrations did not lead to significant effects on *G. mellonella* mortality, indicating fungal specific effects on viability, we wished to conduct an additional early-stage cytotoxicity assessment. A haemolysis assay was carried out whereby ALTOX drugs at the given MIC90 were spotted onto agar plates containing 5% sheep's

blood. Plates were incubated at 37°C and a zone of haemolysis (ZOH) was measured at 2 h and 24 h, whereby alpha-haemolysis (red blood cell damage) was signified by a green-tinge and beta-haemolysis (complete lysis) was signified by a clear area[376]. Interestingly, neither ALTOX094 nor ALTOX102 showed any significant zones of haemolysis or clearing in comparison to the SDS positive control (Fig. 5.10a). No significant haemolytic activity was seen from either ALTOX094 or ALTOX102, even when the concentrations ranged at x2, x5 and x10 of the highest MIC90 of each drug (Fig. 5.10b, 5.10c).

A

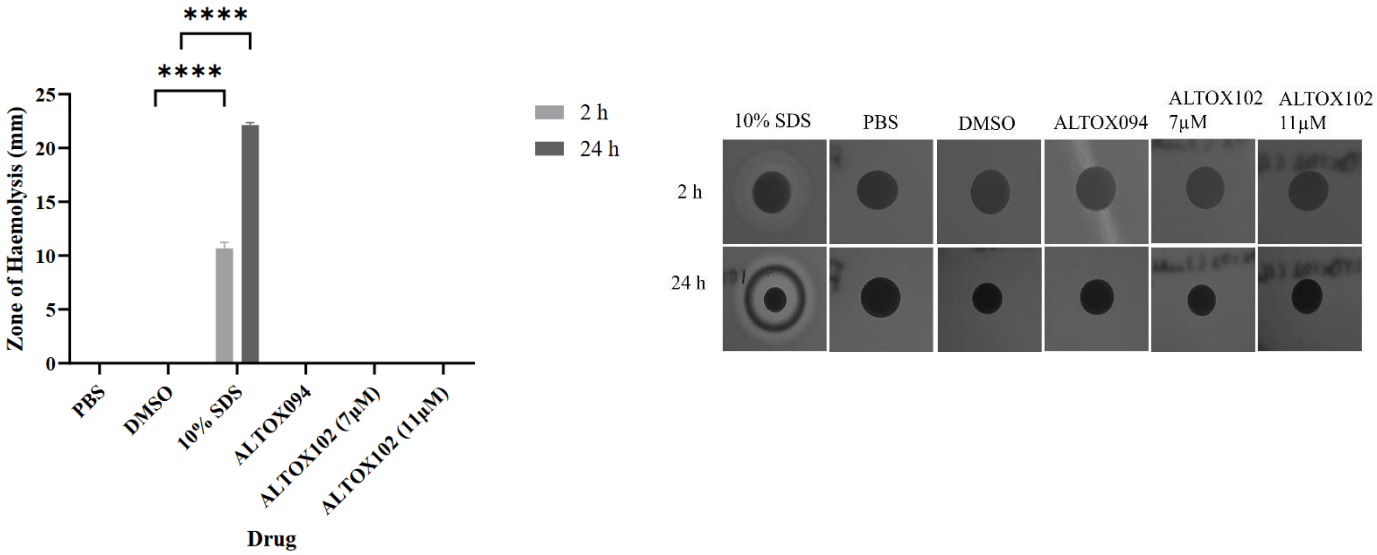

B

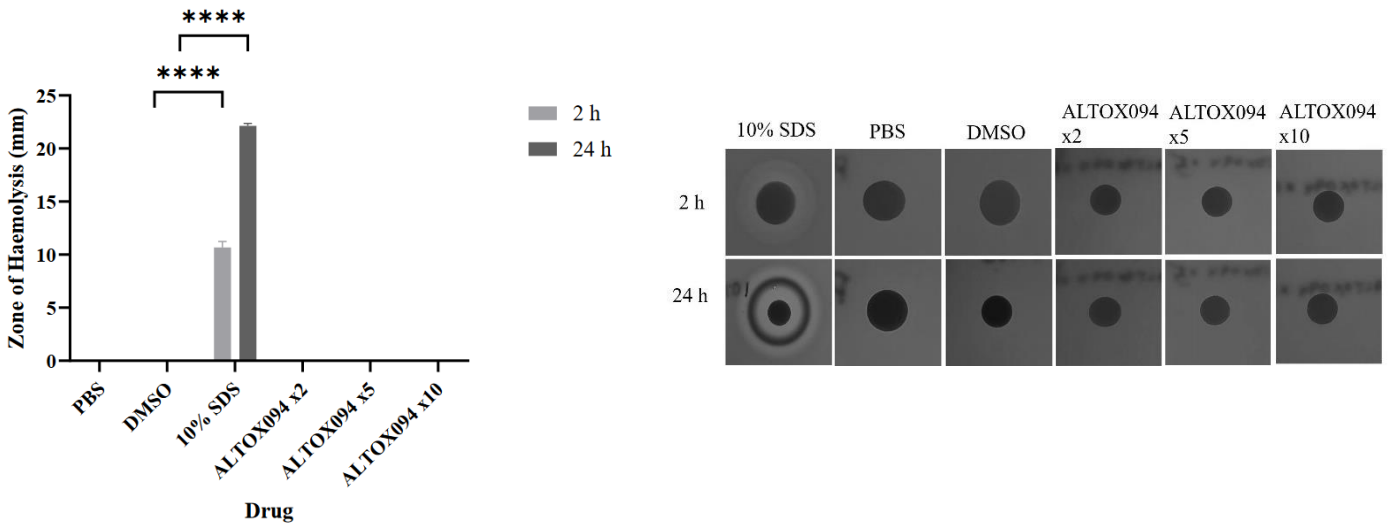

C

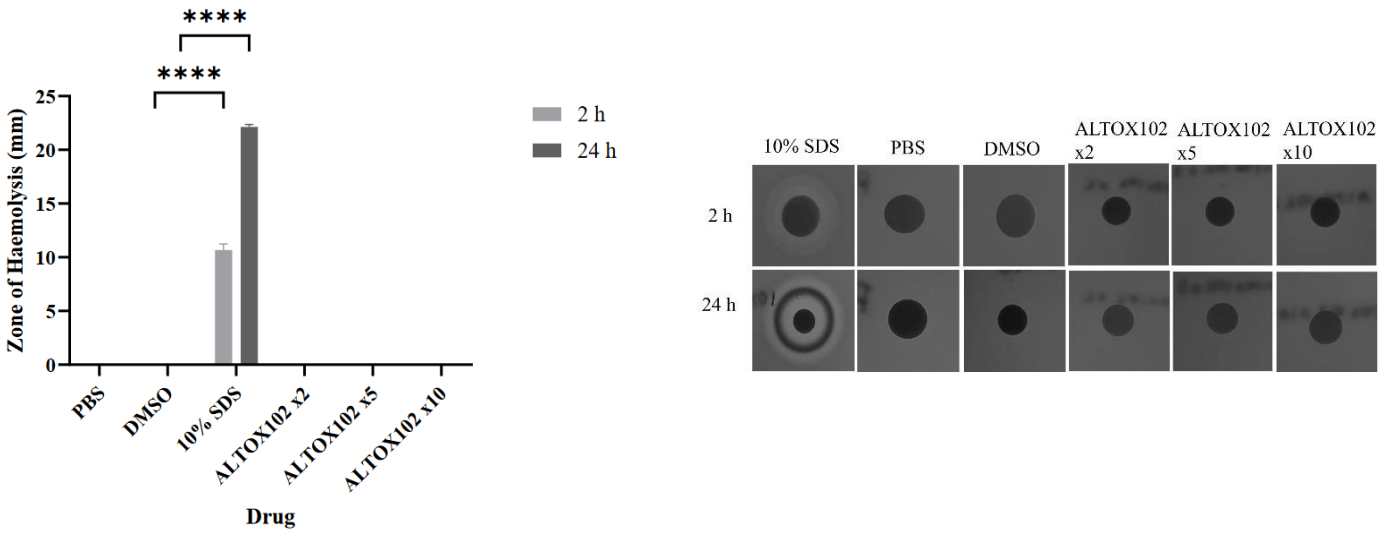

Figure 5.10: Haemolytic effect of ALTOX drugs.
(**A**) ALTOX094 and ALTOX102 were administered to filter paper disks on agar plates containing 5% sheep blood at the MIC90 and incubated at 37°C. The zone of haemolysis (ZOH) was measured after 2 h exposure and 24 h exposure. (**B**) ALTOX094 and (**C**) ALTOX102 was administered at concentrations x2, x5 and x10 the MIC90. The zone of haemolysis (ZOH) was measured after 2 h exposure and 24 h exposure. Significance was calculated using Dunnett's multiple comparisons test following a one-way ANOVA in GraphPad Prism. **** < 0.0001 where P = 0.05. Error bars represent ± SD. n = 3

5.2.12 Determining the active moiety of ALTOX094 and ALTOX102

ALTOX094 and ALTOX102 were designed to target both the mitochondrial bc_1 and Aox enzymes. However, our data suggested that although both could lead to a loss of viability, they exhibited different modes of action. To investigate the active moiety to determine the mechanism of action, controls for both chain length and bromination effect were tested. Controls relating to ALTOX094 (Decyl TPP^+, Dodecyl TPP^+, TPPC3) and ALTOX102 (Octyl TPP^+, ALTOX203) as well as compounds comprising the base molecule for both drugs (TPP+, ISSF31) were compared against the activity of the MALC compound Trimethyloctadecylammonium bromide (STAB) at two different chain lengths (STAB, 10 Carbon (10C) STAB).

5.2.13 Fungistatic action of ALTOX drugs is not reliant on a complete molecule

Wildtype (H99) and *Δaox1* mutant cells were suspended in YPD containing control compounds at the MIC90 relative to either ALTOX094 or ALTOX102 and grown for 48 h at 37°C. TPP^+ and ISSF31 (Fig. 5.11c) had no effect on H99 or *Δaox1* mutant growth. Interestingly, while reference compounds Octyl TPP^+ and ALTOX203 had no effect on wildtype cell growth (Fig. 5.11b) a variable phenotype could be seen for *Δaox1* cells at the 11μM concentration of ALTOX203 (Fig. 5.11b), whereby the effect of ALTOX203 on *Δaox1* populations either inhibited growth (sensitive) or had no apparent effect (non-sensitive). Reference compounds for ALTOX094, Decyl TPP^+ and TPPC3, had fungistatic activity against H99 and *Δaox1* (Fig. 5.11a), while Dodecyl TPP+ had no significant effects on *C. neoformans* growth.

A

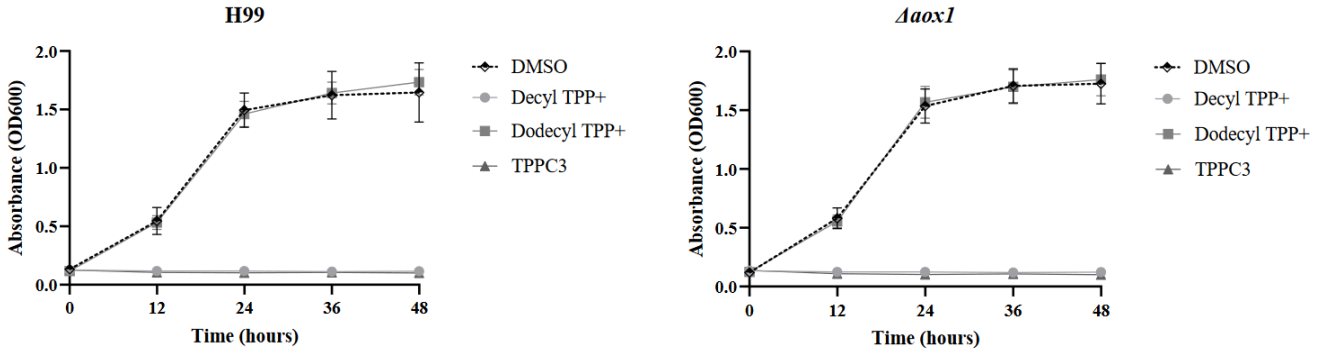

B

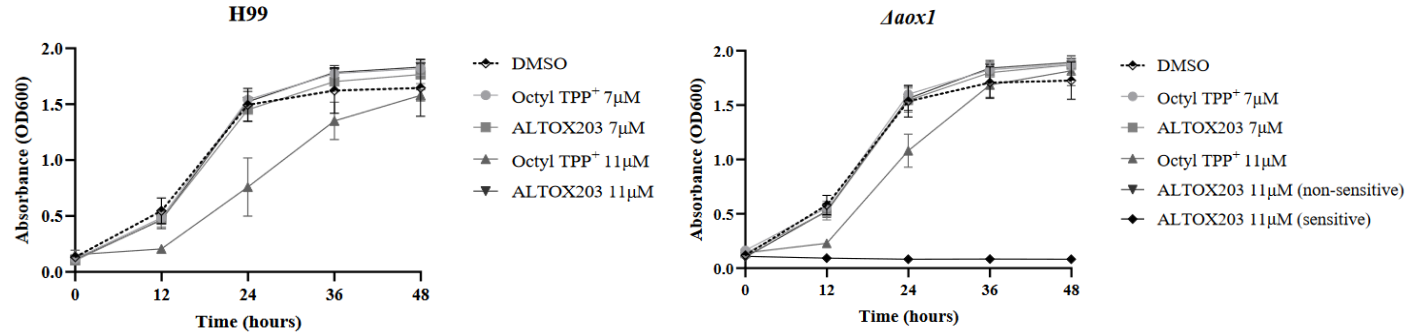

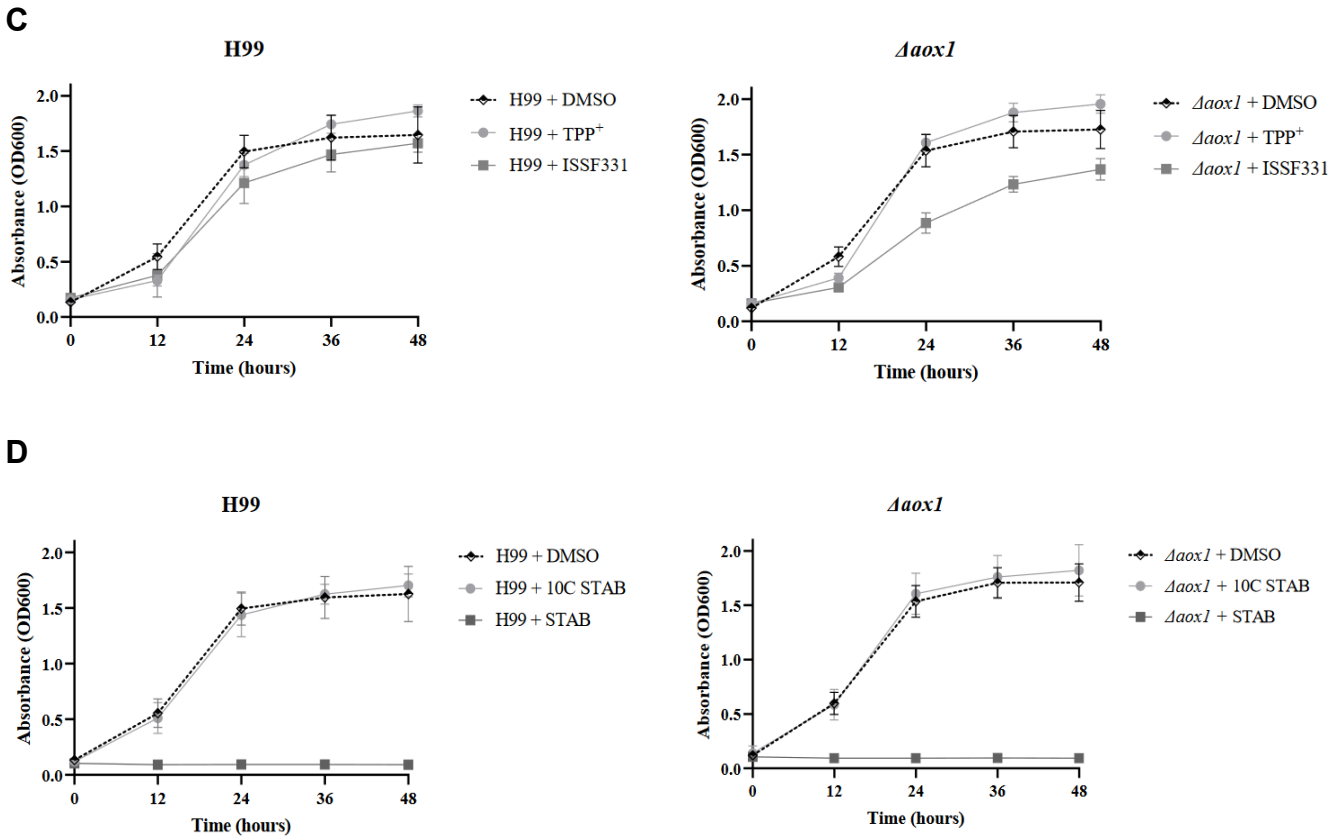

Figure 5.11: Screening of ALTOX reference compounds and their effect on C. neoformans growth.
Growth rates of Wildtype (H99) and *Δaox1* null mutant (*Δaox1*) *C. neoformans* exposed to ALTOX reference compounds Decyl TPP+, Dodecyl TPP+, TPPC3 (**A**), Octyl TPP+ and ALTOX203 (**B**), TPP+ and ISSF331 (**C**) and reference compounds 10C STAB and STAB (**D**). Cultures were grown in YPD containing each compound at the MIC90 for 48 h at 37°C. Error bars represent ± SD. n = 9

To assess whether the lack of growth after Decyl TPP+, TPPC3 and STAB addition at 15 μM, and ALTOX203 addition at 11 μM seen in Fig. 10 was based on fungicidal activity, H99 and *Δaox1* mutant cultures were plated following a 2 h incubation in YPD containing each reference compound at the MIC values of ALTOX094 and ALTOX102. After 48 h, Decyl TPP^+, Dodecyl TPP^+ and TPPC3 significantly reduced viability of both H99 and *Δaox1* cells (Fig. 5.12a), mirroring the viability data following STAB inoculation (Fig. 5.12d). Reference compounds for ALTOX102, however, did not significantly reduce viability of *C. neoformans* (Fig. 5.12b). In fact, addition of both Octyl TPP+ and ALTOX203 at the MIC90 of 7μM exhibited increased cell viability of *Δaox1.* Interestingly, this increase in cell viability was also seen upon addition of ISSF31 to wildtype (H99) cells, and after

addition of 10C STAB to *Δaox1* cells (Fig. 5.12d), although addition of TPP+ at the MIC90 did exhibit a reduction in viability for H99 (Fig. 5.12c). These data indicated that a reduction in viability seen by ALTOX094 may be based on carbon chain length, rather than a proposed dual inhibition of both Cytochrome bc_1 and Aox1, although data for ALTOX102 reference compounds indicated that a different MOA may attribute to the loss of viability seen in Fig. 5.4b.

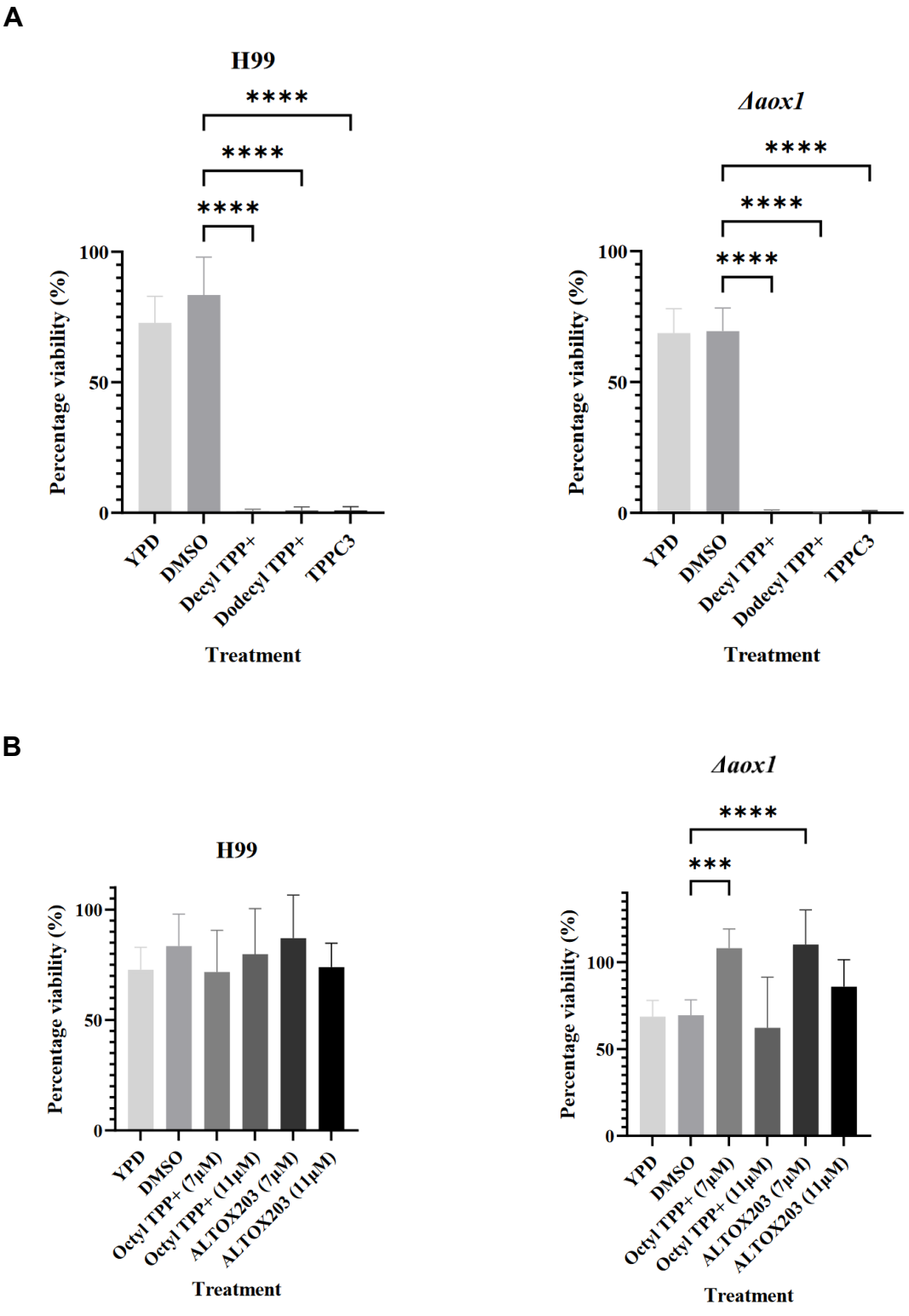

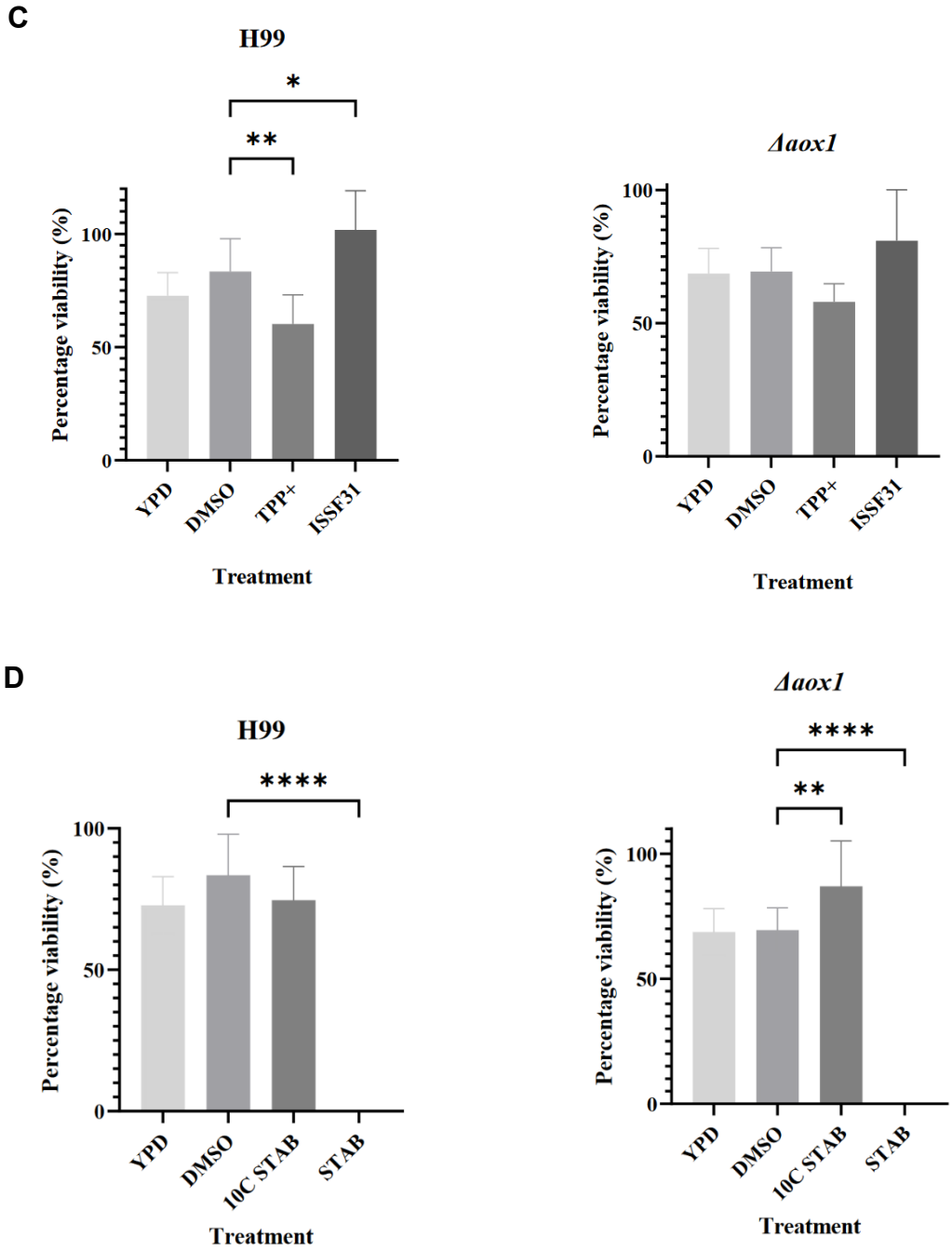

Figure 5.12: Viability assay of C. neoformans exposed to ALTOX reference compounds. The viability of wildtype (H99) and *Δaox1* null mutant (*Δaox1*) *C. neoformans* after a 2 h incubation with Decyl TPP+, Dodecyl TPP+, TPPC3 (**A**), Octyl TPP+ and ALTOX203 (**B**), TPP+ and ISSF331 (**C**) and reference compounds 10C STAB and STAB (**D**). Significance was calculated using Dunnett's multiple comparisons test following a one-way ANOVA in GraphPad Prism. * < 0.05, ** < 0.005, *** < 0.0005, **** <0.0001, where P = 0.05. Error bars represent ± SD. n = 9

5.2.14 Fungicidal activity of ALTOX094 reference compounds is based on a mixture of cell death mechanisms

Following the observation of ALTOX reference compounds on *C. neoformans* viability, we wanted to determine the mechanism of cell death induced by these compounds. H99 and *Δaox1* cultures were treated with the fungicidal reference compounds (Decyl TPP+, Dodecyl TPP+, TPPC3, STAB) at 15μM. Following a 2 h incubation at 37°C, the cultures were co-stained with H_2DCF-DA and PI and analysed using Flow Cytometry. Interestingly, for both H99 (Fig. 5.13a) and *Δaox1* (Fig. 5.13b), all fungicidal compounds tested induced necrosis significantly in comparison to a DMSO control, with Decyl TPP+ inducing necrosis in 65% of H99 and 78% of *Δaox1,* TPPC3 inducing necrosis in 96% and 95% of H99 and *Δaox1* respectively, and STAB inducing 99.7% necrosis in H99 and 99.6% necrosis in *Δaox1.*

Dodecyl TPP+, however, induced significantly less necrosis than the other compounds, only inducing necrotic activity in 18% of H99 and 9% of *Δaox1*. Interestingly, ROS levels between compound treatments differed, with both H99 (Fig. 5.13c) and *Δaox1* (Fig. 5.13d) treated with Decyl TPP+ showing varied ROS levels in the population, although induced ROS in *Δaox1* was significantly lower (Fig. 5.13d). Dodecyl TPP+ treatment showed significantly high ROS levels for *Δaox1* (Fig. 5.13f) although a mixed population of ROS levels for H99 showed no significance after 2 h (Fig. 5.13e). Interestingly, although strains treated with TPPC3 and STAB showed high levels of necrosis for both H99 (Fig. 5.13a) and *Δaox1* (Fig. 5.13b), ROS levels for both strains remained low after TPPC3 treatment (Fig. 5.13g, 5.13h) and STAB treatment (Fig. 5.13i, 5.13j)

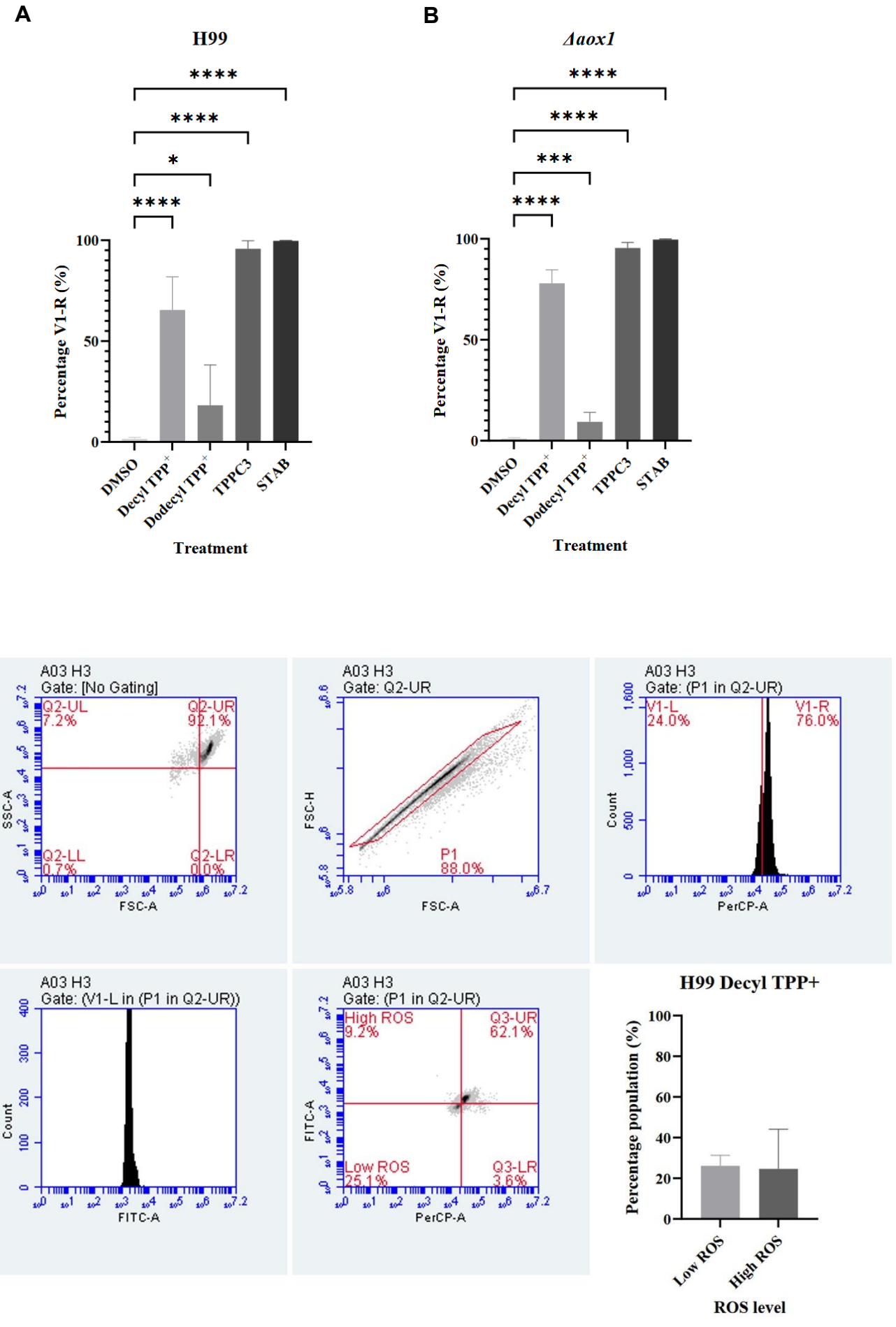
A
H99
****
****
*
****
100
50
0
Percentage V1-R (%)
DMSO
Decyl TPP+
Dodecyl TPP+
TPPC3
STAB
Treatment
B
Δaox1
****
****
***
****
100
50
0
Percentage V1-R (%)
DMSO
Decyl TPP+
Dodecyl TPP+
TPPC3
STAB
Treatment
C
A03 H3
Gate: [No Gating]
Q2-UL
7.2%
Q2-UR
92.1%
Q2-LL
0.7%
Q2-LR
0.0%
SSC-A
FSC-A
A03 H3
Gate: Q2-UR
P1
88.0%
FSC-H
FSC-A
A03 H3
Gate: (P1 in Q2-UR)
V1-L
24.0%
V1-R
76.0%
Count
PerCP-A
A03 H3
Gate: (V1-L in (P1 in Q2-UR))
Count
FITC-A
A03 H3
Gate: (P1 in Q2-UR)
High ROS
9.2%
Q3-UR
62.1%
Low ROS
25.1%
Q3-LR
3.6%
FITC-A
PerCP-A
H99 Decyl TPP+
Percentage population (%)
100
80
60
40
20
0
Low ROS
High ROS
ROS level

D

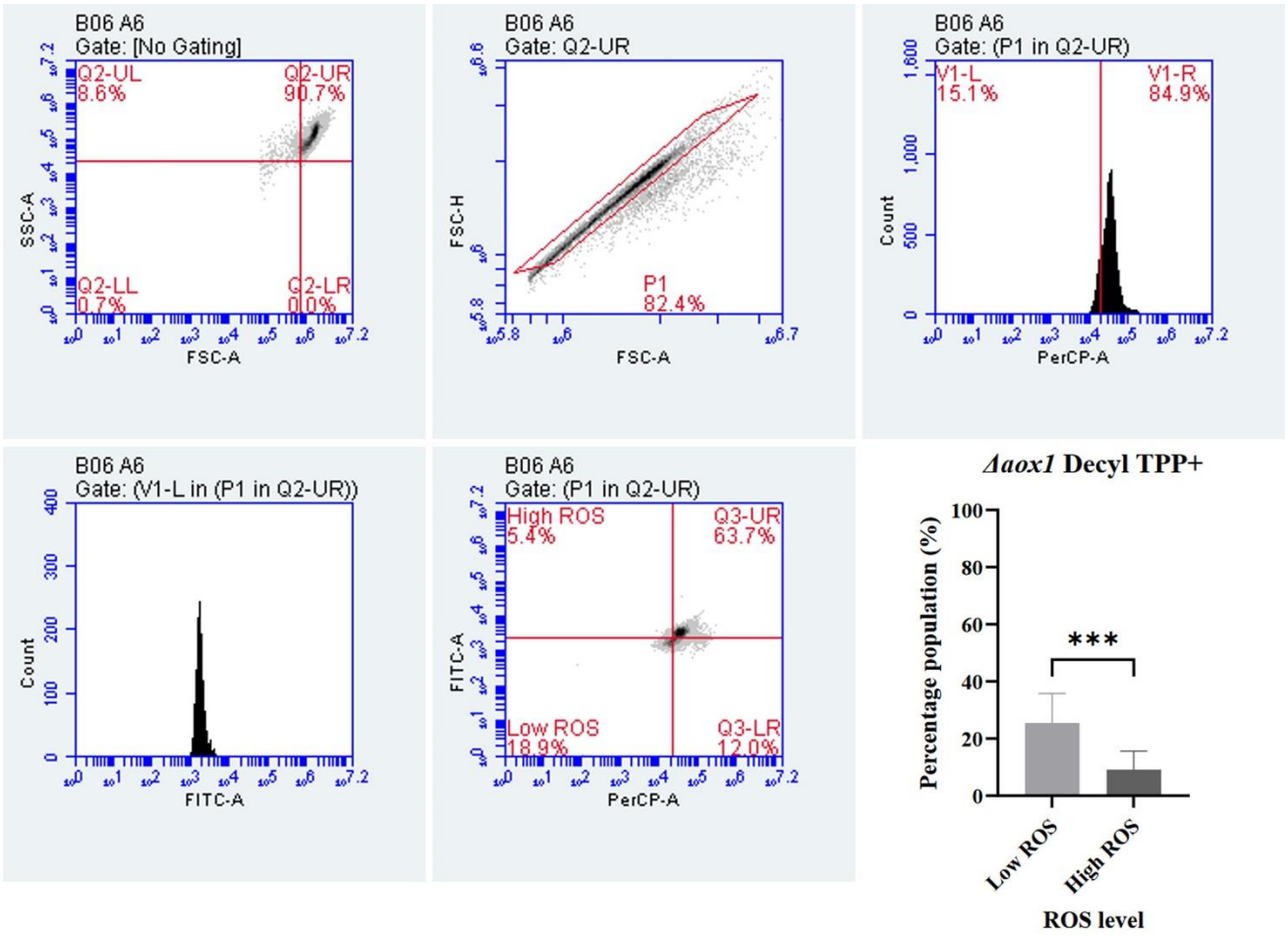
B06 A6
Gate: [No Gating]
Q2-UL
8.6%
Q2-UR
90.7%
Q2-LL
0.7%
Q2-LR
0.0%
SSC-A
FSC-A
B06 A6
Gate: Q2-UR
P1
82.4%
FSC-H
FSC-A
B06 A6
Gate: (P1 in Q2-UR)
V1-L
15.1%
V1-R
84.9%
Count
PerCP-A
B06 A6
Gate: (V1-L in (P1 in Q2-UR))
Count
FITC-A
B06 A6
Gate: (P1 in Q2-UR)
High ROS
5.4%
Q3-UR
63.7%
Low ROS
18.9%
Q3-LR
12.0%
FITC-A
PerCP-A
Δaox1 Decyl TPP+
Percentage population (%)
***
Low ROS
High ROS
ROS level

E

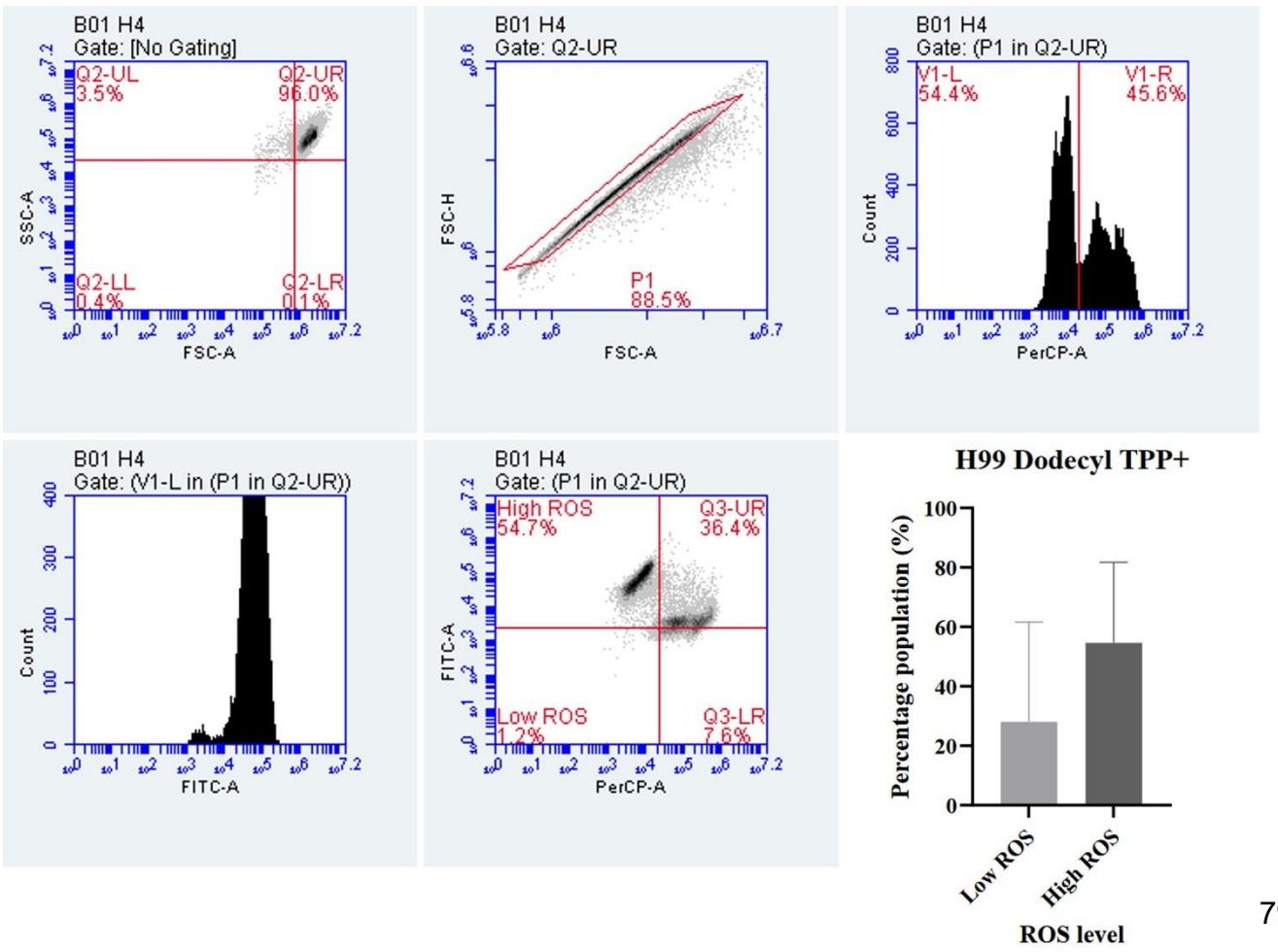
B01 H4
Gate: [No Gating]
Q2-UL
3.5%
Q2-UR
96.0%
Q2-LL
0.4%
Q2-LR
0.1%
SSC-A
FSC-A
B01 H4
Gate: Q2-UR
P1
88.5%
FSC-H
FSC-A
B01 H4
Gate: (P1 in Q2-UR)
V1-L
54.4%
V1-R
45.6%
Count
PerCP-A
B01 H4
Gate: (V1-L in (P1 in Q2-UR))
Count
FITC-A
B01 H4
Gate: (P1 in Q2-UR)
High ROS
54.7%
Q3-UR
36.4%
Low ROS
1.2%
Q3-LR
7.6%
FITC-A
PerCP-A
H99 Dodecyl TPP+
Percentage population (%)
Low ROS
High ROS
ROS level

F

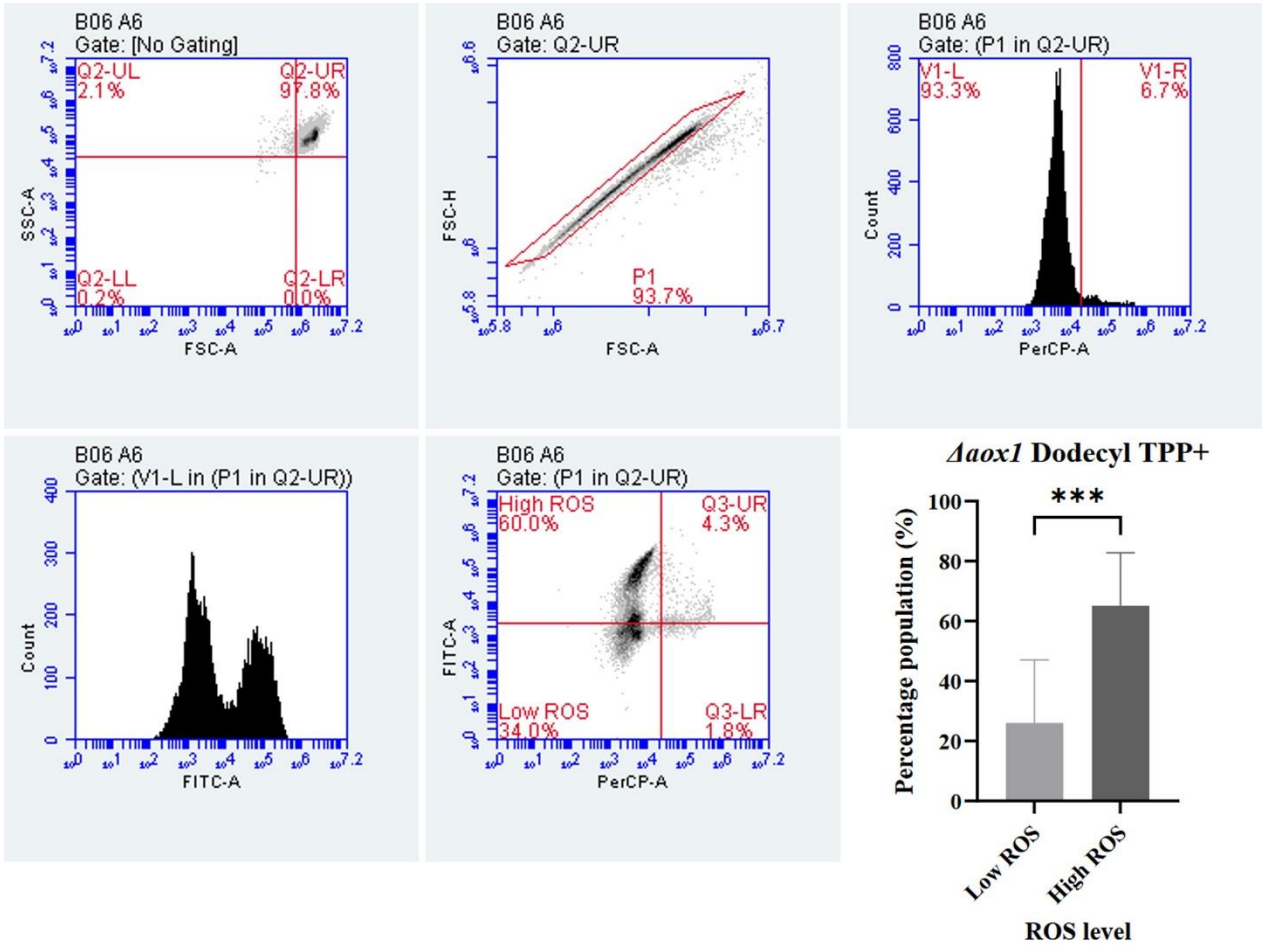
B06 A6
Gate: [No Gating]
Q2-UL
2.1%
Q2-UR
97.8%
Q2-LL
0.2%
Q2-LR
0.0%
SSC-A
FSC-A
B06 A6
Gate: Q2-UR
P1
93.7%
FSC-H
FSC-A
B06 A6
Gate: (P1 in Q2-UR)
V1-L
93.3%
V1-R
6.7%
Count
PerCP-A
B06 A6
Gate: (V1-L in (P1 in Q2-UR))
Count
FITC-A
B06 A6
Gate: (P1 in Q2-UR)
High ROS
60.0%
Q3-UR
4.3%
Low ROS
34.0%
Q3-LR
1.8%
FITC-A
PerCP-A
Δaox1 Dodecyl TPP+
***
Percentage population (%)
Low ROS
High ROS
ROS level

G

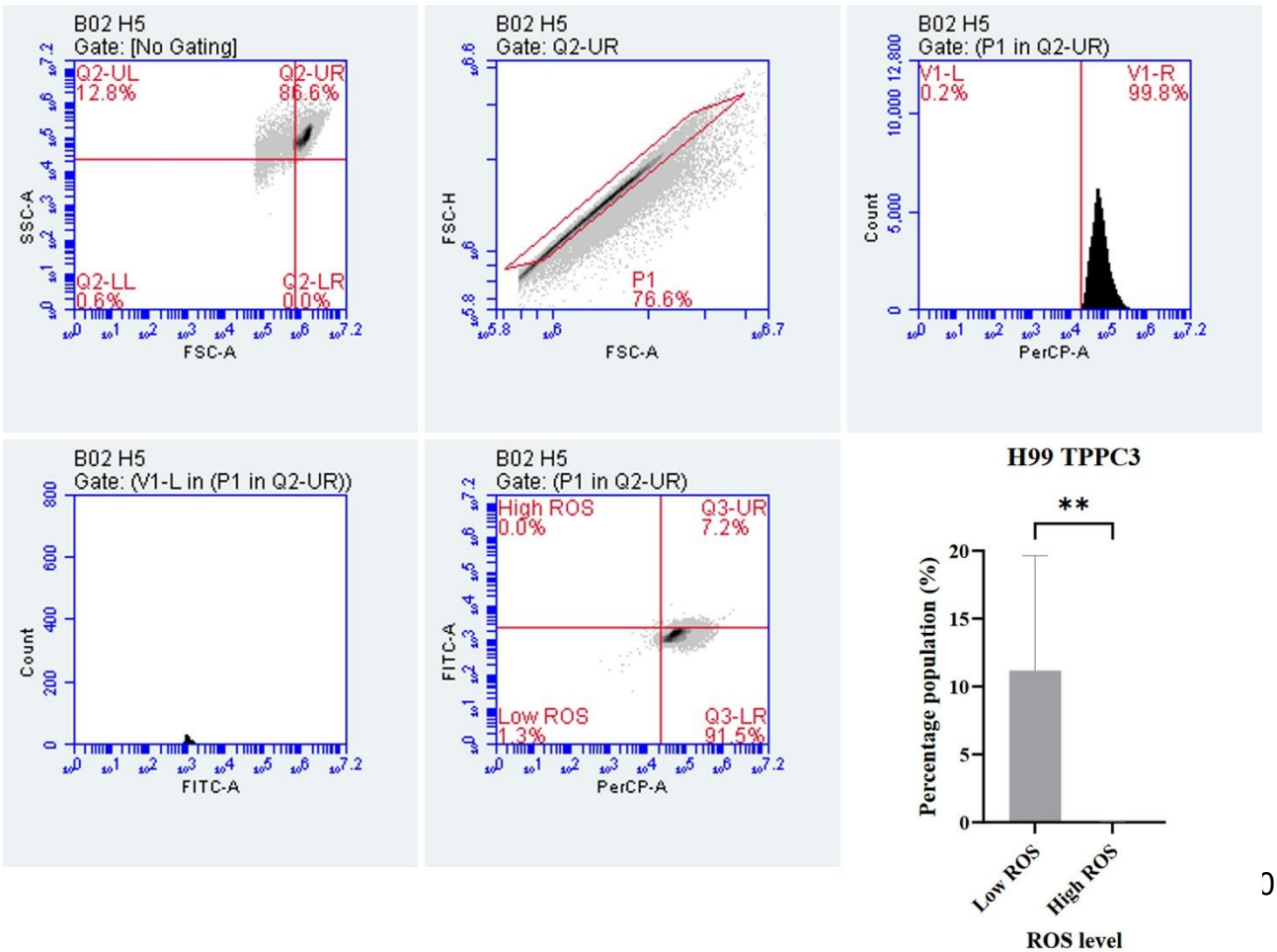
B02 H5
Gate: [No Gating]
Q2-UL
12.8%
Q2-UR
86.6%
Q2-LL
0.6%
Q2-LR
0.0%
SSC-A
FSC-A
B02 H5
Gate: Q2-UR
P1
76.6%
FSC-H
FSC-A
B02 H5
Gate: (P1 in Q2-UR)
V1-L
0.2%
V1-R
99.8%
Count
PerCP-A
B02 H5
Gate: (V1-L in (P1 in Q2-UR))
Count
FITC-A
B02 H5
Gate: (P1 in Q2-UR)
High ROS
0.0%
Q3-UR
7.2%
Low ROS
1.3%
Q3-LR
91.5%
FITC-A
PerCP-A
H99 TPPC3
**
Percentage population (%)
Low ROS
High ROS
ROS level

H

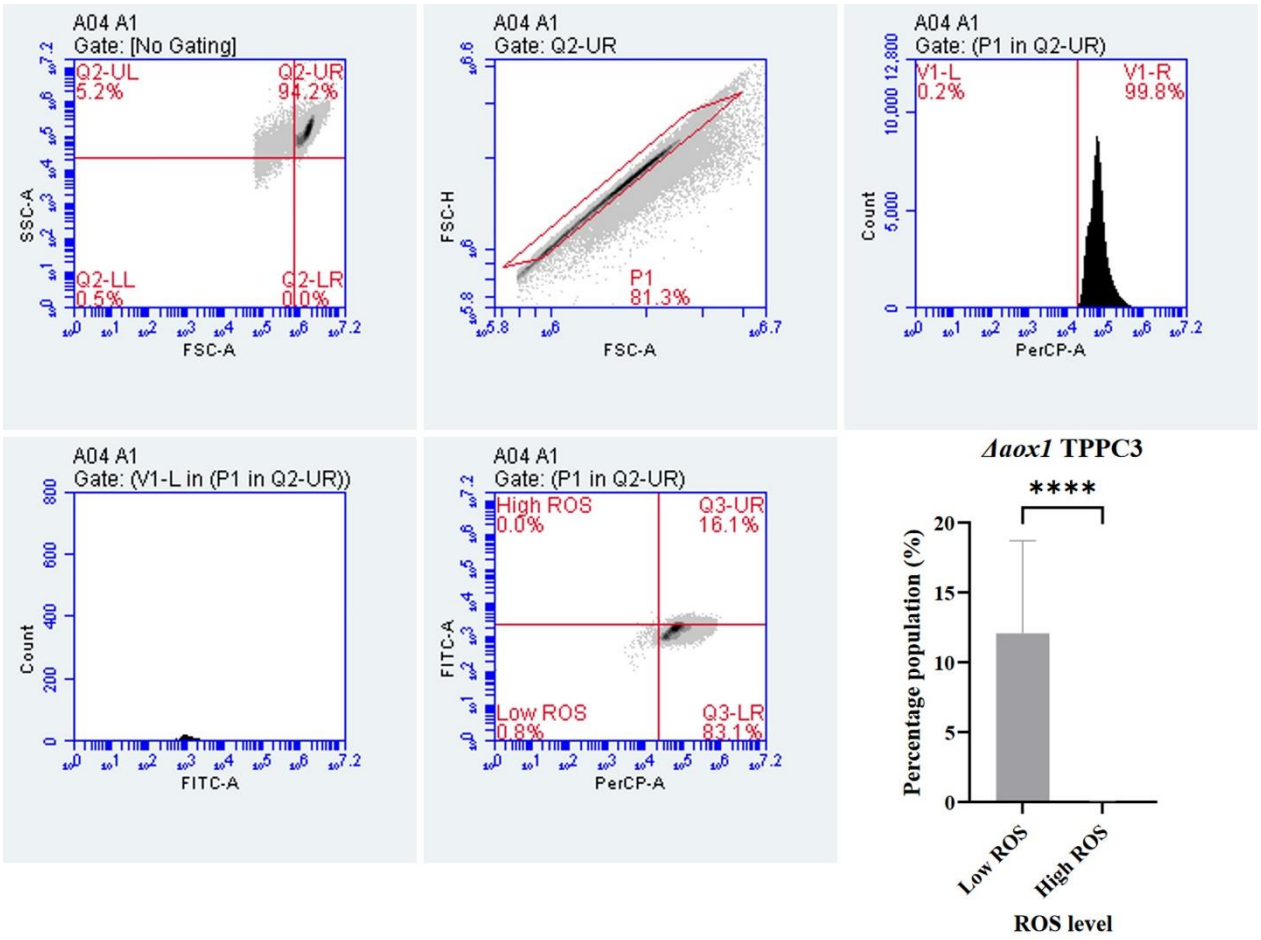
A04 A1
Gate: [No Gating]
Q2-UL
5.2%
Q2-UR
94.2%
Q2-LL
0.5%
C2-LR
0.0%
SSC-A
FSC-A
A04 A1
Gate: Q2-UR
P1
81.3%
FSC-H
FSC-A
A04 A1
Gate: (P1 in Q2-UR)
V1-L
0.2%
V1-R
99.8%
Count
PerCP-A
A04 A1
Gate: (V1-L in (P1 in Q2-UR))
Count
FITC-A
A04 A1
Gate: (P1 in Q2-UR)
High ROS
0.0%
Q3-UR
16.1%
Low ROS
0.8%
Q3-LR
83.1%
FITC-A
PerCP-A
Δaox1 TPPC3
****
Percentage population (%)
Low ROS
High ROS
ROS level

I

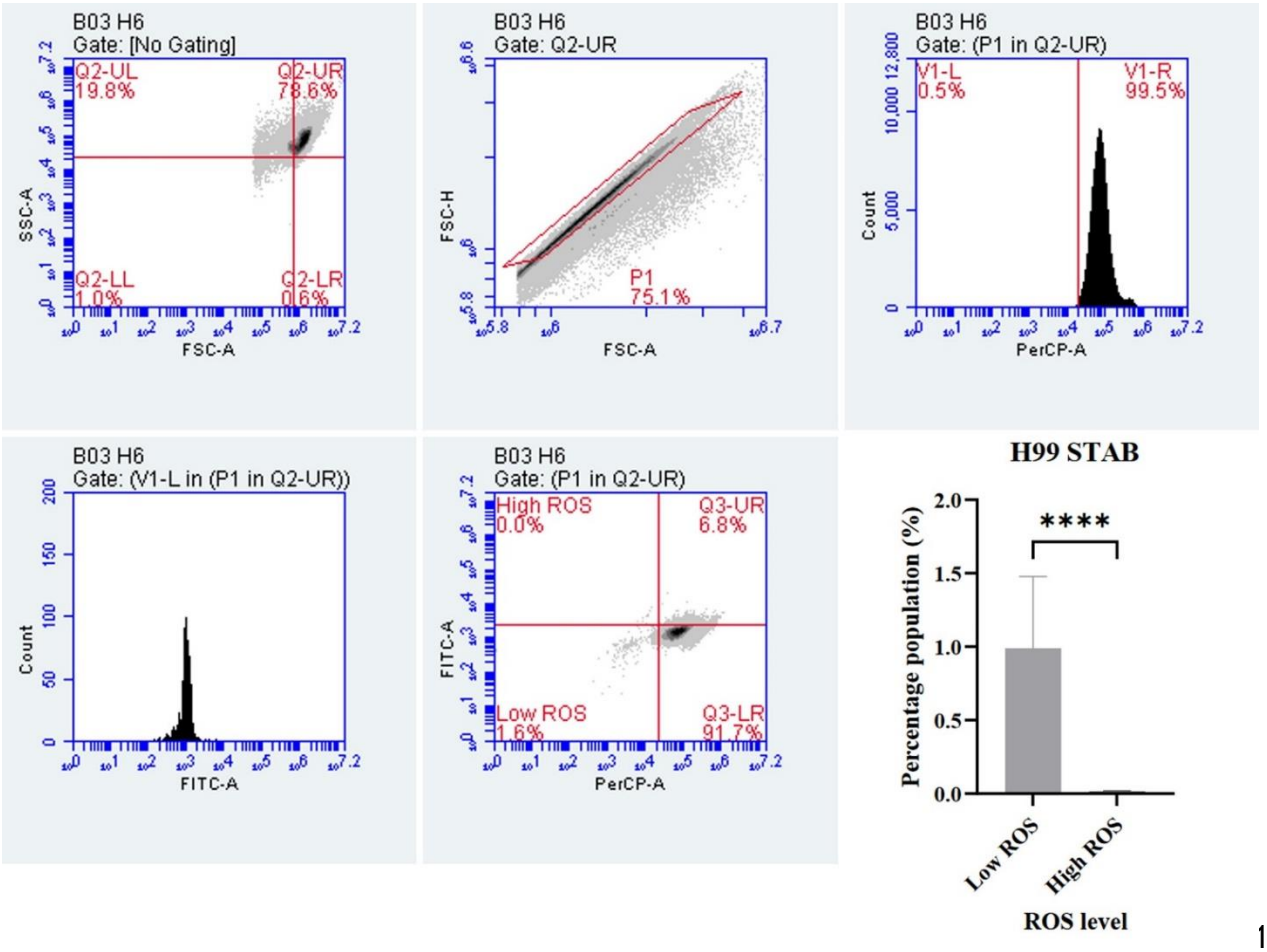
B03 H6
Gate: [No Gating]
Q2-UL
19.8%
Q2-UR
78.6%
Q2-LL
1.0%
C2-LR
0.6%
SSC-A
FSC-A
B03 H6
Gate: Q2-UR
P1
75.1%
FSC-H
FSC-A
B03 H6
Gate: (P1 in Q2-UR)
V1-L
0.5%
V1-R
99.5%
Count
PerCP-A
B03 H6
Gate: (V1-L in (P1 in Q2-UR))
Count
FITC-A
B03 H6
Gate: (P1 in Q2-UR)
High ROS
0.0%
Q3-UR
6.8%
Low ROS
1.6%
Q3-LR
91.7%
FITC-A
PerCP-A
H99 STAB
****
Percentage population (%)
Low ROS
High ROS
ROS level

J

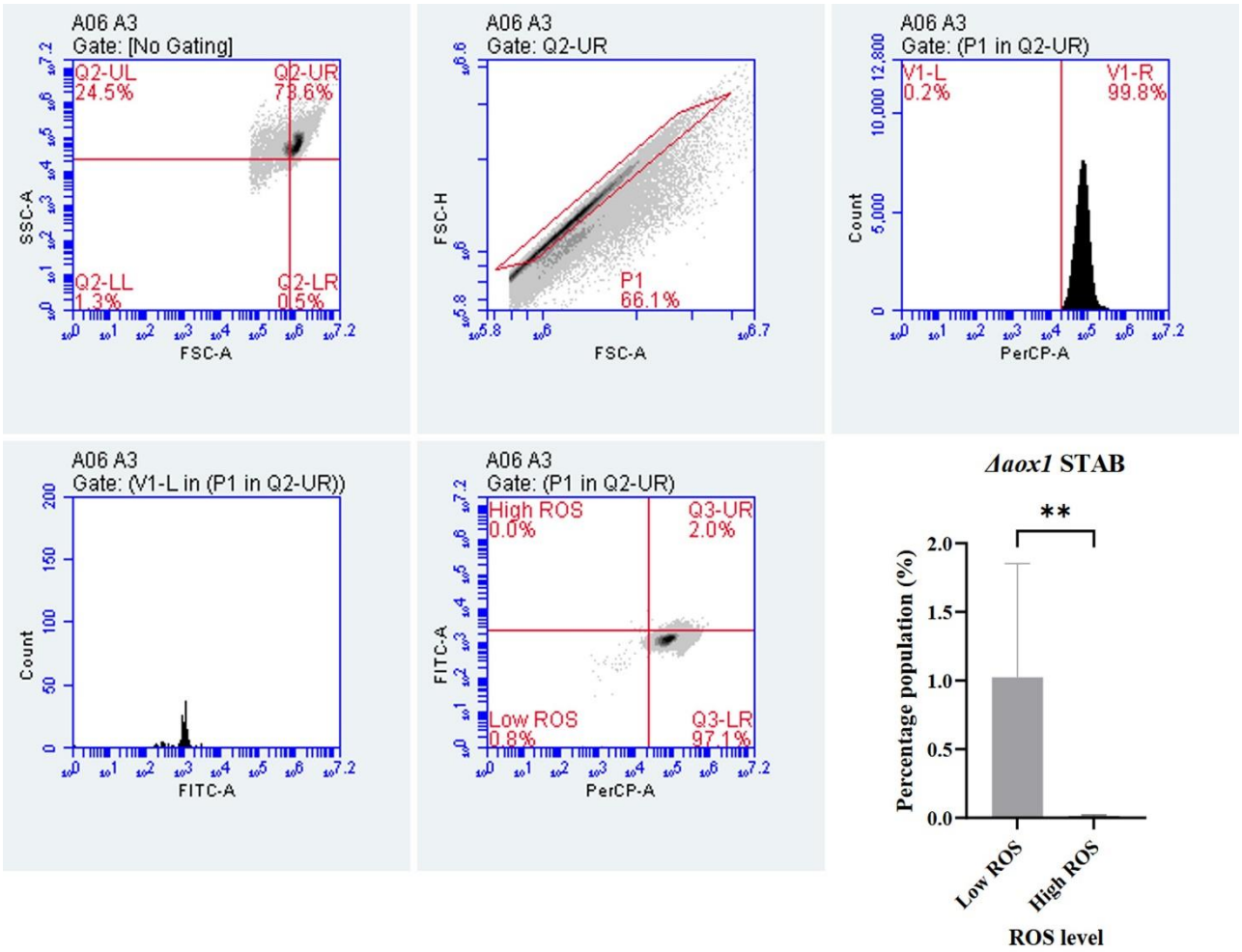

Figure 5.13: Flow cytometry assay of C. neoformans exposed to ALTOX reference drugs. *C. neoformans* strains were stained with H_2DCF-DA and analysed via Flow Cytometry after a 2 h incubation with ALTOX102 at the given MIC90. Percentage necrosis was measured via fluorescence in V1-R. (**A**) Necrosis percentages of H99 treatment, (**B**) Necrosis percentages of *Δaox1* treatment. Percentage population of strains with low ROS and high ROS after ALTOX102 treatment were calculated. Panels: (**C**) H99 + Decyl TPP+, (**D**) *Δaox1* + Decyl TPP+, (**E**) H99 + Dodecyl TPP+, (**F**) *Δaox1* + Dodecyl TPP+, (**G**) H99 TPPC3 (**H**) *Δaox1* + TPPC3, (**I**) H99 + STAB, (**J**) *Δaox1* + STAB. Representative histograms of the population percentage found in V1-L and V1-R after each treatment are included. Significance was calculated using Dunnett's multiple comparisons test following a one-way ANOVA in GraphPad Prism. ** <0.005, *** <0.0005, **** <0.0001, where P = 0.05. Error bars represent ± SD. n = 9

5.2.15 The effects of ALTOX drug components on respiration

To assess whether each drug targets the mitochondria of *C. neoformans*, the respiratory profile of H99 and *Δaox1* was investigated. Respirometer chambers were inoculated with 1 x 10^6 *C. neoformans* cells after 24 h growth and exposed to each listed control compound at the MIC90. Measurements of Maximum and Minimum respiration after exposure to each drug were taken and compared to the routine level of respiration for each strain whereby respiration is regulated according to physiological activity, at intracellular non-saturating ADP levels in routine states of activity. Drug base control compounds (TPP+, ISSF31 and TPPC3) were tested against H99 respiration, with TPP+ (Fig. 5.14a) and ISSF31 (Fig. 5.14b) conferring no significant respiratory losses (Fig. 5.14d) - however, addition of TPPC3 led to a rapid inhibition of respiration (Fig. 5.14c).

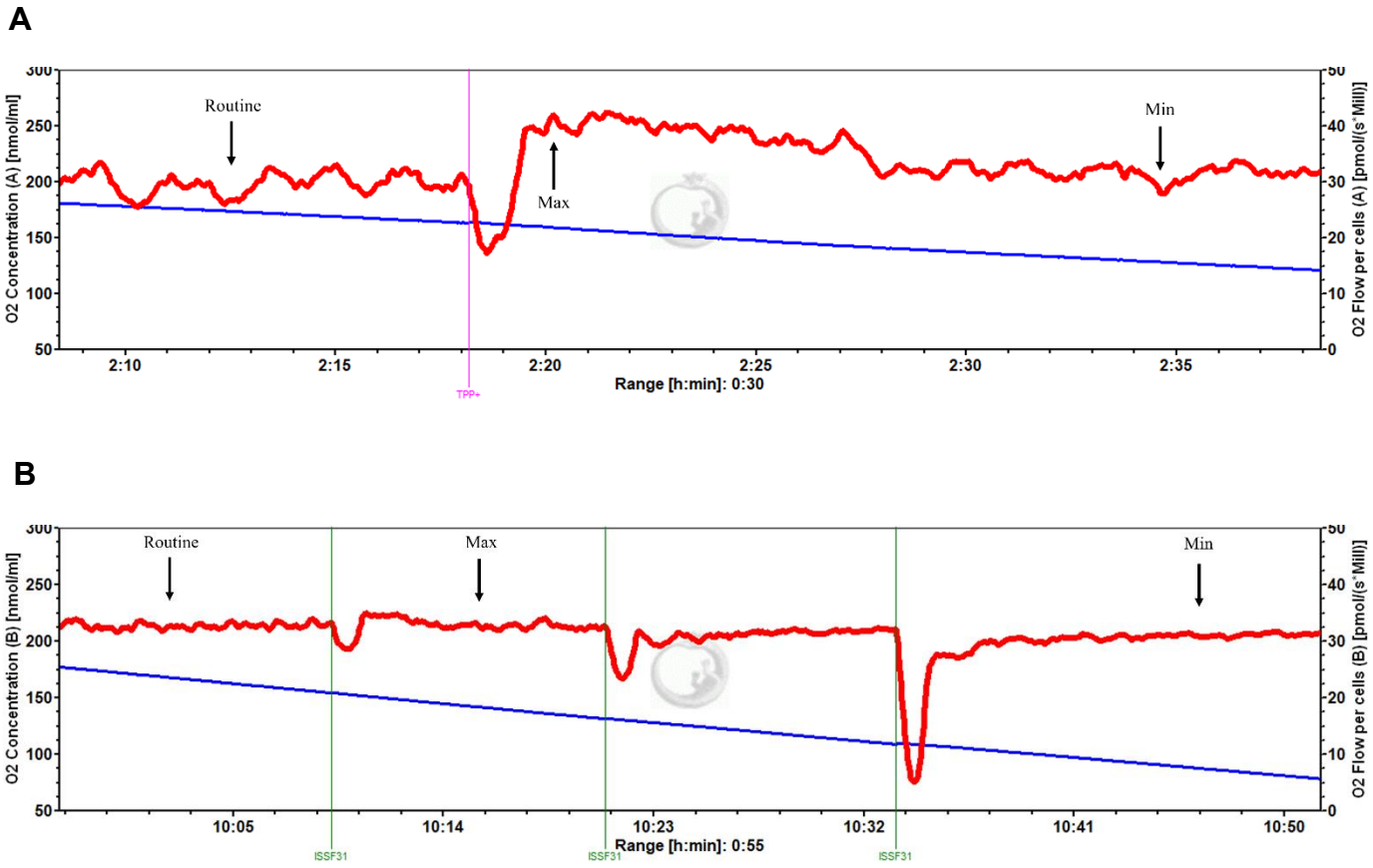

C

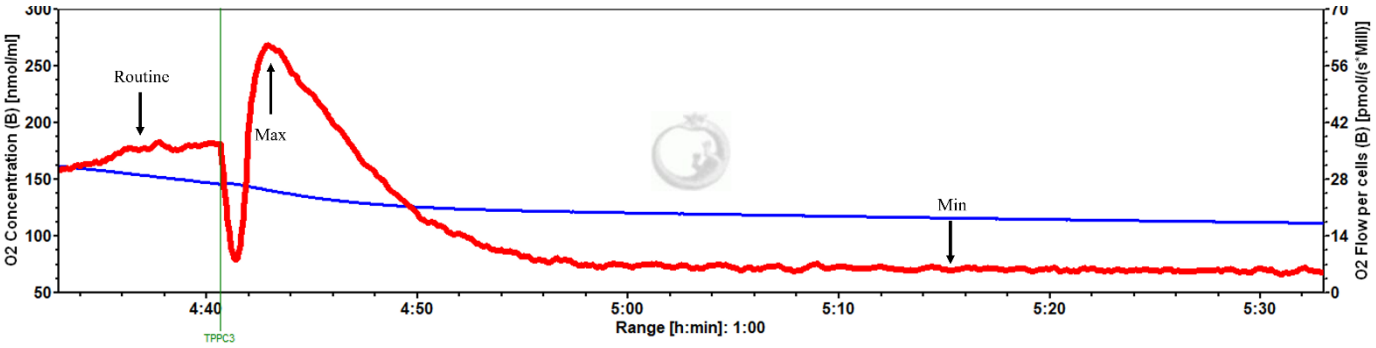

D

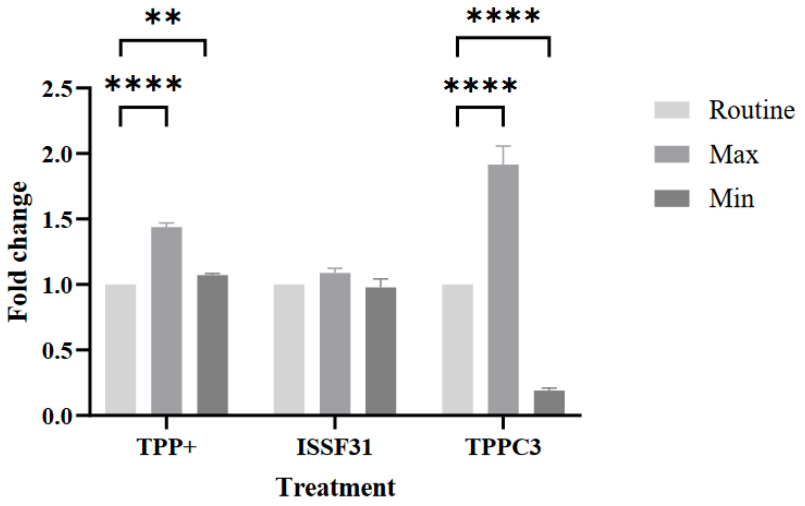

Figure 5.14: Respiratory profiles of C. neoformans exposed to ALTOX094 reference compounds.

Representative example of respiration in H99 determined using HRR. Chambers were inoculated with 1 x 10^6 wildtype cells after 24 h growth and treated with either TPP+ (**A**), ISSF31 (**B**) or TPPC3 (**C**) where indicated to a final concentration of the MIC90 for both drugs. Measurements of Maximum (Max) and Minimum (Min) respiration (O2 flow per cells) after drug exposure were taken and compared to the Routine level of respiration (Routine) for each treatment as indicated. (**D**) Significance was calculated using Dunnett's multiple comparisons test following a one-way ANOVA in GraphPad Prism. ** <0.005, **** <0.0001, where P = 0.05. Error bars represent ± SD. n = 3

5.2.16 Decyl TPP+ inhibits respiration, while Dodecyl TPP+ stimulates respiration

Interestingly, addition of Decyl TPP+ at the MIC90 inhibited respiration in both H99 (Fig. 5.15a) and *Δaox1* (Fig. 5.15b), similar to the action of TPPC3 (Fig. 5.14c). However, Dodecyl TPP+ exhibited a mild stimulation of respiration, in both H99 (Fig. 5.15c, 5.15e) and *Δaox1* (Fig. 5.15d, 5.15f). These

data suggest that inhibition or stimulation of respiration induced by ALTOX drugs were Aox1 independent.

A

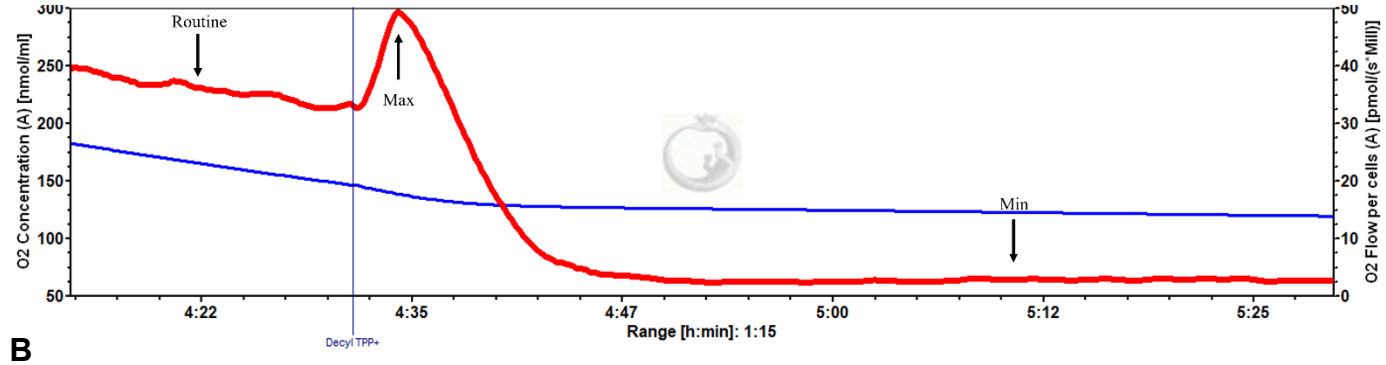

B

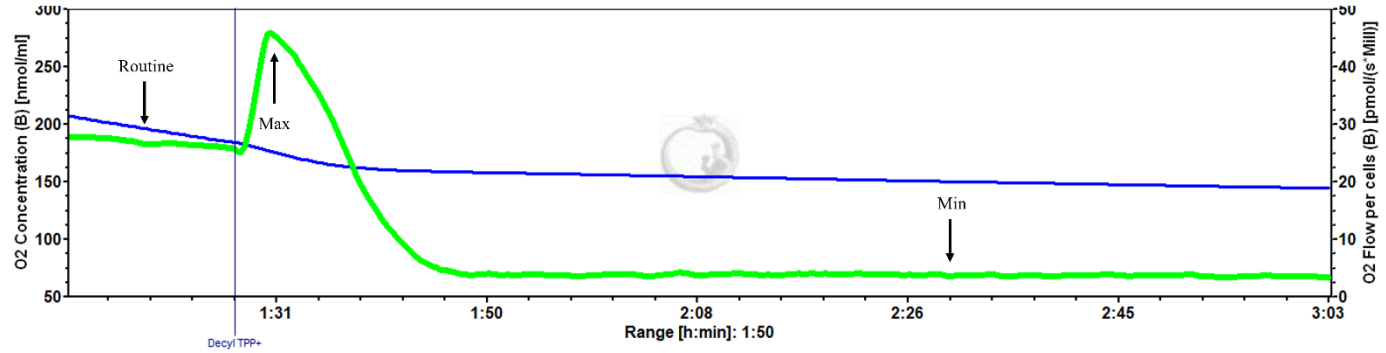

C

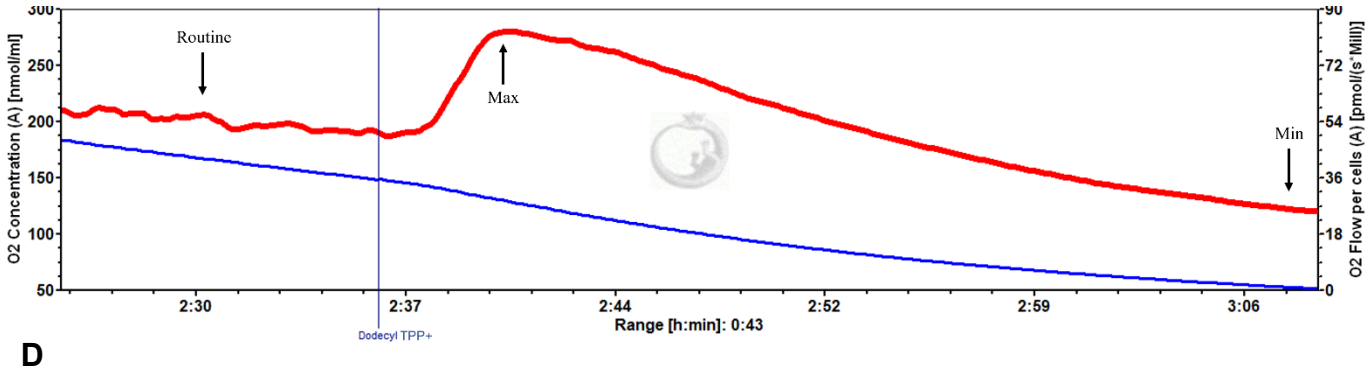

D

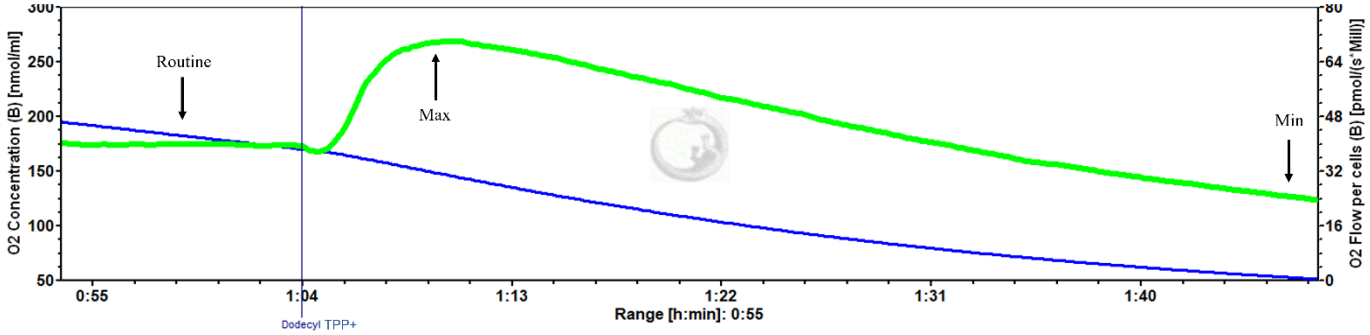

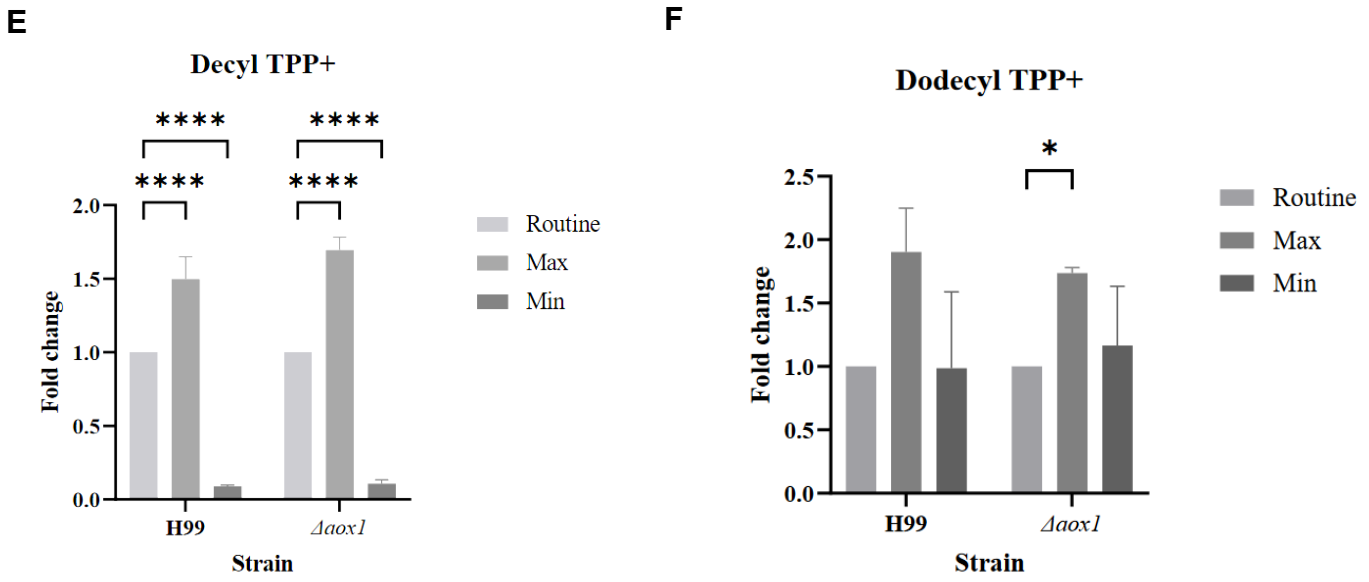

Figure 5.15: Respiratory profiles of C. neoformans exposed to ALTOX094 reference compounds.
Representative example of respiration in H99 and *Δaox1* determined using HRR. Chambers were inoculated with 1 x 10^6 cells after 24 h growth and exposed to either Decyl TPP+ (H99 (**A**), *Δaox1* (**B**)) or Dodecyl TPP+ (H99 (C), *Δaox1* (**D**)) where indicated to a final concentration of the MIC90 for both drugs. Measurements of Maximum (Max) and Minimum (Min) respiration (O2 flow per cells) after drug exposure were taken and compared to the routine level of respiration (Routine) for each strain as indicated. (**E**) Decyl TPP+, (**F**) Dodecyl TPP+. Significance was calculated using Dunnett's multiple comparisons test following a one-way ANOVA in GraphPad Prism. * <0.05, **** <0.0001, where P = 0.05. Error bars represent ± SD. n = 3.

5.2.17 ALTOX102 reference compounds may display a dose-dependent uncoupling activity

Exposure of H99 and *Δaox1* to the ALTOX102 reference compound Octyl TPP+ at the MIC90 of 7μM had no significant effect on respiration in wild type (Fig. 5.16a, 5.16i) or *Δaox1* cells (Fig. 5.16b, 5.16i). While addition of ALTOX203 at 7μM had no effect on *Δaox1* respiration (Fig. 5.16d, 5.16j) it did significantly decrease the minimum respiration value of H99 in comparison to routine respiratory activity (Fig. 5.16c, 5.16j). ALTOX203 did not, however, show a complete inhibition of respiration or increase of the maximum respiratory value (Fig. 5.16c). When both Octyl TPP+ and ALTOX203 were added at the MIC90 of 11μM, there was still no significant effect on *Δaox1* respiration (Fig. 5.16f, 5.16h) but an increase in wildtype respiration was seen for both drugs (Fig. 5.16e, 5.16g) which may indicate an uncoupling activity.

A

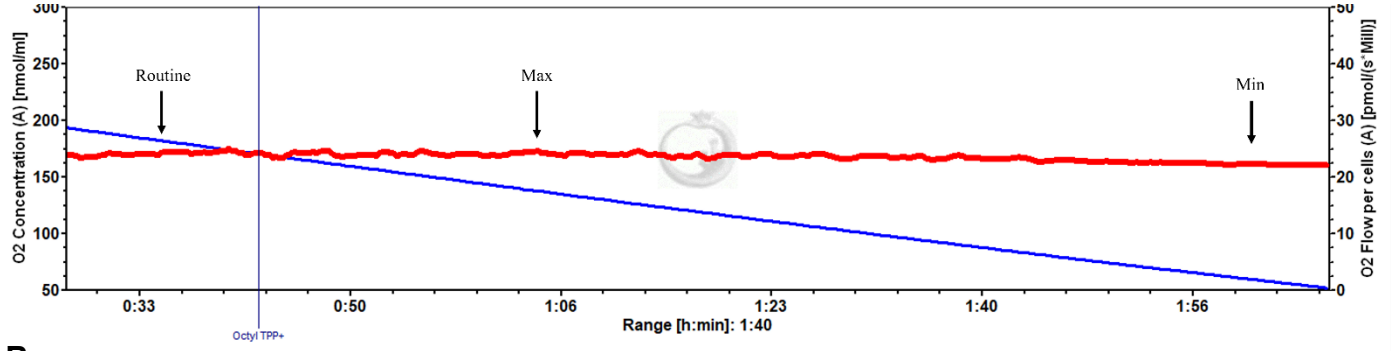
Routine
Max
Min
O2 Concentration (A) [nmol/ml]
O2 Flow per cells (A) [pmol/(s*Mill)]
0:33
0:50
1:06
1:23
1:40
1:56
Range [h:min]: 1:40
Octyl TPP+

B

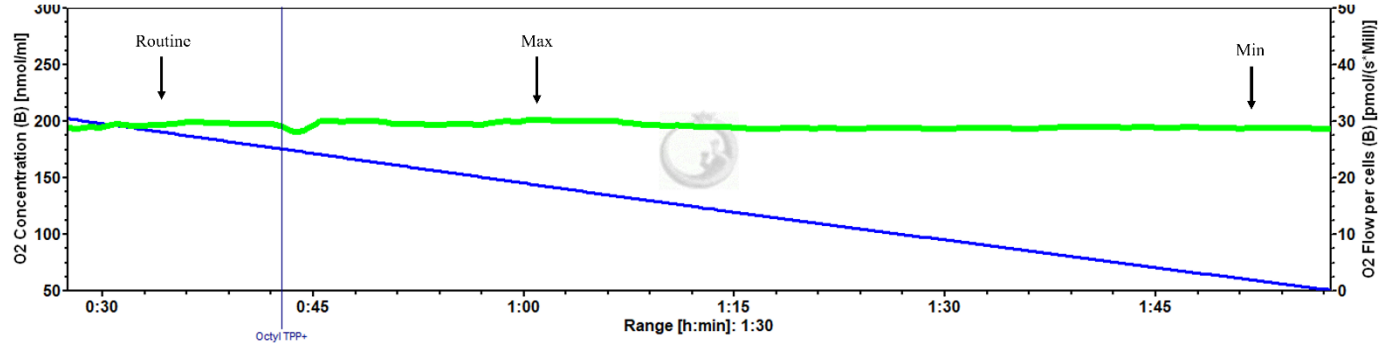
Routine
Max
Min
O2 Concentration (B) [nmol/ml]
O2 Flow per cells (B) [pmol/(s*Mill)]
0:30
0:45
1:00
1:15
1:30
1:45
Range [h:min]: 1:30
Octyl TPP+

C

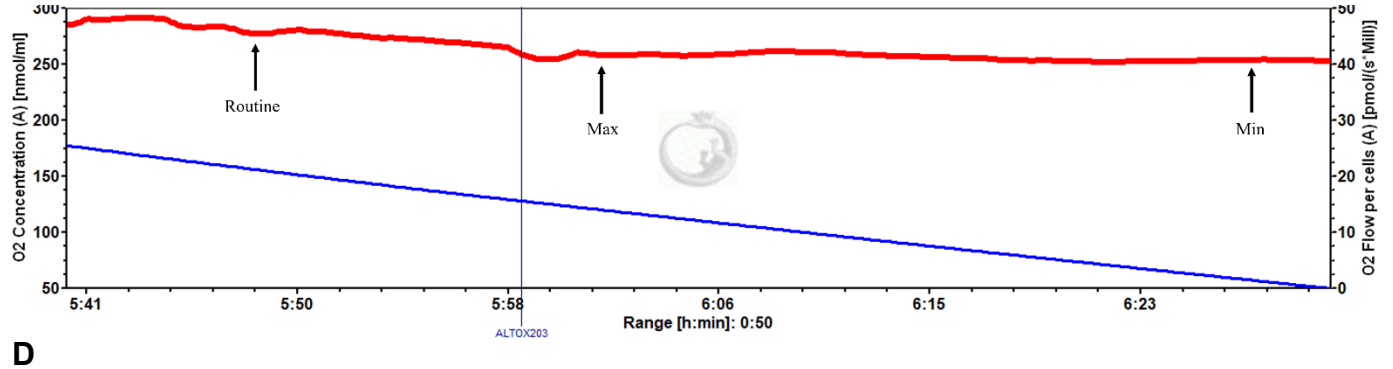
Routine
Max
Min
O2 Concentration (A) [nmol/ml]
O2 Flow per cells (A) [pmol/(s*Mill)]
5:41
5:50
5:58
6:06
6:15
6:23
Range [h:min]: 0:50
ALTOX203

D

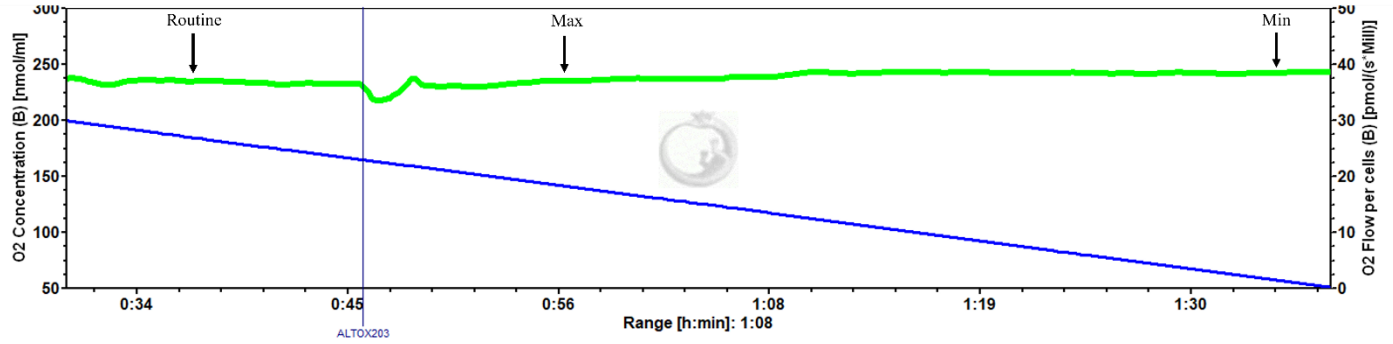
Routine
Max
Min
O2 Concentration (B) [nmol/ml]
O2 Flow per cells (B) [pmol/(s*Mill)]
0:34
0:45
0:56
1:08
1:19
1:30
Range [h:min]: 1:08
ALTOX203

E

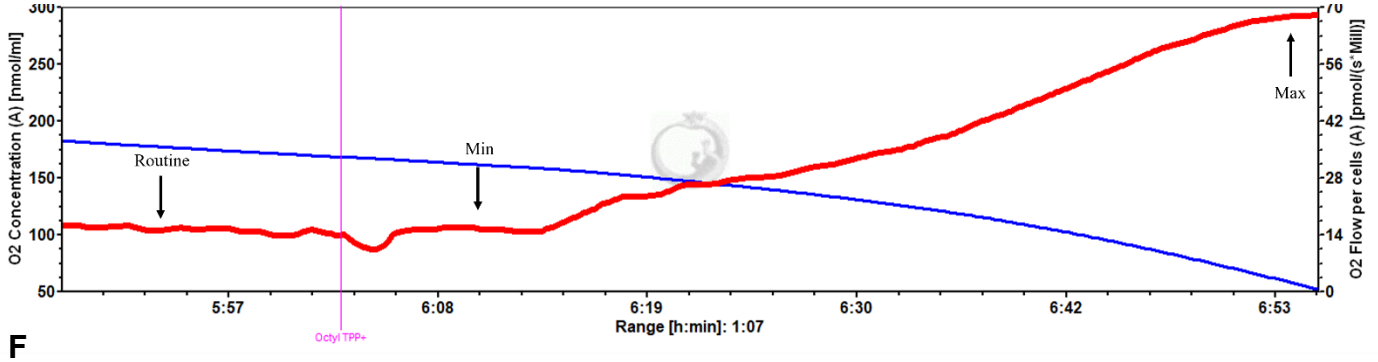
O2 Concentration (A) [nmol/ml]
O2 Flow per cells (A) [pmol/(s*Mill)]
Routine
Min
Max
Octyl TPP+
Range [h:min]: 1:07

F

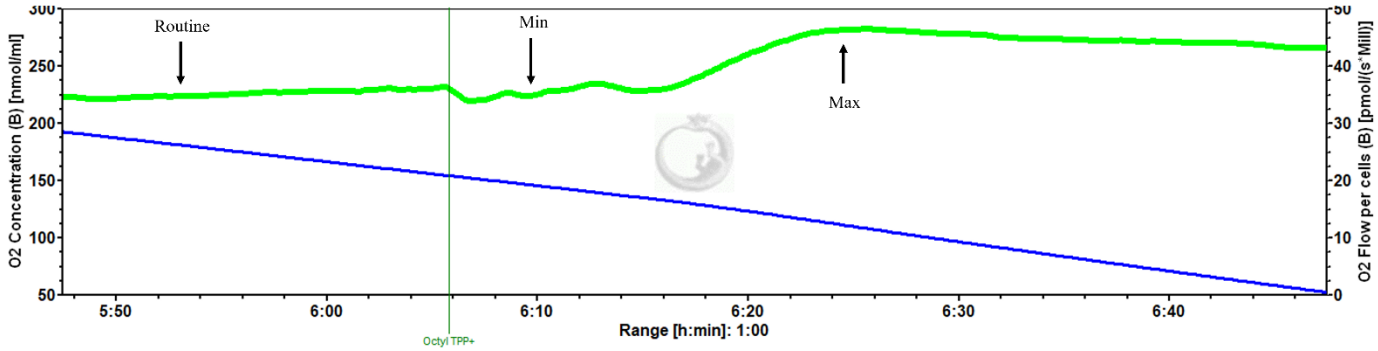
O2 Concentration (B) [nmol/ml]
O2 Flow per cells (B) [pmol/(s*Mill)]
Routine
Min
Max
Octyl TPP+
Range [h:min]: 1:00

G

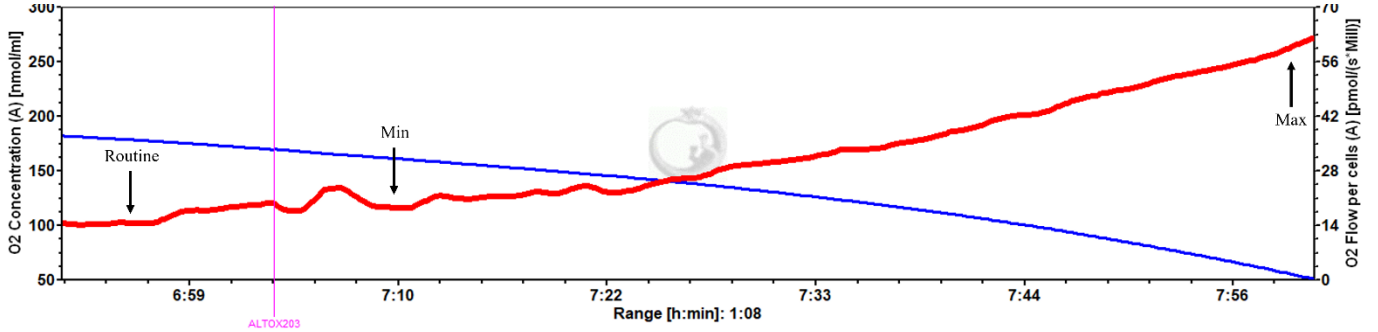
O2 Concentration (A) [nmol/ml]
O2 Flow per cells (A) [pmol/(s*Mill)]
Routine
Min
Max
ALTOX203
Range [h:min]: 1:08

H

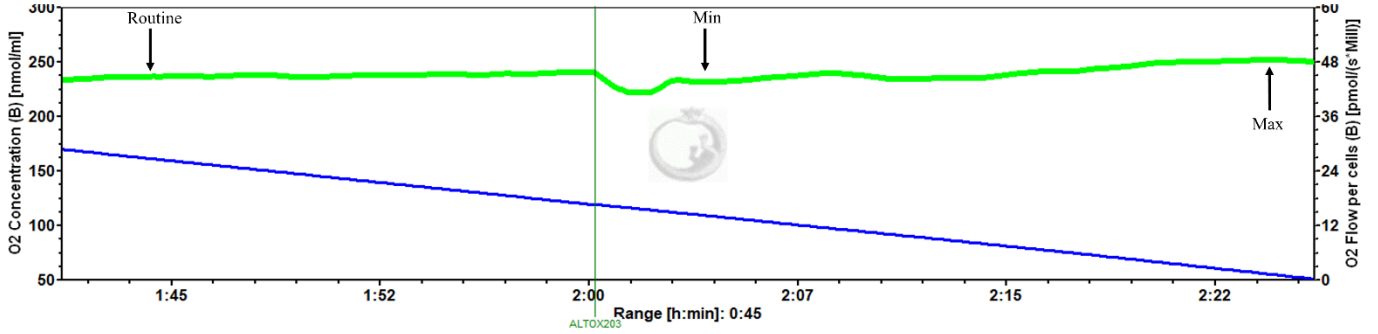
O2 Concentration (B) [nmol/ml]
O2 Flow per cells (B) [pmol/(s*Mill)]
Routine
Min
Max
ALTOX203
Range [h:min]: 0:45

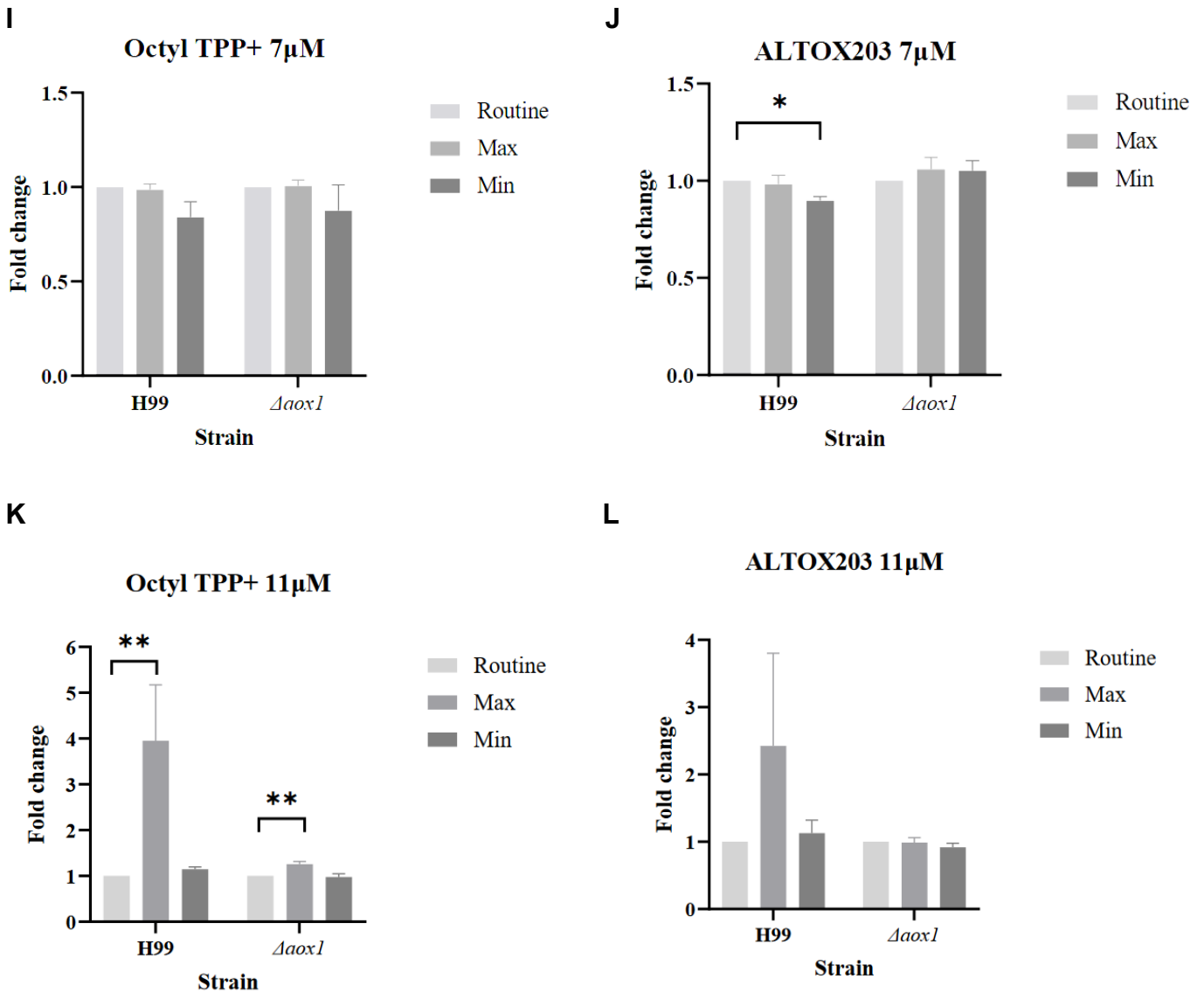

Figure 5.16: Respiratory profiles of C. neoformans exposed to ALTOX102 reference compounds.

Representative example of respiration in H99 and *Δaox1* determined using HRR. Chambers were inoculated with 1 x 10^6 cells after 24 h growth and treated with either Octyl TPP+ or ALTOX203 where indicated to a final concentration of the MIC90 for both drugs. (**A**) H99 + 7µM Octyl TPP+, (**B**) *Δaox1* + 7µM Octyl TPP+, (**C**) H99 + 7µM ALTOX203, (**D**) *Δaox1* + 7µM ALTOX203. (**E**) H99 + 11µM Octyl TPP+, (**F**) *Δaox1* + 11µM Octyl TPP+, (**G**) H99 + 11µM ALTOX203, (**H**) *Δaox1* + 11µM ALTOX203. Measurements of Maximum (Max) and Minimum (Min) respiration (O2 flow per cells) after drug exposure were taken and compared to the routine level of respiration (Routine) for each strain as indicated. (**I**) Octyl TPP+ (7µM), (**J**) ALTOX203 (7µM), (**K**) Octyl TPP+ (11µM), (**L**) ALTOX203 (11µM). Significance was calculated using Dunnett's multiple comparisons test following a one-way ANOVA in GraphPad Prism. * <0.05, ** <0.005, where P = 0.05. Error bars represent ± SD. n = 3

5.2.18 MALC compound respiration stimulation is dependent on carbon chain length

To provide a comparative control, HRR was also carried out on *C. neoformans* exposed to the MALC compound STAB at two separate chain lengths (10C STAB, STAB) at the MIC90 of 15μM. STAB had no significant effect on either wildtype (Fig. 5.17a) or *Δaox1* mutant respiration (Fig. 5.17b) as seen in (Fig. 5.17e). Addition of STAB, however, led to a rapid increase in respiration in both H99 (Fig. 5.17c) and *Δaox1* (Fig. 5.17d) but did not decrease the minimum respiration value for either strain (Fig. 5.17e), which may indicate a strong uncoupling effect.

A

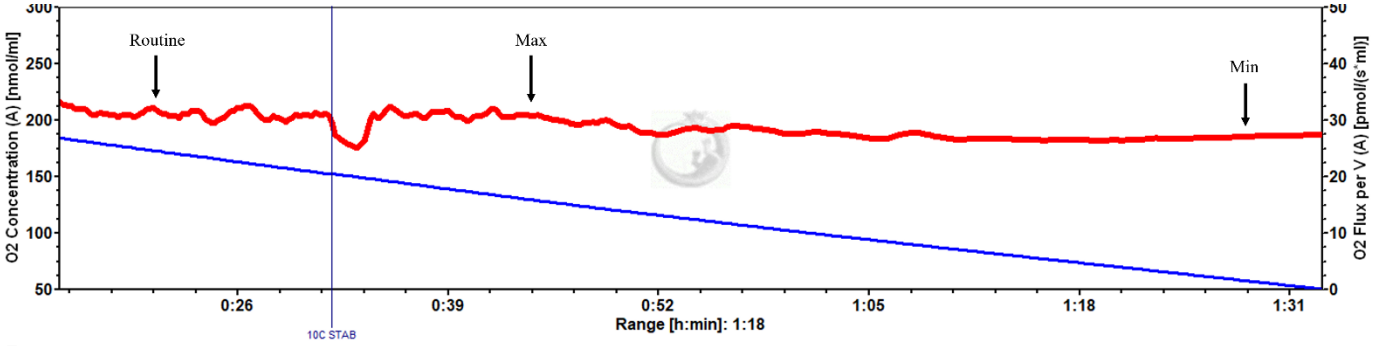
Routine
Max
Min
O2 Concentration (A) [nmol/ml]
O2 Flux per V (A) [pmol/(s*ml)]
0:26
0:39
0:52
1:05
1:18
1:31
10C STAB
Range [h:min]: 1:18

B

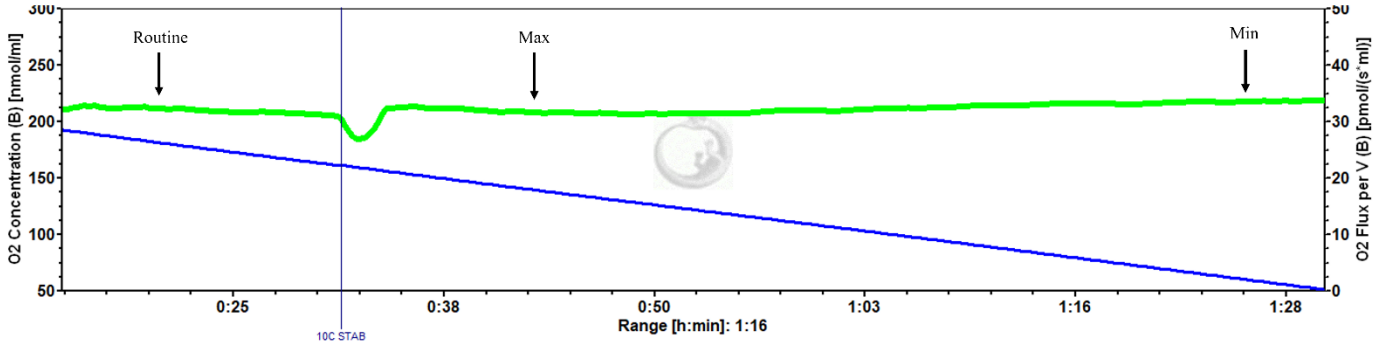
Routine
Max
Min
O2 Concentration (B) [nmol/ml]
O2 Flux per V (B) [pmol/(s*ml)]
0:25
0:38
0:50
1:03
1:16
1:28
10C STAB
Range [h:min]: 1:16

C

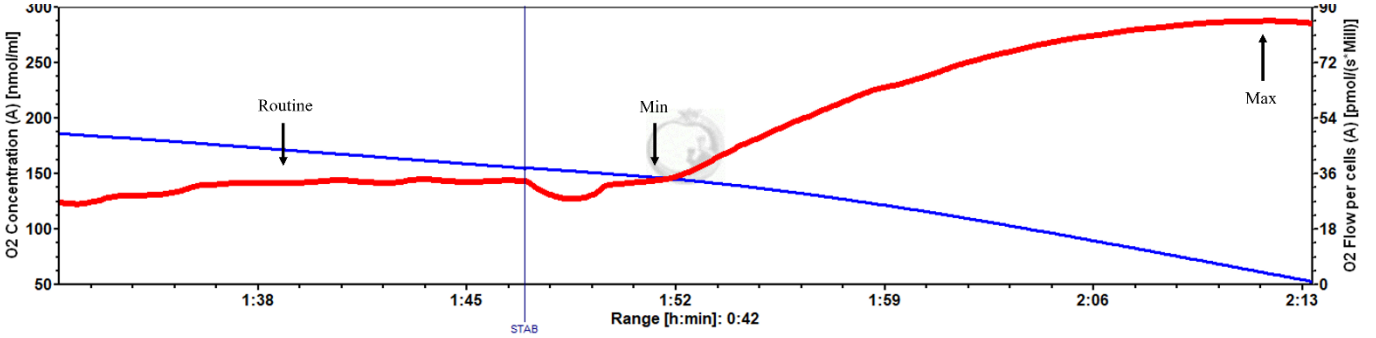
Routine
Min
Max
O2 Concentration (A) [nmol/ml]
O2 Flow per cells (A) [pmol/(s*Mill)]
1:38
1:45
1:52
1:59
2:06
2:13
STAB
Range [h:min]: 0:42

D

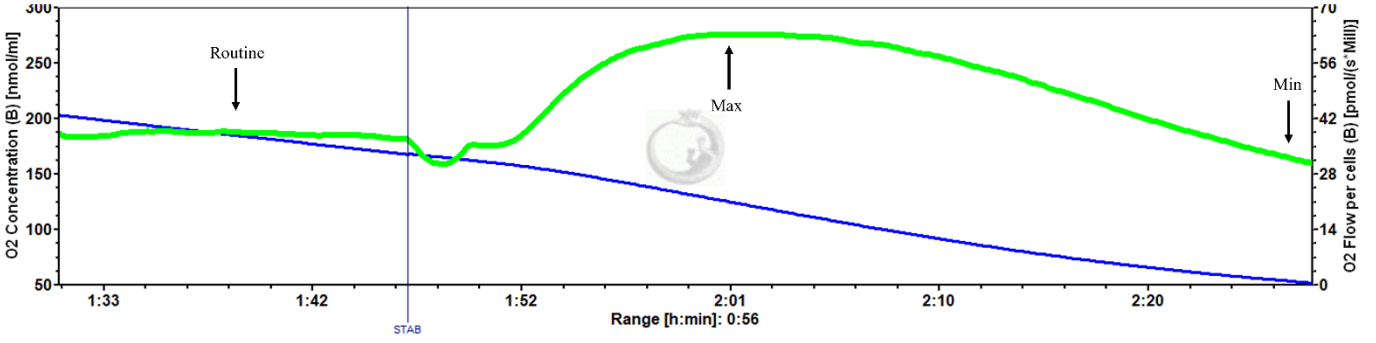
Routine
Max
Min
O2 Concentration (B) [nmol/ml]
O2 Flow per cells (B) [pmol/(s*Mill)]
1:33
1:42
1:52
2:01
2:10
2:20
STAB
Range [h:min]: 0:56

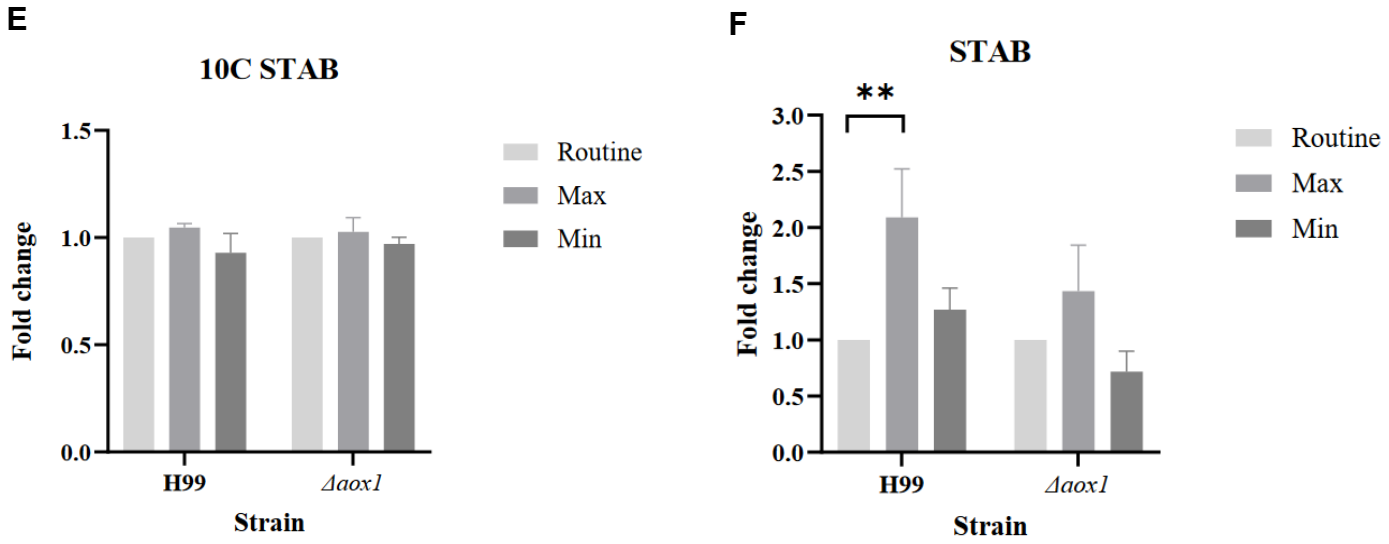

Figure 5.17: Respiratory profiles of C. neoformans exposed to MALC compounds. Representative example of respiration in H99 and *Δaox1* determined using HRR. Chambers were inoculated with 1 x 10^6 cells after 24 h growth and treated with either 10C STAB or STAB where indicated to a final concentration of the MIC90 for both drugs. (**A**) H99 + 10C STAB, (**B**) *Δaox1* + 10C STAB, (**C**) H99 + STAB, (**D**) *Δaox1* + STAB. Measurements of Maximum (Max) and Minimum (Min) respiration (O2 flow per cells) after drug exposure were taken and compared to the routine level of respiration (Routine) for each strain as indicated. (**E**) 10C STAB, (**F**) STAB. Significance was calculated using Dunnett's multiple comparisons test following a one-way ANOVA in GraphPad Prism. *** = 0.0006, where P = 0.05. Error bars represent ± SD. n = 3

5.2.19 ALTOX reference compounds are not haemolytic

To assess whether the effects on mitochondrial membranes exhibited by the ALTOX reference compounds were fungal specific, a haemolysis assay was carried out whereby ALTOX reference compounds at the given MIC90 were spotted onto agar plates containing 5% sheep blood. Plates were incubated at 37°C and a zone of haemolysis (ZOH) was measured at 2 h and 24 h, whereby alpha-haemolysis (red blood cell damage) was signified by a green-tinge and beta-haemolysis (complete lysis) was signified by a clear area. Interestingly, none of the ALTOX094 reference compounds (Fig. 5.18a) or the ALTOX102 reference compounds (Fig. 5.18b) tested showed haemolytic activity. No significant ZOH was determined for either ALTOX094 reference compounds or ALTOX102 reference compounds.

A

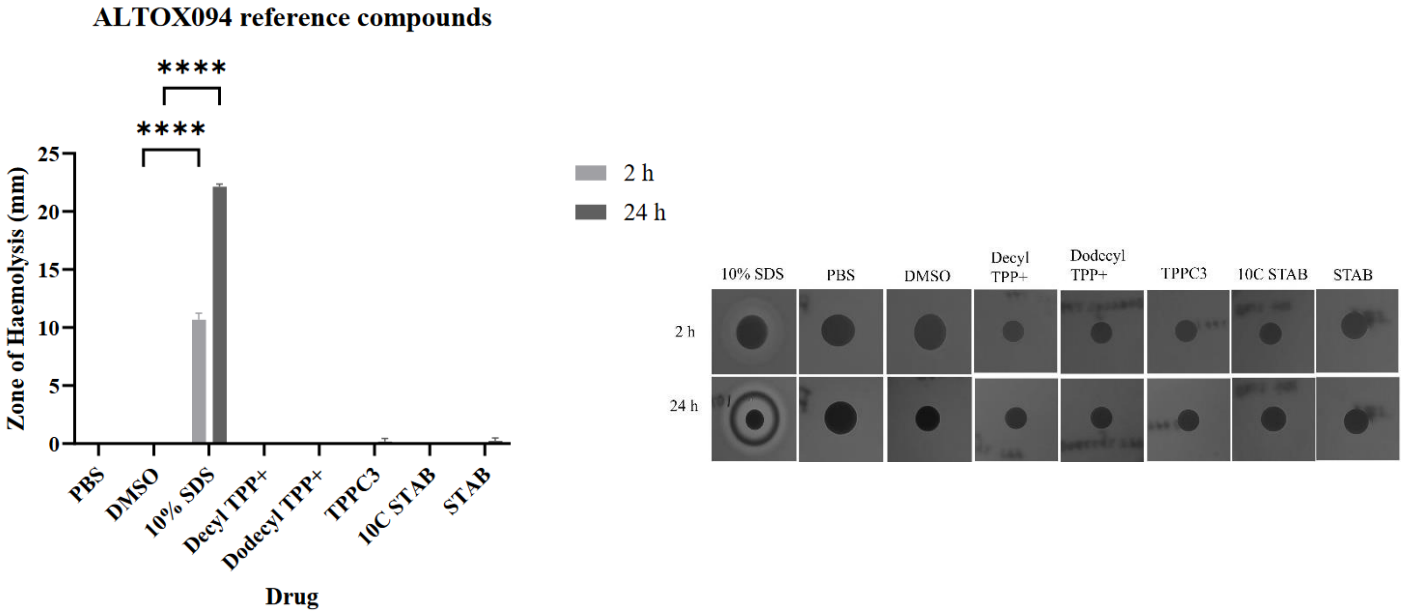

B

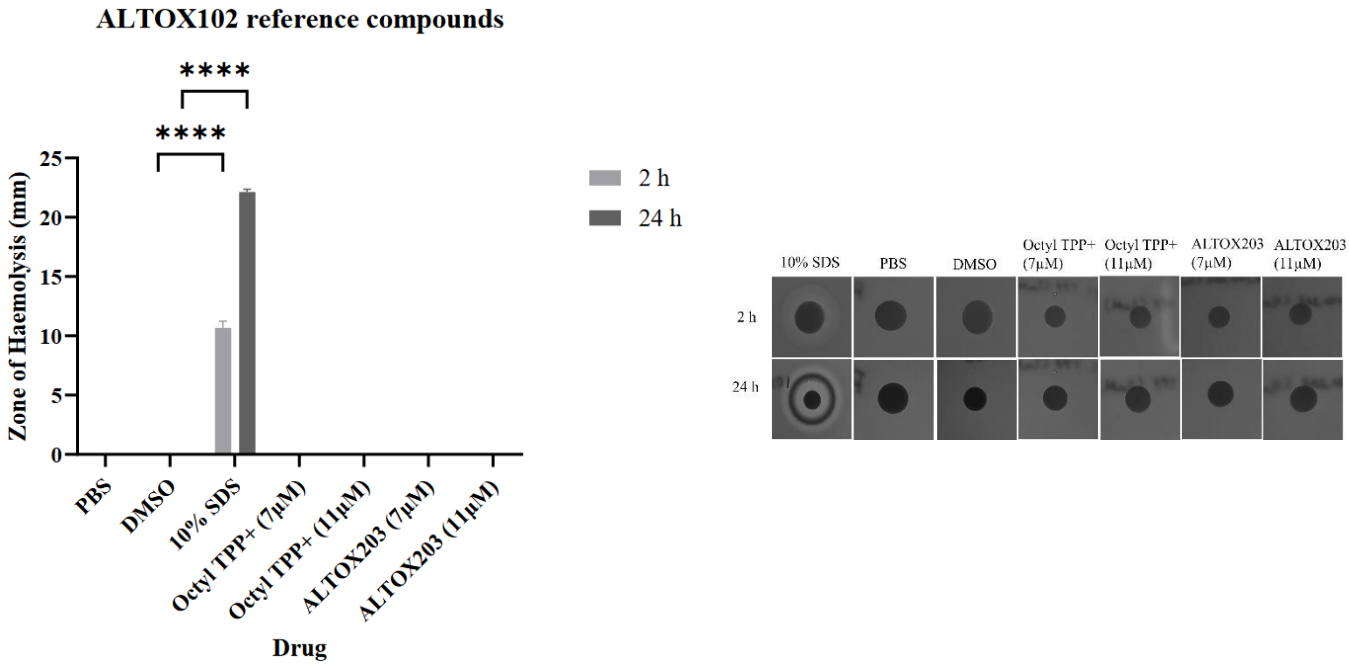

Figure 5.18: Haemolytic effect of ALTOX reference drugs.
(**A**) ALTOX094 reference drugs and (**B**) ALTOX102 reference drugs were administered to filter paper disks on agar plates containing 5% sheep blood at the MIC90 and incubated at 37°C. The zone of haemolysis (ZOH) was measured for ALTOX094 and ALTOX102 after 2 h exposure and 24 h exposure. Significance was calculated using Dunnett's multiple comparisons test following a one-way ANOVA in GraphPad Prism. **** < 0.0001 where P = 0.05. Error bars represent ± SD. n = 3

5.3 Discussion

5.3.1 ALTOX094 and ALTOX102 reduce *C. neoformans* growth and viability

This study aimed to develop compounds capable of the dual inhibition of fungal cytochrome *bc₁* and Aox as a novel approach to antifungal development. Substitution of the chlorine for bromine (**Colletochlorin B** to **ISSF31**) did not lead to a significant reduction in potency (Fig. 5.1), reducing the pIC_{50} from 8.2 ± 0.1 to 7.7 ± 0.2. Addition of the alkyl TPP^+, however, did lead to a significant reduction in inhibition, with both **ALTOX094** and **ALTOX102** being reduced to 4.8 ± 0.1 and 4.9 ± 0.1, respectively. While disappointing, this was not an unexpected result, given that the increased size of the compound is likely to decrease mobility, and the lack of membrane potential in our test system means there is no driving force for accumulation of compound at the target location. However, *in vitro* evidence suggested that both ALTOX094 and ALTOX102 may act as dual inhibitors of *bc₁* complex and Aox activity.

Promisingly, both ALTOX compounds also showed strong effects on *C. neoformans* growth and viability and were selected for further study.

While both ALTOX094 and ALTOX102 led to a loss of viability, ALTOX094 induced high levels of necrosis while ALTOX102 did not, although this necrotic activity was Aox independent. This, in conjunction with evidence that low levels of ROS were seen in ALTOX102 treated strains indicates that both ALTOX094 and ALTOX102 affected *C. neoformans* viability via seemingly separate mechanisms and that in both cases the mode of action was largely separable from Aox function. This may in part be due to variations in the IC50 values observed in Fig. 5.1 whereby ALTOX102 seemed to have a higher potency against cytochrome *bc₁* over Aox2, which suggests that there may be preferential targeting of cytochrome *bc₁*.

5.3.2 ALTOX drugs exhibit fungal specificity

To assess whether the ALTOX drugs could reduce the virulence of *C. neoformans* cells and exhibit fungal specificity at the pre-determined MIC90 concentration, the *Galleria mellonella* infection model

was used for both survival screening and melanisation (immune response). Interestingly, while ALTOX094 did not confer toxicity in *G. mellonella* larvae, addition of ALTOX102 alone showed an increased mortality rate by day 5 and an increase in toxicity was also seen after infection with the *Δaox1* mutant. These findings suggest that pre-treatment of both H99 and *Δaox1* with ALTOX094 exhibited decreased virulence, presenting as a reduction in mortality for larvae by day 5, however this reduction in mortality was not seen for cells pre-treated with ALTOX102. These data indicate that while ALTOX094 treatment of *C. neoformans* showed high necrosis, this is fungal-specific and so did not affect *G. mellonella* larvae. In fact, ALTOX094 addition alone did not induce an increased immune response from *G. mellonella* larvae, although on day 5 larvae infected with the *Δaox1* strain exhibited significant melanisation which was not rescued by ALTOX094 addition. H99-infected larvae inoculated with ALTOX102, however, showed an increased immune response across all conditions on day 5, and larvae infected with *Δaox1* exhibited significant melanisation after just one day and by day 5 significant melanisation was seen across all conditions for *Δaox1* infected larvae inoculated with ALTOX02. While no significant difference in virulence was seen between H99 and *Δaox1* strains for this infection model (Appendix 7.3) differences arising in *G. mellonella* immune response could indicate that a loss of Aox may lead to increased recognition of *C. neoformans* via changes in cryptococcal capsule or cell wall components, leading to PPO activation and melanin production. The increase in larval mortality and melanisation seen upon ALTOX102 addition indicates that the mechanism of action of ALTOX102 may differ to ALTOX094, resulting in an increased host-response to the presence of ALTOX102.

To check whether disparities seen between ALTOX094 and ALTOX102 in the *G. mellonella* infection model were based on fungal specificity, an early-stage cytotoxicity assessment was carried out. Interestingly, neither ALTOX094, ALTOX102, or any of the reference compounds for these drugs showed any haemolytic activity, even up to 10x the MIC90 concentration for each drug. This indicates that while ALTOX094 and ALTOX102 may have shown different effects in the *G. mellonella* infection model, this is unlikely to be based on host cell targeting and provides a large therapeutic window for viable treatment.

5.3.3 ALTOX drugs affect mitochondrial membranes

After establishing the reduction in viability seen after ALTOX094 and ALTOX102 treatment, we wanted to assess whether ALTOX drugs were being targeted to the mitochondrial membrane, by observing the respiratory profiles of *C. neoformans* after drug treatment. Interestingly, while ALTOX094 clearly inhibited respiration in the biphasic effect seen in Fig. 5.7, ALTOX102 did not inhibit respiration, but instead a dose-dependent increase in respiratory activity was seen. While an increase in respiratory activity could be seen for ALTOX102, Dodecyl TPP+, Octyl TPP+ and ALTOX203, we cannot officially define this observed respiratory flux as non-coupled respiration. This definition requires the use of an established uncoupler, such as protonophores like FCCP. As we cannot conclusively establish either ALTOX094, ALTOX102 or any of the reference compounds as protonophores, this increase could only be defined as partial uncoupling, or non-phosphorylating respiration, whereby intrinsic uncoupling occurs via leak of protons across the mitochondrial membrane independently of ADP phosphorylation, dissipating the PMF. The degree of uncoupling for ALTOX102, Octyl TPP+ and ALTOX203 appeared dose-dependent, whereby an increase in respiration for ALTOX102 reference compounds Octyl TPP+ and ALTOX203 was seen only at the MIC90 of 11μM for wildtype *C. neoformans.* However, in conjunction with the viability data seen in Fig. 5.12, this disparity in respiratory traces between strains does not confer a depletion in cell viability. This indicates that addition of ALTOX102 reference compounds at 11μM may induce reversible proton uncoupling which is independent of Aox.

Respiratory activity seen after addition of ALTOX094, Decyl TPP+, and TPPC3 indicated that carbon chain length affected both the degree and permanency of uncoupling and perhaps a bi-phasic shift from proton leak to respiratory inhibition. This is supported by the STAB reference traces, in which a long chain molecule showed strong respiratory stimulation indicative of uncoupling. These data, in combination with the viability data in Fig. 5.12, showed that longer chain length compounds have an increased ability to inhibit respiration, perhaps through irreversible uncoupling and increased membrane porosity, which in turn affects viability. Interestingly, ALTOX drug effect on respiratory activity of *C. neoformans* appeared Aox independent through a lack of disparity between respiratory

traces after ALTOX094 or ALTOX102 addition, which was also seen after addition of Decyl TPP+ and Dodecyl TPP+. Interestingly, Dodecyl TPP+ did not confer the same MOA of fungicidal activity seen by the other reference compounds for ALTOX094. The respiratory profile of Dodecyl TPP+ matched that of Octyl TPP+ and ALTOX203, whereby an increase in maximum respiration was seen, but no inhibition of respiration, like that of ALTOX094, TPPC3 or Decyl TPP+. This may be in part to either a more reversible uncoupling effect, or a lipophilic nature of the drug, whereby the high LogP value seen for Dodecyl TPP+ (Appendix Table 7.3) may lend to low bioavailability of Dodecyl TPP+, loss of targeting and an accumulation within the cell or inability to penetrate the target area itself. This would match the flow cytometry data (Fig. 5.13), where a mixed population of ROS levels was seen after Dodecyl TPP+ treatment for both H99 and *Δaox1* and is perhaps indicative of mixed solubility and targeting ability within cells.

To conclude, our data suggests that ALTOX compound ALTOX094 was a strong fungicidal agent, which inhibited the respiration of *C. neoformans* but did not negatively impact the *G. mellonella* infection model. However, as most of the data was similar for both wildtype H99 and *Δaox1* strains, the mechanism of fungal inhibition appears Aox independent, regardless of drug targeting. Nevertheless, here we have confirmed a novel compound that can target fungal-specific membranes, which led to a loss in viability for *C. neoformans*. Future work should be carried out to assess the exact mechanism behind this loss in viability, and investigation into Aox specific inhibitors, both alone and in combination with other inhibitors of the ETC.

6 Final Discussion

6.1 Introduction

Human fungal pathogens can cause superficial, sub cutaneous or systemic infections, which in the case of immunocompromised individuals can be associated with high mortality. The outcome for patients is also strongly correlated with the speed and accuracy of diagnosis, a rise in antifungal resistance and socioeconomic factors that restrict treatment ability[377-379]. Antifungal resistance is likely to become a major issue, driven by factors such as a limited number of identified cellular targets for antifungal development, the over-use of agricultural fungicides and the emergence of more fungal pathogens in an ever-warming climate[380, 381].

Given the mortality of immunocompromised patients infected with the fungal pathogen *C. neoformans* and the emergence of clinical isolates that are heteroresistant to currently circulating azoles, we wanted to assess whether the mitochondria of *C. neoformans* was a viable target for novel antifungal therapeutics, with a focus on the Aox enzyme.

6.2 Investigating *C. neoformans* metabolism

Metabolic modulation is integral for fungal pathogenicity and dissemination within the host as adaption to limited ranges of metabolites within the harsh host environment, in conjunction with periods of dormancy, can assist both prolonged latency and rapid virulence. We identified several conditions which promoted *C. neoformans* growth in minimal media, including low pH and preferential use of alternative carbon and phosphate sources linked to membrane integrity.

6.2.1 *C. neoformans* shows optimum growth at low pH

Interestingly, *C. neoformans* showed preferential growth at slightly acidic pH (pH 5-7) and could utilise multiple additives for growth at pH 4.5 (Fig. 4.7). The ability of *C. neoformans* to grow in the acidic environment of the phagolysosome has been well reviewed [382], with studies showing that *C.*

neoformans will rapidly replicate inside of the mature phagolysosome and can even manipulate the pH of the phagosome to near its optimum pH of 5 [382, 383]. Interestingly, the use of lysosomotropic agents, such as Chloroquine, have been shown to kill *C. neoformans* directly and indirectly via a rise in phagolysosomal pH and blockage of phagosome maturation [384-386]. However, the adaptability of *C. neoformans* to grow in differing pH conditions is required for not only dissemination throughout the human host outside of macrophage compartments, but perhaps escape from the macrophage itself. This is because *C. neoformans* replies on phagolysosome membrane permeabilisation for lytic expulsion [382], which would include disruption of the low pH, but addition of Chloroquine has been shown to increase non-lytic expulsion [387]. Although the mechanisms behind these phenomena are still unclear, tolerance of fluctuating pH within the processes of engulfment and escape from macrophages may assist *C. neoformans* in dragotcytosis.

While we observed that growth at pH 4.5 with the additives shown in Fig. 4.7d mainly increased *C. neoformans* cell growth, one exception, α-amino malonate, inhibited growth at pH 4.5. Malonate itself is proven to be an inhibitor of complex II of the mitochondria[388], and amino malonate is used as a metabolic precursor to the sphingofungin biosynthetic pathway, which produces sphingolipid inhibitors in pathogenic fungi such as *Aspergillus fumigatus*[389]. Inhibition of growth in the presence of amino malonate may therefore indicate that *C. neoformans* is sensitive to sphingofungin precursors and supports our hypothesis that *C. neoformans* is sensitive to respiratory inhibition.

6.2.2 *C. neoformans* maintenance of membrane integrity

As one of the key virulence traits associated to *C. neoformans* is capsule remodelling and plasma membrane signalling, we wanted to investigate the uptake of supplements that would contribute to these processes. Interestingly, we discovered not only a preferential uptake of phosphates (Fig. 4.5), but a utilisation of carbon sources that contribute to both membrane integrity and capsule biosynthesis (Fig. 4.2). Our data showed that wildtype *C. neoformans* could utilise more carbon sources than the *Δaox1* mutant, but we were particularly interested in the significance of mannitol,

mannose and trehalose. While mannitol and mannose are carbon sources used by both strains, they are key components of capsular GXM [327], and addition of mannitol into growth media has been implicated with a marked increase in capsule size [390]. Trehalose biosynthesis is a key contributor to protection of membrane integrity under stress, which is synthesised from Glucose-6-Phosphate via TPS1 [391], although direct roles of trehalose in pathogenic mechanisms are yet to be elucidated [392]. While our data suggests that wildtype cells could utilise trehalose as a carbon source for increased growth, we observed no significance in *Δaox1* cells. However, on assessment of phosphate source utilisation, cells lacking Aox used markedly more phosphate sources than the wildtype (Fig. 4.5), including those for trehalose biosynthesis. The phosphate sensing and acquisition pathway (PHO) [393], which is controlled through the transcriptional regulator Pho4 [394], is integral for *C. neoformans* dissemination and induction of the seed morphotype, and so uptake of phosphate sources for lipid remodelling and trehalose biosynthesis may take precedence in nutrient-limiting conditions. Given together, it could be suggested that Aox may perhaps have a role in membrane stress mediation, and so cells lacking Aox may actively uptake more phosphate sources to maintain membrane integrity and repair under stress, especially for smaller disseminating morphotypes.

6.3 Assessing *C. neoformans* use of mitochondria

6.3.1 Mitochondrial function is linked to kinases involved in sphingolipid biosynthesis

The developing links between mitochondrial function and pathogenicity have been well reviewed[149], with a focus of mitochondrial involvement in cellular stress management during infection. While exact signalling mechanisms behind diverse mitochondrial function during pathogenesis still require further research, the presumption of high energetic cost to disseminating pathogens led us to screening for kinases required for mitochondrial maintenance under stress. Interestingly, an unbiased kinase knockout screen identified Ypk1, a kinase involved in sphingolipid biosynthesis, as integral for not only routine respiration under normal growth conditions, but also for mitochondrial function under inhibition of Complexes III and IV. We also discovered that active Ypk1 had a role in

melanisation, with identification of the critical residue D386A for Ypk1 activity in relation to melanin synthesis.

Ypk1 is a kinase which is involved with sphingolipid biosynthesis, and studies have proven that it is activated through phosphorylation at multiple sites [395]. Upstream activators of Ypk1 include PKC1, which is part of the Inositol-phosphoryl ceramide synthase (IPC) - Diacylglycerol (DAG) - PKC pathway [396], Pkh202 and TORC2[290], which is critical for mitochondrial function and cell membrane remodelling under stress. The downstream targets of Ypk1 include Orm1 and Orm2 [397], which modulate Serine Palmitoyl Transferase (SPT) activity, the primary enzyme in sphingolipid biosynthesis, and Lac1 and Lag1 ceramide synthases [398], which through ceramides stimulate the synthesis of complex sphingolipids[290, 292]. Interestingly, ceramide is not only synthesised in the endoplasmic reticulum (ER) through Lac1 and Lag1 (Fig. 6.1a), but is also found in mitochondria, both through localised synthesis and translocation from the ER [399]. The roles of ceramide in mitochondrial function and apoptosis has been well reviewed[400], although Ypk1 involvement in these processes is still unclear.

One could speculate that loss of Ypk1 may affect mitochondria by disrupting lipid biosynthesis and autophagy, which may induce cellular sensitivity to mitochondrial ETC inhibition and stress (Fig. 6.1b). This is supported by our data showing that *Δypk1* mutants displayed a lower routine respiration (Fig. 3.14), and the loss of viability in *Δypk1* mutants after Complex III (Fig. 3.13) and Complex IV (Fig. 3.16) inhibition. However, it is important to note that studies have identified Ypk1 in *C. neoformans, C. albicans* and *A. fumigatus* as dispensable for viability during normal growth, which indicates that Ypk1 must have an inducible role under mitochondrial stress but is perhaps not constitutively active for contribution to cell viability during normal growth conditions.

The speculative roles of Ypk1 in sphingolipid cross talk during mitochondrial inhibition and its relation to cell fate are outlined in Fig. 6.1. In order to clarify the effects of Ypk1 loss on cell fate, analysis of cell death mechanisms by flow cytometry and shotgun mass spectrometry for lipid content analysis should be carried out in *Δypk1* mutant *C. neoformans* under mitochondrial stress.

6.3.2 The sphingolipid kinase Ypk1 has a role in *C. neoformans* melanisation

Our data showed that the D386 residue of Ypk1 was essential for the melanisation response. Melanisation is composed of a complex signalling network involving the cAMP/PKA pathway, HOG pathway and RAM pathway, although signalling components and regulation are yet to be fully understood[88, 89]. Melanin is synthesised *in vivo* via laccase enzymes which catalyse melanin polymerisation and deposition at the cell wall. Transcriptional regulation of laccase via LAC1 is multifactorial but is thought to be heavily attributed to four core transcription factors (TFs), Mbs1, Hob1, Bzp4 and Uvs101 [401]. While the epistatic interactions between the HOG, RAM and cAMP/PKA pathways have been investigated[88], little is known about laccase interactions after transcription. However, it has been postulated that laccase localisation to the cell wall for generation of the melanin coat can be controlled by both PKA [402] and PKC1 [403], although the signalling behind this localisation is not well defined.

We can postulate that Ypk1 may act as a central signalling mediator for both plasma membrane lipid homeostasis, through Lac1/Lag1 phosphorylation and acting as a downstream effector of PKC1 for laccase localisation in melanin coat biosynthesis. These roles are dependent on the D386 residue within the catalytic loop of Ypk1, as we have observed that perturbation of this residue led to a loss of melanisation. However, as melanisation in *C. neoformans* is a complex, highly regulated process involving multiple epistatic signalling components, we cannot assume that Ypk1 is solely responsible for melanin biosynthesis. In fact, this is supported by our data showing maintenance of melanisation seen in *Δypk1* mutant *C. neoformans,* which may be a result of activation of alternate signalling pathways. This may include cAMP/PKA, as PKA is shown to be involved in laccase activation and localisation [402], and Cka1, the Casein Kinase II isoform in *C. neoformans*, which has also been implicated in Lac1 activation [404]. As studies have shown that deletion of either Cka1 or PKA lead to a reduction in melanisation [402, 404], this would indicate that melanin signalling is influenced by multiple pathways. Deletion of Ypk1 entirely would likely upregulate PKA, Cka1 and other signalling components found within these pathways to maintain wildtype levels of melanin production. However, one could speculate that the presence of a kinase-dead Ypk1, with a residue D386

alteration, could induce down-regulation of PKA/Cka1 pathway components or block activation of laccase. This would be possible through the multiple phosphorylation sites that have been recorded for Ypk1 [395]. For example, the PDK2 site has unknown, but presumed roles in kinase modulation for downstream processes [395], which remain ambiguous. This indicates that the D836 mutant isoform of Ypk1 would still have functional phosphorylation sites such as K274 in conserved kinase domain II. One could suggest that other phosphorylation sites could have a downstream signalling effect in preventing laccase translocation, so loss of the whole kinase would be required for other melanin biosynthesis pathways to take dominance.

In this way, we can suggest that Ypk1 promotes pleiotropic control of both sphingolipid biosynthesis and laccase localisation, which is attributed to the ambiguity of phosphorylation sites found in the kinase. The proposed interactions of Ypk1 during laccase induction and translocation, and the effects of its loss, can be seen in Fig. 6.1. In order to investigate these proposals, co-immunoprecipitation and fluorescence microscopy should be considered.

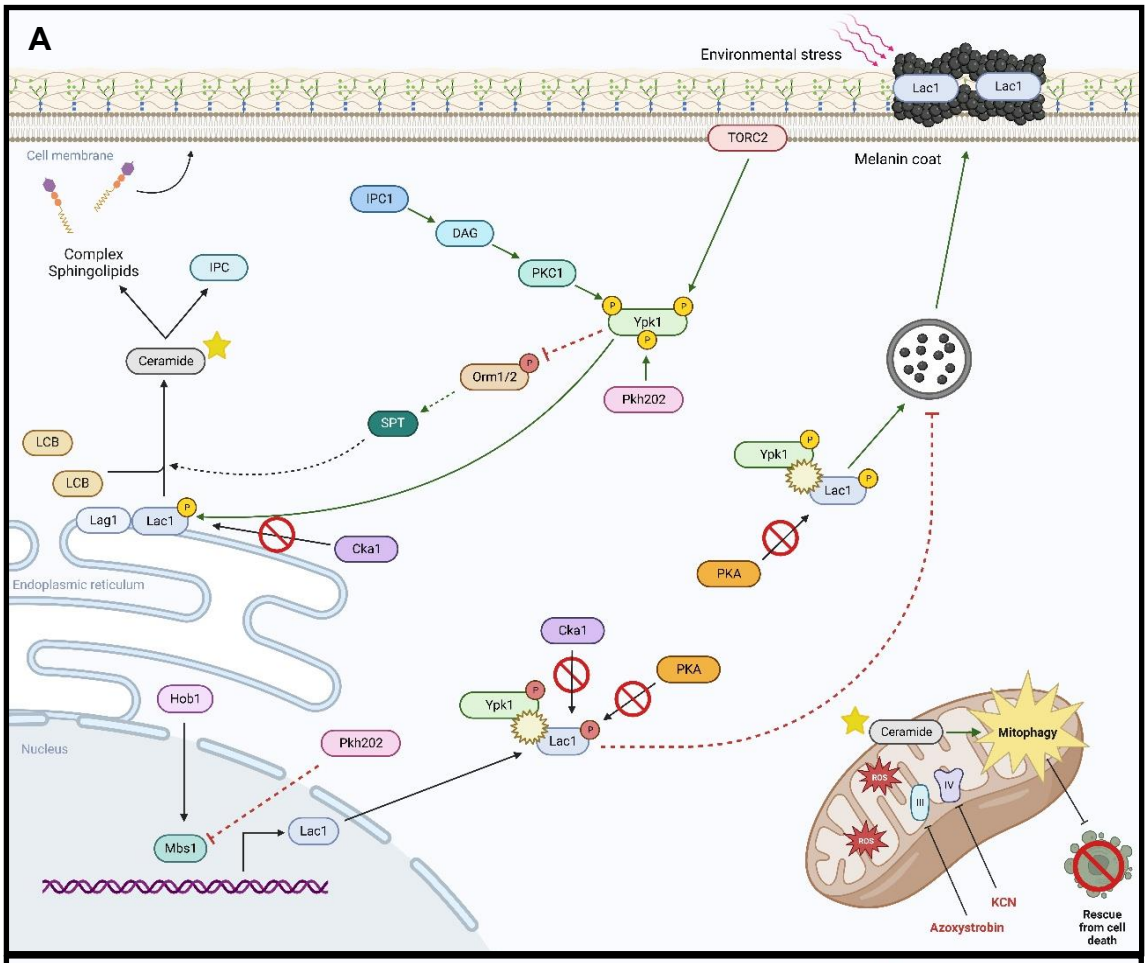
A
Environmental stress
Lac1
Lac1
TORC2
Melanin coat
Cell membrane
Complex Sphingolipids
IPC
IPC1
DAG
PKC1
Ypk1
Ceramide
Orm1/2
Pkh202
SPT
LCB
LCB
Lag1
Lac1
Cka1
Endoplasmic reticulum
Ypk1
Lac1
PKA
Cka1
PKA
Ypk1
Lac1
Hob1
Nucleus
Pkh202
Mbs1
Lac1
Ceramide
Mitophagy
ROS
IV
III
ROS
KCN
Azoxystrobin
Rescue from cell death

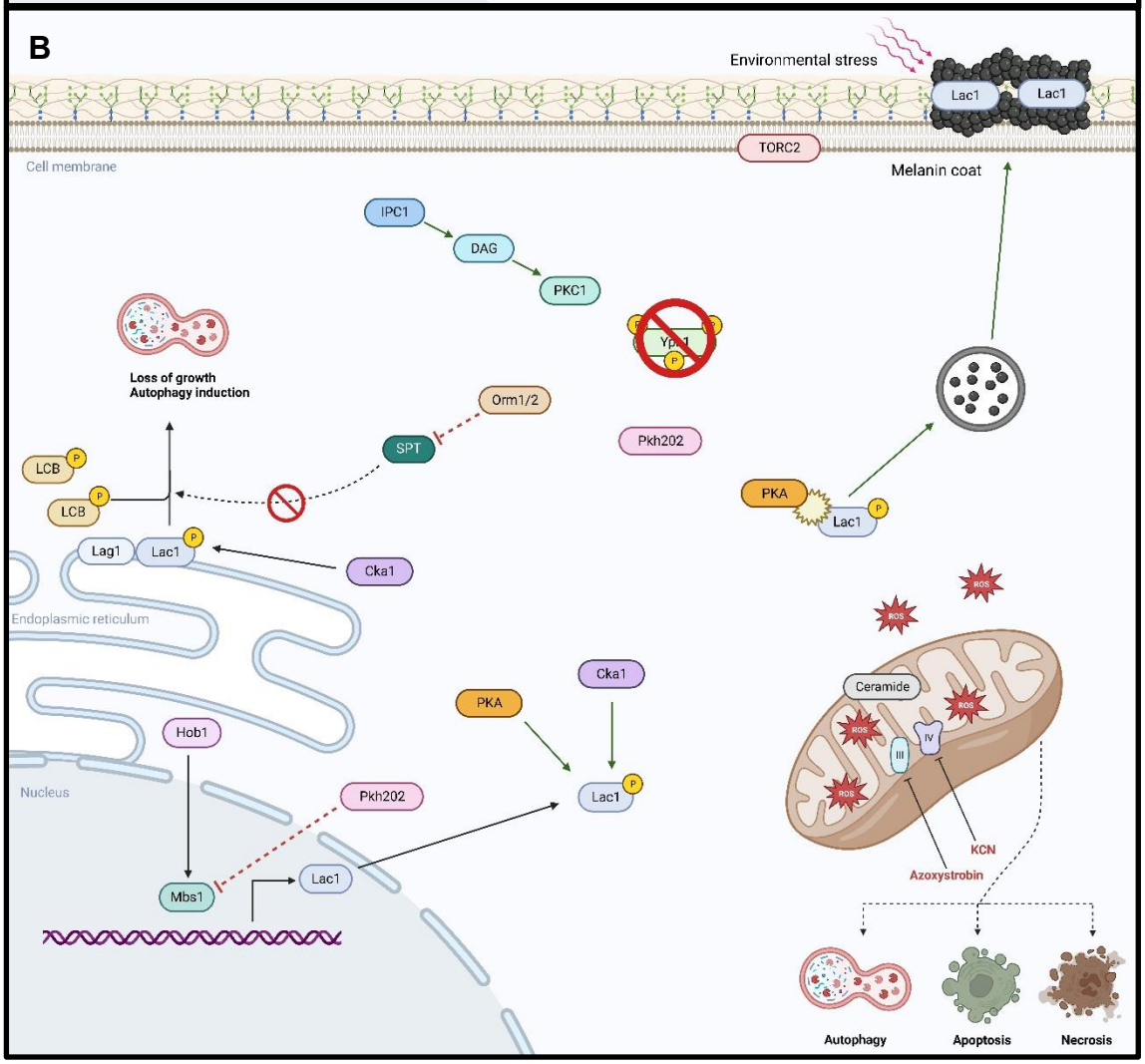
B
Environmental stress
Lac1
Lac1
TORC2
Cell membrane
Melanin coat
IPC1
DAG
PKC1
Loss of growth
Autophagy induction
Orm1/2
SPT
Pkh202
LCB
LCB
Lag1
Lac1
Cka1
PKA
Lac1
Endoplasmic reticulum
Cka1
PKA
Hob1
Nucleus
Pkh202
Lac1
Mbs1
Lac1
ROS
ROS
Ceramide
ROS
IV
III
ROS
KCN
Azoxystrobin
Autophagy
Apoptosis
Necrosis

Figure 6.1: Proposed roles of Ypk1.
Schematic illustrating (**A**) the effect of Ypk1 on melanin production, sphingolipid biosynthesis signalling and mitochondrial physiology under ETC inhibition, with either fully functional Ypk1 or with the D386A substitution. This includes the TORC2 and IPC1-DAG-PKC1 pathway, inhibition of Orm1/2 through phosphorylation, and phosphorylation and translocation of Lac1. Ypk1 is also involved in the production of ceramide, which may be involved in mitophagy and avoidance of cell death. (**B**) The proposed effect of loss of Ypk1 on these processes, where the cAMP/PKA and Cka1 pathways modulate Lac1 phosphorylation, translocation and formation of the melanin coat. Background signalling components and transcription factors, such as Pkh202, Mbs1 and Hob1 are also involved in Lac1 production. Loss of Ypk1 may dysregulate ceramide production, leading to mitochondrial sensitivity to ETC inhibition. Created with BioRender.com.

6.3.3 Roles of Aox in *C. neoformans*

Our data suggests that the Aox of *C. neoformans* contains structural similarities to isoforms found in oleaginous yeasts, rather than other human fungal pathogens such as *C. albicans*. Interestingly, our data also shows that Aox does not contribute to normal growth and respiration but is required for mitochondrial resistance to Complex III inhibition, as wildtype cells show increased respiratory activity and robust growth after Azoxystrobin addition, unlike the *Δaox1* mutant. However, the disparate effects of Complex III and Complex IV inhibition in relation to Aox function supports the given proposal in Section 1.3.8. The lack of Aox response during Complex IV inhibition via KCN, but the induction of Aox under Complex III inhibition, indicates that Aox may provide relief from ETC inhibition though manipulation of electrons from the UQP, perhaps through the induction of quiescence. Interestingly, these findings support studies which have also identified Aox as responsible for RET/FET switching in xenotopic expression of Aox in mice[263].

While dormancy is a well-known process for pathogenic infection of the host in cryptococcosis[114], questions around the induction of a VBNC phenotype and Aox involvement in this process remain. While VBNCs can be reactivated though the addition of quorum sensing vitamins such as pantothenic acid, re-activation of VBNC cells *in vitro* is better in minimal media over rich media[296], thought to be caused by cell death induced by oxidative stress from rapid metabolic activation. *C. neoformans* has interactions with *Acanthamoeba castellanii* [405], *Dictyostelium discoideum* [406] and soil-dwelling cyanogenic bacteria like *Pseudomonas aeruginosa* [407] in the environment, as well as

macrophages in the host, where high levels of cyanide generated by bacteria or NO by macrophages can affect Complex IV activity and *C. neoformans* growth. One could speculate that the VBNC phenotype is an evolutionary adaption to resist these environmental challenges, while Aox induction linked to Complex III and electron transport may be present to moderate ROS production and damage during normal growth.

One possibility is that Aox activation plays a role within a metabolic checkpoint, which helps to halt cellular growth and induce quiescence under conditions of ETC inhibition. This may contribute to the unique VBNC dormancy phenotype observed during infection, where *C. neoformans* can remain metabolically dormant under host-induced antimicrobial stress until latent reactivation. The proposed roles for Aox acting as a metabolic checkpoint for quiescence switching can be found in Fig. 6.2.

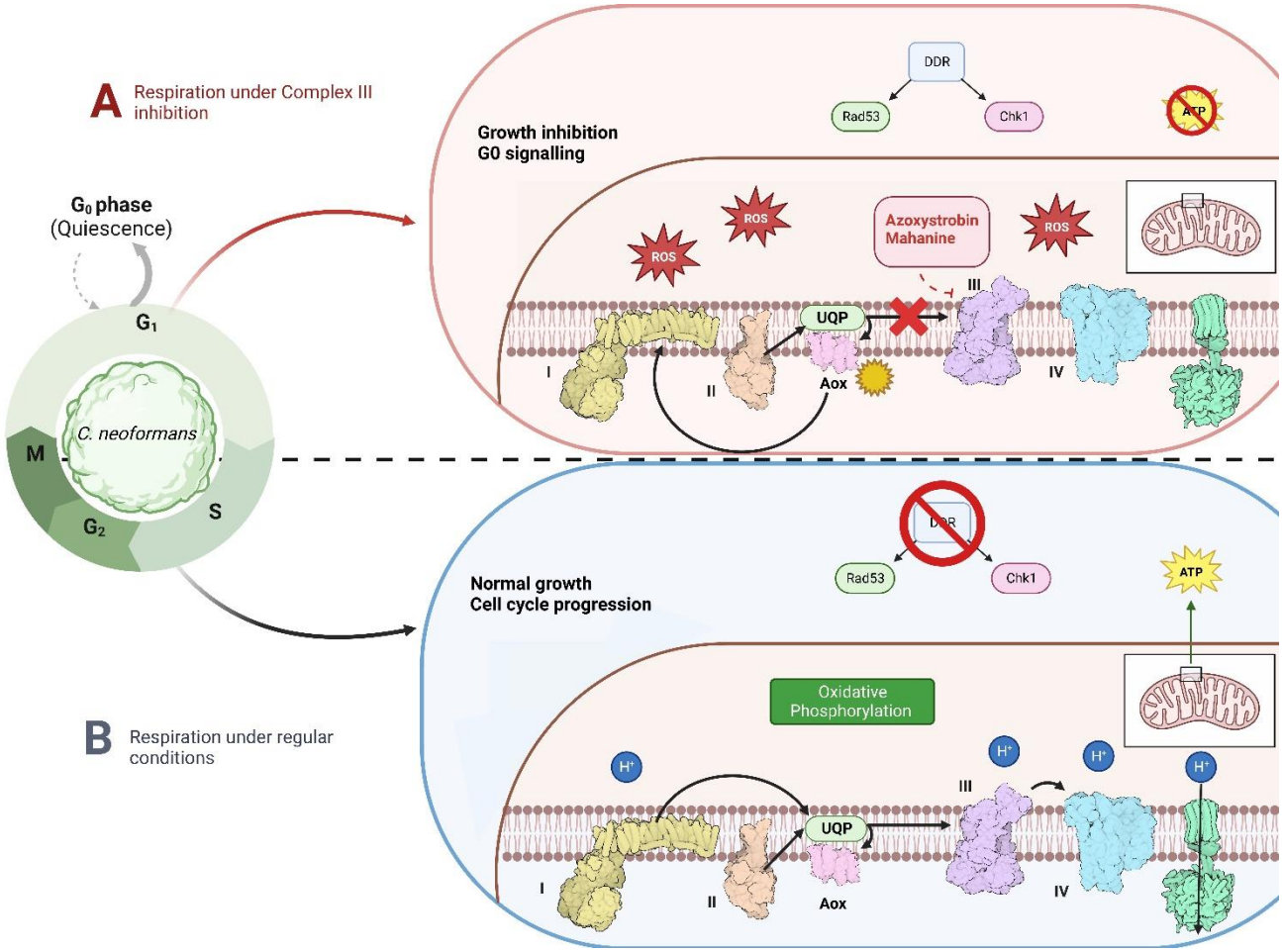

Figure 6.2: Proposed roles of Aox as a quiescence switch.
Schematic illustrating (**A**) the proposed role of Aox under Complex III inhibition by Azoxystrobin or Mahanine, leading to induction into G0 (Quiescence). This may be initiated by ROS production and loss of ATP which induces RET through Complex I and activates the DNA Damage Response (DDR) pathway. (**B**) Respiration processes without Complex III inhibition, including FET, oxidative phosphorylation and production of ATP. This would not induce the DDR pathway and allow for cellular commitment to the G1/S phase of the cell cycle. Black arrows indicate electron movement. Created with BioRender.com.

This postulation is supported by studies in glioblastoma, whereby inhibition of Complex III using Mahanine, which increased ROS, induced the DNA Damage Response (DRR) and led to G0 arrest (quiescence)[237]. Interestingly, DRR leading to quiescence in the G0 section of the cell cycle has been implicated in both fungal pathogenicity and drug resistance[408], and coupling of metabolic checkpoints to the cell cycle has been recently observed, where Ras mislocalisation can alter metabolic homeostasis, inducing quiescence[409]. While these studies support the given proposal,

further research into metabolic checkpoints coupled to cell cycle regulation in *C. neoformans*, and whether this presents a viable target for antifungal therapies, should be explored.

6.4 Antifungal therapeutic strategies

Following our analysis of *C. neoformans* use of mitochondria and metabolic requirements, we wanted to investigate what approach to fungal-specific targeting would be a viable therapeutic option. Firstly, our BIOLOG metabolite screens indicated a preferential uptake of di- and tri-peptides (Fig. 4.4), which have been observed as a potent antifungal against *C. neoformans* as synthetic agents [410-412].

6.4.1 Utilisation of peptides for antifungal targeting

While the mechanism and role of peptide uptake in *C. neoformans* pathogenicity is still unclear, the importance of nitrogen sources in NCR, TOR and SPS-sensing pathways and capsule and melanin synthesis has been investigated [328, 413, 414]. Amino acid uptake is thought to occur through ten amino acid permeases in *C. neoformans* [415], which accounts not only for the increased uptake of peptides for growth that we have seen, but also the attraction to the use of peptides as an antifungal inhibitor. While synthetic peptides are currently being investigated for their potency against *C. neoformans* [410-412], given the observed preferential uptake of di- and tri- peptides for growth, it could be suggested that these peptides could be used for antifungal drug targeting and trafficking into the cell for enhanced drug uptake. This would perhaps address the current issue with enhanced drug efflux seen in both *C. neoformans* and *C. gattii* in response to azole treatment [416], which occurs via the ABC transporters Afr1, Afr2 and Mdr1 [417]. Utilisation of di- and tri-peptides that are readily uptaken by *C. neoformans*, perhaps as part of a drug conjugate, may allow for therapeutic drugs to be retained for longer periods, which would increase efficacy and potentially lower working MICs.

6.4.2 Assessment of *C. neoformans* mitochondria as a viable antifungal target

The BIOLOG screens conducted in this thesis also identified a sensitivity to the antimicrobial compound sodium nitrite (Fig. 4.8). While sodium nitrite has been highlighted as a common antimicrobial in the commercial food industry [418] we were interested in its ability to produce ROS and disrupt the plasma membrane redox system (PMRS) [361]. We were able to show that addition of sodium nitrite disturbed *C. neoformans* membranes, indicated by disruption of respiratory activity conducive with uncoupling of respiration from ATP synthesis (Fig. 4.11). We were also able to confirm that this membrane disruption was detrimental to cell melanisation and viability, which is presumably linked to elevated levels of ROS. While we have postulated that Aox can use ROS as a signal for RET and induction of quiescence, it is important to note that lower levels of ROS can act within signalling pathways, but rapidly generated, high levels of ROS induce cell death. Given the promise of sodium nitrite for therapeutic application, further investigation into its action and cell death mechanisms in *C. neoformans* should be carried out. However, one key finding is that *C. neoformans* was sensitive to mitochondrial membrane disruption.

In support of these findings, our investigations into novel dual inhibitors of both Aox and cytochrome bc_1 (ALTOX094 and ALTOX102) confirmed that *C. neoformans* was sensitive to disruption of mitochondrial membranes (Section 5.3.3). Unfortunately, the dual inhibition of Aox and cytochrome bc_1 could not be confirmed as the mechanism of action responsible for ALTOX094 induced cell death. Interestingly, although we observed a loss of viability for ALTOX102, we could not ascertain a mechanism of cell death, and given our data showing an increase in respiratory activity for cells treated with ALTOX102, we can suggest that ALTOX102 may be inducing a quiescent phenotype. This is supported by the IC50 data suggesting that ALTOX102 preferentially targets cytochrome bc_1 over Aox, which matches our postulation that targeting of Complex III may lead to quiescence through Aox activity. While these drugs were designed to inhibit fungal respiration through dual inhibition, our data suggested that irreversible drug insertion into membranes disrupted cell permeability and membrane integrity and lead to rapid necrosis. We could confirm, however, that this necrosis was fungal specific, which did not affect the *G. mellonella* animal model and did not

confer haemolytic activity. Most interestingly, this finding supports our suggestions that *C. neoformans* is reliant on mitochondrial membrane integrity, of which modulation is Aox independent.

Given our proposals thus far that *C. neoformans* is sensitive to membrane disruption and is heavily reliant on processes involved in lipid and membrane integrity, therapeutics that affect membrane permeability, such as sodium nitrite or ALTOX094, seem to be a viable option. It appears that while Aox may play a key role as a quiescent switch or metabolic checkpoint, this action is still affected by membrane permeability. Aox may account for some avoidance of cell death via quiescence when Complex III of the ETC is targeted, although it does not appear to have a protective role under general membrane perturbation.

6.5 Conclusions and Future Directions

We have investigated the metabolic requirements of *C. neoformans* and its reliance on mitochondria for growth and adaption. Our data suggests that *C. neoformans* uses the classical ETC for respiration, and as such is heavily reliant on maintenance of mitochondrial membrane integrity. We have also seen that mitochondrial function in *C. neoformans* is linked to lipid homeostasis, and perturbation of lipid signalling pathways, particularly involving Ypk1, can result in lower respiration and loss of melanisation. We have also discovered that *C. neoformans* is sensitive to disruption of redox signalling pathways through the rapid induction of ROS and showed sensitivity to membrane disruption, which presents a viable target. Most importantly, our data shows that Aox does not appear to contribute to normal growth or respiration, but we have highlighted a proposed role of Aox as part of a metabolic checkpoint, which through RET induction can induce quiescence in response to mitochondrial Complex III inhibition. We suggest that inducing a VBNC phenotype in a combination therapy with a drug targeting the fatty acid pathway, or presence of a drug that increases oxidative stress after induced VBNC re-activation could be a viable therapy for acute infection, although VBNC host tolerance and signalling should be investigated further.

Future work should be directed towards the analysis of functional membrane targets in *C. neoformans,* and deeper investigation into lipid pathway components linked to mitochondrial morphology and function. Investigations into perturbation of redox signalling, as well as assessing dormancy induction under mitochondrial inhibition should be considered, to perhaps isolate a dual inhibitory mechanism whereby mitochondrial membranes are targeted, but dormancy induction is blocked. Understanding of this signalling within *C. neoformans* and how this relates to stress adaption within the host may allow for new insights into future antifungal therapeutics.

7 Appendix

Gene Names	Organism	Length	50 100 150 200 250 300 350 400
SAPINGB_P001593	Saprochaete ingens	344 AA	52.9% 678 7.6e-83
GX50_07737	Emmonsia crescens	357 AA	50.2% 679 8.1e-83
ASPBRDRAFT_113570 →	Aspergillus brasiliensis (strain CBS 101740 / IMI 381727 / IBT 21946)	351 AA	53.2% 678 9.5e-83
BDW43DRAFT_309613	Petromyces alliaceus (Aspergillus alliaceus)	353 AA	51.3% 678 1e-82
ETB97_009496	Aspergillus burnettii	353 AA	51.3% 678 1e-82
HCAG_03721 →	Ajellomyces capsulatus (strain NAm1 / WU24) (Darling's disease fungus) (Histoplasma capsulatum)	357 AA	46% 678 1.1e-82
BDQ94DRAFT_157850	Aspergillus welwitschiae	325 AA	51.1% 675 1.2e-82
PITG_09890	Phytophthora infestans (strain T30-4) (Potato late blight agent)	316 AA	47.1% 674 1.3e-82
AOX1, CDV55_103685, CFD26_103774	Aspergillus turcosus	345 AA	52.8% 676 1.6e-82
BDV26DRAFT_284853	Aspergillus bertholletiae	353 AA	52.5% 676 2e-82
IFR04_005138	Cadophora malorum	356 AA	50.3% 676 2.2e-82
CNMCM6457_006962, CNMCM6805_007619	Aspergillus fumigatiaffinis	345 AA	50.4% 675 2.2e-82
ASPTUDRAFT_30962	Aspergillus tubingensis (strain CBS 134.48)	351 AA	52.9% 675 2.7e-82
aox1 →	Aspergillus niger	351 AA	52.9% 675 2.7e-82

Figure 7.1a: Similarity scores of Aspergillus brasiliensis, Histoplasma capsulatum and Aspergillus niger Aox, in comparison to C. neoformans Aox (BLAST)[279, 280]***.***

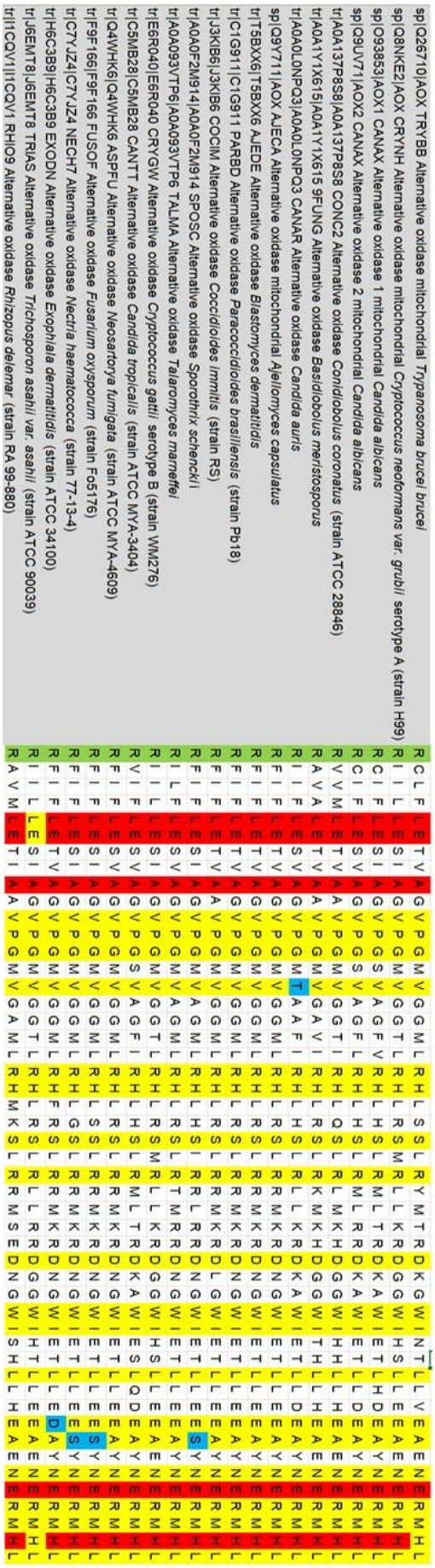

Figure 7.1b: Clustal alignment of the Aox sequences of human fungal pathogens whereby yellow residues indicate conservation, red residues indicate iron binding activity and green residues show quinol binding ability, carried out on Clustal 2.1[424]

Cryptococcus Accession Information 2020

original plate number	original strain number	Plate set description	Plate number	Well	CNAG	Gene name
1	1571	*Cryptococcus* kinase deletion colle	1	B2	CNAG_01333	ALK1
1	1573	*Cryptococcus* kinase deletion colle	1	C2	CNAG_01333	ALK1
1	2216	*Cryptococcus* kinase deletion colle	1	D2	CNAG_06161	VRK1
1	2217	*Cryptococcus* kinase deletion colle	1	E2	CNAG_06161	VRK1
1	1503	*Cryptococcus* kinase deletion colle	1	F2	CNAG_02802	ARG2
1	1504	*Cryptococcus* kinase deletion colle	1	G2	CNAG_02802	ARG2
1	1564	*Cryptococcus* kinase deletion colle	1	B3	CNAG_03369	SWE102
1	1565	*Cryptococcus* kinase deletion colle	1	C3	CNAG_03369	SWE102
1	2157	*Cryptococcus* kinase deletion colle	1	D3	CNAG_01294	IPK1
1	2158	*Cryptococcus* kinase deletion colle	1	E3	CNAG_01294	IPK1
1	n/a	*Cryptococcus* kinase deletion colle	1	F3	disregard	
1	n/a	*Cryptococcus* kinase deletion colle	1	G3	disregard	
1	n/a	*Cryptococcus* kinase deletion colle	1	B4	disregard	
1	n/a	*Cryptococcus* kinase deletion colle	1	C4	disregard	
1	2809	*Cryptococcus* kinase deletion colle	1	D4	CNAG_04821	PAN3
1	2810	*Cryptococcus* kinase deletion colle	1	E4	CNAG_04821	PAN3
1	1438	*Cryptococcus* kinase deletion colle	1	F4	CNAG_00745	HRK1/NPH1
1	1439	*Cryptococcus* kinase deletion colle	1	G4	CNAG_00745	HRK1/NPH1
1	1804	*Cryptococcus* kinase deletion colle	1	C5	CNAG_04408	CKI1
1	1805	*Cryptococcus* kinase deletion colle	1	D5	CNAG_04408	CKI1
1	1235	*Cryptococcus* kinase deletion colle	1	E5	CNAG_02820	PKH201
1	1236	*Cryptococcus* kinase deletion colle	1	F5	CNAG_02820	PKH201
1	1901	*Cryptococcus* kinase deletion colle	1	G5	CNAG_05439	CMK1
1	1902	*Cryptococcus* kinase deletion colle	1	B6	CNAG_05439	CMK1
1	n/a	*Cryptococcus* kinase deletion colle	1	C6	disregard	
1	n/a	*Cryptococcus* kinase deletion colle	1	D6	disregard	
1	1885	*Cryptococcus* kinase deletion colle	1	E6	CNAG_02389	YPK101
1	1886	*Cryptococcus* kinase deletion colle	1	F6	CNAG_02389	YPK101
1	1245	*Cryptococcus* kinase deletion colle	1	G6	CNAG_05097	CKY1
1	1246	*Cryptococcus* kinase deletion colle	1	B7	CNAG_05097	CKY1
1	2415	*Cryptococcus* kinase deletion colle	1	C7	CNAG_06553	GAL83
1	2416	*Cryptococcus* kinase deletion colle	1	D7	CNAG_06553	GAL83
1	2038	*Cryptococcus* kinase deletion colle	1	E7	CNAG_06730	GSK3
1	2039	*Cryptococcus* kinase deletion colle	1	F7	CNAG_06730	GSK3
1	2806	*Cryptococcus* kinase deletion colle	1	G7	CNAG_05965	IRK4
1	n/a	*Cryptococcus* kinase deletion colle	1	C8	disregard	
1	1493	*Cryptococcus* kinase deletion colle	1	B8	CNAG_07744	PIK1
1	1494	*Cryptococcus* kinase deletion colle	1	D8	CNAG_07744	PIK1
1	2941	*Cryptococcus* kinase deletion colle	1	E8	CNAG_03567	CBK1
1	2942	*Cryptococcus* kinase deletion colle	1	F8	CNAG_03567	CBK1
1	1940	*Cryptococcus* kinase deletion colle	1	G8	CNAG_02551	DAK102
1	1941	*Cryptococcus* kinase deletion colle	1	B9	CNAG_02551	DAK102
1	2761	*Cryptococcus* kinase deletion colle	1	C9	CNAG_01155	GUT1
1	1241	*Cryptococcus* kinase deletion colle	1	D9	CNAG_01155	GUT1
1	1410	*Cryptococcus* kinase deletion colle	1	E9	CNAG_06568	SKS1
1	1411	*Cryptococcus* kinase deletion colle	1	F9	CNAG_06568	SKS1
1	1912	*Cryptococcus* kinase deletion colle	1	G9	CNAG_00826	DAK101
1	1913	*Cryptococcus* kinase deletion colle	1	B10	CNAG_00826	DAK101
1	1486	*Cryptococcus* kinase deletion colle	1	C10	CNAG_03048	IRK3
1	1487	*Cryptococcus* kinase deletion colle	1	D10	CNAG_03048	IRK3
1	3056	*Cryptococcus* kinase deletion colle	1	E10	CNAG_07580	TRM7
1	3057	*Cryptococcus* kinase deletion colle	1	F10	CNAG_07580	TRM7
1	2408	*Cryptococcus* kinase deletion colle	1	G10	CNAG_05753	ARG5,6
1	2409	*Cryptococcus* kinase deletion colle	1	B11	CNAG_05753	ARG5,6
1	1514	*Cryptococcus* kinase deletion colle	1	C11	CNAG_05600	IGI1
1	1515	*Cryptococcus* kinase deletion colle	1	D11	CNAG_05600	IGI1
1	278	*Cryptococcus* kinase deletion colle	1	E11	CNAG_01850	TCO1
1	279	*Cryptococcus* kinase deletion colle	1	F11	CNAG_01850	TCO1
1	281	*Cryptococcus* kinase deletion colle	1	G11	CNAG_05590	TCO2
2	282	*Cryptococcus* kinase deletion colle	2	B2	CNAG_05590	TCO2
2	284	*Cryptococcus* kinase deletion colle	2	C2	CNAG_01988	TCO3

2	285	*Cryptococcus*	kinase deletion colle	2	D2	CNAG_01988	TCO3
2	417	*Cryptococcus*	kinase deletion colle	2	E2	CNAG_03355	TCO4
2	418	*Cryptococcus*	kinase deletion colle	2	F2	CNAG_03355	TCO4
2	286	*Cryptococcus*	kinase deletion colle	2	G2	CNAG_00106	TCO5
2	287	*Cryptococcus*	kinase deletion colle	2	B3	CNAG_00106	TCO5
2	2469	*Cryptococcus*	kinase deletion colle	2	C3	CNAG_00363	TCO6
2	2554	*Cryptococcus*	kinase deletion colle	2	D3	CNAG_00363	TCO6
2	n/a	*Cryptococcus*	kinase deletion collection				disregard
2	558	*Cryptococcus*	kinase deletion colle	2	D4	CNAG_00047	PKP1
2	608	*Cryptococcus*	kinase deletion colle	2	E4	CNAG_00047	PKP1
2	270	*Cryptococcus*	kinase deletion colle	2	F4	CNAG_00130	HRK1
2	271	*Cryptococcus*	kinase deletion colle	2	G4	CNAG_00130	HRK1
2	188	*Cryptococcus*	kinase deletion colle	2	B5	CNAG_00396	PKA1
2	189	*Cryptococcus*	kinase deletion colle	2	C5	CNAG_00396	PKA1
2	342	*Cryptococcus*	kinase deletion colle	2	D5	CNAG_01730	STE7
2	343	*Cryptococcus*	kinase deletion colle	2	E5	CNAG_01730	STE7
2	330	*Cryptococcus*	kinase deletion colle	2	F5	CNAG_02357	MKK2
2	331	*Cryptococcus*	kinase deletion colle	2	G5	CNAG_02357	MKK2
2	127	*Cryptococcus*	kinase deletion colle	2	B6	CNAG_02511	CPK1
2	128	*Cryptococcus*	kinase deletion colle	2	C6	CNAG_02511	CPK1
2	373	*Cryptococcus*	kinase deletion colle	2	D6	CNAG_02531	CPK2
2	374	*Cryptococcus*	kinase deletion colle	2	E6	CNAG_02531	CPK2
2	552	*Cryptococcus*	kinase deletion colle	2	F6	CNAG_03670	IRE1
2	554	*Cryptococcus*	kinase deletion colle	2	G6	CNAG_03670	IRE1
2	194	*Cryptococcus*	kinase deletion colle	2	B7	CNAG_04162	PKA2
2	195	*Cryptococcus*	kinase deletion colle	2	C7	CNAG_04162	PKA2
2	n/a	*Cryptococcus*	kinase deletion colle	2	D7		disregard
2	273	*Cryptococcus*	kinase deletion colle	2	E7	CNAG_04755	BCK1
2	274	*Cryptococcus*	kinase deletion colle	2	F7	CNAG_04755	BCK1
2	619	*Cryptococcus*	kinase deletion colle	2	G7	CNAG_06301	SCH9
2	620	*Cryptococcus*	kinase deletion colle	2	B8	CNAG_06301	SCH9
2	313	*Cryptococcus*	kinase deletion colle	2	C8	CNAG_06980	STE11
2	314	*Cryptococcus*	kinase deletion colle	2	D8	CNAG_06980	STE11
2	n/a	*Cryptococcus*	kinase deletion colle	2	E8		disregard
2	1216	*Cryptococcus*	kinase deletion colle	2	F8	CNAG_03024	RIM15
2	1266	*Cryptococcus*	kinase deletion colle	2	G8	CNAG_03367	URK1
2	1267	*Cryptococcus*	kinase deletion colle	2	B9	CNAG_03367	URK1
2	1500	*Cryptococcus*	kinase deletion colle	2	C9	CNAG_02680	VPS15
2	1501	*Cryptococcus*	kinase deletion colle	2	D9	CNAG_02680	VPS15
2	64	*Cryptococcus*	kinase deletion colle	2	E3	CNAG_01523	HOG1
2	1510	*Cryptococcus*	kinase deletion colle	2	E9	CNAG_02296	RBK1
2	1511	*Cryptococcus*	kinase deletion colle	2	F9	CNAG_02296	RBK1
2	1579	*Cryptococcus*	kinase deletion colle	2	G9	CNAG_04631	RIK1
2	1580	*Cryptococcus*	kinase deletion colle	2	B10	CNAG_04631	RIK1
2	1709	*Cryptococcus*	kinase deletion colle	2	C10	CNAG_06193	CRK1
2	1710	*Cryptococcus*	kinase deletion colle	2	D10	CNAG_06193	CRK1
2	n/a	*Cryptococcus*	kinase deletion colle	2	E10		disregard
2	n/a	*Cryptococcus*	kinase deletion colle	2	F10		disregard
2	1736	*Cryptococcus*	kinase deletion colle	2	G10	CNAG_04678	YPK1
2	1737	*Cryptococcus*	kinase deletion colle	2	B11	CNAG_04678	YPK1
2	1800	*Cryptococcus*	kinase deletion colle	2	C11	CNAG_02675	HSL101
2	1801	*Cryptococcus*	kinase deletion colle	2	D11	CNAG_02675	HSL101
2	1825	*Cryptococcus*	kinase deletion colle	2	E11	CNAG_03167	CHK1
2	n/a	*Cryptococcus*	kinase deletion colle	2	F11		disregard
2	1904	*Cryptococcus*	kinase deletion colle	2	G11	CNAG_02542	IRK2
3	1905	*Cryptococcus*	kinase deletion colle	3	B2	CNAG_02542	IRK2
3	1989	*Cryptococcus*	kinase deletion colle	3	G2	CNAG_01062	PSK201
3	n/a	*Cryptococcus*	kinase deletion colle	3	C2		disregard
3	n/a	*Cryptococcus*	kinase deletion colle	3	D2		disregard
3	1990	*Cryptococcus*	kinase deletion colle	3	B3	CNAG_01062	PSK201
3	2040	*Cryptococcus*	kinase deletion colle	3	C3	CNAG_04197	YAK1
3	2096	*Cryptococcus*	kinase deletion colle	3	D3	CNAG_04197	YAK1
3	2443	*Cryptococcus*	kinase deletion colle	3	E3	CNAG_03258	TPK202A
3	2444	*Cryptococcus*	kinase deletion colle	3	F3	CNAG_03258	TPK202A
3	2487	*Cryptococcus*	kinase deletion colle	3	G3	CNAG_02799	DAK202A
3	2489	*Cryptococcus*	kinase deletion colle	3	B4	CNAG_02799	DAK202A

3	2948	*Cryptococcus* kinase deletion colle		3	C4	CNAG_04040	FPK1
3	2949	*Cryptococcus* kinase deletion colle		3	D4	CNAG_04040	FPK1
3	1575	*Cryptococcus* kinase deletion colle		3	E4	CNAG_03216	SNF101
3	1576	*Cryptococcus* kinase deletion colle		3	F4	CNAG_03216	SNF101
3	1807	*Cryptococcus* kinase deletion colle		3	G4	CNAG_01905	KSP1
3	1808	*Cryptococcus* kinase deletion colle		3	B5	CNAG_01905	KSP1
3	1935	*Cryptococcus* kinase deletion colle		3	C5	CNAG_05005	ATG1
3	1936	*Cryptococcus* kinase deletion colle		3	D5	CNAG_05005	ATG1
3	2439	*Cryptococcus* kinase deletion colle		3	E5	CNAG_04108	PKP2
3	2440	*Cryptococcus* kinase deletion colle		3	F5	CNAG_04108	PKP2
3	2072	*Cryptococcus* kinase deletion colle		3	G5	CNAG_06632	ABC1
3	2797	*Cryptococcus* kinase deletion colle		3	B6	CNAG_06632	ABC1
3	2829	*Cryptococcus* kinase deletion colle		3	C6	CNAG_06051	GAL1
3	2830	*Cryptococcus* kinase deletion colle		3	D6	CNAG_06051	GAL1
3	n/a	*Cryptococcus* kinase deletion colle		3	E6		disregard
3	2911	*Cryptococcus* kinase deletion colle		3	F6	CNAG_00636	CDC7
3	3153	*Cryptococcus* kinase deletion colle		3	G6	CNAG_05220	TLK1
3	3188	*Cryptococcus* kinase deletion colle		3	B7	CNAG_05220	TLK1
3	2663	*Cryptococcus* kinase deletion colle		3	C7	CNAG_07779	TDA10
3	3223	*Cryptococcus* kinase deletion colle		3	D7	CNAG_07779	TDA10
3	3240	*Cryptococcus* kinase deletion colle		3	E7	CNAG_06033	MAK3202
3	3241	*Cryptococcus* kinase deletion colle		3	F7	CNAG_06033	MAK3202
3	3236	*Cryptococcus* kinase deletion colle		3	E8	CNAG_04282	MPK2
3	3238	*Cryptococcus* kinase deletion colle		3	F8	CNAG_04282	MPK2
3	1310	*Cryptococcus* kinase deletion colle		3	G8	CNAG_06809	IKS1
3	2119	*Cryptococcus* kinase deletion colle		3	B9	CNAG_06809	IKS1
3	3038	*Cryptococcus* kinase deletion colle		3	C9	CNAG_06086	SSN3
3	3039	*Cryptococcus* kinase deletion colle		3	D9	CNAG_06086	SSN3
3	2892	*Cryptococcus* kinase deletion colle		3	E9	CNAG_04316	UTR1
3	2893	*Cryptococcus* kinase deletion colle		3	F9	CNAG_04316	UTR1
3	3051	*Cryptococcus* kinase deletion colle		3	C10	CNAG_05694	CKA1
3	3052	*Cryptococcus* kinase deletion colle		3	D10	CNAG_05694	CKA1
3	1725	*Cryptococcus* kinase deletion colle		3	G9	CNAG_03843	ARK1
3	1726	*Cryptococcus* kinase deletion colle		3	B10	CNAG_03843	ARK1
3	2372	*Cryptococcus* kinase deletion colle		3	E10	CNAG_06552	SNF1
3	2373	*Cryptococcus* kinase deletion colle		3	F10	CNAG_06552	SNF1
3	3229	*Cryptococcus* kinase deletion colle		3	G10	CNAG_00782	SPS1
3	3325	*Cryptococcus* kinase deletion colle		3	B11	CNAG_00782	SPS1
3	1468	*Cryptococcus* kinase deletion colle		3	C11	CNAG_04230	THI6
3	1469	*Cryptococcus* kinase deletion colle		3	D11	CNAG_04230	THI6
3	1968	*Cryptococcus* kinase deletion colle		3	E11	CNAG_02712	BUD32
3	1969	*Cryptococcus* kinase deletion colle		3	F11	CNAG_02712	BUD32
3	2793	*Cryptococcus* kinase deletion colle		3	G11	CNAG_02947	SCY1
4	2794	*Cryptococcus* kinase deletion colle		4	B2	CNAG_02947	SCY1
4	2370	*Cryptococcus* kinase deletion colle		4	C2	CNAG_00415	CDC2801
4	3699	*Cryptococcus* kinase deletion colle		4	D2	CNAG_00415	CDC2801
4	3219	*Cryptococcus* kinase deletion colle		4	E2	CNAG_03592	THI20
4	3220	*Cryptococcus* kinase deletion colle		4	F2	CNAG_03592	THI20
4	3736	*Cryptococcus* kinase deletion colle		4	G2	CNAG_04433	YAK103
4	3737	*Cryptococcus* kinase deletion colle		4	B3	CNAG_04433	YAK103
4	3632	*Cryptococcus* kinase deletion colle		4	C3	CNAG_06697	MPS1
4	3633	*Cryptococcus* kinase deletion colle		4	D3	CNAG_06697	MPS1
4	3789	*Cryptococcus* kinase deletion colle		4	E3	CNAG_01165	LCB5
4	3790	*Cryptococcus* kinase deletion colle		4	F3	CNAG_01165	LCB5
4	2915	*Cryptococcus* kinase deletion colle		4	G3	CNAG_00405	KIC1
4	2916	*Cryptococcus* kinase deletion colle		4	B4	CNAG_00405	KIC1
4	2852	*Cryptococcus* kinase deletion colle		4	C4	CNAG_03946	GAL101
4	2853	*Cryptococcus* kinase deletion colle		4	D4	CNAG_03946	GAL101
4	3785	*Cryptococcus* kinase deletion colle		4	E4	CNAG_05216	RAD53
4	3786	*Cryptococcus* kinase deletion colle		4	F4	CNAG_05216	RAD53
4	3172	*Cryptococcus* kinase deletion colle		4	G4	CNAG_01209	FAB1
4	2955	*Cryptococcus* kinase deletion colle		4	B5	CNAG_05558	KIN4
4	2136	*Cryptococcus* kinase deletion colle		4	C5	CNAG_06310	IRK7
4	2137	*Cryptococcus* kinase deletion colle		4	D5	CNAG_06310	IRK7
4	3063	*Cryptococcus* kinase deletion colle		4	E5	CNAG_02233	MEC1
4	3611	*Cryptococcus* kinase deletion colle		4	F5	CNAG_02233	MEC1

4	2953	*Cryptococcus* kinase deletion colle	4	G5	CNAG_03811	IRK5
4	1234	*Cryptococcus* kinase deletion colle	4	B6	CNAG_02820	PKH201
4	2808	*Cryptococcus* kinase deletion colle	4	C6	CNAG_05965	IRK4
4	1883	*Cryptococcus* kinase deletion colle	4	D6	CNAG_05439	CMK1
4	4139	*Cryptococcus* kinase deletion colle	4	E6	CNAG_04197	YAK1
4	n/a	*Cryptococcus* kinase deletion colle	4	F6	disregard	
4	4190	*Cryptococcus* kinase deletion colle	4	G6	CNAG_03184	BUB1
4	4191	*Cryptococcus* kinase deletion colle	4	B7	CNAG_03184	BUB1
4	3330	*Cryptococcus* kinase deletion colle	4	C7	CNAG_04215	MET3
4	4212	*Cryptococcus* kinase deletion colle	4	D7	CNAG_02007	ADK1
4	3922	*Cryptococcus* kinase deletion colle	4	E7	CNAG_01612	PSK202
4	3924	*Cryptococcus* kinase deletion colle	4	F7	CNAG_01612	PSK202
4	3926	*Cryptococcus* kinase deletion colle	4	G7	CNAG_06671	YKL1
4	3927	*Cryptococcus* kinase deletion colle	4	B8	CNAG_06671	YKL1
4	2826	*Cryptococcus* kinase deletion colle	4	C8	CNAG_04927	YFH701
4	2410	*Cryptococcus* kinase deletion colle	4	D8	CNAG_05753	ARG5,6
4	3716	*Cryptococcus* kinase deletion colle	4	E8	CNAG_04927	YFH701
4	2912	*Cryptococcus* kinase deletion colle	4	F8	CNAG_00636	CDC7
4	4156	*Cryptococcus* kinase deletion colle	4	G8	CNAG_05558	KIN4
4	4281	*Cryptococcus* kinase deletion colle	4	B9	CNAG_01209	FAB1
4	3211	*Cryptococcus* kinase deletion colle	4	C9	CNAG_03290	KIC102
4	3212	*Cryptococcus* kinase deletion colle	4	D9	CNAG_03290	KIC102
4	3714	*Cryptococcus* kinase deletion colle	4	E9	CNAG_02859	POS5
4	3715	*Cryptococcus* kinase deletion colle	4	F9	CNAG_02859	POS5
4	3930	*Cryptococcus* kinase deletion colle	4	G9	CNAG_01938	KIN1
4	3931	*Cryptococcus* kinase deletion colle	4	B10	CNAG_01938	KIN1
4	n/a	*Cryptococcus* kinase deletion colle	4	C10	CNAG_02233	MEC1
4	n/a	*Cryptococcus* kinase deletion colle	4	D10	CNAG_02233	MEC1
4	3844	*Cryptococcus* kinase deletion colle	4	E10	CNAG_05771	TEL1
4	3845	*Cryptococcus* kinase deletion colle	4	F10	CNAG_05771	TEL1
4	n/a	*Cryptococcus* kinase deletion colle	4	G10	CNAG_06310	IRK7
4	n/a	*Cryptococcus* kinase deletion colle	4	B11	CNAG_06310	IRK7
4	1828	*Cryptococcus* kinase deletion colle	4	C11	CNAG_03167	CHK1
4	3053	*Cryptococcus* kinase deletion colle	4	D11	CNAG_05694	CKA1
4	3814	*Cryptococcus* kinase deletion colle	4	E11	CNAG_04514	MPK1
4	3816	*Cryptococcus* kinase deletion colle	4	F11	CNAG_04514	MPK1
4	3830	*Cryptococcus* kinase deletion colle	4	G11	CNAG_01704	IRK6
5	3831	*Cryptococcus* kinase deletion colle	5	B2	CNAG_01704	IRK6
5	4294	*Cryptococcus* kinase deletion colle	5	C2	CNAG_00266	YFH7
5	4295	*Cryptococcus* kinase deletion colle	5	D2	CNAG_00266	YFH7
5	4341	*Cryptococcus* kinase deletion colle	5	E2	CNAG_04221	FBP26
5	4342	*Cryptococcus* kinase deletion colle	5	F2	CNAG_04221	FBP26
5	4324	*Cryptococcus* kinase deletion colle	5	G2	CNAG_01061	FRK102
5	4325	*Cryptococcus* kinase deletion colle	5	B3	CNAG_01061	FRK102
5	4252	*Cryptococcus* kinase deletion colle	5	C3	CNAG_03796	ENV7
5	4253	*Cryptococcus* kinase deletion colle	5	D3	CNAG_03796	ENV7
5	4269	*Cryptococcus* kinase deletion colle	5	E3	CNAG_05386	PRO1
5	4270	*Cryptococcus* kinase deletion colle	5	F3	CNAG_05386	PRO1
5	4288	*Cryptococcus* kinase deletion colle	5	G3	CNAG_07372	OXK1
5	4289	*Cryptococcus* kinase deletion colle	5	B4	CNAG_07372	OXK1
5	4332	*Cryptococcus* kinase deletion colle	5	C4	CNAG_04314	YEF1
5	4333	*Cryptococcus* kinase deletion colle	5	D4	CNAG_04314	YEF1
5	4327	*Cryptococcus* kinase deletion colle	5	E4	CNAG_04191	CEX1
5	4328	*Cryptococcus* kinase deletion colle	5	F4	CNAG_04191	CEX1
5	4338	*Cryptococcus* kinase deletion colle	5	G4	CNAG_03137	PHO8501
5	4339	*Cryptococcus* kinase deletion colle	5	B5	CNAG_03137	PHO8501
5	4256	*Cryptococcus* kinase deletion colle	5	C5	CNAG_04272	CMK2
5	4257	*Cryptococcus* kinase deletion colle	5	D5	CNAG_04272	CMK2
5	4268	*Cryptococcus* kinase deletion colle	5	E5	CNAG_02915	PKH202
5	4309	*Cryptococcus* kinase deletion colle	5	F5	CNAG_02915	PKH202
5	4321	*Cryptococcus* kinase deletion colle	5	G5	CNAG_06490	SNF102
5	4323	*Cryptococcus* kinase deletion colle	5	B6	CNAG_06490	SNF102
5	4186	*Cryptococcus* kinase deletion colle	5	C6	CNAG_06278	TCO7
5	4187	*Cryptococcus* kinase deletion colle	5	D6	CNAG_06278	TCO7
5	4180	*Cryptococcus* kinase deletion colle	5	E6	CNAG_05243	XKS1
5	4181	*Cryptococcus* kinase deletion colle	5	F6	CNAG_05243	XKS1

5	4275	*Cryptococcus* kinase deletion colle	5	G6	CNAG_00556	YCK2
5	4278	*Cryptococcus* kinase deletion colle	5	B7	CNAG_00556	YCK2
5	4336	*Cryptococcus* kinase deletion colle	5	C7	CNAG_05200	BUD16
5	4337	*Cryptococcus* kinase deletion colle	5	D7	CNAG_05200	BUD16
5	1217	*Cryptococcus* kinase deletion colle	5	E7	CNAG_03024	RIM15
5	123	*Cryptococcus* kinase deletion colle	5	F7	CNAG_00769	PBS2
5	124	*Cryptococcus* kinase deletion colle	5	G7	CNAG_00769	PBS2
5	3702	*Cryptococcus* kinase deletion colle	5	B8	CNAG_08022	PHO85
5	3703	*Cryptococcus* kinase deletion colle	5	C8	CNAG_08022	PHO85
5	1809	*Cryptococcus* kinase deletion colle	5	D8	CNAG_01905	KSP1
5	4211	*Cryptococcus* kinase deletion colle	5	E8	CNAG_02007	ADK1
5	4176	*Cryptococcus* kinase deletion colle	5	F8	CNAG_06366	HRR2502
5	4228	*Cryptococcus* kinase deletion colle	5	G8	CNAG_05104	FRK101
5	4230	*Cryptococcus* kinase deletion colle	5	B9	CNAG_05104	FRK101
5	4174	*Cryptococcus* kinase deletion colle	5	C9	CNAG_06366	HRR2502
5	3824	*Cryptococcus* kinase deletion colle	5	D9	CNAG_01162	MAK3201
5	3825	*Cryptococcus* kinase deletion colle	5	E9	CNAG_01162	MAK3201
5	4347	*Cryptococcus* kinase deletion colle	5	F9	CNAG_07667	SAT4
5	4348	*Cryptococcus* kinase deletion colle	5	G9	CNAG_07667	SAT4
5	2952	*Cryptococcus* kinase deletion colle	5	B10	CNAG_03811	IRK5
5	1950	*Cryptococcus* kinase deletion colle	5	C10	CNAG_07359	IRK1
5	1951	*Cryptococcus* kinase deletion colle	5	D10	CNAG_07359	IRK1
5	65	*Cryptococcus* kinase deletion colle	5	E10	CNAG_01523	HOG1
5	66	*Cryptococcus* kinase deletion colle	5	F10	CNAG_01523	HOG1
5	264	*Cryptococcus* kinase deletion colle	5	G10	CNAG_05063	SSK2
5	265	*Cryptococcus* kinase deletion colle	5	B11	CNAG_05063	SSK2
5	3329	*Cryptococcus* kinase deletion colle	5	C11	CNAG_04215	MET3

Figure 7.2: Plate maps for the C. neoformans kinase knockout series generated by Kyung-Tae Lee et. al[272].

Table 7.1: Summary of additives that increase C. neoformans growth.

Red additives are those that affect both H99 and *Δaox1.*

H99	***Δaox1***
Carbon Sources	**Carbon Sources**
D-Trehalose	D-Mannose
D- Mannose	Dulcitol
Dulcitol	α-D-Glucose
D-Fructose	Gelatin
α-D-Glucose	β-Hydroxy-Butyric Acid
Pectin	
Phosphorus and Sulphur Sources	**Phosphorus and Sulphur Sources**
Adenosine- 2',3'-cyclic monophosphate	Phosphate
	Tri-polyphosphate
	Adenosine- 2',3'-cyclic monophosphate
	Phosphoenol Pyruvate
	D-Glucose-6-Phosphate
	D-Mannose-1-Phosphate
	Cysteamine-S-Phosphate
	Uridine- 3'-monophosphate
	O-Phospho-L-Tyrosine
	O-Phosphoryl-Ethanolamine
	Thymidine- 5'-monophosphate
	Inositol Hexaphosphate
	Sulphate
	Glutathione
Peptide Nitrogen Sources	**Peptide Nitrogen Sources**
Ala-Asn	Ala-Asp

Ala-Lys	Ala-Gln
Ala-Pro	Ala-Val
Arg-Ile	Asp-Gln
Arg-Lys	Asp-Gly
Arg-Met	Gly-Asn
Arg-Trp	Gly-Asp
Asp-Leu	Ile-Asn
Asp-Lys	Lys-Gly
Asp-Phe	Lys-Met
Asp-Val	Gln-Glu
Gln-Gln	Ser-Gln
Glu-Ser	Ser-Glu
Glu-Tyr	Thr-Ser
Gly-Ala	Val-Gln
Gly-Arg	Val-Lys
Gly-Gly	Gly-Gly-Ala
Gly-Phe	Gly-Gly-Leu
Gly-Ser	Gly-Gly-Phe
Gly-Val	Gly-Phe-Phe
Ile-Gln	Leu-Gly-Gly
Lys-Arg	Phe-Gly-Gly
Lys-Phe	Tyr-Gly-Gly
Lys-Trp	
Met-Glu	
Phe-Phe	
Ser-Ser	

Ala-Gln	
Asp-Ala	
Asp-Gln	
Asp-Gly	
Glu-Ala	
Gly-Asn	
Gly-Asp	
Ile-Asn	
Leu-Asn	
Lys-Gly	
Lys-Met	
Gln-Glu	
Phe-Tyr	
Ser-Asn	
Ser-Gln	
Ser-Glu	
Thr-Ser	
Val-Gln	
Val-Phe	
Val-Ser	
Ala-Ala-Ala	
Gly-Gly-Ala	
Gly-Gly-Gly	
Gly-Gly-Ile	
Gly-Gly-Leu	
Gly-Gly-Phe	

Leu-Gly-Gly Phe-Gly-Gly Tyr-Gly-Gly	
	Osmolyte sources Ethylene Glycol 805mM Ethylene Glycol 1610mM Sodium Phosphate pH 7 20mM
pH pH 5 pH 5.5 pH 6 pH 7 pH 4.5 + L-Alanine pH 4.5 + L-Glutamine pH 4.5 + Glycine pH 4.5 + L-Histidine pH 4.5 + L-Lysine pH 4.5 + L-Phenylalanine pH 4.5 + L-Proline pH 4.5 + L-Serine pH 4.5 + L-Tyrosine pH 4.5 + L-Valine pH 4.5 + Hydroxy- L-Proline pH 4.5 + L-Ornithine pH 4.5 + β-Hydroxy Glutamate pH 4.5 + γ-Hydroxy Glutamate	**pH** pH 5 pH 5.5 pH 6 pH 7 pH 4.5 + L-Glutamine pH 4.5 + Glycine pH 4.5 + L-Histidine pH 4.5 + L-Lysine pH 4.5 + L-Phenylalanine pH 4.5 + L-Threonine pH 4.5 + L-Tyrosine pH 4.5 + L-Valine pH 4.5 + Hydroxy- L-Proline pH 4.5 + L-Ornithine pH 4.5 + L-Homoarginine pH 4.5 + L-Norleucine pH 4.5 + β-Hydroxy Glutamate pH 4.5 + 5-Hydroxy Lysine

pH 4.5 + 5-Hydroxy Lysine	pH 4.5 + 5-Hydroxy Tryptophan
pH 4.5 + 5-Hydroxy Tryptophan	pH 4.5 + D, L-Diamino pimelic acid
pH 4.5 + D, L-Diamino pimelic acid	pH 4.5 + Trimethyl amine-N-oxide
pH 4.5 + Trimethyl amine-N-oxide	
pH 4.5 + Urea	

Table 7.2: Summary of additives that inhibit C. neoformans growth.

Red additives are those that affect both H99 and *Δaox1.*

H99	***Δaox1***
Carbon Sources	
Caproic Acid	
Osmolyte sources	**Osmolyte sources**
NaCl 342mM	NaCl 1026mM
NaCl 513mM	NaCl 1112mM
NaCl 855mM	NaCl 1197mM
NaCl 941mM	NaCl 1368mM
NaCl 1026mM	NaCl 1539mM
NaCl 1112mM	NaCl 1710mM
NaCl 1197mM	NaCl 1026mM
NaCl 1368mM	NaCl 1026mM + L- Carnitine
NaCl 1539mM	NaCl 1026mM + Trimethylamine-N-oxide
NaCl 1710mM	NaCl 1026mM + Trigonelline
NaCl 1026mM	Urea 1169mM
NaCl 1026mM + Betaine	Sodium Lactate 979mM
NaCl 1026mM + N-N Dimethyl glycine	Sodium Lactate 1068mM
NaCl 1026mM + Sarcosine	Sodium Benzoate pH 5.2 20mM

NaCl 1026mM + Dimethyl sulphonyl propionate	Sodium Benzoate pH 5.2 50mM
NaCl 1026mM + MOPS	Sodium Benzoate pH 5.2 100mM
NaCl 1026mM + Choline	Sodium Benzoate pH 5.2 200mM
NaCl 1026mM + Creatine	Sodium Nitrite 20mM
NaCl 1026mM + Creatinine	Sodium Nitrite 40mM
NaCl 1026mM + KCl	Sodium Nitrite 60mM
NaCl 1026mM + L-proline	Sodium Nitrite 80mM
NaCl 1026mM + N-Acetyl L-glutamine	Sodium Nitrite 100mM
NaCl 1026mM + β-Glutamic acid	
NaCl 1026mM + Glycerol	
NaCl 1026mM + Trehalose	
NaCl 1026mM + Trimethylamine-N-oxide	
NaCl 1026mM + Trimethylamine	
NaCl 1026mM + Octopine	
NaCl 1026mM + Trigonelline	
Potassium chloride 402mM	
Potassium chloride 537mM	
Potassium chloride 670mM	
Potassium chloride 804mM	
Sodium sulfate 350mM	
Ethylene glycol 2415mM	
Ethylene glycol 3220mM	
Sodium formate 249mM	
Sodium formate 441mM	
Sodium formate 588mM	
Sodium formate 882mM	

Urea 334mM	
Urea 501mM	
Urea 688mM	
Urea 835mM	
Urea 1002mM	
Urea 1169mM	
Sodium Lactate 267mM	
Sodium Lactate 445mM	
Sodium Lactate 534mM	
Sodium Lactate 979mM	
Sodium Lactate 1068mM	
Sodium Phosphate pH 7 100mM	
Sodium Phosphate pH 7 200mM	
Sodium Benzoate pH 5.2 20mM	
Sodium Benzoate pH 5.2 50mM	
Sodium Benzoate pH 5.2 100mM	
Sodium Benzoate pH 5.2 200mM	
Ammonium sulfate pH8 100mM	
Sodium Nitrite 10mM	
Sodium Nitrite 20mM	
Sodium Nitrite 40mM	
Sodium Nitrite 60mM	
Sodium Nitrite 80mM	
Sodium Nitrite 100mM	
pH	**pH**
pH 4.5 + α-Amino malonate	pH 4.5 + Anthranilic acid

pH 9.5	pH 4.5 + α-Amino malonate
pH 10	pH 9.5
pH 9.5 + L-Alanine	pH 10
pH 9.5 + L-Arginine	pH 9.5 + L-Alanine
pH 9.5 + L-Aspartic Acid	pH 9.5 + L-Arginine
pH 9.5 + L-Glutamic Acid	pH 9.5 + L-Asparagine
pH 9.5 + L-Glutamine	pH 9.5 + L-Aspartic Acid
pH 9.5 + Glycine	pH 9.5 + L-Glutamic Acid
pH 9.5 + L-Histidine	pH 9.5 + L-Glutamine
pH 9.5 + L-Isoleucine	pH 9.5 + Glycine
pH 9.5 + L-Leucine	pH 9.5 + L-Histidine
pH 9.5 + L-Lysine	pH 9.5 + L-Isoleucine
pH 9.5 + L-Methionine	pH 9.5 + L-Leucine
pH 9.5 + L-Phenylalanine	pH 9.5 + L-Lysine
pH 9.5 + L-Proline	pH 9.5 + L-Methionine
pH 9.5 + L-Serine	pH 9.5 + L-Phenylalanine
pH 9.5 + L-Threonine	pH 9.5 + L-Proline
pH 9.5 + L-Tryptophan	pH 9.5 + L-Serine
pH 9.5 + L-Valine	pH 9.5 + L-Tryptophan
pH 9.5 + Hydroxy- L-Proline	pH 9.5 + L-Tyrosine
pH 9.5 + L-Ornithine	pH 9.5 + L-Valine
pH 9.5 + L-Homoarginine	pH 9.5 + Hydroxy- L-Proline
pH 9.5 + L-Homoserine	pH 9.5 + L-Ornithine
pH 9.5 + Anthranilic acid	pH 9.5 + L-Homoarginine
pH 9.5 + L-Norleucine	pH 9.5 + L-Homoserine
pH 9.5 + L-Norvaline	pH 9.5 + Anthranilic acid

pH 9.5 + Agmatine	pH 9.5 + L-Norleucine
pH 9.5 + Cadaverine	pH 9.5 + L-Norvaline
pH 9.5 + Putrescine	pH 9.5 + Agmatine
pH 9.5 + Histamine	pH 9.5 + Cadaverine
pH 9.5 + Tyramine	pH 9.5 + Putrescine
pH 9.5 + Tryptamine	pH 9.5 + Histamine
pH 9.5 + Trimethyl amine-N-oxide	pH 9.5 + Tryptamine
pH 9.5 + Urea	pH 9.5 + Trimethyl amine-N-oxide
X-Caprylate	pH 9.5 + Urea
X-α-D-Glucoside	X-Caprylate
X-β-D-Galactoside	X-α-D-Glucoside
X-α-D-Glucuronide	X-β-D-Glucoside
X-β-D-Glucuronide	X-α-D-Galactoside
X-β-D-Glucosaminide	X-β-D-Galactoside
X-β-D-Galactosaminide	X-α-D-Glucuronide
X-SO4	X-β-D-Glucuronide
	X-β-D-Glucosaminide
	X-β-D-Galactosaminide
	X-α-D-Mannoside
	X-PO4
	X-SO4

Table 7.3 cLogP values

Determined using ACD/ChemSketch (freeware) 2020 V1.1. xLOGP3 determined using the method previously defined [419].

Compound	cLogP	xLogP3
Colletochlorin B	6.89	6.00
Colletochlorin D	4.85	4.14
ISSF31	7.29	6.06
ISSF33	5.25	4.21
ALTOX094	-	11.99
ALTOX102	-	9.82
Octyl TPP	-	8.0
Decyl TPP	-	9.1
Dodecyl TPP	-	10.2

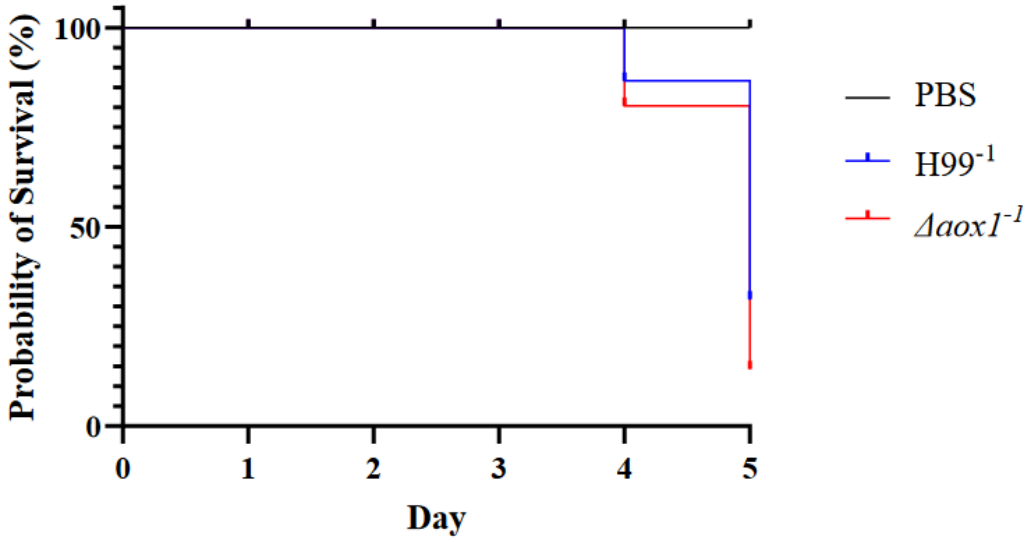

Log-rank (Mantel-Cox) test	
Chi square	2.983
df	1
P value	0.0841
P value summary	ns
Are the survival curves sig different?	No

Figure 7.3: Kaplan-Meyer survival graph comparing wildtype (H99) and Δaox1 mutant C. neoformans virulence.

8 Bibliography

1. Fisher, M. C., Gow, N. A. R. & Gurr, S. J. Tackling emerging fungal threats to animal health, food security and ecosystem resilience. *Philosophical Transactions of the Royal Society B: Biological Sciences* **371**, 20160332 (2023).

2. Brown, B. *et al*. Hidden Killers: Human Fungal Infections. *Sci. Transl. Med.* **4**, 165rv13 (2023).

3. Almeida, F., Rodrigues, M. L. & Coelho, C. The Still Underestimated Problem of Fungal Diseases Worldwide. *Frontiers in Microbiology* **10**, 214 (2019).

4. Fisher Matthew, C. *et al*. Threats Posed by the Fungal Kingdom to Humans, Wildlife, and Agriculture. *mBio* **11**, 10.1128/mbio.00449–20 (2023).

5. Savary, S., Ficke, A., Aubertot, J. & Hollier, C. Crop losses due to diseases and their implications for global food production losses and food security. *Food Security* **4**, 519–537 (2012).

6. Rodrigues, M. L. & Nosanchuk, J. D. Fungal diseases as neglected pathogens: A wake-up call to public health officials. *PLOS Neglected Tropical Diseases* **14**, e0007964 (2020).

7. Kwon-Chung, K. *et al*. *Cryptococcus neoformans* and *Cryptococcus gattii,* the Etiologic Agents of Cryptococcosis. *Cold Spring Harbor perspectives in medicine* **4**, a019760 (2014).

8. Kwon-Chung, K. J. Morphogenesis of Filobasidiella neoformans, the sexual state of *Cryptococcus neoformans* [Fungi]. *Mycologia* **68**, 821–833 (1976).

9. May, R. C., Stone, N. R. H., Wiesner, D. L., Bicanic, T. & Nielsen, K. *Cryptococcus*: from environmental saprophyte to global pathogen. *Nature Reviews Microbiology* **14**, 106–117 (2016).

10. Chowdhary, A., Randhawa, H. S., Prakash, A. & Meis, J. F. Environmental prevalence of *Cryptococcus neoformans* and *Cryptococcus gattii* in India: an update. *Crit. Rev. Microbiol.* **38**, 1–16 (2012).

11. Esher, S. K., Zaragoza, O. & Alspaugh, J. A. Cryptococcal pathogenic mechanisms: a dangerous trip from the environment to the brain. *Memórias do Instituto Oswaldo Cruz* **113**, e180057 (2018).

12. Rajasingham, R. *et al*. The global burden of HIV-associated cryptococcal infection in adults in 2020: a modelling analysis. *The Lancet Infectious Diseases* **22**, 1748–1755 (2023).

13. Rajasingham, R. *et al*. Global burden of disease of HIV-associated cryptococcal meningitis: an updated analysis. *The Lancet Infectious Diseases* **17**, 873–881 (2023).

14. Chang, W. *et al*. Pulmonary cryptococcosis: comparison of clinical and radiographic characteristics in immunocompetent and immunocompromised patients. *Chest* **129**, 333–340 (2006).

15. Sabiiti, W. & May, R. C. Mechanisms of infection by the human fungal pathogen *Cryptococcus neoformans*. *Future Microbiol.* **7**, 1297–1313 (2012).

16. Bratton, E. W. *et al*. Comparison and temporal trends of three groups with cryptococcosis: HIV-infected, solid organ transplant, and HIV-negative/non-transplant. *PLoS One* **7**, e43582 (2012).

17. Williamson, P. *et al*. Cryptococcal meningitis: epidemiology, immunology, diagnosis and therapy. *Nature Reviews Neurology* **13** (2016).

18. William, H. *et al*. Fluconazole Monotherapy Is a Suboptimal Option for Initial Treatment of Cryptococcal Meningitis Because of Emergence of Resistance. *mBio* **10**, 10.1128/mbio.02575–19 (2023).

19. Bermas, A. & Geddes-McAlister, J. Combatting the evolution of antifungal resistance in *Cryptococcus neoformans*. *Mol. Microbiol.* **114**, 721–734 (2023).

20. Stone, N. R. H. *et al*. Dynamic ploidy changes drive fluconazole resistance in human cryptococcal meningitis. *J. Clin. Invest.* **129**, 999–1014 (2019).

21. Feng, Y. *et al*. Adaptation to Fluconazole via Aneuploidy Enables Cross-Adaptation to Amphotericin B and Flucytosine in *Cryptococcus neoformans*. *Microbiology Spectrum* **9**, 723 (2023).

22. Greene, G., Lawrence, D. S., Jordan, A., Chiller, T. & Jarvis, J. N. Cryptococcal meningitis: a review of cryptococcal antigen screening programs in Africa. *Expert Review of Anti-infective Therapy* **19**, 233–244 (2021).

23. Hull, C. M. & Heitman, J. Genetics of *Cryptococcus neoformans*. *Annu. Rev. Genet.* **36**, 557–615 (2023).

24. Erke, K. H. Light microscopy of basidia, basidiospores, and nuclei in spores and hyphae of *Filobasidiella neoformans* (*Cryptococcus neoformans*). *J. Bacteriol.* **128**, 445–455 (1976).

25. Botts Michael, R., Giles Steven, S., Gates Marcellene, A., Kozel Thomas, R. & Hull Christina, M. Isolation and Characterization of *Cryptococcus neoformans* Spores Reveal a Critical Role for Capsule Biosynthesis Genes in Spore Biogenesis. *Eukaryotic Cell* **8**, 595–605 (2023).

26. Giles, S. S., Dagenais, T. R. T., Botts, M. R., Keller, N. P. & Hull, C. M. Elucidating the Pathogenesis of Spores from the Human Fungal Pathogen *Cryptococcus neoformans*. *Infect. Immun.* **77**, 3491–3500 (2009).

27. Levitz Stuart, M. *et al*. *Cryptococcus neoformans* Resides in an Acidic Phagolysosome of Human Macrophages. *Infect. Immun.* **67**, 885–890 (1999).

28. Fountain, A., Inpanathan, S., Alves, P., Verdawala, M. B. & Botelho, R. J. Phagosome maturation in macrophages: Eat, digest, adapt, and repeat. *Advances in Biological Regulation* **82**, 100832 (2021).

29. Uribe-Querol, E. & Rosales, C. in *Encyclopedia of Infection and Immunity* (ed Rezaei, N.) 99–109 (Elsevier, Oxford, 2022).

30. Greene, C. J. *et al*. Macrophages disseminate pathogen associated molecular patterns through the direct extracellular release of the soluble content of their phagolysosomes. *Nature Communications* **13**, 3072 (2022).

31. Onyishi, C. U. *et al*. Toll-like receptor 4 and macrophage scavenger receptor 1 crosstalk regulates phagocytosis of a fungal pathogen. *Nature Communications* **14**, 4895 (2023).

32. Bryan, A. M. *et al*. Cholesterol and sphingomyelin are critical for Fcγ receptor–mediated phagocytosis of *Cryptococcus neoformans* by macrophages. *J. Biol. Chem.* **297** (2021).

33. Cruz-Acuña Melissa, Noah, P. & Lewis Jamal, S. Vomocytosis: Too Much Booze, Base, or Calcium? *mBio* **10**, 10.1128/mbio.02526–19 (2023).

34. Diamond, R. D. & Bennett, J. E. Growth of *Cryptococcus neoformans* within human macrophages in vitro. *Infect. Immun.* **7**, 231–236 (1973).

35. May, R. C. & Casadevall, A. In fungal intracellular pathogenesis, form determines fate. *MBio* **9**, 10.1128/mbio. 02092–18 (2018).

36. O'Meara, T. R. *et al*. Global analysis of fungal morphology exposes mechanisms of host cell escape. *Nature Communications* **6**, 6741 (2015).

37. Pauwels, A., Trost, M., Beyaert, R. & Hoffmann, E. Patterns, Receptors, and Signals: Regulation of Phagosome Maturation. *Trends Immunol.* **38**, 407–422 (2017).

38. Gilbert, A. S. *et al*. Vomocytosis of live pathogens from macrophages is regulated by the atypical MAP kinase ERK5. *Sci. Adv.* **3**, e1700898 (2017).

39. Lei, G. *et al*. Biofilm from a clinical strain of Cryptococcus neoformans activates the NLRP3 inflammasome. *Cell Res.* **23**, 965–968 (2013).

40. Stukes, S. *et al*. The Membrane Phospholipid Binding Protein Annexin A2 Promotes Phagocytosis and Nonlytic Exocytosis of Cryptococcus neoformans and Impacts Survival in Fungal Infection. *J. Immunol.* **197**, 1252–1261 (2016).

41. Alvarez, M. & Casadevall, A. Phagosome extrusion and host-cell survival after *Cryptococcus neoformans* phagocytosis by macrophages. *Current Biology* **16**, 2161–2165 (2006).

42. Alvarez, M., Saylor, C. & Casadevall, A. Antibody action after phagocytosis promotes Cryptococcus neoformans and Cryptococcus gattii macrophage exocytosis with biofilm-like microcolony formation. *Cell. Microbiol.* **10**, 1622–1633 (2023).

43. Dragotakes, Q., Fu, M. S. & Casadevall, A. Dragotcytosis: Elucidation of the Mechanism for *Cryptococcus neoformans* Macrophage-to-Macrophage Transfer. *J. Immunol.* **202**, 2661–2670 (2019).

44. Salazar, A. S. *et al*. Potential missed opportunities for diagnosis of cryptococcosis and the association with mortality: A cohort study. *EClinicalMedicine* **27**, 100563 (2020).

45. Chang, Y. *et al*. Glycosaminoglycan Binding Facilitates Entry of a Bacterial Pathogen into Central Nervous Systems. *PLOS Pathogens* **7**, e1002082 (2011).

46. Charlier, C. *et al*. Capsule Structure Changes Associated with *Cryptococcus neoformans* Crossing of the Blood-Brain Barrier. *The American Journal of Pathology* **166**, 421–432 (2005).

47. Chen, S. H. M. *et al*. *Cryptococcus neoformans* induces alterations in the cytoskeleton of human brain microvascular endothelial cells. *J. Med. Microbiol.* **52**, 961–970 (2003).

48. Santiago-Tirado Felipe, H., Onken Michael, D., Cooper John, A., Klein Robyn, S. & Doering Tamara, L. Trojan Horse Transit Contributes to Blood-Brain Barrier Crossing of a Eukaryotic Pathogen. *mBio* **8**, 10.1128/mbio.02183–16 (2017).

49. Woo, Y. H. & Martinez, L. R. *Cryptococcus neoformans*–astrocyte interactions: effect on fungal blood brain barrier disruption, brain invasion, and meningitis progression. *Crit. Rev. Microbiol.* **47**, 206–223 (2021).

50. Chrisman, C. J., Albuquerque, P., Guimaraes, A. J., Nieves, E. & Casadevall, A. Phospholipids Trigger *Cryptococcus neoformans* Capsular Enlargement during Interactions with Amoebae and Macrophages. *PLOS Pathogens* **7**, e1002047 (2011).

51. Cross, C. E. & Bancroft, G. J. Ingestion of acapsular *Cryptococcus neoformans* occurs via mannose and beta-glucan receptors, resulting in cytokine production and increased phagocytosis of the encapsulated form. *Infect. Immun.* **63**, 2604–2611 (1995).

52. O'Meara Teresa, R. & Andrew, A. J. The *Cryptococcus neoformans* Capsule: a Sword and a Shield. *Clin. Microbiol. Rev.* **25**, 387–408 (2012).

53. Zaragoza, O. *et al*. Capsule enlargement in *Cryptococcus neoformans* confers resistance to oxidative stress suggesting a mechanism for intracellular survival. *Cell. Microbiol.* **10**, 2043–2057 (2008).

54. Granger, D. L., Perfect, J. R. & Durack, D. T. Virulence of *Cryptococcus neoformans*. Regulation of capsule synthesis by carbon dioxide. *J. Clin. Invest.* **76**, 508–516 (1985).

55. Vartivarian, S. E. *et al*. Regulation of Cryptococcal Capsular Polysaccharide by Iron. *J. Infect. Dis.* **167**, 186–190 (1993).

56. Zaragoza, O. & Casadevall, A. Experimental modulation of capsule size in *Cryptococcus neoformans*. *Biol. Proc. Online* **6**, 10–15 (2004).

57. Cordero Radames, J. B., Aviv, B. & Arturo, C. Temporal Behavior of Capsule Enlargement by *Cryptococcus neoformans*. *Eukaryotic Cell* **12**, 1383–1388 (2013).

58. Trevijano-Contador, N., Rossi, S. A., Alves, E., Landín-Ferreiroa, S. & Zaragoza, O. Capsule Enlargement in *Cryptococcus neoformans* Is Dependent on Mitochondrial Activity. *Frontiers in Microbiology* **8**, 1423 (2017).

59. Kozel, T. R. *et al*. Antigenic and biological characteristics of mutant strains of *Cryptococcus neoformans* lacking capsular O acetylation or xylosyl side chains. *Infect. Immun.* **71**, 2868–2875 (2003).

60. Feldmesser, M., Kress, Y. & Casadevall, A. 2. Dynamic changes in the morphology of *Cryptococcus neoformans* during murine pulmonary infection. *Microbiology* **147**, 2355–2365.

61. McFadden Diane, C., Fries Bettina, C., Fang, W. & Arturo, C. Capsule Structural Heterogeneity and Antigenic Variation in *Cryptococcus neoformans*. *Eukaryotic Cell* **6**, 1464–1473 (2007).

62. Kuttel, M. M., Casadevall, A. & Oscarson, S. *Cryptococcus neoformans* Capsular GXM Conformation and Epitope Presentation: A Molecular Modelling Study. *Molecules* **25** (2020).

63. McFadden, D. C., De Jesus, M. & Casadevall, A. The physical properties of the capsular polysaccharides from *Cryptococcus neoformans* suggest features for capsule construction. *J. Biol. Chem.* **281**, 1868–1875 (2006).

64. Heiss, C., Klutts, J. S., Wang, Z., Doering, T. L. & Azadi, P. The structure of *Cryptococcus neoformans* galactoxylomannan contains beta-D-glucuronic acid. *Carbohydr. Res.* **344**, 915–920 (2009).

65. Lortholary, O. *et al*. Immune mediators in cerebrospinal fluid during cryptococcosis are influenced by meningeal involvement and human immunodeficiency virus serostatus. *J. Infect. Dis.* **183**, 294–302 (2001).

66. Lortholary, O. *et al*. Cytokine profiles of AIDS patients are similar to those of mice with disseminated *Cryptococcus neoformans* infection. *Infect. Immun.* **67**, 6314–6320 (1999).

67. Fleuridor, R., Lyles, R. H. & Pirofski, L. Quantitative and Qualitative Differences in the Serum Antibody Profiles of Human Immunodeficiency Virus—Infected Persons with and without *Cryptococcus neoformans* Meningitis. *J. Infect. Dis.* **180**, 1526–1535 (1999).

68. Denham, S. T. *et al*. A dissemination-prone morphotype enhances extrapulmonary organ entry by *Cryptococcus neoformans*. *Cell Host & Microbe* **30**, 1382–1400.e8 (2022).

69. Freitas, G. J. C. *et al*. The Dynamics of *Cryptococcus neoformans* Cell and Transcriptional Remodeling during Infection. *Cells* **11** (2022).

70. Zaragoza, O. & Nielsen, K. Titan cells in *Cryptococcus neoformans*: cells with a giant impact. *Curr. Opin. Microbiol.* **16**, 409–413 (2013).

71. Hommel, B. *et al*. Titan cells formation in *Cryptococcus neoformans* is finely tuned by environmental conditions and modulated by positive and negative genetic regulators. *PLOS Pathogens* **14**, e1006982 (2018).

72. Li, Z. & Nielsen, K. Morphology Changes in Human Fungal Pathogens upon Interaction with the Host. *Journal of Fungi* **3** (2017).

73. Okagaki Laura, H. & Kirsten, N. Titan Cells Confer Protection from Phagocytosis in *Cryptococcus neoformans* Infections. *Eukaryotic Cell* **11**, 820–826 (2012).

74. Jang Eun-Ha, Kim Ji-Seok, Yu Seong-Ryong & Bahn Yong-Sun. Unraveling Capsule Biosynthesis and Signaling Networks in *Cryptococcus neoformans*. *Microbiology Spectrum* **10**, 2866 (2022).

75. Rizzo, J. *et al*. Analysis of multiple components involved in the interaction between *Cryptococcus neoformans* and *Acanthamoeba castellanii*. *Fungal Biology* **121**, 602–614 (2017).

76. Rodrigues, M. L. *et al*. Vesicular polysaccharide export in *Cryptococcus neoformans* is a eukaryotic solution to the problem of fungal trans-cell wall transport. *Eukaryot. Cell.* **6**, 48–59 (2007).

77. Zamith-Miranda Daniel *et al*. Comparative Molecular and Immunoregulatory Analysis of Extracellular Vesicles from *Candida albicans* and *Candida auris*. *mSystems* **6**, 10.1128/msystems.00822–21 (2021).

78. Albuquerque, P. C. *et al*. Vesicular transport in *Histoplasma capsulatum*: an effective mechanism for trans-cell wall transfer of proteins and lipids in ascomycetes. *Cell. Microbiol.* **10**, 1695–1710 (2008).

79. Vallejo, M. C. *et al*. Lipidomic Analysis of Extracellular Vesicles from the Pathogenic Phase of *Paracoccidioides brasiliensis*. *PLOS ONE* **7**, e39463 (2012).

80. Juliana, R. *et al*. Coregulation of extracellular vesicle production and fluconazole susceptibility in Cryptococcus neoformans. *mBio* **14**, 870 (2023).

81. Huang, S. *et al*. *Cryptococcus neoformans*-Derived Microvesicles Enhance the Pathogenesis of Fungal Brain Infection. *PLOS ONE* **7**, e48570 (2012).

82. Bitencourt Tamires, A. *et al*. Fungal Extracellular Vesicles Are Involved in Intraspecies Intracellular Communication. *mBio* **13**, 3272 (2022).

83. Watkins, R. A. *et al*. *Cryptococcus neoformans* Escape From Dictyostelium Amoeba by Both WASH-Mediated Constitutive Exocytosis and Vomocytosis. *Frontiers in Cellular and Infection Microbiology* **8** (2018).

84. Steenbergen, J. N., Shuman, H. A. & Casadevall, A. *Cryptococcus neoformans* interactions with amoebae suggest an explanation for its virulence and intracellular pathogenic strategy in macrophages. *Proc. Natl. Acad. Sci. U. S. A.* **98**, 15245–15250 (2001).

85. Basso, A. M. M. *et al*. Immunomodulatory activity of β-glucan-containing exopolysaccharides from Auricularia auricular in phagocytes and mice infected with *Cryptococcus neoformans*. *Med. Mycol.* **58**, 227–239 (2020).

86. Ding, C. *et al*. *Cryptococcus neoformans* Copper Detoxification Machinery Is Critical for Fungal Virulence. *Cell Host & Microbe* **13**, 265–276 (2013).

87. Sun, T. *et al*. Reciprocal functions of *Cryptococcus neoformans* copper homeostasis machinery during pulmonary infection and meningoencephalitis. *Nature Communications* **5**, 5550 (2014).

88. Dongpil, L. *et al*. Unraveling Melanin Biosynthesis and Signaling Networks in *Cryptococcus neoformans*. *mBio* **10**, 10.1128/mbio.02267–19 (2019).

89. Cordero Radames, J. B., Emma, C. & Arturo, C. Melanization in *Cryptococcus neoformans* Requires Complex Regulation. *mBio* **11**, 10.1128/mbio.03313–19 (2020).

90. Williamson, P. R. Biochemical and molecular characterization of the diphenol oxidase of *Cryptococcus neoformans*: identification as a laccase. *J. Bacteriol.* **176**, 656–664 (1994).

91. Nosanchuk, J. D. & Casadevall, A. The contribution of melanin to microbial pathogenesis. *Cell. Microbiol.* **5**, 203–223 (2003).

92. Liu, L., Tewari, R. P. & Williamson, P. R. Laccase Protects *Cryptococcus neoformans* from Antifungal Activity of Alveolar Macrophages. *Infect. Immun.* **67**, 6034–6039 (1999).

93. Saikia, S., Oliveira, D., Hu, G. & Kronstad, J. Role of ferric reductases in iron acquisition and virulence in the fungal pathogen Cryptococcus neoformans. *Infect. Immun.* **82**, 839–850 (2014).

94. Saikia, S., Oliveira, D., Hu, G. & Kronstad, J. Role of ferric reductases in iron acquisition and virulence in the fungal pathogen *Cryptococcus neoformans*. *Infect. Immun.* **82**, 839–850 (2014).

95. Barluzzi, R. *et al*. Iron overload exacerbates experimental meningoencephalitis by *Cryptococcus neoformans*. *J. Neuroimmunol.* **132**, 140–146 (2002).

96. Perfect, J. R., Lang, S. D. & Durack, D. T. Chronic cryptococcal meningitis: a new experimental model in rabbits. *The American journal of pathology* **101**, 177 (1980).

97. Araújo, G. R. d. S. *et al*. Dexamethasone and Methylprednisolone Promote Cell Proliferation, Capsule Enlargement, and in vivo Dissemination of C. neoformans. *Frontiers in Fungal Biology* **2**, 643537 (2021).

98. Perfect, J. R., Lang, S. D. & Durack, D. T. Chronic cryptococcal meningitis: a new experimental model in rabbits. *The American journal of pathology* **101**, 177 (1980).

99. Perfect, J. R. *Cryptococcus neoformans:* the yeast that likes it hot. *FEMS Yeast Res* **6**, 463–468 (2006).

100. Petter, R., Kang, B. S., Boekhout, T., Davis, B. J. & Kwon-Chung, K. A survey of heterobasidiomycetous yeasts for the presence of the genes homologous to virulence factors of *Filobasidiella neoformans*, CNLAC1 and CAP59. *Microbiology* **147**, 2029–2036 (2001).

101. Giles, S. S., Batinic-Haberle, I., Perfect, J. R. & Cox, G. M. *Cryptococcus neoformans* mitochondrial superoxide dismutase: an essential link between antioxidant function and high-temperature growth. *Eukaryotic Cell* **4**, 46–54 (2005).

102. Petzold, E. W. *et al*. Characterization and Regulation of the Trehalose Synthesis Pathway and Its Importance in the Pathogenicity of *Cryptococcus neoformans*. *Infect. Immun.* **74**, 5877–5887 (2006).

103. Bahn, Y., Kojima, K., Cox, G. M. & Heitman, J. Specialization of the HOG Pathway and Its Impact on Differentiation and Virulence of *Cryptococcus neoformans*. *Mol. Biol. Cell* **16**, 2285–2300 (2005).

104. Nichols, C. B., Perfect, Z. H. & Alspaugh, J. A. A Ras1-Cdc24 signal transduction pathway mediates thermotolerance in the fungal pathogen *Cryptococcus neoformans*. *Mol. Microbiol.* **63**, 1118–1130 (2023).

105. Probst, C. *et al*. A fungal lytic polysaccharide monooxygenase is required for cell wall integrity, thermotolerance, and virulence of the fungal human pathogen *Cryptococcus neoformans*. *PLOS Pathogens* **19**, e1010946 (2023).

106. O'Meara Teresa, R., Christie, H., Price Michael, S., Steve, G. & Andrew, A. J. *Cryptococcus neoformans* Histone Acetyltransferase Gcn5 Regulates Fungal Adaptation to the Host. *Eukaryotic Cell* **9**, 1193–1202 (2010).

107. Xu, J. Genotype-Environment Interactions of Spontaneous Mutations for Vegetative Fitness in the Human Pathogenic Fungus *Cryptococcus neoformans*. *Genetics (Austin)* **168**, 1177–1188 (2004).

108. Vande Zande, P., Zhou, X. & Selmecki, A. The Dynamic Fungal Genome: Polyploidy, Aneuploidy and Copy Number Variation in Response to Stress. *Annu. Rev. Microbiol.* **77**, 341–361 (2023).

109. Hu, G. *et al*. Variation in chromosome copy number influences the virulence of *Cryptococcus neoformans* and occurs in isolates from AIDS patients. *BMC Genomics* **12**, 526 (2011).

110. Todd, R. T. & Selmecki, A. Copy Number Variation and Allele Ratio Analysis in *Candida albicans* Using Whole Genome Sequencing Data. *Methods Mol. Biol.* **2658**, 105–125 (2023).

111. Morrow, C. A. & Fraser, J. A. Ploidy variation as an adaptive mechanism in human pathogenic fungi. *Semin. Cell Dev. Biol.* **24**, 339–346 (2013).

112. Gerstein Aleeza, C. *et al*. Polyploid Titan Cells Produce Haploid and Aneuploid Progeny To Promote Stress Adaptation. *mBio* **6**, 10.1128/mbio.01340–15 (2023).

113. Edward, S., Chang Yun, C., Martin, G. H. & Kwon-Chung Kyung, J. Heteroresistance to Fluconazole in *Cryptococcus neoformans* Is Intrinsic and Associated with Virulence. *Antimicrob. Agents Chemother.* **53**, 2804–2815 (2009).

114. Alanio, A. Dormancy in *Cryptococcus neoformans*: 60 years of accumulating evidence. *J. Clin. Invest.* **130**, 3353–3360 (2020).

115. Ke, W. *et al*. Fungicide-tolerant persister formation during cryptococcal pulmonary infection. *Cell Host & Microbe* **32**, 276–289.e7 (2024).

116. Moreira, I. d. M. B. *et al*. Investigation of fluconazole heteroresistance in clinical and environmental isolates of *Cryptococcus neoformans* complex and *Cryptococcus gattii* complex in the state of Amazonas, Brazil. *Med. Mycol.* **60**, myac005 (2022).

117. Keerativasee, S. *et al*. Heteroresistance to fluconazole among isolates of *Cryptococcus neoformans* in Northern Thailand. *African Journal of Microbiology Research* **7**, 4096–4102 (2013).

118. Sar, B. *et al*. Increasing in vitro resistance to fluconazole in *Cryptococcus neoformans* Cambodian isolates: April 2000 to March 2002. *J. Antimicrob. Chemother.* **54**, 563–565 (2004).

119. Medina, R. *et al*. Fungal Mitogenomes: Relevant Features to Planning Plant Disease Management. *Frontiers in Microbiology* **11** (2020).

120. Duvenage, L., Munro, C. A. & Gourlay, C. W. The potential of respiration inhibition as a new approach to combat human fungal pathogens. *Curr. Genet.* **65**, 1347–1353 (2019).

121. Yulin, Q., Jinxin, W., Quanzhen, L. & Bing, H. Recent Progress in Research on Mitochondrion-Targeted Antifungal Drugs: a Review. *Antimicrob. Agents Chemother.* **67**, 3 (2023).

122. Gibbs, E. T. *et al*. Site IQ in mitochondrial complex I generates S1QEL-sensitive superoxide/hydrogen peroxide in both the reverse and forward reactions. *Biochem. J.* **480**, 363–384 (2023).

123. Roca, R., Whitworth, W., Prag, P., Murphy, M. & Ramakrishnan, R. Tumor necrosis factor induces pathogenic mitochondrial ROS in tuberculosis through reverse electron transport. *Science* **376**, eabh2841 (2023).

124. Warris, A. & Ballou, E. R. Oxidative responses and fungal infection biology. *Semin. Cell Dev. Biol.* **89**, 34–46 (2019).

125. Kirkinezos, I. G. & Moraes, C. T. Reactive oxygen species and mitochondrial diseases. *Semin. Cell Dev. Biol.* **12**, 449–457 (2001).

126. Delattin, N., Cammue, B. P. A. & Thevissen, K. Reactive oxygen species-inducing antifungal agents and their activity against fungal biofilms. *Future Medicinal Chemistry* **6**, 77–90 (2023).

127. Shekhova, E., Kniemeyer, O. & Brakhage, A. A. Induction of Mitochondrial Reactive Oxygen Species Production by Itraconazole, Terbinafine, and Amphotericin B as a Mode of Action against *Aspergillus fumigatus*. *Antimicrob. Agents Chemother.* **61**, e00978–17. Print 2017 Nov (2017).

128. Joseph-Horne, T., Hollomon, D. W. & Wood, P. M. Fungal respiration: a fusion of standard and alternative components. *Biochimica et Biophysica Acta (BBA) - Bioenergetics* **1504**, 179–195 (2001).

129. Joseph-Horne, T. & Hollomon, D. W. Functional diversity within the mitochondrial electron transport chain of plant pathogenic fungi. *Pest Manag. Sci.* **56**, 24–30 (2023).

130. Tamura, H. *et al*. Effect of the methoxyiminoacetamide fungicide, SSF129, on respiratory activity in *Botrytis cinerea*. *Pestic. Sci.* **55**, 681–686 (1999).

131. Joseph-Horne, T. *et al*. Characterization of a Split Respiratory Pathway in the Wheat “Take-all” Fungus, *Gaeumannomyces graminis var.tritici* *. *J. Biol. Chem.* **273**, 11127–11133 (1998).

132. Tian, F., Lee, S. Y., Woo, S. Y. & Chun, H. S. Alternative Oxidase: A Potential Target for Controlling Aflatoxin Contamination and Propagation of *Aspergillus flavus*. *Frontiers in Microbiology* **11** (2020).

133. Huh, W. & Kang, S. Characterization of the gene family encoding alternative oxidase from *Candida albicans*. *Biochem. J.* **356**, 595–604 (2001).

134. Malina, C., Yu, R., Björkeroth, J., Kerkhoven, E. J. & Nielsen, J. Adaptations in metabolism and protein translation give rise to the Crabtree effect in yeast. *Proceedings of the National Academy of Sciences* **118**, e2112836118 (2023).

135. Childers, D. S. *et al*. The Rewiring of Ubiquitination Targets in a Pathogenic Yeast Promotes Metabolic Flexibility, Host Colonization and Virulence. *PLOS Pathogens* **12**, e1005566 (2016).

136. Burgain, A. *et al*. A novel genetic circuitry governing hypoxic metabolic flexibility, commensalism and virulence in the fungal pathogen *Candida albicans*. *PLOS Pathogens* **15**, e1007823 (2019).

137. Bouklas, T., Masone, L. & Fries, B. C. Differences in Sirtuin Regulation in Response to Calorie Restriction in *Cryptococcus neoformans*. *Journal of Fungi* **4**, 26 (2018).

138. Martins, V. d. P., Dinamarco, T. M., Curti, C. & Uyemura, S. A. Classical and alternative components of the mitochondrial respiratory chain in pathogenic fungi as potential therapeutic targets. *J. Bioenerg. Biomembr.* **43**, 81–88 (2011).

139. Moore, A. L. *et al*. Unraveling the Heater: New Insights into the Structure of the Alternative Oxidase. *Annu. Rev. Plant Biol.* **64**, 637–663 (2023).

140. Vanlerberghe, G. C. & McIntosh, L. ALTERNATIVE OXIDASE: From Gene to Function. *Annu. Rev. Plant Physiol. Plant Mol. Biol.* **48**, 703–734 (2023).

141. Molnár, Á P. *et al*. Analysis of the Relationship between Alternative Respiration and Sterigmatocystin Formation in *Aspergillus nidulans*. *Toxins* **10**, 168 (2018).

142. Duvenage, L. *et al*. Inhibition of Classical and Alternative Modes of Respiration in *Candida albicans* Leads to Cell Wall Remodeling and Increased Macrophage Recognition. *mBio* **10**, 10.1128/mbio.02535–18 (2019).

143. Milani, G. *et al*. Respiratory chain network in mitochondria of *Candida parapsilosis:* ADP/O appraisal of the multiple electron pathways. *FEBS Lett.* **508**, 231–235 (2001).

144. Baishya, J. & Wakeman, C. A. Selective pressures during chronic infection drive microbial competition and cooperation. *npj Biofilms and Microbiomes* **5**, 16 (2019).

145. Morales, D. K. *et al*. Control of *Candida albicans* metabolism and biofilm formation by *Pseudomonas aeruginosa* phenazines. *mBio* **4**, 526 (2013).

146. Hoffman, L. R. *et al*. Nutrient Availability as a Mechanism for Selection of Antibiotic Tolerant *Pseudomonas aeruginosa* within the CF Airway. *PLOS Pathogens* **6**, e1000712 (2010).

147. Zhao, Y., Lim, J., Xu, J., Yu, J. & Zheng, W. Nitric oxide as a developmental and metabolic signal in filamentous fungi. *Mol. Microbiol.* **113**, 872–882 (2023).

148. Pradhan, A. *et al*. Anticipatory Stress Responses and Immune Evasion in Fungal Pathogens. *Trends Microbiol.* **29**, 416–427 (2023).

149. Black, B., Lee, C., Horianopoulos, L. C., Jung, W. H. & Kronstad, J. W. Respiring to infect: Emerging links between mitochondria, the electron transport chain, and fungal pathogenesis. *PLOS Pathogens* **17**, e1009661 (2021).

150. Aoki, S., Ito-Kuwa, S., Nakamura, Y. & Masuhara, T. Comparative Pathogenicity of a Wild-Type Strain and Respiratory Mutants of *Candida albicans* in Mice. *Zentralblatt für Bakteriologie* **273**, 332–343 (1990).

151. Shuna, C. *et al*. Inhibition of Respiration of *Candida albicans* by Small Molecules Increases Phagocytosis Efficacy by Macrophages. *mSphere* **5**, 10.1128/msphere.00016–20 (2020).

152. Grahl, N. *et al*. Mitochondrial Activity and Cyr1 Are Key Regulators of Ras1 Activation of *C. albicans* Virulence Pathways. *PLOS Pathogens* **11**, e1005133 (2015).

153. Lin, C. & Chen, Y. Conserved and Divergent Functions of the cAMP/PKA Signaling Pathway in *Candida albicans* and *Candida tropicalis*. *Journal of Fungi* **4** (2018).

154. Silao, F. G. S. *et al*. Mitochondrial proline catabolism activates Ras1/cAMP/PKA-induced filamentation in *Candida albicans*. *PLOS Genetics* **15**, e1007976 (2019).

155. Gupta, A. & Chattoo, B. B. Functional analysis of a novel ABC transporter ABC4 from *Magnaporthe grisea*. *FEMS Microbiol. Lett.* **278**, 22–28 (2008).

156. Urban, M., Bhargava, T. & Hamer, J. E. An ATP-driven efflux pump is a novel pathogenicity factor in rice blast disease. *EMBO J.* **18**, 512–521 (2023).

157. Wasi, M. *et al*. ABC Transporter Genes Show Upregulated Expression in Drug-Resistant Clinical Isolates of *Candida auris*: A Genome-Wide Characterization of ATP-Binding Cassette (ABC) Transporter Genes. *Frontiers in Microbiology* **10** (2019).

158. Zhang, Y. *et al*. Requirement for Ergosterol in V-ATPase Function Underlies Antifungal Activity of Azole Drugs. *PLOS Pathogens* **6**, e1000939 (2010).

159. Yan, Z. & Xu, J. Mitochondria are inherited from the MATa parent in crosses of the basidiomycete fungus *Cryptococcus neoformans*. *Genetics* **163**, 1315–1325 (2003).

160. Chang Andrew, L. & Doering Tamara, L. Maintenance of Mitochondrial Morphology in *Cryptococcus neoformans* Is Critical for Stress Resistance and Virulence. *mBio* **9**, 10.1128/mbio.01375–18 (2023).

161. Horianopoulos, L. C. & Kronstad, J. W. Connecting iron regulation and mitochondrial function in *Cryptococcus neoformans*. *Curr. Opin. Microbiol.* **52**, 7–13 (2019).

162. Ingavale, S. S. *et al*. Importance of Mitochondria in Survival of *Cryptococcus neoformans* Under Low Oxygen Conditions and Tolerance to Cobalt Chloride. *PLOS Pathogens* **4**, e1000155 (2008).

163. Duarte, M., Sousa, R. & Videira, A. Inactivation of genes encoding subunits of the peripheral and membrane arms of *neurospora* mitochondrial complex I and effects on enzyme assembly. *Genetics* **139**, 1211–1221 (1995).

164. Duarte, M. & Videira, A. Respiratory Chain Complex I Is Essential for Sexual Development in *Neurospora* and Binding of Iron Sulfur Clusters Are Required for Enzyme Assembly. *Genetics* **156**, 607–615 (2000).

165. Duarte, M., Mota, N., Pinto, L. & Videira, A. Inactivation of the gene coding for the 30.4-kDa subunit of respiratory chain NADH dehydrogenase: is the enzyme essential for *Neurospora*? *Molecular and General Genetics MGG* **257**, 368–375 (1998).

166. Harkness, T. A. A. *et al*. Disruption of the gene encoding the 78-kilodalton subunit of the peripheral arm of complex I in *Neurospora crassa* by repeat induced point mutation (RIP). *Curr. Genet.* **27**, 339–350 (1995).

167. Navarro-Espíndola, R., Suaste-Olmos, F. & Peraza-Reyes, L. Dynamic Regulation of Peroxisomes and Mitochondria during Fungal Development. *Journal of Fungi* **6** (2020).

168. Isabel, M., Dencher Norbert, A., Arnaldo, V. & Frank, K. Supramolecular Organization of the Respiratory Chain in *Neurospora crassa* Mitochondria. *Eukaryotic Cell* **6**, 2391–2405 (2023).

169. Krause, F. *et al*. Supramolecular Organization of Cytochrome c Oxidase- and Alternative Oxidase-dependent Respiratory Chains in the Filamentous Fungus *Podospora anserina**. *J. Biol. Chem.* **279**, 26453–26461 (2004).

170. Maas, M. F. P. M., Sellem, C. H., Krause, F., Dencher, N. A. & Sainsard-Chanet, A. Molecular Gene Therapy: Overexpression of the Alternative NADH Dehydrogenase NDI1 Restores Overall Physiology in a Fungal Model of Respiratory Complex I Deficiency. *J. Mol. Biol.* **399**, 31–40 (2010).

171. Chae, M. S. & Nargang, F. E. Investigation of regulatory factors required for alternative oxidase production in *Neurospora crassa*. *Physiol. Plantarum* **137**, 407–418 (2023).

172. Merryman, M., Crigler, J., Seipelt-Thiemann, R. & McClelland, E. A mutation in *C. neoformans* mitochondrial NADH dehydrogenase results in increased virulence in mice. *Virulence* **11**, 1366–1378 (2020).

173. Geißel, B., Penka, M., Neubauer, M. & Wagener, J. The ER-mitochondria encounter structure contributes to hyphal growth, mitochondrial morphology and virulence of the pathogenic mold *Aspergillus fumigatus*. *International Journal of Medical Microbiology* **307**, 37–43 (2017).

174. Enkler, L. *et al*. Arf1 coordinates fatty acid metabolism and mitochondrial homeostasis. *Nat. Cell Biol.* (2023).

175. Ruf, D., Brantl, V. & Wagener, J. Mitochondrial Fragmentation in *Aspergillus fumigatus* as Early Marker of Granulocyte Killing Activity. *Frontiers in Cellular and Infection Microbiology* **8** (2018).

176. Schertl, P. & Braun, H. Respiratory electron transfer pathways in plant mitochondria. *Frontiers in Plant Science* **5** (2014).

177. Braun, H. *et al*. The life of plant mitochondrial complex I. *Mitochondrion* **19**, 295–313 (2014).

178. Umbach, A. & Siedow, J. The Cyanide-Resistant Alternative Oxidases from the Fungi *Pichia stipitis* and *Neurospora crassa* Are Monomeric and Lack Regulatory Features of the Plant Enzyme. *Arch. Biochem. Biophys.* **378**, 234–45 (2000).

179. Huang, S. & Millar, A. H. Succinate dehydrogenase: the complex roles of a simple enzyme. *Curr. Opin. Plant Biol.* **16**, 344–349 (2013).

180. Millar, A. H. *et al*. Mitochondrial cytochrome c oxidase and succinate dehydrogenase complexes contain plant specific subunits. *Plant Mol. Biol.* **56**, 77–90 (2004).

181. Thomazella, D. P. T. *et al*. The hemibiotrophic cacao pathogen *Moniliophthora perniciosa* depends on a mitochondrial alternative oxidase for biotrophic development. *New Phytol.* **194**, 1025–1034 (2012).

182. Xu, T. *et al*. Involvement of alternative oxidase in the regulation of sensitivity of *Sclerotinia sclerotiorum* to the fungicides azoxystrobin and procymidone. *Journal of Microbiology* **51**, 352–358 (2013).

183. Szibor, M., Schenkl, C., Barsottini, M. R. O., Young, L. & Moore, A. L. Targeting the alternative oxidase (AOX) for human health and food security, a pharmaceutical and agrochemical target or a rescue mechanism? *Biochem. J.* **479**, 1337–1359 (2022).

184. Pandey, A. K., Samota, M. K., Kumar, A., Silva, A. S. & Dubey, N. K. Fungal mycotoxins in food commodities: present status and future concerns. *Frontiers in Sustainable Food Systems* **7**, 2571–2581 (2023).

185. Tian, F. *et al*. Effect of plant-based compounds on the antifungal and antiaflatoxigenic efficiency of strobilurins against *Aspergillus flavus*. *J. Hazard. Mater.* **415**, 125663 (2021).

186. Li-Jun Fu *et al*. Systemic Induction and Role of Mitochondrial Alternative Oxidase and Nitric Oxide in a Compatible Tomato–Tobacco mosaic virus Interaction. *MPMI* **23**, 39–48 (2023).

187. Keunen, E., Jozefczak, M., Remans, T., Vangronsveld, J. & Cuypers, A. Alternative respiration as a primary defence during cadmium-induced mitochondrial oxidative challenge in *Arabidopsis thaliana*. *Environ. Exp. Bot.* **91**, 63–73 (2013).

188. Oh, G. G. K., O'Leary, B. M., Signorelli, S. & Millar, A. H. Alternative oxidase (AOX) 1a and 1d limit proline-induced oxidative stress and aid salinity recovery in *Arabidopsis*. *Plant Physiol.* **188**, 1521–1536 (2022).

189. Simons, B. H., Millenaar, F. F., Mulder, L., Van Loon, L. C. & Lambers, H. Enhanced Expression and Activation of the Alternative Oxidase during Infection of Arabidopsis with Pseudomonas syringae pv tomato1. *Plant Physiol.* **120**, 529–538 (1999).

190. Zhang, L., Oh, Y., Li, H., Baldwin, I. T. & Galis, I. Alternative oxidase in resistance to biotic stresses: *Nicotiana attenuata* AOX contributes to resistance to a pathogen and a piercing-sucking insect but not *Manduca sexta* larvae. *Plant Physiol.* **160**, 1453–1467 (2012).

191. Cruz Avila-Adame & Wolfram Köller. Disruption of the Alternative Oxidase Gene in *Magnaporthe grisea* and Its Impact on Host Infection. *MPMI* **15**, 493–500 (2023).

192. Sierra-Campos, E., Velázquez, I., Matuz-Mares, D., Villavicencio-Queijeiro, A. & Pardo, J. P. Functional properties of the *Ustilago maydis* alternative oxidase under oxidative stress conditions. *Mitochondrion* **9**, 96–102 (2009).

193. Cárdenas-Monroy, C. A. *et al*. The mitochondrial alternative oxidase Aox1 is needed to cope with respiratory stress but dispensable for pathogenic development in *Ustilago maydis*. *PLOS ONE* **12**, e0173389 (2017).

194. Lin, Z., Wu, J., Jamieson, P. A. & Zhang, C. Alternative Oxidase Is Involved in the Pathogenicity, Development, and Oxygen Stress Response of *Botrytis cinerea*. *Phytopathology*® **109**, 1679–1688 (2019).

195. Fernández-Ortuño, D., Tores, J., Vicente, A. & Pérez-García, A. Mechanisms of resistance to QoI fungicides in phytopathogenic fungi. *International Microbiology* **11**, 1–9 (2008).

196. Oliveira, T. Y. K. *et al*. Evidence of Resistance to QoI Fungicides in Contemporary Populations of *Mycosphaerella fijiensis, M. musicola* and *M. thailandica* from Banana Plantations in Southeastern Brazil. *Agronomy* **12** (2022).

197. Sautua, F. J. & Carmona, M. A. Detection and characterization of QoI resistance in *Pyrenophora tritici-repentis* populations causing tan spot of wheat in Argentina. *Plant Pathol.* **70**, 2125–2136 (2021).

198. Miguez, M., Reeve, C., Wood, P. M. & Hollomon, D. W. Alternative oxidase reduces the sensitivity of *Mycosphaerella graminicola* to QOI fungicides. *Pest Manag. Sci.* **60**, 3–7 (2023).

199. Kaneko, I. & Ishii, H. Effect of azoxystrobin on activities of antioxidant enzymes and alternative oxidase in wheat head blight pathogens *Fusarium graminearum* and *Microdochium nivale*. *Journal of General Plant Pathology* **75**, 388–398 (2009).

200. Li, S., Li, X., Zhang, H., Wang, Z. & Xu, H. The research progress in and perspective of potential fungicides: Succinate dehydrogenase inhibitors. *Bioorg. Med. Chem.* **50**, 116476 (2021).

201. Chen, W. *et al*. Resistance risk assessment for a novel succinate dehydrogenase inhibitor pydiflumetofen in *Fusarium asiaticum*. *Pest Manag. Sci.* **77**, 538–547 (2021).

202. Avenot, H. F. & Michailides, T. J. Progress in understanding molecular mechanisms and evolution of resistance to succinate dehydrogenase inhibiting (SDHI) fungicides in phytopathogenic fungi. *Crop Protection* **29**, 643–651 (2010).

203. Karelov, A. *et al*. Wheat Genes Associated with Different Types of Resistance against Stem Rust (*Puccinia graminis Pers.*). *Pathogens* **11** (2022).

204. Cullis, C. A. in *Genetics and Genomics of Linum* (ed Cullis, C. A.) 215–225 (Springer International Publishing, Cham, 2019).

205. Shamima, A. *et al*. Role of Alternative Oxidase Gene in Pathogenesis of *Cryptococcus neoformans*. *Infect. Immun.* **71**, 5794–5802 (2003).

206. Martins Vicente, P. *et al*. Involvement of an Alternative Oxidase in Oxidative Stress and Mycelium-to-Yeast Differentiation in *Paracoccidioides brasiliensis*. *Eukaryotic Cell* **10**, 237–248 (2011).

207. Hernández Ruiz, O. *et al*. Alternative Oxidase Mediates Pathogen Resistance in *Paracoccidioides brasiliensis* Infection. *PLOS Neglected Tropical Diseases* **5**, e1353 (2011).

208. Grahl, N., Dinamarco, T. M., Willger, S. D., Goldman, G. H. & Cramer, R. A. *Aspergillus fumigatus* mitochondrial electron transport chain mediates oxidative stress homeostasis, hypoxia responses and fungal pathogenesis. *Mol. Microbiol.* **84**, 383–399 (2012).

209. Magnani, T. *et al*. Silencing of mitochondrial alternative oxidase gene of *Aspergillus fumigatus* enhances reactive oxygen species production and killing of the fungus by macrophages. *J. Bioenerg. Biomembr.* **40**, 631–636 (2008).

210. Del-Saz, N. *et al*. An In Vivo Perspective of the Role(s) of the Alternative Oxidase Pathway. *Trends Plant Sci.* **23**, 206–219 (2023).

211. McDonald, A. E. & Gospodaryov, D. V. Alternative NAD(P)H dehydrogenase and alternative oxidase: Proposed physiological roles in animals. *Mitochondrion* **45**, 7–17 (2019).

212. Copsey, A. C. *et al*. Kinetic characterisation and inhibitor sensitivity of *Candida albicans* and *Candida auris* recombinant AOX expressed in a self-assembled proteoliposome system. *Sci. Rep.* **11**, 14748–3 (2021).

213. Duvenage, L. *et al*. Alternative oxidase induction protects *Candida albicans* from respiratory stress and promotes hyphal growth. *bioRxiv*, 405670 (2018).

214. Wang, T., Xie, X., Li, K., Deng, Y. & Chen, H. Alternative Oxidase Promotes Biofilm Formation of *Candida albicans*. *Current Medical Science* **38**, 443–448 (2018).

215. Yan, L. *et al*. The alternative oxidase of *Candida albicans* causes reduced fluconazole susceptibility. *J. Antimicrob. Chemother.* **64**, 764–773 (2009).

216. Liu, Z. *et al*. Multifactor transcriptional control of alternative oxidase induction integrates diverse environmental inputs to enable fungal virulence. *Nature Communications* **14**, 4528 (2023).

217. Ittarat, I., Asawamahasakda, W., Bartlett, M. S., Smith, J. W. & Meshnick, S. R. Effects of atovaquone and other inhibitors on *Pneumocystis carinii* dihydroorotate dehydrogenase. *Antimicrob. Agents Chemother.* **39**, 325–328 (1995).

218. Merali, S., Vargas, D., Franklin, M. & Clarkson, A. B. J. S-adenosylmethionine and *Pneumocystis carinii*. *J. Biol. Chem.* **275**, 14958–14963 (2000).

219. Gabaldón, T. & Carreté, L. The birth of a deadly yeast: tracing the evolutionary emergence of virulence traits in *Candida glabrata*. *FEMS Yeast Res* **16**, fov110 (2016).

220. Apostolopoulou, A. & Fishman, J. A. The Pathogenesis and Diagnosis of *Pneumocystis jiroveci* Pneumonia. *Journal of Fungi* **8** (2022).

221. Badiee, P., Rezapour, A., Abbasian, A., Foroutan, H. R. & Jafarian, H. Prevalence of colonization and mitochondrial large subunit rRNA mutation of *Pneumocystis jiroveci* among Iranian children. *Iran. J. Microbiol.* **8**, 326–330 (2016).

222. Clarkson, A. B. C., J., Bienen, E. J., Pollakis, G. & Grady, R. W. Respiration of Bloodstream Forms of the Parasite *Trypanosoma brucei brucei* Is Dependent on a Plant-like Alternative Oxidase *. *J. Biol. Chem.* **264**, 17770–17776 (1989).

223. Shiba, T. *et al*. Structure of the trypanosome cyanide-insensitive alternative oxidase. *Proceedings of the National Academy of Sciences* **110**, 4580–4585 (2023).

224. Menzies, S. K., Tulloch, L. B., Florence, G. J. & Smith, T. K. The trypanosome alternative oxidase: a potential drug target? *Parasitology* **145**, 175–183 (2018).

225. Goughenour, K. D. *et al*. Murine Inducible Nitric Oxide Synthase Expression Is Essential for Antifungal Defenses in Kidneys during Disseminated *Cryptococcus deneoformans* Infection. *J. Immunol.* **207**, 2096–2106 (2021).

226. Millar, A. H. & Day, D. A. Nitric oxide inhibits the cytochrome oxidase but not the alternative oxidase of plant mitochondria. *FEBS Lett.* **398**, 155–158 (1996).

227. Bai, Z., Harvey, L. M. & McNeil, B. Physiological responses of chemostat cultures of *Aspergillus niger* (B1-D) to simulated and actual oxidative stress. *Biotechnol. Bioeng.* **82**, 691–701 (2023).

228. Kot, E. J., Olson, V. L., Rolewic, L. J. & McClary, D. O. An alternate respiratory pathway in *Candida albicans*. *Antonie Van Leeuwenhoek* **42**, 33–48 (1976).

229. Nasrin, F. Study of Antimicrobial and Antioxidant Potentiality of Anti-diabetic Drug Metformin. *International Journal of Pharmaceutics and Drug Analysis* **2**, 220–224 (2014).

230. Mascaraque, V., Navas, C., Hernaéz, M. L., Gil, C. & Molero, G. R. 2. Proteomic study of the effect of metformin on *C. albicans*. *Access Microbiology,* **3**, po0078.

231. Meherunisa, Jaiswal, S. & Seth, V. Study of Metformin Effect on Antimicrobial Property. *Int Arch BioMed Clin Res* **4** (2023).

232. Pernicova, I. & Korbonits, M. Metformin—mode of action and clinical implications for diabetes and cancer. *Nature Reviews Endocrinology* **10**, 143–156 (2014).

233. Liu, W. *et al*. Beneficial Effects of Gracillin From Rhizoma Paridis Against Gastric Carcinoma via the Potential TIPE2-Mediated Induction of Endogenous Apoptosis and Inhibition of Migration in BGC823 Cells. *Frontiers in Pharmacology* **12** (2021).

234. Li, Y. *et al*. Gracillin Shows Potential Efficacy Against Non-Small Cell Lung Cancer Through Inhibiting the mTOR Pathway. *Frontiers in Oncology* **12** (2022).

235. Zhang, X. *et al*. Synthesis and Antifungal Activities of New Type β-Methoxyacrylate-Based Strobilurin Analogues. *Chin. J. Chem.* **30**, 1517–1524 (2023).

236. Gao, A. *et al*. Azoxystrobin, a mitochondrial complex III Qo site inhibitor, exerts beneficial metabolic effects in vivo and in vitro. *Biochimica et Biophysica Acta (BBA) - General Subjects* **1840**, 2212–2221 (2014).

237. Bhattacharya, K. *et al*. Mahanine, a novel mitochondrial complex-III inhibitor induces G0/G1 arrest through redox alteration-mediated DNA damage response and regresses glioblastoma multiforme. *Am. J. Cancer. Res.* **4**, 629–647 (2014).

238. Georgios, C., Lewis Russell, E. & Kontoyiannis Dimitrios, P. Inhibition of *Candida parapsilosis* Mitochondrial Respiratory Pathways Enhances Susceptibility to Caspofungin. *Antimicrob. Agents Chemother.* **50**, 744–747 (2023).

239. Chen, H. *et al*. Azoxystrobin Reduces Oral Carcinogenesis by Suppressing Mitochondrial Complex III Activity and Inducing Apoptosis. *Cancer Management and Research* **12**, 11573–11583 (2020).

240. Takahashi, S., Shinomiya, T. & Nagahara, Y. Azoxystrobin Induces Apoptosis and Cell Cycle Arrest in Human Leukemia Cells Independent of p53 Expression. *Anticancer Res.* **42**, 1307 (2022).

241. Kapur, A. *et al*. Atovaquone: An Inhibitor of Oxidative Phosphorylation as Studied in Gynecologic Cancers. *Cancers* **14** (2022).

242. Luo, M. *et al*. Bedaquiline inhibits the yeast and human mitochondrial ATP synthases. *Communications Biology* **3**, 452 (2020).

243. Symersky, J., Osowski, D., Walters, D. E. & Mueller, D. M. Oligomycin frames a common drug-binding site in the ATP synthase. *Proceedings of the National Academy of Sciences* **109**, 13961–13965 (2023).

244. Mackieh, R. *et al*. Inhibitors of ATP Synthase as New Antibacterial Candidates. *Antibiotics* **12**, 650 (2023).

245. Hendrickson, J. A., Hu, C., Aitken, S. L. & Beyda, N. Antifungal Resistance: a Concerning Trend for the Present and Future. *Curr. Infect. Dis. Rep.* **21**, 47 (2019).

246. Shannon, K. *et al*. Antifungal Resistance Trends of *Candida auris* Clinical Isolates in New York and New Jersey from 2016 to 2020. *Antimicrob. Agents Chemother.* **66**, 2242 (2022).

247. Gonçalves, S. S., Souza, A. C. R., Chowdhary, A., Meis, J. F. & Colombo, A. L. Epidemiology and molecular mechanisms of antifungal resistance in *Candida* and *Aspergillus*. *Mycoses* **59**, 198–219 (2016).

248. Rex, J. H., Cooper, C. R., Merz, W. G., Galgiani, J. N. & Anaissie, E. J. Detection of amphotericin B-resistant *Candida* isolates in a broth-based system. *Antimicrob. Agents Chemother.* **39**, 906–909 (1995).

249. Patrick, V. *et al*. Mechanisms of Azole Resistance in a Clinical Isolate of *Candida tropicalis*. *Antimicrob. Agents Chemother.* **49**, 4608–4615 (2005).

250. Forastiero, A. *et al*. *Candida tropicalis* Antifungal Cross-Resistance Is Related to Different Azole Target (Erg11p) Modifications. *Antimicrob. Agents Chemother.* **57**, 4769–4781 (2013).

251. Kelly, S. L. *et al*. Resistance to fluconazole and cross-resistance to amphotericin B in *Candida albicans* from AIDS patients caused by defective sterol Δ5,6-desaturation. *FEBS Lett.* **400**, 80–82 (2023).

252. Whaley, S. G. *et al*. Azole Antifungal Resistance in *Candida albicans* and Emerging Non-albicans *Candida* Species. *Frontiers in Microbiology* **7**, 2173 (2017).

253. Young Laura, Y., Hull Christina, M. & Joseph, H. Disruption of Ergosterol Biosynthesis Confers Resistance to Amphotericin B in *Candida lusitaniae*. *Antimicrob. Agents Chemother.* **47**, 2717–2724 (2003).

254. Scott Nancy, E., Edwin, E. S., Kline Susan, E. & Anna, S. Rapid Evolution of Multidrug Resistance in a *Candida lusitaniae* Infection during Micafungin Monotherapy. *Antimicrob. Agents Chemother.* **0**, 543 (2023).

255. Su, S. *et al*. The antifungal activity of caspofungin in combination with antifungals or non-antifungals against *Candida* species in vitro and in clinical therapy. *Expert Review of Anti-infective Therapy* **20**, 161–178 (2022).

256. Colley, T. *et al*. Antifungal synergy of a topical triazole, PC945, with a systemic triazole against respiratory *Aspergillus fumigatus* infection. *Scientific Reports* **9**, 9482 (2019).

257. Perfect, J. R. *et al*. Clinical Practice Guidelines for the Management of Cryptococcal Disease: 2010 Update by the Infectious Diseases Society of America. *Clin. Infect. Dis.* **50**, 291–322 (2010).

258. Iyer, K. R., Revie, N. M., Fu, C., Robbins, N. & Cowen, L. E. Treatment strategies for cryptococcal infection: challenges, advances and future outlook. *Nature Reviews Microbiology* **19**, 454–466 (2021).

259. Vincent, B. M. *et al*. A Fungal-Selective Cytochrome bc1 Inhibitor Impairs Virulence and Prevents the Evolution of Drug Resistance. *Cell Chemical Biology* **23**, 978–991 (2023).

260. Shi, J., Li, S., Gao, A., Zhu, K. & Zhang, H. Tetrandrine enhances the antifungal activity of fluconazole in a murine model of disseminated candidiasis. *Phytomedicine* **46**, 21–31 (2018).

261. Li, L. *et al*. The Synergism of the Small Molecule ENOblock and Fluconazole Against Fluconazole-Resistant Candida albicans. *Frontiers in Microbiology* **10**, 2071 (2019).

262. Li, Q. *et al*. Oxidative stress in fungal fermentation processes: the roles of alternative respiration. *Biotechnol. Lett.* **33**, 457–467 (2011).

263. Szibor, M. *et al*. Bioenergetic consequences from xenotopic expression of a tunicate AOX in mouse mitochondria: Switch from RET and ROS to FET. *Biochim. Biophys. Acta Bioenerg.* **1861**, 148137 (2020).

264. Cao, R. *et al*. The germination of fungal spores in water and enhanced their resistance to chlor(am)ine: Characteristics and mechanisms. *Chem. Eng. J.* **454**, 140184 (2023).

265. Jarmuszkiewicz, W., Hryniewiecka, L. & Sluse, F. E. The Effect of pH on the Alternative Oxidase Activity in Isolated *Acanthamoeba castellanii* Mitochondria. *J. Bioenerg. Biomembr.* **34**, 221–226 (2002).

266. Vanlerberghe, G. C. Alternative Oxidase: A Mitochondrial Respiratory Pathway to Maintain Metabolic and Signaling Homeostasis during Abiotic and Biotic Stress in Plants. *International Journal of Molecular Sciences* **14**, 6847 (2013).

267. El-Khoury, R. *et al*. Engineering the alternative oxidase gene to better understand and counteract mitochondrial defects: state of the art and perspectives. *Br. J. Pharmacol.* **171**, 2243–2249 (2023).

268. Hoenigl, M. *et al*. The Antifungal Pipeline: Fosmanogepix, Ibrexafungerp, Olorofim, Opelconazole, and Rezafungin. *Drugs* **81**, 1703–1729 (2021).

269. Jim, K. *et al*. Adaptation of *Cryptococcus neoformans* to Mammalian Hosts: Integrated Regulation of Metabolism and Virulence. *Eukaryotic Cell* **11**, 109–118 (2012).

270. Tezcan, E. F., Demirtas, Y., Cakar, Z. P. & Ulgen, K. O. Comprehensive genome-scale metabolic model of the human pathogen Cryptococcus neoformans: A platform for understanding pathogen metabolism and identifying new drug targets. *Frontiers in Bioinformatics* **3** (2023).

271. Chun, C. D. & Madhani, H. D. Applying genetics and molecular biology to the study of the human pathogen *Cryptococcus neoformans*. *Methods Enzymol.* **470**, 797–831 (2010).

272. Lee, K. *et al*. Systematic functional analysis of kinases in the fungal pathogen *Cryptococcus neoformans*. *Nat. Commun.* **7**, 12766 (2016).

273. Lee, H., Khanal Lamichhane, A., Garraffo, H. M., Kwon-Chung, K. & Chang, Y. C. Involvement of PDK1, PKC and TOR signalling pathways in basal fluconazole tolerance in *Cryptococcus neoformans*. *Mol. Microbiol.* **84**, 130–146 (2012).

274. Doyle, K. in *Investigating metabolic dysfunction in a Saccharomyces cerevisiae model of SOD1-associated amyotrophic lateral sclerosis* (University of Kent (United Kingdom), 2022).

275. Champion, O. L., Titball, R. W. & Bates, S. Standardization of *G. mellonella* Larvae to Provide Reliable and Reproducible Results in the Study of Fungal Pathogens. *J. Fungi (Basel)* **4**, 108. doi: 10.3390/jof4030108 (2018).

276. Loh, J. M. S., Adenwalla, N., Wiles, S. & Proft, T. *Galleria mellonella* larvae as an infection model for group A streptococcus. *Virulence* **4**, 419–428 (2013).

277. O'Reilly, M. *et al*. Gentamicin Affects the Bioenergetics of Isolated Mitochondria and Collapses the Mitochondrial Membrane Potential in Cochlear Sensory Hair Cells. *Front. Cell. Neurosci.* **13**, 416 (2019).

278. McDonald, A. E. & Vanlerberghe, G. C. Branched Mitochondrial Electron Transport in the Animalia: Presence of Alternative Oxidase in Several Animal Phyla. *IUBMB Life* **56**, 333–341 (2023).

279. Altschul, S. F., Gish, W., Miller, W., Myers, E. W. & Lipman, D. J. Basic local alignment search tool. *J. Mol. Biol.* **215**, 403–410 (1990).

280. Altschul, S. F. *et al*. Gapped BLAST and PSI-BLAST: a new generation of protein database search programs. *Nucleic Acids Res.* **25**, 3389–3402 (1997).

281. Tamura, K., Stecher, G. & Kumar, S. MEGA11: Molecular Evolutionary Genetics Analysis Version 11. *Mol. Biol. Evol.* **38**, 3022–3027 (2021).

282. Ciccarelli, F. D. *et al*. Toward automatic reconstruction of a highly resolved tree of life. *Science* **311**, 1283–1287 (2006).

283. Madeira, F. *et al*. Search and sequence analysis tools services from EMBL-EBI in 2022. *Nucleic Acids Res.* **50**, W276–W279 (2022).

284. Statzell-Tallman, A., Belloch, C. & Fell, J. W. *Kwoniella mangroviensis* gen. nov., sp.nov. (*Tremellales, Basidiomycota*), a teleomorphic yeast from mangrove habitats in the Florida Everglades and Bahamas. *FEMS Yeast Res.* **8**, 103–113 (2008).

285. Gomes, F. C. O., Safar, S. V. B., Santos, A. R. O., Lachance, M. & Rosa, C. A. *Kockovaella libkindii* sp. nov., a yeast species isolated from water tanks of bromeliad. *Int. J. Syst. Evol. Microbiol.* **66**, 5066–5069 (2016).

286. The, U. C. UniProt: the universal protein knowledgebase in 2021. *Nucleic Acids Res.* **49**, D480–D489 (2021).

287. Yang, J. *et al*. The I-TASSER Suite: protein structure and function prediction. *Nat. Methods* **12**, 7–8 (2015).

288. Roy, A., Kucukural, A. & Zhang, Y. I-TASSER: a unified platform for automated protein structure and function prediction. *Nature Protocols* **5**, 725–738 (2010).

289. Zhang, Y. I-TASSER server for protein 3D structure prediction. *BMC Bioinformatics* **9**, 40 (2008).

290. Niles, B. J., Joslin, A. C., Fresques, T. & Powers, T. TOR Complex 2-Ypk1 Signaling Maintains Sphingolipid Homeostasis by Sensing and Regulating ROS Accumulation. *Cell Reports* **6**, 541–552 (2014).

291. Niles, B. J. & Powers, T. TOR complex 2–Ypk1 signaling regulates actin polarization via reactive oxygen species. *Mol. Biol. Cell* **25**, 3962–3972 (2014).

292. Rego, A., Mendes, F., Costa, V., Chaves, S. R. & Côrte-Real, M. Pkh1p-Ypk1p and Pkh1p-Sch9p Pathways Are Activated by Acetic Acid to Induce a Mitochondrial-Dependent Regulated Cell Death. *Oxidative Medicine and Cellular Longevity* **2020**, 7095078 (2020).

293. Wolf, D. G. *et al*. Multidrug-resistant *Trichosporon asahii* infection of nongranulocytopenic patients in three intensive care units. *J. Clin. Microbiol.* **39**, 4420–4425 (2001).

294. Salvador López, J. M., Vandeputte, M. & Van Bogaert, I. N. A. Oleaginous yeasts: Time to rethink the definition? *Yeast* **39**, 553–606 (2022).

295. Yaguchi, A. *et al*. Identification of oleaginous yeasts that metabolize aromatic compounds. *J. Ind. Microbiol. Biotechnol.* **47**, 801–813 (2020).

296. Hommel, B. *et al*. *Cryptococcus neoformans* resists to drastic conditions by switching to viable but non-culturable cell phenotype. *PLOS Pathogens* **15**, e1007945 (2019).

297. Ma, X. *et al*. Mitochondrial electron transport chain complex III is required for antimycin A to inhibit autophagy. *Chem. Biol.* **18**, 1474–1481 (2011).

298. Hommel, B. *et al*. Cryptococcus neoformans resists to drastic conditions by switching to viable but non-culturable cell phenotype. *PLOS Pathogens* **15**, e1007945 (2019).

299. Muir, A., Ramachandran, S., Roelants, F. M., Timmons, G. & Thorner, J. TORC2-dependent protein kinase Ypk1 phosphorylates ceramide synthase to stimulate synthesis of complex sphingolipids. *Elife* **3**, 10.7554/eLife.03779 (2014).

300. Kihara, A., Mitsutake, S., Mizutani, Y. & Igarashi, Y. Metabolism and biological functions of two phosphorylated sphingolipids, sphingosine 1-phosphate and ceramide 1-phosphate. *Prog. Lipid Res.* **46**, 126–144 (2007).

301. Kim, S., Fyrst, H. & Saba, J. Accumulation of Phosphorylated Sphingoid Long Chain Bases Results in Cell Growth Inhibition in *Saccharomyces cerevisiae*. *Genetics* **156**, 1519–1529 (2000).

302. Mrad, M., Bou Dargham, T., Moumneh, M. B. & Dbaibo, G. in *Handbook of Cancer and Immunology* 1–19 (Springer, 2022).

303. Quinville, B. M., Deschenes, N. M., Ryckman, A. E. & Walia, J. S. A comprehensive review: sphingolipid metabolism and implications of disruption in sphingolipid homeostasis. *International journal of molecular sciences* **22**, 5793 (2021).

304. Mizutani, Y., Kihara, A. & Igarashi, Y. Identification of the human sphingolipid C4-hydroxylase, hDES2, and its up-regulation during keratinocyte differentiation. *FEBS Lett.* **563**, 93–97 (2004).

305. Turpin-Nolan, S. M. & Brüning, J. C. The role of ceramides in metabolic disorders: when size and localization matters. *Nature Reviews Endocrinology* **16**, 224–233 (2020).

306. Uchida, Y. Ceramide signaling in mammalian epidermis. *Biochim. Biophys. Acta* **1841**, 453–462 (2014).

307. Munshi, M. A. *et al*. The role of ceramide synthases in the pathogenicity of *Cryptococcus neoformans*. *Cell reports* **22**, 1392–1400 (2018).

308. Singh, A., MacKenzie, A., Girnun, G. & Del Poeta, M. Analysis of sphingolipids, sterols, and phospholipids in human pathogenic *Cryptococcus* strains [S]. *J. Lipid Res.* **58** (2017).

309. Rhome, R. *et al*. Biosynthesis and immunogenicity of glucosylceramide in *Cryptococcus neoformans* and other human pathogens. *Eukaryotic cell* **6**, 1715–1726 (2007).

310. Loftus, B. J. *et al*. The genome of the basidiomycetous yeast and human pathogen *Cryptococcus neoformans*. *Science* **307**, 1321–1324 (2005).

311. Ryan, R. *et al*. Biosynthesis and Immunogenicity of Glucosylceramide in *Cryptococcus neoformans* and Other Human Pathogens. *Eukaryotic Cell* **6**, 1715–1726 (2007).

312. Usmani, S. A. *et al*. Beyond membrane components: uncovering the intriguing world of fungal sphingolipid synthesis and regulation. *Res. Microbiol.* **174**, 104087 (2023).

313. Geeraert, L., Mannaerts, G. P. & van Veldhoven, P. P. Conversion of dihydroceramide into ceramide: involvement of a desaturase. *Biochem. J.* **327 (Pt 1)**, 125–132 (1997).

314. Baker, R. P., Chrissian, C., Stark, R. E. & Casadevall, A. *Cryptococcus neoformans* melanization incorporates multiple catecholamines to produce polytypic melanin. *J. Biol. Chem.* **298**, 101519 (2022).

315. Megyeri, M. *et al*. Yeast ceramide synthases, Lag1 and Lac1, have distinct substrate specificity. *J. Cell. Sci.* **132**, jcs228411 (2019).

316. Roelants, F. M., Torrance, P. D. & Thorner, J. R. 2. Differential roles of PDK1- and PDK2-phosphorylation sites in the yeast AGC kinases Ypk1, Pkc1 and Sch9. *Microbiology* **150**, 3289–3304.

317. Thorner, J. TOR complex 2 is a master regulator of plasma membrane homeostasis. *Biochem. J.* **479**, 1917–1940 (2022).

318. Williamson, P. R. Biochemical and molecular characterization of the diphenol oxidase of *Cryptococcus neoformans*: identification as a laccase. *J. Bacteriol.* **176**, 656–664 (1994).

319. Salas, S. D., Bennett, J. E., Kwon-Chung, K., Perfect, J. R. & Williamson, P. R. Effect of the laccase gene CNLAC1, on virulence of *Cryptococcus neoformans*. *J. Exp. Med.* **184**, 377–386 (1996).

320. Walton, F. J., Idnurm, A. & Heitman, J. Novel gene functions required for melanization of the human pathogen *Cryptococcus neoformans*. *Mol. Microbiol.* **57**, 1381–1396 (2005).

321. Zaragoza, O. Basic principles of the virulence of *Cryptococcus*. *Virulence* **10**, 490–501 (2019).

322. Coelho, C., Bocca, A. L. & Casadevall, A. The Intracellular Life of *Cryptococcus neoformans*. *Annu. Rev. Pathol. Mech. Dis.* **9**, 219–238 (2014).

323. Shea, J. M., Henry, J. L. & Del Poeta, M. Lipid metabolism in *Cryptococcus neoformans*. *FEMS Yeast Res* **6**, 469–479 (2006).

324. Jung, W. H., Sánchez-León, E. & Kronstad, J. W. Coordinated regulation of iron metabolism in *Cryptococcus neoformans* by GATA and CCAAT transcription factors: connections with virulence. *Curr. Genet.* **67**, 583–593 (2021).

325. Toplis, B. *et al*. A link between urease and polyamine metabolism in *Cryptococcus neoformans*. *Microb. Pathog.* **158**, 105076 (2021).

326. Yu, C. *et al*. Landscape of gene expression variation of natural isolates of *Cryptococcus neoformans* in response to biologically relevant stresses. *Microb. Genom.* **6**, e000319. doi: 10.1099/mgen.0.000319 (2020).

327. Robert, C., O'Neill Eric, B. & Shuqun, S. Assimilation of Xylose, Mannose, and Mannitol for Synthesis of Glucuronoxylomannan of Cryptococcus neoformansDetermined by 13C Nuclear Magnetic Resonance Spectroscopy. *Infect. Immun.* **66**, 2996–2998 (1998).

328. Ngamskulrungroj, P., Chang, Y., Roh, J. & Kwon-Chung, K. Differences in Nitrogen Metabolism between Cryptococcus neoformans and C. gattii, the Two Etiologic Agents of Cryptococcosis. *PLOS ONE* **7**, e34258 (2012).

329. Lee, S. *et al*. Microbiological safety of processed meat products formulated with low nitrite concentration — A review. *Asian-Australas J Anim Sci* **31**, 1073–1077 (2018).

330. Hu, G., Cheng, P., Sham, A., Perfect, J. R. & Kronstad, J. W. Metabolic adaptation in Cryptococcus neoformans during early murine pulmonary infection. *Mol. Microbiol.* **69**, 1456–1475 (2008).

331. Schmitz, K., Protzko, R., Zhang, L. & Benz, J. P. Spotlight on fungal pectin utilization—from phytopathogenicity to molecular recognition and industrial applications. *Appl. Microbiol. Biotechnol.* **103**, 2507–2524 (2019).

332. Lee, K. -., Gimore, D. F. & Huss, M. J. Fungal Degradation of the Bioplastic PHB (Poly-3-hydroxy-butyric acid). *Journal of Polymers and the Environment* **13**, 213–219 (2005).

333. Ruma-Haynes, P., Brownlee, A. G. & Sorrell, T. C. A rapid method for detecting extracellular proteinase activity in Cryptococcus neoformans and a survey of 63 isolates. *Journal of Medical Microbiology,* **49**, 733–737 (2000).

334. Calvete, C. L. *et al*. Amino acid permeases in *Cryptococcus neoformans* are required for high temperature growth and virulence; and are regulated by Ras signaling. *PLoS One* **14**, e0211393 (2019).

335. Garbe, E. & Vylkova, S. Role of Amino Acid Metabolism in the Virulence of Human Pathogenic Fungi. *Current Clinical Microbiology Reports* **6**, 108–119 (2019).

336. Kwak, M., Liu, R. & Kang, S. Antimicrobial activity of cyclic dipeptides produced by *Lactobacillus plantarum* LBP-K10 against multidrug-resistant bacteria, pathogenic fungi, and *influenza A* virus. *Food Control* **85**, 223–234 (2018).

337. Kwak, M. *et al*. Cyclic dipeptides from lactic acid bacteria inhibit the proliferation of pathogenic fungi. *Journal of Microbiology* **52**, 64–70 (2014).

338. Castaldi, S., Cimmino, A., Masi, M. & Evidente, A. Bacterial Lipodepsipeptides and Some of Their Derivatives and Cyclic Dipeptides as Potential Agents for Biocontrol of Pathogenic Bacteria and Fungi of Agrarian Plants. *J. Agric. Food Chem.* **70**, 4591–4598 (2022).

339. Rai, N., Rathore, S., Tiwari, R. T., Patil, S. & Gajbhiye, A. Synthesis, Characterization and Pharmacological Evaluation of Ultra Short Dipeptides as Antimicrobial and Anticancer Agents. *International Journal of Pharmaceutical Investigation* **13** (2023).

340. Poonia, B. K., Sidhu, A. & Sharma, A. B. Cyclo(l-proline-l-serine) Dipeptide Suppresses Seed Borne Fungal Pathogens of Rice: Altered Cellular Membrane Integrity of Fungal Hyphae and Seed Quality Benefits. *J. Agric. Food Chem.* **70**, 2160–2168 (2022).

341. Lev, S. *et al*. The PHO signaling pathway directs lipid remodeling in *Cryptococcus neoformans* via DGTS synthase to recycle phosphate during phosphate deficiency. *PLOS ONE* **14**, e0212651 (2019).

342. Washington, E. J. *et al*. Structures of trehalose-6-phosphate synthase, Tps1, from the fungal pathogen *Cryptococcus neoformans*: a target for novel antifungals. *bioRxiv*, 2023.03.14.530545 (2023).

343. Benaroudj, N., Lee, D. H. & Goldberg, A. L. Trehalose Accumulation during Cellular Stress Protects Cells and Cellular Proteins from Damage by Oxygen Radicals *. *J. Biol. Chem.* **276**, 24261–24267 (2023).

344. Crowe, J. H., Crowe, L. M., Carpenter, J. F. & Aurell Wistrom, C. Stabilization of dry phospholipid bilayers and proteins by sugars. *Biochem. J.* **242**, 1–10 (1987).

345. Crowe, C., Crowe, C. & Chapman, C. Preservation of Membranes in Anhydrobiotic Organisms: The Role of Trehalose. *Science* **223**, 701–703 (2023).

346. Fernandez, O., Béthencourt, L., Quero, A., Sangwan, R. S. & Clément, C. Trehalose and plant stress responses: friend or foe? *Trends Plant Sci.* **15**, 409–417 (2023).

347. Hottiger, T., De Virgilio, C., Hall, M. N., Boller, T. & Wiemken, A. The role of trehalose synthesis for the acquisition of thermotolerance in yeast. *European Journal of Biochemistry* **219**, 187–193 (1994).

348. Steen, B. R. *et al*. *Cryptococcus neoformans* Gene Expression during Experimental Cryptococcal Meningitis. *Eukaryotic Cell* **2**, 1336–1349 (2003).

349. Petzold, E. W. *et al*. Characterization and Regulation of the Trehalose Synthesis Pathway and Its Importance in the Pathogenicity of Cryptococcus neoformans. *Infect. Immun.* **74**, 5877–5887 (2006).

350. Levitz, S. M., Harrison, T. S., Tabuni, A. & Liu, X. Chloroquine induces human mononuclear phagocytes to inhibit and kill *Cryptococcus neoformans* by a mechanism independent of iron deprivation. *J. Clin. Invest.* **100**, 1640–1646 (1997).

351. Nessa, K., Gross, N. T., Jarstrand, C., Johansson, A. & Camner, P. In vivo interaction between alveolar macrophages and *Cryptococcus neoformans*. *Mycopathologia* **139**, 1–7 (1997).

352. DeLeon-Rodriguez, C. & Casadevall, A. *Cryptococcus neoformans*: Tripping on Acid in the Phagolysosome. *Frontiers in Microbiology* **7** (2016).

353. Stanojevic, D., Comic, L. J., Stefanovic, O. & Solujic-Sukdolak, S. Antimicrobial effects of sodium benzoate, sodium nitrite and potassium sorbate and their synergistic action in vitro. *Bulgarian Journal of Agricultural Science* **15**, 307–311 (2009).

354. Fraqueza, M. J., Laranjo, M., Elias, M. & Patarata, L. Microbiological hazards associated with salt and nitrite reduction in cured meat products: control strategies based on antimicrobial effect of natural ingredients and protective microbiota. *Current Opinion in Food Science* **38**, 32–39 (2021).

355. Ramachandraiah, K. & Chin, K. B. Antioxidant, Antimicrobial, and Curing Potentials of Micronized Celery Powders added to Pork Sausages. *Food Sci. Anim. Resour.* **41**, 110–121 (2021).

356. Nandi, A., Yan, L., Jana, C. K. & Das, N. Role of Catalase in Oxidative Stress- and Age-Associated Degenerative Diseases. *Oxid Med. Cell. Longev* **2019**, 9613090 (2019).

357. Rossman, M. J. *et al*. Inorganic Nitrite Supplementation Improves Endothelial Function With Aging. *Hypertension* **77**, 1212–1222 (2023).

358. Parthasarathy, D. K. & Bryan, N. S. Sodium nitrite: The “cure” for nitric oxide insufficiency. *Meat Sci.* **92**, 274–279 (2012).

359. Baskin, S. I., Horowitz, A. M. & Nealley, E. W. The Antidotal Action of Sodium Nitrite and Sodium Thiosulfate Against Cyanide Poisoning. *The Journal of Clinical Pharmacology* **32**, 368–375 (2023).

360. Rowe, J. J., Yarbrough, J. M., Rake, J. B. & Eagon, R. G. Nitrite inhibition of aerobic bacteria. *Curr. Microbiol.* **2**, 51–54 (1979).

361. Ansari, F. A. & Mahmood, R. Sodium nitrite enhances generation of reactive oxygen species that decrease antioxidant power and inhibit plasma membrane redox system of human erythrocytes. *Cell Biol. Int.* **40**, 887–894 (2016).

362. Missall Tricia, A., Lodge Jennifer, K. & McEwen Joan, E. Mechanisms of Resistance to Oxidative and Nitrosative Stress: Implications for Fungal Survival in Mammalian Hosts. *Eukaryotic Cell* **3**, 835–846 (2004).

363. Maliehe, M. *et al*. Environmental Factors That Contribute to the Maintenance of Cryptococcus neoformans Pathogenesis. *Microorganisms* **8**, 180 (2020).

364. de Nadal, E. & Posas, F. The HOG pathway and the regulation of osmoadaptive responses in yeast. *FEMS Yeast Res.* **22**, foac013. doi: 10.1093/femsyr/foac013 (2022).

365. Meng, Y. & Ding, C. Mitochondria in *Cryptococcus*: an update of mitochondrial transcriptional regulation in *Cryptococcus*. *Curr. Genet.* **69**, 1–6 (2023).

366. Moore, A. L. *et al*. Unraveling the Heater: New Insights into the Structure of the Alternative Oxidase. *Annu. Rev. Plant Biol.* **64**, 637–663 (2023).

367. Elliott, C. *et al*. Purification and characterisation of recombinant DNA encoding the alternative oxidase from Sauromatum guttatum. *Mitochondrion* **19 Pt B**, 261–268 (2014).

368. Barsottini, M. R. O. *et al*. Biochemical characterization and inhibition of the alternative oxidase enzyme from the fungal phytopathogen *Moniliophthora perniciosa*. *Communications Biology* **3**, 263 (2020).

369. Kido, Y. *et al*. Purification and kinetic characterization of recombinant alternative oxidase from *Trypanosoma brucei brucei*. *Biochim. Biophys. Acta* **1797**, 443–450 (2010).

370. Cortes, L. A. *et al*. Novel Gallate Triphenylphosphonium Derivatives with Potent Antichagasic Activity. *PLOS ONE* **10**, e0136852 (2015).

371. Battogtokh, G. *et al*. Mitochondria-targeting drug conjugates for cytotoxic, anti-oxidizing and sensing purposes: current strategies and future perspectives. *Acta Pharm. Sin. B.* **8**, 862–880 (2018).

372. Ebiloma, G. U. *et al*. Inhibition of trypanosome alternative oxidase without its N-terminal mitochondrial targeting signal (ΔMTS-TAO) by cationic and non-cationic 4-hydroxybenzoate and 4-alkoxybenzaldehyde derivatives active against T. brucei and T. congolense. *Eur. J. Med. Chem.* **150**, 385–402 (2018).

373. Yousif, L. F., Stewart, K. M. & Kelley, S. O. Targeting mitochondria with organelle-specific compounds: strategies and applications. *Chembiochem* **10**, 1939–1950 (2009).

374. Young, L. *et al*. Kinetic and structural characterisation of the ubiquinol-binding site and oxygen reduction by the trypanosomal alternative oxidase. *Biochim. Biophys. Acta Bioenerg.* **1861**, 148247 (2020).

375. Trevijano-Contador, N. & Zaragoza, O. Immune Response of *Galleria mellonella* against Human Fungal Pathogens. *J. Fungi (Basel)* **5**, 3. doi: 10.3390/jof5010003 (2018).

376. Buxton, R. Blood Agar Plates and Hemolysis Protocols. *American Society for Microbiology*, 1–9 (2005).

377. Cowen, L. E., Sanglard, D., Howard, S. J., Rogers, P. D. & Perlin, D. S. Mechanisms of Antifungal Drug Resistance. *Cold Spring Harb Perspect. Med.* **5**, a019752 (2014).

378. Havlickova, B., Czaika, V. A. & Friedrich, M. Epidemiological trends in skin mycoses worldwide. *Mycoses* **51 Suppl 4**, 2–15 (2008).

379. Baker, J. & Denning, D. W. The SSS revolution in fungal diagnostics: speed, simplicity and sensitivity. *Br. Med. Bull.*, ldad011 (2023).

380. Ball, B., Langille, M. & Geddes-McAlister, J. Fun(gi)omics: Advanced and Diverse Technologies to Explore Emerging Fungal Pathogens and Define Mechanisms of Antifungal Resistance. *mBio* **11**, 10.1128/mbio.01020–20 (2023).

381. Lucas, J. A., Hawkins, N. J. & Fraaije, B. A. Chapter Two - The Evolution of Fungicide Resistance. *Adv. Appl. Microbiol.* **90**, 29–92 (2015).

382. DeLeon-Rodriguez, C. & Casadevall, A. Cryptococcus neoformans: Tripping on Acid in the Phagolysosome. *Frontiers in Microbiology* **7**, 164 (2016).

383. Levitz Stuart, M. *et al*. Cryptococcus neoformans Resides in an Acidic Phagolysosome of Human Macrophages. *Infect. Immun.* **67**, 885–890 (2023).

384. Levitz, S. M., Harrison, T. S., Tabuni, A. & Liu, X. Chloroquine induces human mononuclear phagocytes to inhibit and kill Cryptococcus neoformans by a mechanism independent of iron deprivation. *J. Clin. Invest.* **100**, 1640–1646 (1997).

385. Harrison, T. S., Griffin, G. E. & Levitz, S. M. Conditional Lethality of the Diprotic Weak Bases Chloroquine and Quinacrine against Cryptococcus neoformans. *J. Infect. Dis.* **182**, 283–289 (2000).

386. Weber, S. M., Levitz, S. M. & Harrison, T. S. Chloroquine and the fungal phagosome. *Curr. Opin. Microbiol.* **3**, 349–353 (2000).

387. Nicola André Moraes, Robertson Emma, J., Albuquerque Patrícia, Derengowski Lorena, d. S. & Arturo, C. Nonlytic Exocytosis of Cryptococcus neoformans from Macrophages Occurs In Vivo and Is Influenced by Phagosomal pH. *mBio* **2**, 10.1128/mbio.00167–11 (2011).

388. Lin, J. *et al*. Synthetic Derivatives of Ciclopirox are Effective Inhibitors of *Cryptococcus neoformans*. *ACS Omega* **6**, 8477–8487 (2021).

389. Bissell, A. U. *et al*. Biosynthesis of the Sphingolipid Inhibitors Sphingofungins in Filamentous Fungi Requires Aminomalonate as a Metabolic Precursor. *ACS Chem. Biol.* **17**, 386–394 (2022).

390. Guimarães, A. J. *et al*. Cryptococcus neoformans responds to mannitol by increasing capsule size in vitro and in vivo. *Cell. Microbiol.* **12**, 740–753 (2010).

391. Washington, E. J. *et al*. Structures of trehalose-6-phosphate synthase, Tps1, from the fungal pathogen Cryptococcus neoformans: a target for novel antifungals. *bioRxiv*, 2023.03.14.530545 (2023).

392. Thammahong, A., Puttikamonkul, S., Perfect, J. R., Brennan, R. G. & Cramer, R. A. Central Role of the Trehalose Biosynthesis Pathway in the Pathogenesis of Human Fungal Infections: Opportunities and Challenges for Therapeutic Development. *Microbiol. Mol. Biol. Rev.* **81**, e00053–16. Print 2017 Jun (2017).

393. Lev, S. *et al*. The PHO signaling pathway directs lipid remodeling in Cryptococcus neoformans via DGTS synthase to recycle phosphate during phosphate deficiency. *PLOS ONE* **14**, e0212651 (2019).

394. Sophie, L. *et al*. Pho4 Is Essential for Dissemination of Cryptococcus neoformans to the Host Brain by Promoting Phosphate Uptake and Growth at Alkaline pH. *mSphere* **2**, 10.1128/msphere.00381–16 (2017).

395. Roelants, F. M., Torrance, P. D. & Thorner, J. R. 2. Differential roles of PDK1- and PDK2-phosphorylation sites in the yeast AGC kinases Ypk1, Pkc1 and Sch9. *Microbiology* **150**, 3289–3304.

396. Heung, L. J., Kaiser, A. E., Luberto, C. & Del Poeta, M. The Role and Mechanism of Diacylglycerol-Protein Kinase C1 Signaling in Melanogenesis by *Cryptococcus neoformans**. *J. Biol. Chem.* **280**, 28547–28555 (2005).

397. Sun, Y. *et al*. Orm protein phosphoregulation mediates transient sphingolipid biosynthesis response to heat stress via the Pkh-Ypk and Cdc55-PP2A pathways. *Mol. Biol. Cell* **23**, 2388–2398 (2012).

398. Muir, A., Ramachandran, S., Roelants, F. M., Timmons, G. & Thorner, J. TORC2-dependent protein kinase Ypk1 phosphorylates ceramide synthase to stimulate synthesis of complex sphingolipids. *eLife* **3**, e03779 (2014).

399. Stiban, J., Caputo, L. & Colombini, M. Ceramide synthesis in the endoplasmic reticulum can permeabilize mitochondria to proapoptotic proteins. *J. Lipid Res.* **49**, 625–634 (2008).

400. Hernández-Corbacho, M. J., Salama, M. F., Canals, D., Senkal, C. E. & Obeid, L. M. Sphingolipids in mitochondria. *Biochim. Biophys. Acta Mol. Cell. Biol. Lipids* **1862**, 56–68 (2017).

401. Dongpil, L. *et al*. Unraveling Melanin Biosynthesis and Signaling Networks in Cryptococcus neoformans. *mBio* **10**, 10.1128/mbio.02267–19 (2023).

402. Choi, J., Vogl, A. W. & Kronstad, J. W. Regulated expression of cyclic AMP-dependent protein kinase A reveals an influence on cell size and the secretion of virulence factors in Cryptococcus neoformans. *Mol. Microbiol.* **85**, 700–715 (2012).

403. Heung, L. J., Luberto, C., Plowden, A., Hannun, Y. A. & Del Poeta, M. The Sphingolipid Pathway Regulates Pkc1 through the Formation of Diacylglycerol in *Cryptococcus neoformans**. *J. Biol. Chem.* **279**, 21144–21153 (2004).

404. Ong, B. X. *et al*. Structural analysis of fungal pathogenicity-related casein kinase α subunit, Cka1, in the human fungal pathogen Cryptococcus neoformans. *Scientific Reports* **9**, 14398 (2019).

405. Rizzo, J. *et al*. Analysis of multiple components involved in the interaction between Cryptococcus neoformans and Acanthamoeba castellanii. *Fungal Biology* **121**, 602–614 (2017).

406. Watkins, R. A. *et al*. Cryptococcus neoformans Escape From Dictyostelium Amoeba by Both WASH-Mediated Constitutive Exocytosis and Vomocytosis. *Frontiers in Cellular and Infection Microbiology* **8**, 108 (2018).

407. Rella, A. *et al*. Pseudomonas aeruginosa Inhibits the Growth of Cryptococcus Species. *Mycopathologia* **173**, 451–461 (2012).

408. Jung Kwang-Woo *et al*. Rad53- and Chk1-Dependent DNA Damage Response Pathways Cooperatively Promote Fungal Pathogenesis and Modulate Antifungal Drug Susceptibility. *mBio* **10**, 10.1128/mbio.01726–18 (2023).

409. Piper-Brown, E., Dresel, F., Badr, E. & Gourlay, C. W. Elevated Levels of Mislocalised, Constitutive Ras Signalling Can Drive Quiescence by Uncoupling Cell-Cycle Regulation from Metabolic Homeostasis. *Biomolecules* **13** (2023).

410. Sharma, K. *et al*. Synthetic amino acids-derived peptides target Cryptococcus neoformans by inducing cell membrane disruption. *Bioorg. Chem.* **130**, 106252 (2023).

411. Mahindra, A. *et al*. Synthetically modified l-histidine-rich peptidomimetics exhibit potent activity against Cryptococcus neoformans. *Bioorg. Med. Chem. Lett.* **24**, 3150–3154 (2014).

412. Mahindra, A. *et al*. Discovery of Short Peptides Exhibiting High Potency against Cryptococcus neoformans. *ACS Med. Chem. Lett.* **5**, 315–320 (2014).

413. Lee, I. R., Chow, E. W. L., Morrow, C. A., Djordjevic, J. T. & Fraser, J. A. Nitrogen Metabolite Repression of Metabolism and Virulence in the Human Fungal Pathogen Cryptococcus neoformans. *Genetics* **188**, 309–323 (2011).

414. Garbe, E. & Vylkova, S. Role of Amino Acid Metabolism in the Virulence of Human Pathogenic Fungi. *Current Clinical Microbiology Reports* **6**, 108–119 (2019).

415. Calvete, C. L. *et al*. Amino acid permeases in Cryptococcus neoformans are required for high temperature growth and virulence; and are regulated by Ras signaling. *PLoS One* **14**, e0211393 (2019).

416. Basso,Luiz R.,,Jr, Gast, C. E., Bruzual, I. & Wong, B. Identification and properties of plasma membrane azole efflux pumps from the pathogenic fungi Cryptococcus gattii and Cryptococcus neoformans. *J. Antimicrob. Chemother.* **70**, 1396–1407 (2015).

417. Miwha, C., Edward, S., Khanal, L. A., Kwon-Chung Kyung, J. & Chang Yun, C. Roles of Three Cryptococcus neoformans and Cryptococcus gattii Efflux Pump-Coding Genes in Response to Drug Treatment. *Antimicrob. Agents Chemother.* **62**, 10.1128/aac.01751–17 (2018).

418. Ramachandraiah, K. & Chin, K. B. Antioxidant, Antimicrobial, and Curing Potentials of Micronized Celery Powders added to Pork Sausages. *Food Sci. Anim. Resour.* **41**, 110–121 (2021).

419. Cheng, T. *et al*. Computation of octanol-water partition coefficients by guiding an additive model with knowledge. *J. Chem. Inf. Model.* **47**, 2140–2148 (2007).

420. Efremov, R. G., Baradaran, R. & Sazanov, L. A. The architecture of respiratory complex I. *Nature* **465**, 441–445 (2010).

421. Shimizu, H. *et al*. Crystal structure of mitochondrial quinol–fumarate reductase from the parasitic nematode *Ascaris suum*. *J Biochem* **151**, 589–592 (2012).

422. Lange, C. & Hunte, C. Crystal structure of the yeast cytochrome *bc1* complex with its bound substrate cytochrome c. *Proceedings of the National Academy of Sciences* **99**, 2800–2805 (2023).

423. Stock, S., Leslie, L. & Walker, W. Molecular Architecture of the Rotary Motor in ATP Synthase. *Science* **286**, 1700–1705 (2023).

424. Larkin, M. A. *et al*. Clustal W and Clustal X version 2.0. *Bioinformatics* **23**, 2947–2948 (2007).